Statistics and Operations Research Transactions,

vol. 43, n. 1 (2019)

SORT 43 (1) January-June 2019, 3-24 DOI: 10.2436/20.8080.02.77

A simheuristic for routing electric vehicles with limited driving ranges and stochastic travel times

Lorena Reyes-Rubiano[1,*], Daniele Ferone[2], Angel A. Juan[3,4] and Javier Faulin[1]

Abstract

Green transportation is becoming relevant in the context of smart cities, where the use of electric vehicles represents a promising strategy to support sustainability policies. However the use of electric vehicles shows some drawbacks as well, such as their limited driving-range capacity. This paper analyses a realistic vehicle routing problem in which both driving-range constraints and stochastic travel times are considered. Thus, the main goal is to minimize the expected time-based cost required to complete the freight distribution plan. In order to design reliable routing plans, a simheuristic algorithm is proposed. It combines Monte Carlo simulation with a multi-start metaheuristic, which also employs biased-randomization techniques. By including simulation, simheuristics extend the capabilities of metaheuristics to deal with stochastic problems. A series of computational experiments are performed to test our solving approach as well as to analyse the effect of uncertainty on the routing plans.

MSC: 90B08.

Keywords: Vehicle routing problem, electric vehicles, green transport and logistics, smart cities, simheuristics, biased-randomized heuristics.

1. Introduction

The growing public concern about living conditions and environmental preservation, specially in the context of modern cities, leads to the emergence and consolidation of the sustainable city concept, which integrates social, environmental, and economic dimensions (McKinnon et al., 2015). Smart sustainable cities call for an intelligent management of resources considering the social welfare in order to achieve a sustainable growth (Bibri and Krogstie, 2017). On the one hand, companies need to satisfy an in-

* *Corresponding author:* lorena.reyes@unavarra.es

[1] Institute of Smart Cities, Public University of Navarra, Pamplona, Spain

[2] Dept. of Informatics, Systems and Communication (DISCo), University of Milano-Bicocca, Milano, Italy

[3] IN3 – Computer Science Dept., Open University of Catalonia, Barcelona, Spain

[4] Euncet Business School, Terrassa, Spain

Received: March 2018
Accepted: November 2018

creasing consumers' demand that requires an intense freight transportation activity. This activity has to be carried out without generating economic inefficiencies. On the other hand, the welfare and environmental deterioration brings to light the need for smarter distribution systems that guarantee sustainability of this transportation activity. Nowadays, the main initiatives and policies in the area of transportation and logistics consider pollution targets. Typically, governmental urban guidelines focus on improving passenger and freight transportation due to their noticeable impact on the citizens' quality of life. Indeed, freight transportation generates around 10% of the greenhouse gases and ozone precursors released in the atmosphere (Eurostat, 2016). Since these emissions affect people's health, their reduction does not only generate an environmental benefit, but also social and economic gains. According to The World Bank (2018), 60% of the operation costs in developing countries are referred to energy bills. This reinforces the idea of a strong correlation between the different sustainability dimensions.

Consequently, the sustainability concept promotes the use of vehicles running on alternative fuel technologies. In particular, electric vehicles (EVs) represent a promising option to mitigate the negative impacts caused by transport activities in city logistics. Governments in many countries promote initiatives and regulations that aim at increasing the use of EVs, specially in city logistics and transportation activities. As a result, urban mobility is evolving to incorporate EVs. These incentives are motivated by the potential of zero-emission vehicles to reduce externalities on the citizens and the environment (Eurostat, 2016). As a way of responding to the aforementioned challenges related to sustainable logistics, a number of relevant initiatives have been released, e.g.: *(i)* Lean and Green Europe (www.lean-green.eu); *(ii)* US / Canada Smartway Transport Partnership (www.nrcan.gc.ca); or *(iii)* UNCTAD Sustainable Freight Transport and Finance (www.unctad.org). Some of these initiatives are supported and sponsored by private companies that acknowledge the importance of an environmentally sustainable growth. Responding to social and business needs, a large number of enterprises are incorporating both EVs and hybrid vehicles in their supply chain activities. In summary, the traditional paradigm of freight distribution in modern cities is changing with the introduction of these new technologies and the adoption of distribution concepts based on horizontal cooperation (Pérez-Bernabeu et al., 2015, Serrano-Hernández et al., 2017).

However, despite these technological advances there are still barriers to the full development of sustainable freight transportation. Examples of these barriers are: inefficient operations, poor infrastructures, or lack of sustainable policies. EVs require extra operational efforts due to the limited life of their batteries, the amount of time required to refill them, and the lack of recharging stations in modern cities. These technical limitations introduce driving-range constraints that do not exist in the case of traditional internal combustion vehicles (Juan et al., 2016). In addition to the previously described barriers, one has to take into account that the battery consumption rate depends on a wide range of random or difficult to predict factors, such as traffic congestion, road characteristics affecting the energy consumption, weather conditions, driving style, etc. In other words, real-life is full of uncertainty that has to be taken into account when consider-

ing travel times. Accordingly, this paper analyses the electric vehicle routing problem with stochastic travel times (EVRPST), which also considers time-based driving-range constraints (Figure 1). Being a rich extension of the classical vehicle routing problem (VRP), the EVRPST is also an *NP-hard* optimization problem, which justifies the use of heuristic-based solving approaches. Our main goal is to design an 'efficient' routing plan that satisfies a set of customers' demands using a homogeneous fleet of electric vehicles, each of them characterized by a limited loading capacity and driving range. Furthermore, we consider a more realistic VRP in which transport times are not deterministic but random variables instead. Efficiency will be measured in terms of total transport time. In other words, our main goal is to minimize the total expected time necessary to complete the delivery. Notice that random travel times could cause the exhaustion of the vehicle battery before completing its assigned route. Such a route failure will require a costly corrective action, which will be also measured in time units (Eshtehadi, Fathian and Demir, 2017).

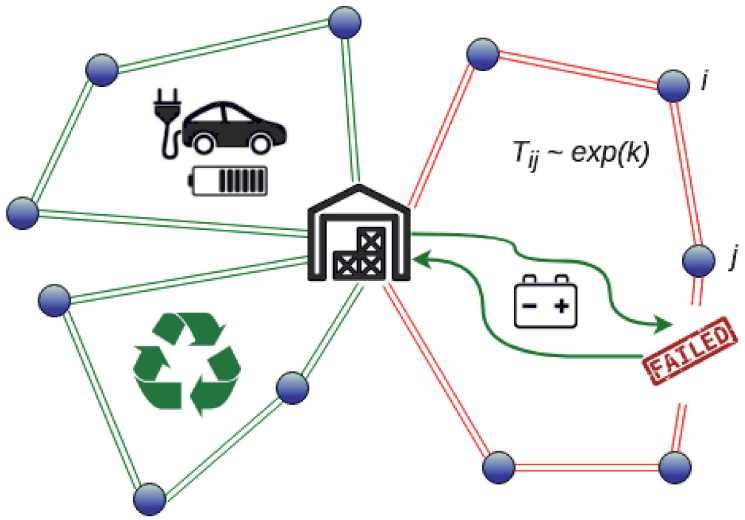

Figure 1: *A simple representation of the EVRPST with driving-range constraints.*

To solve the EVRPST, a novel simheuristic approach integrating Monte Carlo simulation within a multi-start framework is proposed. A review on basic concepts of simheuristic algorithms can be found in Juan et al. (2015). Also, the generation of solutions inside the multi-start framework is based on the use of biased-randomized techniques, which allow to extend deterministic heuristic into enhanced probabilistic algorithms. Grasas et al. (2017) provide an updated review of biased-randomized algorithms. Our solving approach considers the use of energy safety stocks: that is, during the design of the routing plan, a certain percentage of the battery is reserved for covering emergency situations with higher-than-expected travel times. Notice that using higher levels of safety stock leads to shorter routes and a higher number of required vehicles.

In contrast, using lower levels of safety stock will increase the probability of suffering a route failure. Whenever this occurs, we assume that the failing battery has to be replaced by a new one. In our computational experiments, this corrective action has a time-based penalty cost equivalent to a round-trip from the depot to the current position of the battery that needs to be replaced. All in all, the main contributions of this paper are: (i) to mitigate the lack of works on vehicle routing problems considering both driving-range limitations and uncertainty conditions; (ii) to develop and test a simheuristic approach for the EVRPST; and (iii) to analyse the effect of random travel times and the use of energy safety stocks on the routing plans.

The remaining of the paper is organized as follows: Section 2 reviews related work in the transportation literature; Section 3 provides some additional details on the problem under study; our simheuristic solving approach is explained in Section 4; Section 5 describes a series of computational experiments, while the associated results are discussed in Section 6; finally, Section 7 concludes the paper and identifies potential lines for future research.

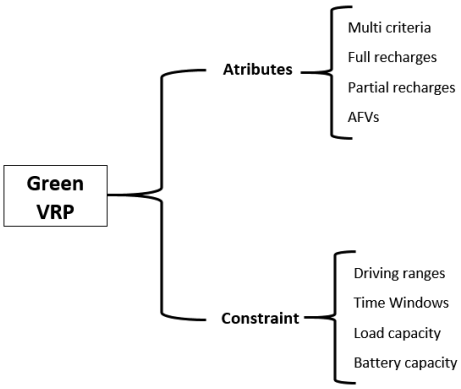

Figure 2: *Frequent attributes and constraints in the G-VRP.*

2. Literature review

The use of EVs in transport activities is related to several urban changes in terms of infrastructure and distribution strategies. On the one hand, some of these challenges relate to infrastructure and fleet configurations (Juan, Goentzel and Bektaş, 2014b, Shao, Guan and Bi, 2018). On the other hand, EVs have started to replace conventional vehicles in city logistics, redefining transport operations (Hof, Schneider and Goeke, 2017). Many logistics and transportation problems in smart cities can be modeled as rich VRP variants (Cáceres-Cruz et al., 2014). The rich VRP has been a very active research line in combinatorial optimization problems. This is partly due to the difficulty of managing multiple attributes and constraints, such as the different sustainability dimensions: economic, social, and environmental (McKinnon et al., 2015). In particular, the 'green'

VRP (G-VRP) is a rich VRP which considers routing problems using alternative fuel vehicles (AFVs) (Erdoğan and Miller-Hooks, 2012). One popular G-VRP variant is the so-called pollution routing problem or PRP (Bektaş and Laporte, 2011). In the PRP, the main objective is to minimize the energy consumption. It also includes time windows as a realistic constraint. Figure 2 provides a scheme that summarizes different attributes and constraints frequently associated with the G-VRP (Lin et al., 2014).

2.1. The deterministic G-VRP

A key restriction in VRPs with EVs is the limited capacity of their batteries, which might require multiple recharging stops. Hence, (Erdoğan and Miller-Hooks, 2012) solve a G-VRP allowing intermediate stops by implementing procedures based on the well-known savings heuristics (Clarke and Wright, 1964) and the popular density-based clustering algorithm. Demir, Bektaş and Laporte (2012) solves a PRP with time windows, where customer sequences are first defined and, afterwards, the travel speeds are optimized by means of an adaptive large neighbourhood search (ALNS) metaheuristic. Juan et al. (2014b) address the G-VRP with multiple driving ranges. The goal of this work is to define alternative fleet configurations based on EVs and hybrid-electric vehicles. The authors describe an integer programming formulation and a multi-round heuristic algorithm that iteratively constructs a solution. Schneider, Stenger and Goeke (2014) propose an ALNS metaheuristic with some local searches with the aim of minimizing the total distribution cost, which includes the cost of using a fleet of vehicles plus the actual routing cost. Additionally, these authors considered intermediate stops in recharging stations. Similarly, the ALNS metaheuristic is hybridized with the adaptive variable neighbourhood search framework by Schneider, Stenger and Hof (2015), who deal with a routing problem with EVs-related constraints and also consider intermediate stops. Koç and Karaoglan (2016) design a simulated annealing metaheuristic, based on an exact method, to solve the G-VRP for the small-scale instances proposed by Erdoğan and Miller-Hooks (2012). Hiermann et al. (2016) study the VRP with EVs, time windows, and recharging stations. Hof et al. (2017) consider EVs to solve a location-routing problem where the objective is to determine whether the battery swap stations should be defined from candidate locations or closer to the set of customers. Finally, the G-VRP with multiple objectives – including both monetary and environmental costs – is discussed by Sawik, Faulin and Pérez-Bernabeu (2017a, b, c).

2.2. The stochastic G-VRP

Stochastic combinatorial optimization has received increasing interest during the last decades (Bianchi et al., 2009, Ritzinger, Puchinger and Hartl, 2015). Solving a stochastic VRP requires a methodology able to deal with the random components of the problem, which is not straightforward, as discussed in Juan et al. (2011a, 2013). The most frequent random variables are: customers' demands, service and travel times, and fre-

quency of order placing (Bozorgi, Farasat and Mahmoud, 2017). The previous articles highlight the importance of dealing with uncertainty, and study realistic characteristics such as urban transport dynamics. In most existing works, travel times are assumed to be constant, but this is not a realistic assumption. Hence, Ritzinger et al. (2015) propose to deal with uncertain travel times by modelling them as stochastic and time-dependent variables.

Uncertainty conditions are sometimes addressed by means of stochastic programming. This approach provides high quality solutions for small instances (Bozorgi-Amiri, Jabalameli and Al-e Hashem, 2013). Erdoğan and Miller-Hooks (2012) present an exact model to solve the VRP with stochastic travel times. These authors assess the influence of route duration on environmental indicators, such as energy consumption. Another relevant problem is the time-dependent VRP, where the travel times are different depending on the specific period. Gendreau, Ghiani and Guerriero (2015) provides a literature review on these topics. Travel times may vary by exogenous variables, such as traffic congestion, weather conditions, moving targets, or mobile obstacles. They might also be influenced by endogenous variables: for example, by varying the vehicles' speeds or by choosing highways over standard roads.

Recently, Eshtehadi et al. (2017) address a VRP with stochastic demands and travel times. These authors develop a solving approach based on an exact method that is able to solve instances with up to 20 nodes considering multiple scenarios. The authors tackle the stochasticity describing two scenarios that represent the best and the worst conditions for demand and travel times. To conclude this literature review, Table 1

Table 1: *An illustrative set of works covering the most popular G-VRP variants.*

Papers	Atributes	Constraints	Solution Approach
Shao et al. (2018)		Driving range	GA
Eshtehadi et al. (2017)	Stochastic demands Stochastic travel times	Driving range	SP
Sawik et al. (2017a,b,c)	Multi criteria	Driving range	EM
Koç and Karaoglan (2016)		Driving range	SAM and EM
Hiermann et al. (2016)	Full recharges	Time windows	EM
Desaulniers et al. (2016)	Full recharges Partial recharges	Driving range Time windows	EM
Schneider et al. (2015)	Full recharges	Driving range	ALNS
Felipe et al. (2014)	Full recharges	Driving range	GSA
Juan et al. (2014a)	Heterogeneous fleet	Driving range	RMS
Schneider et al. (2014)	Full recharges	Driving range	ALNS
Erdoğan and Miller-Hooks (2012)	Stochastic travel time Full recharges	Driving range	SP

ALNS: Adaptive large neighbourhood search. EM: Exact method. SP: Stochastic programming.
RMS: A randomized multi-start algorithm. GA: Genetic algorithm.GSA: Greedy algorithm. SH: Savings heuristic.
SAM: Simulated annealing metaheuristic. DC: Density-based clustering algorithm

summarizes some illustrative works providing evidence about the most studied G-VRP variants.

3. Additional details on the EVRPST

The EVRPST is defined on an undirected graph $G = (N, A)$. Here, N contains the depot (node 0) and a set of customers $N^* = \{1, 2, \ldots, n\}$. Also, $A = \{(i, j) \mid i, j \in N, i \neq j\}$ is the set of edges connecting any two nodes in N. Each customer $i \in N^*$ has a demand $d_i > 0$. There is a set V of homogeneous vehicles, each of them with a loading capacity of $q >> max\{d_i\}$. As it is usual in most VRPs (Toth and Vigo, 2014), the following assumptions hold: (i) all customers' demands must be satisfied; (ii) each vehicle route starts and ends at the depot; (iii) each customer is visited exactly once; and (iv) the demand to be served in each route does not exceed the vehicle loading capacity. Moreover, the time-based cost of traversing each edge (i, j) is given by an independent random variable $T_{ij} = T_{ji} > 0$, which follows a known probability distribution with mean $E(T_{ij}) = t_{ij}$. Thus, the additional constraint is considered as well: the expected travel time employed by a vehicle to complete its route is limited by the battery duration, $t_{max} > \{\sum E[T_{ij}]\}$.

However, considering stochastic travel times implies introducing uncertainty about how much energy will be required to complete a route. Energy consumption and travel times depend on multiple factors, such as current load of the vehicle, road type, vehicle speed, driving skills, etc. This uncertainty makes it hard to guarantee feasible solutions when hard time-related constraints on batteries duration are considered. In particular, electric vehicles have a risk of batteries exhaustion during the trip, which is considered as a *route failure*. Decision makers may define corrective actions to properly address these failures when they happen. They might also define preventive actions to be applied before the vehicle runs out of battery. Figure 3 illustrates some examples of these types of actions.

On the one hand, a corrective action to resume the routing plan is required when a vehicle A runs out of energy after visiting a customer j (failure type I). In our computational experiments, we will assume that the cost of this corrective action is the time needed for a new vehicle B to complete a round-trip from the depot to the current location of A to supply a new battery. On the other hand, a preventive action could also be applied: if there is a high risk of running out of battery after serving a customer j, vehicle A might decide to return from j to the depot for recharging or swapping batteries (failure type II); after that, it might resume its planned route from the next customer, k. The time-based cost of such a preventive action could be estimated as the time requested to visit the depot for recharging batteries plus the time employed in moving from the depot to the next customer in the original route, k.

Although the simheuristic methodology introduced in this paper is quite flexible and could be easily extended to consider preventive actions, in our computational experiments we have only considered corrective actions (i.e., type I failures). Accordingly,

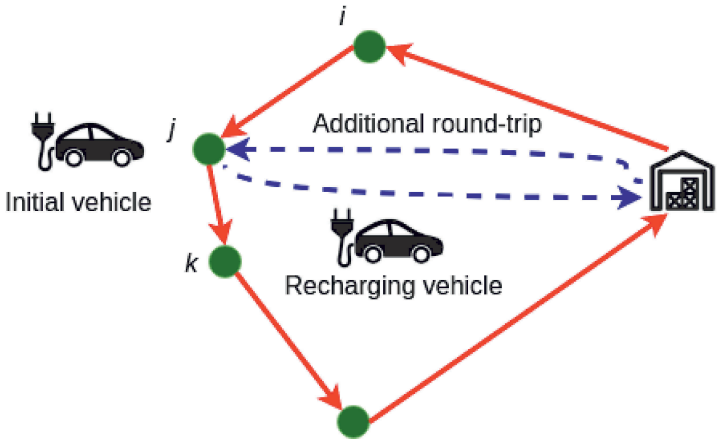

(a) Preventive action for type II failure

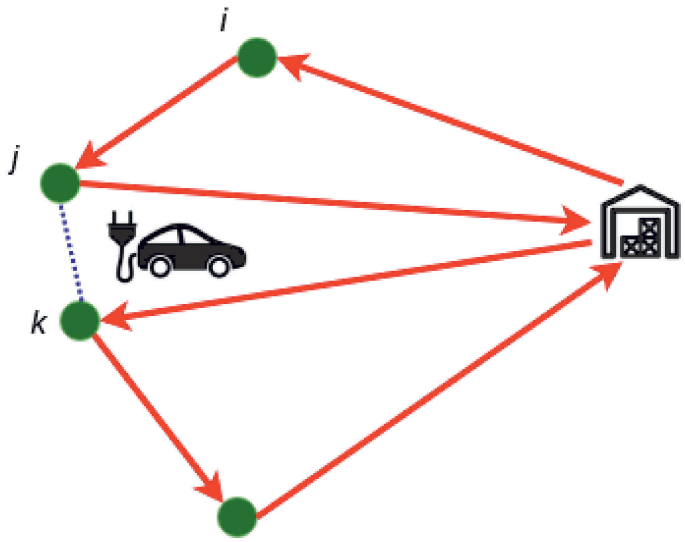

(b) Corrective action for type I failure

Figure 3: *Different actions to deal with route failures while using electric vehicles.*

the objective function minimizes the expected time-based cost required to complete the delivery process. Notice that this time-based cost is a non-smooth function, since it includes the 'penalty' cost associated with applying these corrective actions whenever route failures occur. Hence, if T_v represents the total time employed by vehicle v in completing its route, the objective function can be expressed as:

$$\min E\left(\sum_{v\in V} T_v\right) \tag{1}$$

with:

$$T_v = \begin{cases} \sum\limits_{\substack{i,j \in N \\ i \neq j}} T_{ij} \cdot z_{ijv} & \text{if } \sum\limits_{\substack{i,j \in N \\ i \neq j}} T_{ij} \cdot z_{ijv} \leq t_{max} \\ \sum\limits_{\substack{i,j \in N \\ i \neq j}} T_{ij} \cdot z_{ijv} + 2 \cdot T_{j0} & \text{otherwise} \end{cases} \tag{2}$$

where the decision variable z_{ijv} takes the value 1 if vehicle v covers the edge (i, j), while it takes the value 0 otherwise.

4. A simulation-optimization approach

Some of the first works employing simulation-optimization methods to deal with the VRP are due to Faulin and Juan (2008) and Faulin et al. (2008). Our solving methodology relies on a simheuristic approach, which proposes the integration of simulation techniques within a heuristic framework to address stochastic optimization problems in a natural way (Juan et al., 2015). In a simheuristic approach, the metaheuristic component is responsible for searching and filtering out promising solutions, while the simulation component is responsible for estimating different statistics associated with these promising solutions when considered in a stochastic environment. When properly designed, the simulation component can also provide feedback that is then used by the heuristic framework to better guide the search process De Armas et al. (2017). In this paper, we propose to integrate Monte Carlo simulation (MCS) into a biased-randomized multi-start framework. Biased-randomized versions of a constructive heuristic allow for fast generation of high-quality solutions (Grasas et al., 2017). These techniques have been successfully applied in solving different combinatorial optimization problems in areas such as vehicle routing (Dominguez, Juan and Faulin, 2014, Dominguez et al., 2016b, a, c), scheduling (Juan et al., 2014c, Ferone et al., 2018, Gonzalez-Neira et al., 2017) and facility location (Alvarez Fernandez et al., 2018). When complemented with some local search and encapsulated inside a multi-start (or similar) framework, they constitute a strong basis that can be easily extended into a simheuristic framework (Grasas, Juan and Lourenço, 2016). Our biased-randomized multi-start (BR-MS) simheuristic approach builds upon the biased-randomized version of Clarke and Right Savings (BRCWS) procedure proposed by Juan et al. (2011b). The complete algorithm is summarized in Pseudo-code 1 and described next in more detail.

First, the stochastic instance is transformed into a deterministic one by using expected travel times as initial estimates for the real stochastic values. Then, following the Clarke and Wright (1964) heuristics, a dummy solution is created and the savings associated with traversing each edge are computed. This initial solution (*initSol*) is improved by the classical *2-Opt* local search operator, and its expected travel time (stochastic cost) is estimated by using a fast MCS with just *sSim* runs – typically in the order of a few hundreds. Notice that, as any other solution we will generate, *initSol* will have

Algorithm 1: *BR-MS simheuristic for the EVRPST.*

```
1: procedure SIMHEURISTIC solve(test, nodes, edges)
                                          ▷ test: maxTime, β, sSim, lSim, s
                                          ▷ nodes: coordinates, demand
                                          ▷ edges: travel time
2:     savings ← computeSavings (nodes, edges)
3:     initSol ← savingsHeuristic (nodes, savings)   ▷ Clarke and Wright (1964)
4:     initSol ← localSearch (initSol)                              ▷ 2-Opt
5:     stochCost(initSol) ← simulation (initSol, sSim)
6:     baseSol ← initSol
7:     bestStochSolList ← add (initSol)                        ▷ elite solutions
8:     while (elapsedTime < maxTime) do
9:         newSol ← BRCWS (nodes, savings, β, s)          ▷ Juan et al. (2011b)
10:        newSol ← localSearch (newSol)                            ▷ 2-Opt
11:        if (detCost(newSol) < detCost(baseSol)) then
12:            stochCost(newSol) ← simulation (newSol, sSim)
13:            if (stochCost(newSol) < detCost(baseSol)) then
14:                baseSol ← newSol
15:            end if
16:            update (bestStochSolList)
17:        end if
18:    end while
19:    for (each sol in bestStochSolList) do
20:        stochCost(sol) ← simulation (sol, lSim)
21:    end for
22:    return bestSol in bestStochSolList
23: end procedure
```

two time-based costs: the one associated with the deterministic version of the problem (*detCost*) and the one associated with the stochastic one (*stochCost*). At this stage, *initSol* is stored as our temporary reference or 'base' solution (*baseSol*) and included in a list of 'elite' stochastic solutions (*bestStochSolList*). Afterwards, a multi-start process is repeated until a termination criterion (*maxTime*) is met. In each iteration, a new deterministic solution (*newSol*) is generated by using the BRCWS procedure. Once a fast local search is applied, this solution is labeled as 'promising' if its deterministic time-based cost is lower than that of *baseSol*. If it is not promising, *newSol* is discarded

and a new iteration starts. If it is promising, a new fast MCS is applied to estimate the stochastic cost (expected time) associated with *newSol*. Whenever appropriate, *baseSol* is replaced by *newSol* and the *bestStochSolList* is updated. Once the ending criterion is met, the expected time associated with each elite solution in *bestStochSolList* is assessed again, this time using a more intensive MCS with *lSim* runs, typically in the order of a few thousands. Notice that while the assessments in the main loop are required to be fast, because the number of solutions to assess may be extraordinarily high, those applied to a reduced list of elite solutions can employ more computing time.

The computational time of the algorithm is bounded by *maxTime*. Regarding its computational complexity, each iteration has three stages: the construction with BRCWS, the local search, and the simulation phase. The computational complexity of BRCWS is bounded by the number of the edges m, since the merging can be done in constant time but it is necessary to examine all savings. Since each client is served exactly once, the local search swapping moves are bounded to $O(n^2) = O(m)$. Finally, the complexity of the simulation stage is $O(m \cdot sSim)$. Therefore, the complexity of each iteration is dominated by the simulation phase, and it is $O(m \cdot sSim)$.

As usually done in the related literature (Grasas et al., 2017), the biased-randomized procedure is based on the use of a geometric probability distribution, which makes use of a parameter β ($0 < \beta < 1$). The BRCWS heuristic is adapted from the one proposed by Juan et al. (2011b) to ensure the feasibility of the generated solutions. In particular, it is guaranteed that the expected travel time of each vehicle will not exceed the duration of the batteries. However, as discussed before, under stochastic conditions it is not possible to guarantee that a route is failure-free. Accordingly, the reliability of each solution (i.e., the probability that a solution does not suffer any route failure) is also estimated from the data obtained in the previous simulation runs. As a way to increase these reliability levels, different levels of safety stock are considered for each vehicle. In other words, during the route-design stage, a given percentage of the vehicle driving-range capacity ($s\%$) is reserved as a safety stock to be used in case of higher-than-expected travel times. The specific value of s is a decision variable to be determined during the simulation-optimization process, since it will depend on the specific instance being analysed as well as on the probability distribution used to model travel times.

Notice that a relatively high value of s leads to short and reliable routes, i.e., routes employing short travel times and with a low probability of experiencing a failure due to the existence of a noticeable safety stock. Unfortunately, this also requires the use of more vehicles to cover all customers. On the contrary, a relatively value of s produces longer routes with a higher probability of suffering a failure (low reliability), but it requires a lower number of routes to cover all customers.

Regarding the MCS module, the steps followed to assess the stochastic performance (expected travel time) of a given solution are: (i) using random sampling from the assigned probability distributions, we run different executions of the routing plan in order to obtain random observations of the total travel time associated with it; (ii) from these random observations, different statistics can be computed for each routing plan, e.g.:

average time, variability of these times, etc.; (iii) using the same simulation outcomes, we estimate the reliability of each routing plan as the quotient between the number of route failures and the number of simulation runs. These experiments are repeated for different percentages of the safety stock level, s.

5. Computational experiments

This section presents a set of extensive computational experiments carried out to test our simheuristic approach for the EVRPST. Firstly, we introduce the instances that will be used to test our approach. Secondly, the algorithm parameters are discussed. Finally, the computational results are provided – they will be fully analysed in the next section. The algorithm has been implemented as a Java application. A standard personal computer with an Intel Core i5 CPU at 3.2 GHz and 4 GB RAM has been employed to perform all the experiments.

5.1. Benchmark instances

As a benchmark for our test, a set of 27 instances originally proposed by Uchoa et al. (2017) are selected. The original instances already included a maximum distance per route. They have been adapted so they use time-based costs instead of distance-based ones; i.e., Euclidean distances are considered to be travel times and the maximum distance per route is transformed into a maximum time per route. These instances are derived from the ones proposed by Christofides (1976), Golden et al. (1998), and Li, Golden and Wasil (2005). Table 2 shows the main characteristics of these instances.

In order to perform numerical experiments under uncertainty conditions, the aforementioned deterministic instances have been extended to consider stochastic travel times as follows: if the original instance shows a determinisitic travel time $t_{ij} = t_{ji} > 0$ when moving from node i to node j (with $i \neq j$), then we consider that the stochastic travel time T_{ij} is a random variable following an exponential probability distribution with $E[T_{ij}] = t_{ij}$ and $Var[T_{ij}] = t_{ij}^2$. In a real-life scenario, the specific probability distributions associated with each stochastic travel time would need to be fitted from historical observations, but our solving approach would still be valid. Furthermore, different levels of safety stock – as a percentage of the battery capacity (i.e., vehicle driving range) – have been considered in our experiments: $s \in \{0\%, 5\%, 10\%, \ldots, 35\%\}$.

5.2. Parameter settings

One of the advantages of our algorithm is that it does not require a complex fine-tuning process. In fact, after some quick trial-and-error experiments, the following values were set for each parameter:

Table 2: *Characteristics of the benchmark instances.*

Instance	n	$\|V\|$	q	t_{max}
Golden_1	240	9	550	650
Golden_2	320	10	700	900
Golden_3	400	10	900	1200
Golden_4	480	10	1000	1600
Golden_5	200	5	900	1800
Golden_6	280	7	900	1500
Golden_7	260	9	900	1300
Golden_8	440	10	900	1200
CMT6	50	6	160	200
CMT7	75	11	140	160
CMT8	100	9	200	230
CMT9	150	14	200	200
CMT10	199	18	200	200
CMT13	120	11	200	720
CMT14	100	11	200	1040
Li_21	560	10	1200	1800
Li_22	600	15	900	1000
Li_23	640	10	1400	2200
Li_24	720	10	1500	2400
Li_25	760	19	900	900
Li_26	800	10	1700	2500
Li_27	840	20	900	900
Li_28	880	10	1800	2800
Li_29	960	10	2000	3000
Li_30	1040	10	2100	3200
Li_31	1120	10	2300	3500
Li_32	1200	11	2500	3600

n = number of customers; $|V|$ = number of vehicles
q = capacity of each vehicle
t_{max} = maximum time allowed per route

- The biased-randomized selection during the construction process was generated by using a geometric probability distribution with parameter $\beta \in (0.23, 0.30)$ – i.e., at each iteration a random value inside the previous interval was assigned to β.
- The number of simulation runs was set to $sSim = 400$ for fast simulations (on each promising solution) and to $lSim = 10,000$ for intensive simulations (on each elite solution).
- For each instance, the algorithm was run 20 times, each time employing a different seed for the pseudo-random number generator.
- For each instance and seed, the algorithm was executed for $maxTime = 90$ seconds. Notice that this time does not include the time employed in computing the intensive simulations – however, since the number of elite solutions is reduced, this final step takes just a few additional seconds.

5.3. Computational results

Table 3 summarizes the results obtained both using the BRCWS procedure – a deterministic component inside the simheuristic – and the complete MS-BR simheuristic algorithm. Both approaches were run using the same parameters setting as described in Section 5.2. Also, in this comparison, no safety stock is considered, i.e., $s = 0\%$.

Table 3: *Performance of best deterministic and stochastic solutions.*

	BRCWS (deterministic component)			MS-BR Simheuristic	
Instance	BDS-Det	BDS-Stoch (a)	Reliability	BSS-Stoch	Reliability
CMT6	546.59	586.75	0.97	586.75	0.97
CMT7	856.26	1060.14	0.86	1040.29	0.88
CMT8	870.60	911.39	0.97	911.14	0.97
CMT9	1118.03	1189.43	0.95	1183.26	0.96
CMT10	1375.31	1439.11	0.95	1431.04	0.96
CMT13	1537.88	1544.24	0.99	1539.03	0.99
CMT14	823.11	823.24	0.99	823.24	0.99
Golden_1	5786.96	9939.65	0.02	9298.79	0.05
Golden_2	8646.93	13376.35	0.01	12754.47	0.03
Golden_3	12828.23	17757.94	0.01	16416.42	0.06
Golden_4	17963.58	23019.70	0.02	21764.50	0.06
Golden_5	7334.24	7679.08	0.78	7602.17	0.83
Golden_6	9829.11	12119.12	0.14	11371.87	0.30
Golden_7	12270.11	15998.37	0.04	15274.38	0.08
Golden_8	13753.22	18831.50	0.01	17869.64	0.03
Li_21	20465.47	24826.35	0.03	23939.78	0.08
Li_22	16612.02	23985.19	0.00	23330.96	0.00
Li_23	23192.07	27986.58	0.02	27176.38	0.07
Li_24	26160.76	30327.41	0.04	30086.13	0.06
Li_25	17618.46	27426.64	0.00	26942.85	0.00
Li_26	28728.31	34534.97	0.01	32076.98	0.09
Li_27	18460.02	28341.25	0.00	28160.91	0.00
Li_28	32654.00	35986.88	0.08	35547.75	0.20
Li_29	35230.52	38188.93	0.10	36485.80	0.87
Li_30	40363.61	44088.03	0.07	42891.96	0.48
Li_31	44248.09	47195.81	0.13	46263.44	0.58
Li_32	45959.99	50720.75	0.04	49407.09	0.15
Average	16490.84	19996.24	0.31	19340.31	0.40

BDS-Det: Best deterministic solution in a deterministic scenario.
BDS-Stoch: Best deterministic solution in a stochastic scenario.
BSS-Stoch: Best stochastic solution in a stochastic scenario.

Hence, column *BDS-Det* shows the cost (in total travel time) associated with the best-found solution obtained for the deterministic version of the problem when it is applied in a deterministic scenario (without uncertainty); column *BDS-Stoch* provides the expected cost of the same solution when it is employed in a stochastic scenario; the reliability column gives an estimate of the probability that the best deterministic solution can be used in a stochastic scenario without suffering any route failure – notice

that reliabilities can be low in some cases since no safety stock is considered. Similarly, column *BSS-Stoch* shows the expected cost of the best-found solution for the stochastic version of the problem when applied in a stochastic scenario. Finally, the reliability column provides an estimate of the probability that this solution can be completed as designed – without route failures. As depicted in Figure 4, *BDS-Det* and *BDS-Stoch* act as a lower bound and an upper bound, respectively, for *BSS-Stoch*. Thus, in general, it is not a good idea to apply the best-found solution for the deterministic version of the problem to a scenario under uncertainty, since it might often result in a sub-optimal plan. Instead, it is better to use a simulation-optimization approach to generate solutions with a better performance under stochastic conditions (usually by offering a higher reliability level and thus avoiding expensive corrective actions).

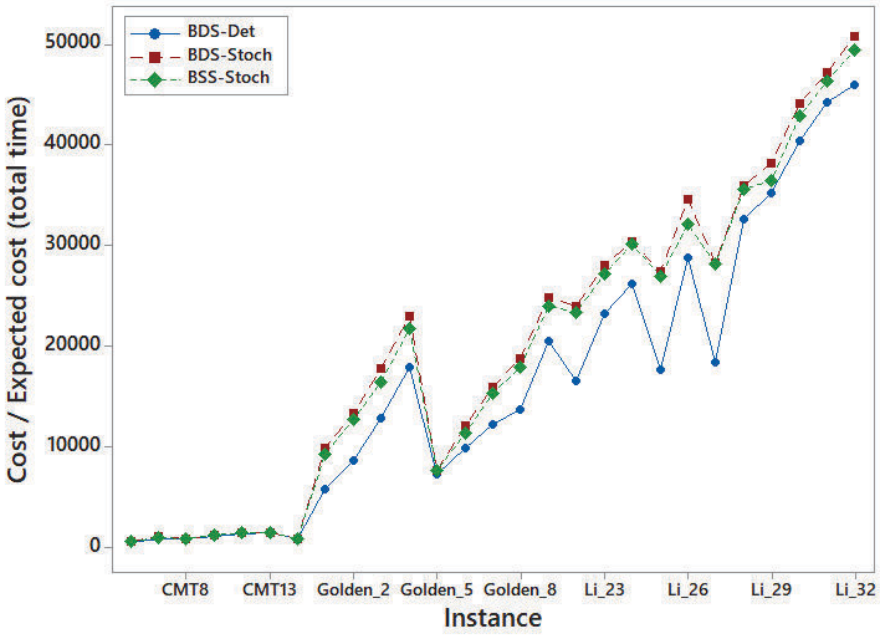

Figure 4: *Visual comparison among BDS-Det, BDS-Stoch, and BSS-Stoch.*

For each instance and safety stock level s, Table 4 shows the expected cost (in total travel time) provided by our simheuristic algorithm in a stochastic scenario. The table also shows the reliability associated with each solution – which tends to increase with the safety stock level –, as well as the gap with respect to the solution obtained without using any safety stock.

Table 4: *Solution performance considering different safety stock levels.*

	BDS-Stoch	BSS-Stoch with s = 5%			BSS-Stoch with s = 15%			BSS-Stoch with s = 25%			BSS-Stoch with s = 35%		
Instance	E[Cost] (a)	E[Cost] (c)	Reliab.	Gap (c)-(a)	E[Cost] (e)	Reliab.	Gap (e)-(a)	E[Cost] (g)	Reliab.	Gap (g)-(a)	E[Cost] (i)	Reliab.	Gap (i)-(a)
CMT6	586.75	584.80	0.97	−0.33%	586.94	0.97	0.03%	580.22	0.97	−1.11%	577.34	0.98	−1.60%
CMT7	1060.14	1044.42	0.87	−1.48%	1040.23	0.87	−1.88%	1041.44	0.88	−1.76%	1021.55	0.89	−3.64%
CMT8	911.39	910.92	0.97	−0.05%	909.31	0.97	−0.23%	895.55	0.99	−1.74%	890.08	0.98	−2.34%
CMT9	1189.43	1185.18	0.96	−0.36%	1180.13	0.96	−0.78%	1165.24	0.96	−2.03%	1150.64	0.97	−3.26%
CMT10	1439.11	1433.89	0.96	−0.36%	1429.24	0.96	−0.69%	1440.93	0.95	0.13%	1423.00	0.98	−1.12%
CMT13	1544.24	1554.70	1.00	0.68%	1552.56	1.00	0.54%	1554.78	1.00	0.68%	1555.34	1.00	0.72%
CMT14	823.24	820.79	1.00	−0.30%	819.92	1.00	−0.40%	822.17	1.00	−0.13%	820.66	1.00	−0.31%
Golden_1	9939.65	8814.54	0.09	−11.32%	7911.15	0.27	−20.41%	7698.07	0.56	−22.55%	8094.93	0.81	−18.56%
Golden_2	13376.35	12159.70	0.07	−9.10%	10669.63	0.32	−20.24%	10373.62	0.59	−22.45%	10883.65	0.87	−18.64%
Golden_3	17757.94	16135.89	0.09	−9.13%	14569.99	0.34	−17.95%	13520.73	0.75	−23.86%	13127.24	0.95	−26.08%
Golden_4	23019.70	20693.91	0.15	−10.10%	19188.46	0.48	−16.64%	18460.61	0.82	−19.81%	18498.44	0.97	−19.64%
Golden_5	7679.08	7584.29	0.95	−1.23%	7585.41	0.95	−1.22%	7335.11	0.97	−4.48%	7231.07	0.99	−5.83%
Golden_6	12119.12	10963.40	0.45	−9.54%	10206.53	0.76	−15.78%	9812.63	0.91	−19.03%	9657.49	0.97	−20.31%
Golden_7	15998.37	14250.60	0.22	−10.92%	13333.32	0.44	−16.66%	12568.18	0.75	−21.44%	12115.77	0.96	−24.27%
Golden_8	18831.50	16971.04	0.08	−9.88%	15499.76	0.32	−17.69%	14579.05	0.69	−22.58%	14314.21	0.93	−23.99%
Li_21	24826.35	22865.97	0.19	−7.90%	21736.92	0.47	−12.44%	20683.79	0.85	−16.69%	20724.91	0.97	−16.52%
Li_22	23985.19	21542.09	0.02	−10.19%	20772.52	0.11	−13.39%	19038.31	0.49	−20.62%	20424.35	0.78	−14.85%
Li_23	27986.58	25514.42	0.24	−8.83%	24106.71	0.59	−13.86%	23381.52	0.90	−16.45%	23126.42	0.99	−17.37%
Li_24	30327.41	29102.20	0.11	−4.04%	26439.78	0.87	−12.82%	26200.40	0.93	−13.61%	26121.15	1.00	−13.87%
Li_25	27426.64	26020.12	0.00	−5.13%	24084.62	0.06	−12.19%	24501.08	0.32	−10.67%	N/A	N/A	N/A
Li_26	34534.97	29439.93	0.75	−14.75%	29316.25	0.80	−15.11%	28893.00	0.96	−16.34%	29010.87	0.99	−16.00%
Li_27	28341.25	27203.26	0.00	−4.02%	25756.63	0.04	−9.12%	26592.44	0.23	−6.17%	N/A	N/A	N/A
Li_28	35986.88	33494.04	0.76	−6.93%	32982.25	0.76	−8.35%	31505.10	0.98	−12.45%	31559.27	1.00	−12.30%
Li_29	38188.93	36379.32	0.92	−4.74%	35586.57	0.71	−6.81%	33713.97	0.99	−11.72%	34091.61	1.00	−10.73%
Li_30	44088.03	42149.09	0.31	−4.40%	40709.81	0.90	−7.66%	40839.56	1.00	−7.37%	40826.65	1.00	−7.40%
Li_31	47195.81	45952.96	0.45	−2.63%	44212.40	0.88	−6.32%	44151.37	0.99	−6.45%	44985.68	1.00	−4.68%
Li_32	50720.75	48539.65	0.16	−4.30%	46575.65	1.00	−8.17%	46595.38	0.99	−8.13%	46018.94	1.00	−9.27%
Averages			0.47	−5.60%		0.66	−9.49%		0.83	−11.44%		0.96	−11.67%

One should notice that, in most cases, using a safety stock during the design stage might be a good strategy to reduce the impact of route failures whenever travel times are higher than expected. This concept is further discussed in the next section. Also, note that for a safety stock level of 35% (or higher), there are some instances that cannot be solved during the design stage; i.e., assuming such a high safety stock level, some customers in instances *Li_25* and *Li_27* cannot be reached from the depot in the reduced 'standard' time of the batteries (i.e., without considering the extra time that can be provided by the energy safety stock). That justifies that we focus on safety stock levels between 0% and 35% of the original battery capacity.

6. Analysis of results

For each considered safety stock level, $s \in \{0\%, 5\%, 10\%, \ldots, 35\%\}$, Figure 5 uses boxplots to illustrate the distribution of the reliability indices associated with the best-found stochastic solutions for each instance.

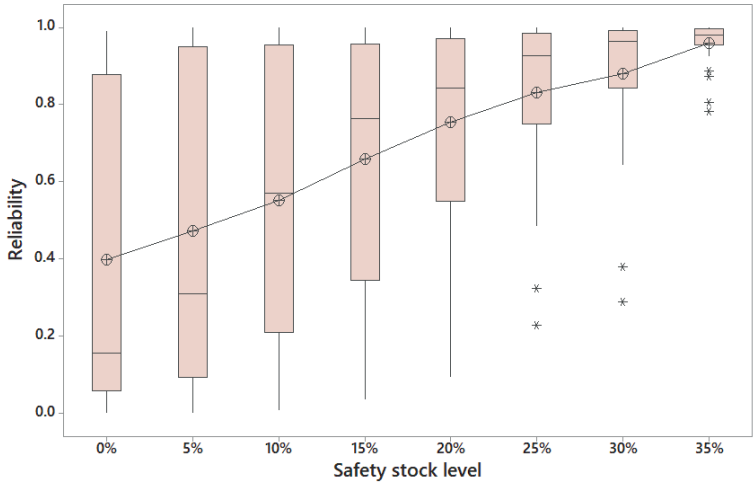

Figure 5: *Reliability values for different safety stock levels.*

Notice that the higher the safety stock level, the higher the average reliability index is. Moreover, increasing the safety stock level also contributes to reduce the variability in these reliability indices – i.e., increasing the safety stock has the expected effect of reducing the number of route failures, which in turn reduces the extra costs generated by corrective actions. Of course, increasing the safety stock level makes the solution more 'robust' against uncertainty (thus reducing the cost due to corrective actions), but it also requires the use of additional routes in the solution, which raises the cost (total time employed) of the final distribution plan. Therefore, this trade-off must be taken into account when finding the right level of safety stock for each individual instance.

Finally, Figure 6 shows the expected travel times, across all instances, for each safety stock level. The most relevant observation here, is that the expected cost (total travel time) can be reduced, on average, by using safety stock levels between 20% and 25% of the original capacity. Of course, the specific safety stock level to use will depend upon the actual instance as well as on the probability distribution employed to model the travel times. Still, the point here is that the use of safety stocks can contribute to reduce the total expected cost of the distribution plan by making this plan less sensitive to the risk of route failures.

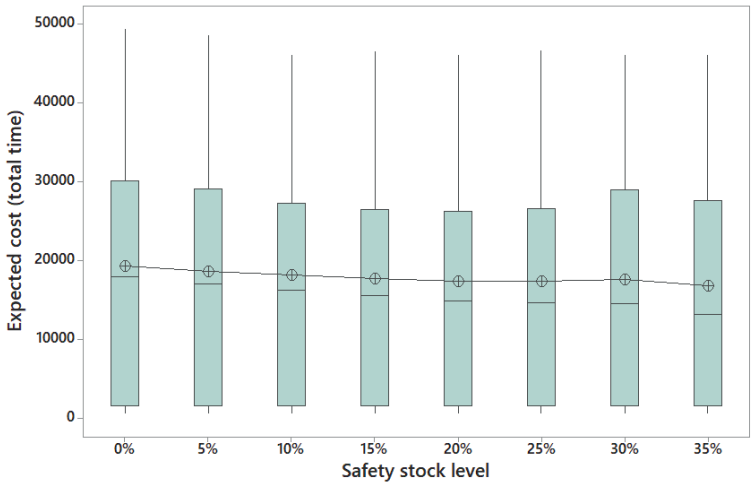

Figure 6: *Expected travel times for different safety stock levels.*

7. Conclusions and future research

The transportation sector is one of the most pollutant ones in modern societies. As a consequence, a number of government regulations have been set to promote the use of electric vehicles in order to reduce the air pollution. However, the current infrastructure of cities makes it difficult to fully develop green logistics and transportation practices. For instance, the use of electric vehicles for freight distribution has to deal with multiple obstacles, such as scattered network configuration and the technical limitations of those vehicles. So far, only a reduced number of works have studied the electric vehicle routing problem with stochastic travel times. Aiming at reducing this gap in the literature, the paper analyses the aforementioned problem considering also driving-range limitations, which might cause route failures when the vehicle runs out of battery.

Our methodology combines Monte Carlo simulation with a multi-start framework, which also integrates a biased-randomized constructive heuristic. Our simheuristic algorithm also makes use of safety stocks during the routing design stage, thus decreasing

the risk of suffering route failures. In other words, we focus on constructing reliable solutions with a low risk of requesting corrective actions. Our results prove that using deterministic solutions in stochastic scenarios might lead to sub-optimal distribution plans that can be easily improved by using a simulation-optimization technique such as the one proposed here. They also illustrate how the use of the suitable energy safety stock levels during the routing design stage can increase the reliability of the distribution plans, thus reducing the total expected costs.

Some future lines can extend this work. In particular, we are interested in: (i) analysing the effect of preventive strategies – such as the ones already described in this paper – on the expected cost of the considered instances; (ii) extending our methodology (e.g., by hybridizing it with Petri nets) so it can also take into account possible correlations among travel times associated with different edges; (iii) extending our results to the heterogeneous fleet scenario, where vehicles might have different driving ranges and batteries; and (iv) including different sustainability dimensions related to environmental and social costs of these distribution activities, specially in the context of smart cities.

Acknowledgments

This work has been partially supported by the Spanish Ministry of Economy and Competitiveness (TRA2015-71883-REDT), and the Ibero-American Program for Science and Technology for Development (CYTED2014-515RT0489). Moreover, we appreciate the financial support of the Erasmus+ Program (2018-1-ES01-KA103-049767) as well as the support of the UPNA doctoral program.

References

Alvarez Fernandez, S., Ferone, D., Juan, A.A., Silva, D.G. and de Armas, J. (2018). A 2-stage biased-randomized iterated local search for the uncapacitated single allocation p-hub median problem. *Transactions on Emerging Telecommunications Technologies*, 29, e3418.

Bektaş, T. and Laporte, G. (2011). The pollution-routing problem. *Transportation Research Part B: Methodological*, 45, 1232–50.

Bianchi, L., Dorigo, M., Gambardella, L.M. and Gutjahr, W.J. (2009). A survey on metaheuristics for stochastic combinatorial optimization. *Natural Computing*, 8, 239–87.

Bibri, S.E. and Krogstie, J. (2017). Smart sustainable cities of the future: An extensive interdisciplinary literature review. *Sustainable Cities and Society*, 31, 183–212.

Bozorgi, A.M., Farasat, M. and Mahmoud. (2017). A. A time and energy efficient routing algorithm for electric vehicles based on historical driving data. *IEEE Transactions on Intelligent Vehicles*, 2, 308–20.

Bozorgi-Amiri, A., Jabalameli, M. and Al-e Hashem, S.M. (2013). A multi-objective robust stochastic programming model for disaster relief logistics under uncertainty. *OR spectrum*, 35, 905–33.

Cáceres-Cruz, J., Arias, P., Guimarans, D., Riera, D. and Juan, A.A. (2014). Rich vehicle routing problem: A survey. *ACM Computing Surveys*, 47, 1-28.

Christofides, N. (1976). The vehicle routing problem. *Revue française d'automatique, informatique, recherche opérationnelle. Recherche opérationnelle*, 10, 55–70.

Clarke, G. and Wright, J.W. (1964). Scheduling of vehicles from a central depot to a number of delivery points. *Operations Research*, 12, 568–81.

De Armas, J., Juan, A.A., Marquès, J.M. and Pedroso, J.P. (2017). Solving the deterministic and stochastic uncapacitated facility location problem: from a heuristic to a simheuristic. *Journal of the Operational Research Society*, 68, 161–76.

Demir, E., Bektaş, T. and Laporte, G. (2012). An adaptive large neighborhood search heuristic for the pollution-routing problem. *European Journal of Operational Research*, 223, 346–59.

Desaulniers, G., Errico, F., Irnich, S. and Schneider, M. (2016). Exact algorithms for electric vehicle-routing problems with time windows. *Operations Research*, 64, 1388–1405.

Dominguez, O., Guimarans, D., Juan, A.A. and de la Nuez, I. (2016a). A biased-randomised large neighbourhood search for the two-dimensional vehicle routing problem with backhauls. *European Journal of Operational Research*, 255, 442–62.

Dominguez, O., Juan, A.A., Barrios, B., Faulin, J. and Agustin, A. (2016b). Using biased randomization for solving the two-dimensional loading vehicle routing problem with heterogeneous fleet. *Annals of Operations Research*, 236, 383–404.

Dominguez, O., Juan, A.A. and Faulin, J. (2014). A biased-randomized algorithm for the two-dimensional vehicle routing problem with and without item rotations. *International Transactions in Operational Research*, 21, 375–98.

Dominguez, O., Juan, A.A., de la Nuez Pestana, I.A. and Ouelhadj, D. (2016c). An ils-biased randomization algorithm for the two-dimensional loading hfvrp with sequential loading and items rotation. Journal of the Operational Research Society, 67, 37–53.

Erdoğan, S. and Miller-Hooks, E. (2012). A green vehicle routing problem. *Transportation Research Part E: Logistics and Transportation Review*, 48, 100–14.

Eshtehadi, R., Fathian, M. and Demir, E. (2017). Robust solutions to the pollution-routing problem with demand and travel time uncertainty. *Transportation Research Part D: Transport and Environment*, 51, 351–63.

Eurostat. Energy, transport and environment indicators (2016). Available at: http://ec.europa.eu (accessed August, 2018).

Faulin, J., Gilibert, M., Juan, A.A., Vilajosana, X. and Ruiz, R. (2008). Sr-1: A simulation-based algorithm for the capacitated vehicle routing problem. In: *Simulation Conference, 2008. WSC 2008. Winter. IEEE*, 2708–16.

Faulin, J. and Juan, A.A. (2008). The algacea-1 method for the capacitated vehicle routing problem. *International Transactions in Operational Research*, 15, 599–621.

Felipe, A., Ortuño, M.T., Righini, G. and Tirado, G. (2014). A heuristic approach for the green vehicle routing problem with multiple technologies and partial recharges. *Transportation Research Part E: Logistics and Transportation Review*, 71, 111–28.

Ferone, D., Gruler, A., Festa, P. and Juan, A.A. (2018). Enhancing and extending the classical GRASP framework with biased randomization and simulation. *Journal of the Operational Research Society*.

Gendreau, M., Ghiani, G. and Guerriero, E. (2015). Time-dependent routing problems: A review. *Computers & Operations Research*, 64, 189–97.

Golden, B.L., Wasil, E.A., Kelly, J.P. and Chao, I.M. (1998). The impact of metaheuristics on solving the vehicle routing problem: algorithms, problem sets, and computational results. In: *Fleet management and logistics*. Springer, 33–56.

Gonzalez-Neira, E.M., Ferone, D., Hatami, S. and Juan, A.A. (2017). A biased-randomized simheuristic for the distributed assembly permutation flowshop problem with stochastic process-ing times. *Simulation Modelling Practice and Theory*, 79(Supplement C), 23–36.

Grasas, A., Juan, A.A., Faulin, J., de Armas, J. and Ramalhinho, H. (2017). Biased randomization of heuristics using skewed probability distributions: a survey and some applications. *Computers & Industrial Engineering*, 110, 216–28.

Grasas, A., Juan, A.A. and Lourenço, HR. (2016). SimILS: a simulation-based extension of the iterated local search metaheuristic for stochastic combinatorial optimization. *Journal of Simulation*, 10, 69–77.

Hiermann, G., Puchinger, J., Ropke, S. and Hartl, R.F. (2016). The electric fleet size and mix vehicle routing problem with time windows and recharging stations. *European Journal of Operational Research*, 252, 995–1018.

Hof, J., Schneider, M. and Goeke, D. (2017). Solving the battery swap station location-routing problem with capacitated electric vehicles using an AVNS algorithm for vehicle-routing problems with intermediate stops. *Transportation Research Part B*, 97, 102–12.

Juan, A.A., Faulin, J., Grasman, S., Riera, D., Marull, J. and Mendez, C. (2011a). Using safety stocks and simulation to solve the vehicle routing problem with stochastic demands. *Transportation Research Part C: Emerging Technologies*, 19, 751–65.

Juan, A.A., Faulin, J., Jorba, J., Caceres, J. and Marquès, J.M. (2013). Using parallel & distributed computing for real-time solving of vehicle routing problems with stochastic demands. *Annals of Operations Research*, 207, 43–65.

Juan, A.A., Faulin, J., Jorba, J., Riera, D., Masip, D. and Barrios, B. (2011b). On the use of monte carlo simulation, cache and splitting techniques to improve the clarke and wright savings heuristics. *Journal of the Operational Research Society*, 62, 1085–97.

Juan, A.A., Faulin, J., Pérez-Bernabeu, E. and Jozefowiez, N. (2014a). Horizontal cooperation in vehicle routing problems with backhauling and environmental criteria. *Procedia - Social and Behavioral Sciences*, 111, 1133–41.

Juan, A.A., Goentzel, J. and Bektaş, T. (2014b). Routing fleets with multiple driving ranges: Is it possible to use greener fleet configurations? *Applied Soft Computing Journal*, 21, 84–94.

Juan, A.A., Lourenço, H.R., Mateo, M., Luo, R. and Castella, Q. (2014c). Using iterated local search for solving the flow-shop problem: Parallelization, parametrization, and randomization issues. *International Transactions in Operational Research*, 21, 103–26.

Juan, A.A., Mendez, C.A., Faulin, J., De Armas, J. and Grasman, S.E. (2016). Electric vehicles in logistics and transportation: A survey on emerging environmental, strategic, and operational challenges. *Energies*, 9, 1–21.

Juan, A.A., Pascual, I., Guimarans, D. and Barrios, B. (2015). Combining biased randomization with iterated local search for solving the multidepot vehicle routing problem. *International Transactions in Operational Research*, 22, 647–67.

Koç, C. and Karaoglan, I. (2016). The green vehicle routing problem: A heuristic based exact solution approach. *Applied Soft Computing Journal*, 39, 154–64.

Li, F., Golden, B. and Wasil, E. (2005). Very large-scale vehicle routing: New test problems, algorithms, and results. *Computers and Operations Research*, 32, 1165–79.

Lin, C., Choy, K.L., Ho, G.T.S., Chung, S.H. and Lam, H.Y. (2014). Survey of green vehicle routing problem: past and future trends. *Expert Systems with Applications*, 41(4 part 1), 1118–38.

McKinnon, A., Cullinane, S., Browne, M. and Whiteing, A. (2015). Green Logistics: Improving the Environmental Sustaintability of Logistics. 2nd ed. London: Kogan Page. ISBN: 978-0-7494-6625-1.

Pérez-Bernabeu, E., Juan, A.A., Faulin, J. and Barrios, B.B. (2015). Horizontal cooperation in road transportation: a case illustrating savings in distances and greenhouse gas emissions. *International Transactions in Operational Research*, 22, 585–606.

Ritzinger, U., Puchinger, J. and Hartl, R.F. (2015). A survey on dynamic and stochastic vehicle routing problems. *International Journal of Production Research*, 7543, 1–17.

Sawik, B., Faulin, J. and Pérez-Bernabeu, E. (2017a). A multicriteria analysis for the green VRP: a case discussion for the distribution problem of a Spanish retailer. *Transportation Research Procedia*, 22, 305–13.

Sawik, B., Faulin, J. and Pérez-Bernabeu, E. (2017b). Multi-criteria optimization for fleet size with environmental aspects. *Transportation Research Procedia*, 27, 61–8.

Sawik, B., Faulin, J. and Pérez-Bernabeu, E. (2017c). Selected multi criteria green vehicle routing problems. In: *Applications of Management Science*, 57–83.

Schneider, M., Stenger, A. and Goeke, D. (2014). The electric vehicle-routing problem with time windows and recharging stations. *Transportation Science*, 48, 500–20.

Schneider, M., Stenger, A. and Hof, J. (2015). An adaptive VNS algorithm for vehicle routing problems with intermediate stops. *OR Spectrum*, 37, 353–87.

Serrano-Hernández, A., Juan, A.A., Faulin, J. and Perez-Bernabeu, E. (2017). Horizontal collaboration in freight transport: Concepts, benefits, and environmental challenges. *Statistics and Operations Research Transactions*, 41, 1–22.

Shao, S., Guan, W. and Bi. J. (2018). Electric vehicle-routing problem with charging demands and energy consumption. *The Institute of Engineering and Technology*, 12, 202–12.

The World Bank. (2018). Connecting to compete: trade logistics in the global economy. Technical Report; World Bank; Washington, DC. Available at: https://elibrary.worldbank.org/doi/abs/10.1596/29971 (accessed: August 2018).

Toth, P. and Vigo, D. (2014). Vehicle routing: problems, methods, and applications. *SIAM*.

Uchoa, E., Pecin, D., Pessoa, A., Poggi, M., Vidal, T. and Subramanian, A. (2017). New benchmark instances for the capacitated vehicle routing problem. *European Journal of Operational Research*, 257, 845–58.

SORT 43 (1) January-June 2019, 25-50 DOI: 10.2436/20.8080.02.78

New L^2-type exponentiality tests

Marija Cuparić[1], Bojana Milošević[2] and Marko Obradović[3]

Abstract

We introduce new consistent and scale-free goodness-of-fit tests for the exponential distribution based on the Puri-Rubin characterization. For the construction of test statistics we employ weighted L^2 distance between V-empirical Laplace transforms of random variables that appear in the characterization. We derive the asymptotic behaviour under the null hypothesis as well as under fixed alternatives. We compare our tests, in terms of the Bahadur efficiency, to the likelihood ratio test, as well as some recent characterization based goodness-of-fit tests for the exponential distribution. We also compare the power of our tests to the power of some recent and classical exponentiality tests. According to both criteria, our tests are shown to be strong and outperform most of their competitors.

MSC: 62G10, 62G20.

Keywords: Goodness-of-fit, exponential distribution, Laplace transform, Bahadur efficiency, V-statistics with estimated parameters.

1. Introduction

The exponential distribution is one of the most widely studied distributions in theoretical and applied statistics, and many models assume exponentiality of the data. For this reason, a great variety of goodness-of-fit tests, for the case of the exponential distribution, have been proposed in the literature.

The classical approach is to use the time-honoured goodness-of-fit tests based on an empirical distribution function, such as Kolmogorov-Smirnov, Cramer-von Mises, Anderson-Darling, applied to the case of the exponential distributions. The alternative approach is to use tests specifically designed for testing exponentiality. These test statistics are mainly based on empirical counterparts of certain special properties of the exponential distribution. Some of the tests employ properties related to different integral transforms such as: characteristic functions (see e.g. Henze, 1992, Henze and Meintanis, 2002b, Henze and Meintanis, 2005); Laplace transforms (see e.g. Henze

[1] Faculty of Mathematics, University of Belgrade, marijar@matf.bg.ac.rs

[2] Faculty of Mathematics, University of Belgrade, bojana@matf.bg.ac.rs (Corresponding author)

[3] Faculty of Mathematics, University of Belgrade, marcone@matf.bg.ac.rs

Received: September 2018
Accepted: November 2018

and Meintanis, 2002a, Klar, 2003, Meintanis, Nikitin and Tchirina, 2007); and other integral transforms (see e.g. Klar, 2005, Meintanis, 2008). Other tests exploit properties such as maximal correlations (see Grané and Fortiana, 2009, Grané and Fortiana, 2011, Strzalkowska-Kominiak and Grané, 2017), entropy (see Alizadeh Noughabi and Arghami, 2011), etc.

Among the various properties, those that characterize the distribution stand out. The simple form of the exponential distribution give rise to many equidistribution type characterizations. The equality in distribution can be expressed in many ways (equality of distribution functions, densities, integral transforms, etc.), and hence is suitable for building different types of test statistics. Such tests have become very popular in recent times, as they are proven to be rather efficient. Tests that use U-empirical and V-empirical distribution functions, of integral-type (integrated difference) and supremum-type, can be found in Nikitin and Volkova (2010), Volkova (2015), Jovanović et al.(2015), Milošević and Obradović (2016b), Milošević (2016), Nikitin and Volkova (2016). A class of weighted integral-type tests that uses U-empirical Laplace transforms is presented in Milošević and Obradović (2016a).

Motivated by the power and efficiency of those tests, we create a similar test based on an equidistribution characterization. The test statistics, measuring the distance between two V-empirical Laplace transforms of the random variables that appear in the characterization, are, for the first time, of weighted L^2-type. This guarantees the consistency of the test against all alternatives.

The paper is organized as follows. In Section 2 we introduce the test statistics and derive their asymptotic properties, both under the null and the alternative hypotheses. In Section 3 we calculate the approximate Bahadur slope of our tests, for different close alternatives, and inspect the impact of the tuning parameter to the efficiencies of the test. We also compare the proposed tests to their recent competitors via approximate local relative Bahadur efficiency. In Section 4 we conduct a power study. We obtain empirical powers of the tests, against different common alternatives, and compare them to some recent and classical exponentiality tests. We also apply an algorithm for data driven selection of the tuning parameter and obtain the corresponding powers in the small sample case. Real data applications are presented in Section 5, while the proofs, the datasets, and the code can be found in the appendices.

2. Test statistic

Consider the following characterization by Puri and Rubin (1970).

Characterization 2.1. *Let X_1 and X_2 be two independent copies of a random variable X with pdf $f(x)$. Then X and $|X_1 - X_2|$ have the same distribution, if and only if for some $\lambda > 0$, $f(x) = \lambda e^{-\lambda x}$, for $x \geq 0$.*

Let $X_1, X_2, \ldots, X_n$ be independent and identically distributed (i.i.d.) non-negative random variables with an unknown absolutely continuous distribution function F. We consider the transformed sample $Y_i = \widehat{\lambda}_n X_i$, $i = 1, 2.., n.$, where $\widehat{\lambda}_n$ is the reciprocal sample mean. For testing the null hypothesis $H_0 : F(x) = 1 - e^{-\lambda x}$, $\lambda > 0$, in view of the characterization 2.1, we propose the following family of test statistics, depending on the tuning parameter $a > 0$:

$$M_{n,a}(\widehat{\lambda}_n) = \int_0^\infty \left(L_n^{(1)}(t) - L_n^{(2)}(t) \right)^2 e^{-at} dt, \tag{1}$$

where

$$L_n^{(1)}(t) = \frac{1}{n} \sum_{i_1=1}^{n} e^{-tY_{i_1}}$$

$$L_n^{(2)}(t) = \frac{1}{n^2} \sum_{i_1,i_2=1}^{n} e^{-t|Y_{i_1} - Y_{i_2}|}$$

are V-empirical Laplace transforms of Y_1 and $|Y_1 - Y_2|$ respectively.

In order to explore the asymptotic properties we rewrite (1) as

$$\begin{aligned} M_{n,a}(\widehat{\lambda}_n) &= \int_0^\infty \left(\frac{1}{n} \sum_{i_1=1}^{n} e^{-tX_{i_1}\widehat{\lambda}_n} - \frac{1}{n^2} \sum_{i_1,i_2=1}^{n} e^{-t|X_{i_1} - X_{i_2}|\widehat{\lambda}_n} \right)^2 e^{-at} dt \\ &= \frac{1}{n^4} \int_0^\infty \sum_{i_1,i_2,i_3,i_4} \left(e^{-tX_{i_1}\widehat{\lambda}_n} - e^{-t|X_{i_1} - X_{i_2}|\widehat{\lambda}_n} \right) \left(e^{-tX_{i_3}\widehat{\lambda}_n} - e^{-t|X_{i_3} - X_{i_4}|\widehat{\lambda}_n} \right) e^{-at} dt \\ &= \frac{1}{n^4} \sum_{i_1,i_2,i_3,i_4} \int_0^\infty g(X_{i_1}, X_{i_2}, t; \widehat{\lambda}_n) g(X_{i_3}, X_{i_4}, t; \widehat{\lambda}_n) e^{-at} dt \\ &= \frac{1}{n^4} \sum_{i_1,i_2,i_3,i_4} h(X_{i_1}, X_{i_2}, X_{i_3}, X_{i_4}, a; \widehat{\lambda}_n), \end{aligned}$$

where $\widehat{\lambda}_n = \overline{X}_n^{-1}$ is a consistent estimator of λ and

$$h(X_1, X_2, X_3, X_4, a; \widehat{\lambda}_n) = \frac{1}{4!} \sum_{\pi(4)} \int_0^\infty g(X_{i_1}, X_{i_2}, t; \widehat{\lambda}_n) g(X_{i_3}, X_{i_4}, t; \widehat{\lambda}_n) e^{-at} dt,$$

with $\pi(4)$ being the set of all 4! permutations of the numbers $1, 2, 3, 4$.

Let us first focus on $M_{n,a}(\lambda)$, for a fixed $\lambda > 0$. Notice that $M_{n,a}(\lambda)$ is a V-statistic with kernel h. Moreover, under the null hypothesis, its distribution does not depend on λ, so we may assume $\lambda = 1$. It is easy to show that its first projection on a basic observation is equal to zero. After some calculations, one can obtain its second projection given by

$$\begin{aligned}\widetilde{h}_2(x,y,a) &= E(h(X_1,X_2,X_3,X_4,a)|X_1 = x, X_2 = y)\\ &= -\frac{1}{2} + \frac{1}{3}(e^{-x}+e^{-y}) + \frac{1}{6}e^{a-x-y}\mathrm{Ei}(-a)\Big(a(e^x-2)(e^y-2) - e^x - e^y + 4\Big)\\ &+ \frac{1}{6}e^{-a-x-y}\Big(\mathrm{Ei}(a)(4a+e^x+e^y-4) - (\mathrm{Ei}(a+x)(4(a+x-1)+e^y)\\ &+ \mathrm{Ei}(a+y)(4(a+y-1)+e^x) - 4(a+x+y-1)\mathrm{Ei}(a+x+y))\Big) + \frac{1}{6(a+x+y)},\end{aligned}$$

where $\mathrm{Ei}(x) = -\int_{-x}^{\infty}\frac{e^{-t}}{t}dt$ is the exponential integral. The function $\widetilde{h}_2$ is non-constant for any $a > 0$. Hence, kernel h is degenerate with degree 2.

Since kernel h is bounded and degenerate, from the theorem for the asymptotic distribution of U-statistics with degenerate kernels (Korolyuk and Borovskikh, 1994, Corollary 4.4.2), and the Hoeffding representation of V-statistics, we get that, $M_{n,a}(1)$, being a V-statistic of degree 2, has the following asymptotic distribution

$$nM_{n,a}(1) \xrightarrow{d} 6\sum_{k=1}^{\infty}\delta_k W_k^2, \tag{2}$$

where $\{\delta_k\}$ are the eigenvalues of the integral operator $\mathcal{M}_a$ defined by

$$\mathcal{M}_a q(x) = \int_0^{+\infty}\widetilde{h}_2(x,y,a)q(y)dF(y), \tag{3}$$

and $\{W_k\}$ is the sequence of i.i.d. standard Gaussian random variables.

Our statistic $M_{n,a}(\widehat{\lambda}_n)$ can be rewritten as

$$\begin{aligned}M_{n,a}(\widehat{\lambda}_n) &= \int_0^{\infty}\left(\frac{1}{n^2}\sum_{i_1,i_2=1}^{n} g(X_{i_1},X_{i_2},t,a;\widehat{\lambda}_n)\right)^2 e^{-at}dt\\ &= \int_0^{\infty} V_n(\widehat{\lambda}_n)^2 e^{-at}dt.\end{aligned}$$

Here $V_n(\widehat{\lambda}_n)$ is a V-statistic of order 2 with an estimated parameter, and kernel $g(X_{i_1},X_{i_2},t,a;\widehat{\lambda}_n)$.

Since the function $g(x_1,x_2,t,a;\gamma)$ is continuously differentiable with respect to γ at the point $\gamma=\lambda$, the mean-value theorem gives

$$V_n(\widehat{\lambda}_n) = V_n(\lambda) + (\widehat{\lambda}_n - \lambda)\frac{\partial V_n(\gamma)}{\partial \gamma}|_{\gamma=\lambda^*},$$

for some λ^* between λ and $\widehat{\lambda}_n$.

From the Law of large numbers for V-statistics (Serfling, 2009, 6.4.2.), the partial derivative $\frac{\partial V_n(\gamma)}{\partial \gamma}$ converges to

$$E\left(t|X_1 - X_2|e^{-t|X_1-X_2|\gamma} - tX_1e^{-tX_1\gamma}\right) = 0.$$

Since $\sqrt{n}(\widehat{\lambda}_n - \lambda)$ is stochastically bounded, it follows that statistics $\sqrt{n}V_n(\widehat{\lambda}_n)$ and $\sqrt{n}V_n(1)$ are asymptotically equally distributed. Therefore, $nM_{n,a}(\widehat{\lambda}_n)$ and $nM_{n,a}(1)$ will have the same limiting distribution. We summarize this in the following theorem.

Theorem 2.2. *Let $X_1,\ldots,X_n$ be an i.i.d. sample with distribution function $F(x) = 1 - e^{-\lambda x}$ for some $\lambda > 0$. Then*

$$nM_{n,a}(\widehat{\lambda}_n) \xrightarrow{d} 6\sum_{k=1}^{\infty}\delta_k W_k^2, \tag{4}$$

where $\{\delta_k\}$ are the eigenvalues of the integral operator $\mathcal{M}_a$ defined in (3)*, and $\{W_k\}$ is the sequence of i.i.d standard Gaussian random variables.*

2.1. Limiting distribution under fixed alternative

Now we consider the asymptotic behaviour of our statistics $M_{n,a}$ under a fixed alternative with finite expectation μ. Here, it is also easy to show that the first projection of kernel h,

$$h_1(s,a) = E(h(X_1,X_2,X_3,X_4,a;\mu)|X_1 = s)$$

is a non-constant function, hence the kernel is non-degenerate. Therefore, the limiting distribution will differ from the null case. We present this in Theorem 2.3, where, for brevity, we introduce the following notation: $\boldsymbol{x} = (x_1,x_2,x_3,x_4)$; $\boldsymbol{G}(\boldsymbol{x}) = \prod_{i=1}^4 G(x_i)$; $h'(\boldsymbol{x},a;\mu) = \frac{\partial h(\boldsymbol{x},a;\gamma)}{\partial \gamma}\Big|_{\gamma=\mu}$.

Theorem 2.3. *Let $X_1,\ldots,X_n$ be an i.i.d. sample from an alternative distribution with distribution function G. Then*

$$\sqrt{n}(M_{n,a}(\widehat{\mu}) - \Delta) \xrightarrow{d} \mathcal{N}(0,\Sigma),$$

where $\widehat{\mu} = \overline{X}_n$, $\Delta = E(M_{n,a}(\mu))$, *and*

$$\Sigma = 16Var\left(h_1(X_1,a)\right) + \left(\int\limits_{(R^+)^4} h'(\boldsymbol{x},a;\mu)d\boldsymbol{G}(\boldsymbol{x})\right)^2 Var(X_1) + 8\Bigg(\int\limits_{(R^+)^4} x_1 h(\boldsymbol{x},a;\mu)d\boldsymbol{G}(\boldsymbol{x}) - \int\limits_{R^+} x_1 dG(x_1) \int\limits_{(R^+)^4} h(\boldsymbol{x},a;\mu)d\boldsymbol{G}(\boldsymbol{x})\Bigg). \tag{5}$$

Proof. See Appendix A. ∎

3. Local approximate Bahadur efficiency

One way to compare tests is to calculate their relative Bahadur efficiency. We briefly present it here. For more details we refer to Bahadur (1971) and Nikitin (1995).

For two tests with the same null and alternative hypotheses, $H_0 : \theta \in \Theta_0$ and $H_1 : \theta \in \Theta_1$, the asymptotic relative Bahadur efficiency is defined as the ratio of sample sizes needed to reach the same test power, when the level of significance approaches zero. For two sequences of test statistics, it can be expressed as the ratio of Bahadur exact slopes, functions proportional to the exponential rates of the decrease of their sizes, for the increasing number of observations and a fixed alternative. The calculation of these slopes depends on large deviation functions which are often hard to obtain. For this reason, in many situations, the tests are compared using the approximate Bahadur efficiency, which is shown to be a good approximation in the local case (when $\theta \to \partial\Theta_0$).

Suppose that $T_n = T_n(X_1,\ldots,X_n)$ is a test statistic with its large values being significant. Let the limiting distribution function of T_n, under H_0, be F_T, whose tail behaviour is given by $\log(1-F_T(t)) = -\frac{a_T t^2}{2}(1+o(1))$, where a_T is a positive real number, and $o(1) \to 0$ as $t \to \infty$. Suppose also that the limit in probability $\lim_{n\to\infty} T_n/\sqrt{n} = b_T(\theta) > 0$ exists for $\theta \in \Theta_1$. Then the relative approximate Bahadur efficiency of T_n, with respect to another test statistic V_n (whose large values are significant), is

$$e^*_{T,V} = \frac{c^*_T(\theta)}{c^*_V(\theta)},$$

where $c^*_T(\theta) = a_T b^2_T(\theta)$ i $c^*_V(\theta) = a_V b^2_V(\theta)$ are approximate Bahadur slopes of T_n and V_n, respectively.

We may suppose, without loss of generality, that $\Theta_0 = \{0\}$. Consequently, the approximate local relative Bahadur efficiency is given by

$$e^*_{T,V} = \lim_{\theta\to 0} e^*_{T,V}(\theta).$$

Let $\mathcal{G} = \{G(x,\theta),\ \theta > 0\}$ be a family of alternative distribution functions with finite expectations, such that $G(x,\theta) = 1 - e^{-\lambda x}$, for some $\lambda > 0$, if and only if $\theta = 0$, and the regularity conditions for V-statistics with weakly degenerate kernels from (Nikitin and Peaucelle, 2004, Assumptions WD) are satisfied.

The logarithmic tail behaviour of the limiting distribution of $M_{n,a}(\widehat{\lambda}_n)$, under the null hypothesis, is derived in the following lemma.

Lemma 3.1. *For the statistic $M_{n,a}(\widehat{\lambda}_n)$ and a given alternative density $g(x,\theta)$ from $\mathcal{G}$, the Bahadur approximate slope satisfies the relation $c_M(\theta) \sim \frac{b_M(\theta)}{6\delta_1}$, where $b_M(\theta)$ is the limit in P_θ probability of $M_{n,a}(\widehat{\lambda}_n)$, and δ_1 is the largest eigenvalue of the sequence $\{\delta_k\}$ from* (2).

Proof. See Appendix A.

The limit in probability of our test statistic, under a close alternative, can be derived using the following lemma.

Lemma 3.2. *For a given alternative density $g(x;\theta)$ whose distribution belongs to $\mathcal{G}$, we have that the limit in probability of the statistic $M_{n,a}(\widehat{\lambda}_n)$ is*

$$b_M(\theta) = 6 \int_0^\infty \int_0^\infty \widetilde{h}_2(x,y) f(x) f(y) dx dy \cdot \theta^2 + o(\theta^2), \theta \to 0,$$

where $f(x) = \frac{\partial}{\partial\theta} g(x;\theta)|_{\theta=0}$.

Proof. See Appendix A.

To calculate the efficiency one needs to find δ_1, the largest eigenvalue. Since we can not obtain it analytically, we use the following approximation, introduced in Božin et al. (2018).

It can be shown that δ_1 is the limit of the sequence of the largest eigenvalues of linear operators defined by $(m+1)\times(m+1)$ matrices $M^{(m)} = ||m_{i,j}^{(m)}||$, $0 \le i \le m, 0 \le j \le m$, where

$$m_{i,j}^{(m)} = \widetilde{h}_2\left(\frac{Bi}{m}, \frac{Bj}{m}\right) \sqrt{e^{\frac{B(i)}{m}} - e^{\frac{B(i+1)}{m}}} \cdot \sqrt{e^{\frac{B(j)}{m}} - e^{\frac{B(j+1)}{m}}} \cdot \frac{1}{1-e^{-B}}, \tag{6}$$

when m tends to infinity and $F(B)$ approaches 1.

In Table 1, we present the largest eigenvalues for a =0.5, 1, 2 and 5, obtained using (6) with $m = 4500$ and $B = 10$.

Table 1: *Approximate eigenvalues of* $\mathcal{M}_a$.

a	0.5	1	2	5
δ_1	$1.32 \cdot 10^{-2}$	$5.32 \cdot 10^{-3}$	$1.73 \cdot 10^{-3}$	$2.80 \cdot 10^{-4}$

3.1. Efficiencies with respect to likelihood ratio tests

Lacking a theoretical upper bound, the approximate Bahadur slopes are often compared (see e.g. Meintanis et al., 2007) to the approximate Bahadur slopes of the likelihood ratio tests (LRT), which are known to be optimal parametric tests in terms of Bahadur efficiency. Hence, we may consider the approximate relative Bahadur efficiencies against the LRT as a sort of "absolute" local approximate Bahadur efficiencies. We calculate it for the following alternatives:

- a Weibull distribution with density

$$g(x,\theta) = e^{-x^{1+\theta}}(1+\theta)x^{\theta}, \theta > 0, x \geq 0; \tag{7}$$

- a Gamma distribution with density

$$g(x,\theta) = \frac{x^{\theta}e^{-x}}{\Gamma(\theta+1)}, \theta > 0, x \geq 0; \tag{8}$$

- a Linear failure rate (LFR) distribution with density

$$g(x,\theta) = e^{-x-\theta\frac{x^2}{2}}(1+\theta x), \theta > 0, x \geq 0; \tag{9}$$

- a mixture of exponential distributions with negative weights (EMNW(β)) with density (see Jevremovic (1991))

$$g(x,\theta) = (1+\theta)e^{-x} - \theta\beta e^{-\beta x}, \theta \in \left(0, \frac{1}{\beta-1}\right], x \geq 0; \tag{10}$$

It is easy to show that all densities given above belong to the family $\mathcal{G}$.

The efficiencies, as functions of the tuning parameter a, are shown on Figure 1.

We can notice that the local efficiencies range from reasonable to high, and for some values of a they are very high. Also, their behaviour with respect to the tuning parameter a is very different. In the cases of Weibull and Linear failure rate alternatives, they are increasing functions of a, while in the Gamma case, the function is decreasing. In the case of EMNW(3), the efficiencies increase up to a certain point and then decrease.

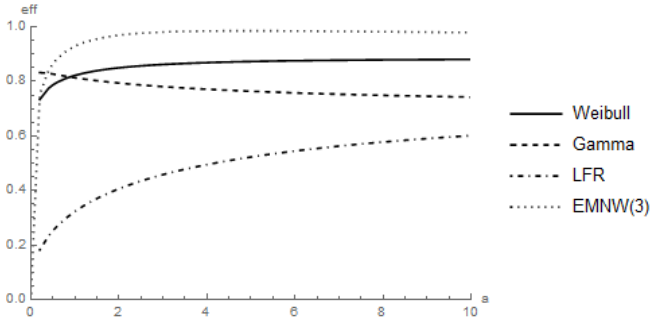

Figure 1: *Local approximate Bahadur efficiencies w.r.t. LRT.*

3.2. Comparison of efficiencies

In this section, we calculate the local approximate Bahadur relative efficiency of our tests against some recent, characterization based integral-type tests, for the previously mentioned alternatives.

The characterizations are of the equidistribution type and take the following form.

Let $X_1,\dots,X_{\max(m,p)}$ be i.i.d with d.f. F, $\omega_1 : R^m \mapsto R^1$ and $\omega_2 : R^p \mapsto R^1$ two sample functions. Then the following relation holds

$$\omega_1(X_1,\dots,X_m) \stackrel{d}{=} \omega_2(X_1,\dots,X_p)$$

if and only if $F(x) = 1 - e^{-\lambda x}$, for some $\lambda > 0$.

Notice that the Puri-Rubin characterization 2.1 is an example of such characterizations.

The first class of competitor tests consists of the integral-type tests with test statistic

$$I_n = \int_0^\infty \Big(G_n^{(1)}(t) - G_n^{(2)}(t)\Big) dF_n(t),$$

where $G_n^{(1)}(t)$ and $G_n^{(2)}(t)$ are V-empirical distribution functions of ω_1 and ω_2, respectively and F_n is the empirical distribution function.

In particular, we consider the following integral-type test statistics:

- $I_{n,k}^{(1)}$, proposed in Jovanović et al. (2015), based on the Arnold and Villasenor characterization, where $\omega_1(X_1,\dots,X_k) = \max(X_1,\dots,X_k)$ and $\omega_2(X_1,\dots,X_k) = X_1 + \frac{X_2}{2} + \cdots \frac{X_k}{k}$ (see Arnold and Villasenor, 2013, Milošević and Obradović, 2016c);

- $I_n^{(2)}$, proposed in Milošević and Obradović (2016b), based on the Milošević-Obradović characterization, where $\omega_1(X_1,X_2) = \max(X_1.X_2)$ and $\omega_2(X_1,X_2,X_3) = \min(X_1,X_2)+X_3$ (see Milošević and Obradović, 2016c);
- $I_n^{(3)}$, proposed in Milošević (2016), based on the Obradović characterization, where $\omega_1(X_1,X_2,X_3) = \max(X_1,X_2,X_3)$ and $\omega_2(X_1,X_2,X_3,X_4) = X_1+\text{med}(X_2,X_3,X_4)$ (see Obradović, 2015);
- $I_n^{(4)}$, proposed in Volkova (2015), based on the Yanev-Chakraborty characterization, where $\omega_1(X_1,X_2,X_3) = \max(X_1,X_2,X_3)$ and $\omega_2(X_1,X_2,X_3) = \frac{X_1}{3}+\max(X_2,X_3)$ (see Yanev and Chakraborty, 2013).

We also consider integral-type tests of the form

$$J_{n,a} = \int_0^\infty \left(L_n^{(1)}(t) - L_n^{(2)}(t)\right)\overline{X}_n e^{-at}dt, \tag{11}$$

where $L_n^{(1)}(t)$ and $L_n^{(2)}(t)$ are V-empirical Laplace transforms of ω_1 and ω_2, respectively. This approach has been originally proposed in Milošević and Obradović (2016a). There, particular cases of Desu characterization, with $\omega_1(X_1) = X_1$ and $\omega_2(X_1,X_2) = 2\min(X_1,X_2)$, and Puri-Rubin characterization were examined. We denote the corresponding test statistics with $J_{n,a}^{\mathcal{D}}$ and $J_{n,a}^{\mathcal{P}}$, respectively. The results are presented in Table 2. We can notice that in most cases tests that employ V-empirical Laplace transforms are more efficient than those based on V-empirical distribution functions. On the other hand, new tests are comparable with $J_{n,a}^{\mathcal{P}}$ and more efficient than $J_{n,a}^{\mathcal{D}}$.

4. Power study

In this section we compare the empirical powers of our tests with those of some common competitors. We choose the values of the tuning parameter to be 0.5, 1, 2 and 5. We also consider the limiting case when a tends to infinity. The expression for this limiting statistic is given in the following theorem.

Theorem 4.1. *For fixed n, we have*

$$\lim_{a\to\infty} a^3 M_{n,a}(\hat{\lambda}_n) = 2\left(\frac{1}{n^2}\sum_{i,j=1}^{n}|Y_i - Y_j| - \overline{Y}_n\right)^2,$$

where $Y_i = \hat{\lambda}_n X_i$, $i = 1,2,\ldots,n$.

Table 2: *Relative Bahadur efficiency of $M_{n,a}$ with respect to its competitors.*

$I_{n,2}^{(1)}$	*Weibull*	1.27	1.33	1.37	1.42
	Gamma	1.14	1.13	1.10	1.06
	LFR	2.44	3.13	3.93	5.08
	$EMNW(3)$	1.25	1.34	1.40	1.42
$I_{n,3}^{(1)}$	*Weibull*	1.19	1.24	1.28	1.32
	Gamma	1.17	1.15	1.12	1.09
	LFR	1.59	2.04	2.56	3.31
	$EMNW(3)$	1.08	1.17	1.22	1.23
$I_n^{(2)}$	*Weibull*	1.05	1.10	1.14	1.17
	Gamma	1.04	1.02	1.00	0.97
	LFR	1.22	1.56	1.96	2.53
	$EMNW(3)$	1.02	1.10	1.15	1.17
$I_n^{(3)}$	*Weibull*	1.06	1.10	1.14	1.18
	Gamma	1.18	1.16	1.14	1.10
	LFR	0.82	1.05	1.32	1.71
	$EMNW(3)$	0.94	1.02	1.06	1.08
$I_n^{(4)}$	*Weibull*	1.21	1.27	1.31	1.35
	Gamma	1.30	1.28	1.25	1.21
	LFR	1.23	1.57	1.98	2.56
	$EMNW(3)$	1.04	1.12	1.16	1.18
$J_{n,a}^{\mathcal{P}}$	*Weibull*	0.97	0.97	1.01	1.00
	Gamma	0.98	0.99	1.00	1.02
	LFR	0.97	0.93	0.91	0.93
	$EMNW(3)$	0.97	0.98	0.99	1.00
$J_{n,a}^{\mathcal{D}}$	*Weibull*	1.00	0.95	0.93	0.95
	Gamma	2.16	1.64	1.33	1.13
	LFR	1.17	1.07	1.01	0.99
	$EMNW(3)$	1.42	1.18	1.06	0.99

Proof. See Appendix A.

As competitor tests we use the following tests, listed in Henze and Meintanis (2005), Milošević and Obradović (2016a) and Torabi, Montazeri and Grané (2018):

- the test based on mean density (see Epps and Pulley, 1986):
  $EP_n = \sqrt{48n}\left(\frac{1}{n}\sum_{j=1}^{n} e^{-Y_j} - \frac{1}{2}\right)$, where $Y_j = \frac{X_j}{\overline{X}_n}$;
- the tests based on the mean residual life function (see Baringhaus and Henze, 2000a):

$$\overline{KS}_n = \sqrt{n}\sup_{t\geq 0}\left|\frac{1}{n}\sum_{j=1}^{n}\min(Y_j,t) - \frac{1}{n}\sum_{j=1}^{n} I\{Y_j \leq t\}\right|;$$

$$\overline{CM}_n = n\int_0^\infty \left(\frac{1}{n}\sum_{j=1}^{n}\min(Y_j,t) - \frac{1}{n}\sum_{j=1}^{n} I\{Y_j \leq t\}\right)^2 e^{-t}dt;$$

- the Cramer-von Mises test: $\omega_n^2 = \int_0^\infty (F_n(x) - (1-e^{-x}))^2 e^{-x}dx$;
- the Kolmogorov-Smirnov test: $KS_n = \sup_{x\geq 0}|F_n(x) - (1-e^{-x})|$;
- the test based on the integrated distribution function (see Klar, 2001):
  $KL_{n,a} = na^3\int_0^\infty (\psi_n(t) - \psi(t))^2 e^{-at}dt$, where
  $\psi(t) = \int_t^\infty (1-F(x))dx = e^{-t}$ and $\psi_n(t) = \int_t^\infty (1-F_n(x))dx$;
- the test based on spacings and Gini index (see D'Agostino and Stephens, 1986):
  $S_n = \sum_{j=1}^{n-1} U_j$, where $U_j = \frac{\sum_{i=1}^{j} D_i}{\sum_{i=1}^{n} X_i}$ and $D_j = (n+1-j)(X_{(j)} - X_{(j-1)})$;
- the score test of Cox and Oakes (1984): $CO_n = n + \sum_{j=1}^{n}(1-Y_j)\log Y_j$;
- the test of Milošević and Obradović: $J_{n,a}^{\mathcal{D}}$ and $J_{n,a}^{\mathcal{P}}$ from (11);
- the tests based on discrepancy measure (see Torabi et al., 2018):
  $H_n^{(k)} = \frac{1}{n}\sum_{j=1}^{n} h_k\left(\frac{1+F_0(\frac{X_j}{\overline{X}_n})}{1+F_n(X_j)}\right)$, where $h_1(x) = (e^{x-1}-x)I_{[0,1]}(x) + \sqrt[3]{|x^3-1|}I_{[1,\infty)}(x)$ and $h_2(x) = (e^{x-1}-x)I_{[0,1]}(x) + \frac{(x-1)^2}{(x+1)^2}I_{[1,\infty)}(x)$;
- the test based on maximal correlations (see Fortiana and Grané, 2003): $Q_n = \frac{s_n}{\overline{X}_n}\rho^+(F_n,F_0)$, where s_n^2 is sample variance and $\rho^+(F_1,F_2)$ is Hoeffding maximum correlation.

The Monte Carlo study is done for the small sample size $n = 20$, and a moderate sample size $n = 50$, with $N = 10000$ replicates, for the level of significance $\alpha = 0.05$ and the following alternative distributions:

- a Weibull $W(\theta)$ distribution with density (7);
- a Gamma $\Gamma(\theta)$ distribution with density (8);

- a half-normal HN distribution with density

$$g(x) = \sqrt{\frac{2}{\pi}} e^{-\frac{x^2}{2}}, x \geq 0;$$

- a uniform U distribution with density

$$g(x) = 1, 0 \leq x \leq 1;$$

- a Chen's $CH(\theta)$ distribution with density

$$g(x,\theta) = 2\theta x^{\theta-1} e^{x^\theta - 2(1-e^{x^\theta})}, x \geq 0;$$

- a linear failure rate $LF(\theta)$ distribution with density (9);
- a modified extreme value $EV(\theta)$ distributions with density

$$g(x,\theta) = \frac{1}{\theta} e^{\frac{1-e^x}{\theta}+x}, x \geq 0.$$

The powers are presented in Tables 3 and 4.

Table 3: *Percentage of rejected hypotheses for $n = 20$.*

Alt.	$Exp(1)$	$W(1.4)$	$\Gamma(2)$	HN	U	$CH(0.5)$	$CH(1)$	$CH(1.5)$	$LF(2)$	$LF(4)$	$EV(1.5)$	$LN(0.8)$	$LN(1.5)$	$DL(1)$	$DL(1.5)$
EP	5	36	48	21	66	63	15	84	28	42	45	25	67	20	64
$\overline{KS}$	5	35	46	24	72	47	18	79	32	44	48	28	55	22	6
$\overline{CM}$	5	35	47	22	70	61	16	83	30	43	47	27	66	21	63
ω^2	5	34	47	21	66	61	14	79	28	41	43	33	62	23	65
KS	5	28	40	18	52	56	13	67	24	34	35	30	58	20	56
KL	5	29	44	16	61	77	11	76	23	34	37	35	66	21	63
S	5	35	46	21	70	63	15	84	29	42	46	24	67	19	62
CO	5	37	54	19	50	**80**	13	81	25	37	37	33	60	25	72
$J^{\mathcal{D}}_{n,1}$	5	42	64	20	45	15	15	15	29	40	36	47	32	28	72
$J^{\mathcal{D}}_{n,5}$	5	48	64	28	70	20	21	21	36	52	53	33	57	24	70
$J^{\mathcal{P}}_{n,1}$	5	49	65	29	73	21	22	21	38	51	54	34	41	24	68
$J^{\mathcal{P}}_{n,5}$	5	48	62	**32**	79	23	23	23	**41**	**56**	58	27	59	21	65
$H^{(1)}_n$	5	49	60	31	78	0	**24**	**91**	40	55	23	33	0	30	74
$H^{(2)}_n$	5	6	10	2	18	79	2	29	4	7	8	8	**71**	4	20
Q_n	5	32	38	23	**86**	43	17	85	30	42	54	18	61	15	50
$M_{n,0.5}$	5	46	66	25	64	19	18	19	35	49	46	**57**	1	**39**	**81**
$M_{n,1}$	5	49	66	28	72	21	21	21	38	52	53	51	2	37	**81**
$M_{n,2}$	5	**50**	**67**	31	75	22	23	23	40	55	56	45	6	37	**81**
$M_{n,5}$	5	48	62	**32**	80	22	23	24	40	**56**	58	42	21	33	80
$M_{n,\infty}$	5	47	59	31	81	23	23	23	40	56	**59**	33	51	26	73

Table 4: *Percentage of rejected hypotheses for $n = 50$.*

Alt.	$Exp(1)$	$W(1.4)$	$\Gamma(2)$	HN	U	$CH(0.5)$	$CH(1)$	$CH(1.5)$	$LF(2)$	$LF(4)$	$EV(1.5)$	$LN(0.8)$	$LN(1.5)$	$DL(1)$	$DL(1.5)$
EP	5	80	91	54	98	94	38	**100**	69	87	90	45	**95**	39	97
$\overline{KS}$	5	71	86	50	99	90	36	**100**	65	82	88	62	92	43	96
$\overline{CM}$	5	77	90	53	99	94	37	**100**	69	87	90	65	**95**	44	97
ω^2	5	75	90	48	98	95	32	**100**	64	83	86	76	94	52	98
KS	5	64	83	39	93	92	26	98	53	72	75	71	91	46	95
KL	5	72	93	37	97	**99**	23	**100**	54	75	79	92	94	66	99
S	5	79	90	54	99	94	38	**100**	69	87	90	47	**95**	39	97
CO	5	82	96	45	91	**99**	30	**100**	60	80	78	66	92	55	99
$J^{\mathcal{D}}_{n,1}$	5	78	96	36	76	23	24	23	51	71	64	93	64	72	**100**
$J^{\mathcal{D}}_{n,5}$	5	86	**97**	55	97	41	40	40	72	89	89	70	90	55	**100**
$J^{\mathcal{P}}_{n,1}$	5	85	96	54	97	38	38	38	70	87	87	77	78	58	99
$J^{\mathcal{P}}_{n,5}$	5	86	96	63	99	46	46	45	77	91	93	58	92	47	98
$H^{(1)}_n$	5	**88**	94	**65**	99	0	**50**	**100**	**79**	**92**	94	51	0	50	98
$H^{(2)}_n$	5	37	62	13	78	98	7	94	24	44	46	47	**95**	23	87
Q_n	5	73	79	59	**100**	77	47	**100**	74	89	**96**	26	93	25	86
$M_{n,0.5}$	5	84	**97**	48	95	34	33	33	65	83	81	**94**	36	**77**	**100**
$M_{n,1}$	5	85	**97**	54	97	38	38	38	69	87	86	89	50	72	**100**
$M_{n,2}$	5	86	96	57	98	41	41	41	73	89	90	83	65	67	**100**
$M_{n,5}$	5	87	96	63	99	45	45	45	76	91	93	71	80	59	99
$M_{n,\infty}$	5	84	94	63	99	47	46	46	78	**92**	94	53	92	48	98

It can be noticed that our tests have good empirical sizes and their power ranges from reasonable to high. In the majority of cases, our tests are either the most powerful or their power is very close to the one of the most powerful competitor.

4.1. On a data-dependent choice of the tuning parameter

The powers of the proposed tests depend on the values of the tuning parameter a. Therefore, a well-chosen value of a would help underpin making the right decision. However, since the "right" value of a is rather different for various alternatives, a general conclusion on which a is most suitable in practice, can not be made. Hence, in what follows, we present an algorithm for a data driven selection of the tuning parameter, proposed initially by Allison and Santana (2015):

1. fix a grid of positive values of $a, (a_1, \ldots, a_k)$;
2. obtain a bootstrap sample $\boldsymbol{X}^*_n$ from the empirical distribution function of $\boldsymbol{X}_n$;
3. determine the value of the test statistic $M_{n,a_i}, i = 1, \ldots, k$, for the obtained sample;
4. repeat steps 2 and 3 B times and obtain series of values of test statistics for every a, $M^*_{j,a_i}, i = 1, \ldots, k, j = 1, \ldots, B$;

5. determine the empirical power of the test for every a, i.e.

$$\hat{P}_{a_i} = \frac{1}{B}\sum_{j=1}^{B} \mathrm{I}\{M_{j,a_i} \geq \check{C}_{n,a_i}(\alpha)\}, i = 1,\ldots,k,$$

   where $\mathrm{I}\{\cdot\}$ is the indicator function;
6. for the next calculation $\hat{a} = \underset{a\in\{a_1,\ldots,a_k\}}{argmax}\ \hat{P}_a$ will be used.

The critical value $\check{C}_{n,\hat{a}}$ is determined using the Monte Carlo procedure with N_1 replicates. Then, the empirical power of the test is determined based on the new sample from the alternative distribution

$$p = \frac{1}{N_1}\sum_{i=1}^{N_1} \mathrm{I}\{M_{n,\hat{a}} \geq \check{C}_{n,\hat{a}}(\alpha)\}.$$

The previously described procedure is repeated N times and the average value is taken as the estimated power:

$$\widetilde{P} = \frac{1}{N}\sum_{i=1}^{N} p_i.$$

The code of this algorithm is provided in Appendix C.

The results are presented in Tables 5 and 6. The numbers in the parentheses represent the percentage of times that each value of a equals the estimated optimal one. It is important to note that these bootstrap powers are comparable to the maximum achievable power for the tests calculated over a grid of values of the tuning parameter.

Table 5: *Percentage of rejected samples for different value of a, $n = 20$, $\alpha = 0.05$.*

	0.5	1	2	5	$\hat{a}$
$W(1.4)$	46(**50**)	49(12)	50(15)	48(23)	48
$\Gamma(2)$	66 (**63**)	65(12)	65(10)	63(15)	65
HN	25(**35**)	28(14)	30(17)	32(34)	29
U	64(20)	72(9)	75(21)	80 (**50**)	75
$CH(0.5)$	19(**37**)	21(15)	22(17)	22(31)	21
$CH(1)$	18(**35**)	21(15)	23(16)	23(34)	21
$CH(1.5)$	19(**35**)	20(11)	20(20)	24(34)	21
$LF(2)$	35(33)	37(12)	38(20)	41 (**35**)	38
$LF(4)$	49(**35**)	53(14)	54(16)	54(**35**)	52
$EW(1.5)$	46(24)	53(12)	56(20)	58(**44**)	54
$LN(0.8)$	57(**92**)	51(3)	45(4)	42(1)	56
$LN(1.5)$	2(13)	3(2)	6(2)	20(**83**)	17
$DL(1)$	39(**73**)	37(8)	37(10)	33(9)	38
$DL(1.5)$	82(**71**)	81(6)	82(12)	79(11)	82

Table 6: *Percentage of rejected samples for different value of a, $n = 50$, $\alpha = 0.05$.*

	0.5	1	2	5	$\hat{a}$
$W(1.4)$	84(**43**)	86(19)	86(16)	87(22)	85
$\Gamma(2)$	97(**68**)	97(15)	96(11)	95(6)	97
HN	48(21)	53(13)	57(23)	62(**43**)	57
U	95(31)	97(12)	98(20)	99(**37**)	98
$CH(0.5)$	34(19)	37(11)	41(20)	44(**50**)	41
$CH(1)$	33(18)	37(13)	41(18)	46(**51**)	41
$CH(1.5)$	33(18)	37(13)	42(19)	44(**50**)	41
$LF(2)$	65(20)	69(12)	74(24)	76(**44**)	72
$LF(4)$	83(25)	86(16)	89(20)	91(**39**)	88
$EW(1.5)$	81(17)	87(13)	89(22)	93(**48**)	89
$LN(0.8)$	95(**92**)	89(6)	82(2)	70 (0)	94
$LN(1.5)$	38(2)	50(1)	64(4)	79(**93**)	78
$DL(1)$	77(**81**)	72(11)	68(4)	60(4)	67
$DL(1.5)$	100(**84**)	100(11)	100(4)	99(1)	100

5. Real data examples

In this section we apply our tests to three real datasets. The first dataset represents inter-occurrence times of fatal accidents to British-registered passenger aircraft, 1946-1963, measured in number of days and listed in the order of their occurrence in time (see Pyke, 1965).

The second dataset represents failure times for right rear breaks on D9G-66A Caterpillar tractors (see Barlow and Campo (1975)). The third dataset represents failure and running times (1000 cycles) of a sample of 30 units of a larger electrical system (see Meeker and Escobar (2014)). The third set was also analysed in Shakeel et al. (2016). The datasets are given in Tables 8-10 of Appendix B, while their empirical and theoretical density, cumulative distribution function, Q-Q and P-P plots, are shown in Figures 2-4. The figures suggest that the exponential distribution provides a good fit for the first dataset, unlike for the remaining two.

In Table 7 we present, for all three datasets, the p-values of our test with data driven selection of the tuning parameter, as well as for $M_{n,\infty}$. For comparison purposes, we also include some exponentiality tests that were shown to have good power performance in Tables 3 and 4.

We can see that our tests confirm the conclusions suggested by the plots 2-4. While the competitor tests mostly point to the same decisions, it is worth noting that, at the 5% level of significance, few of them fail to reject the null hypothesis for the third dataset.

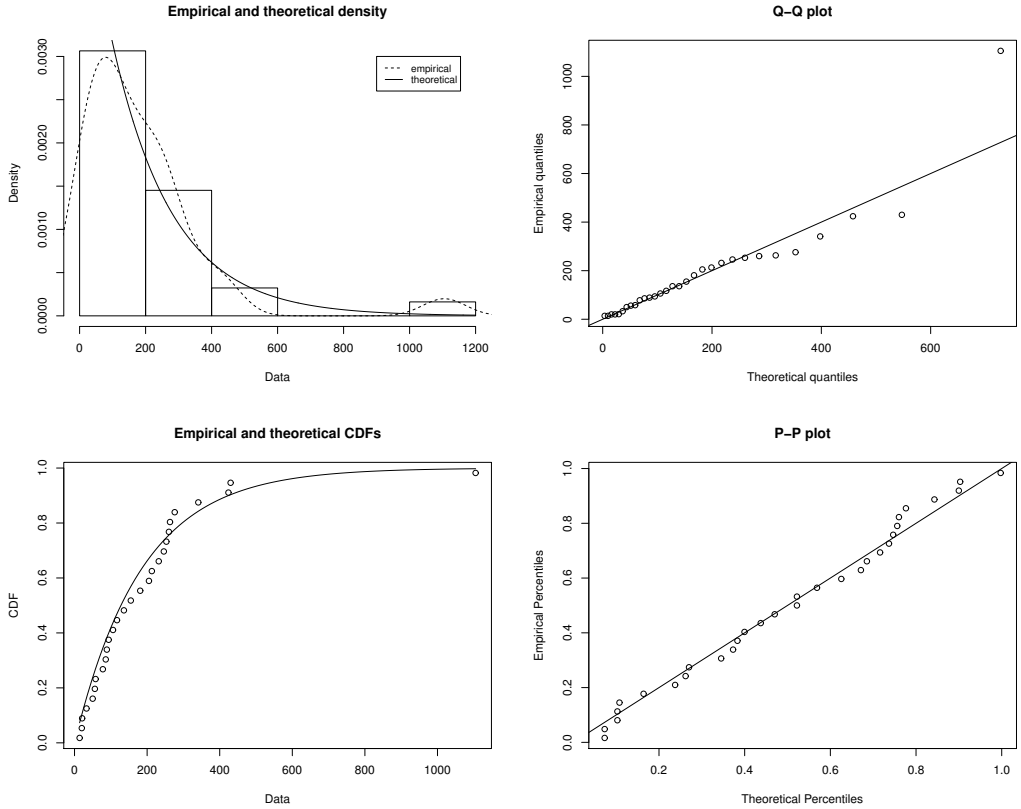

Figure 2: *Plots for dataset 1.*

Table 7: *p-values for three datasets.*

Stat.	EP	ω^2	CO	$H_n^{(1)}$	$H_n^{(2)}$	$J_{n,1}^{\mathfrak{P}}$	$M_{n,\hat{a}}$	$M_{n,\infty}$
Dataset 1	0.4037	0.9103	0.4907	0.6062	0.8737	0.3708	0.4902	0.8917
Dataset 2	0	0	0	0	0.0005	0	0	0
Dataset 3	0.0279	0.0059	0.1536	0.0420	0.0940	0.0163	0.0092	0.0074

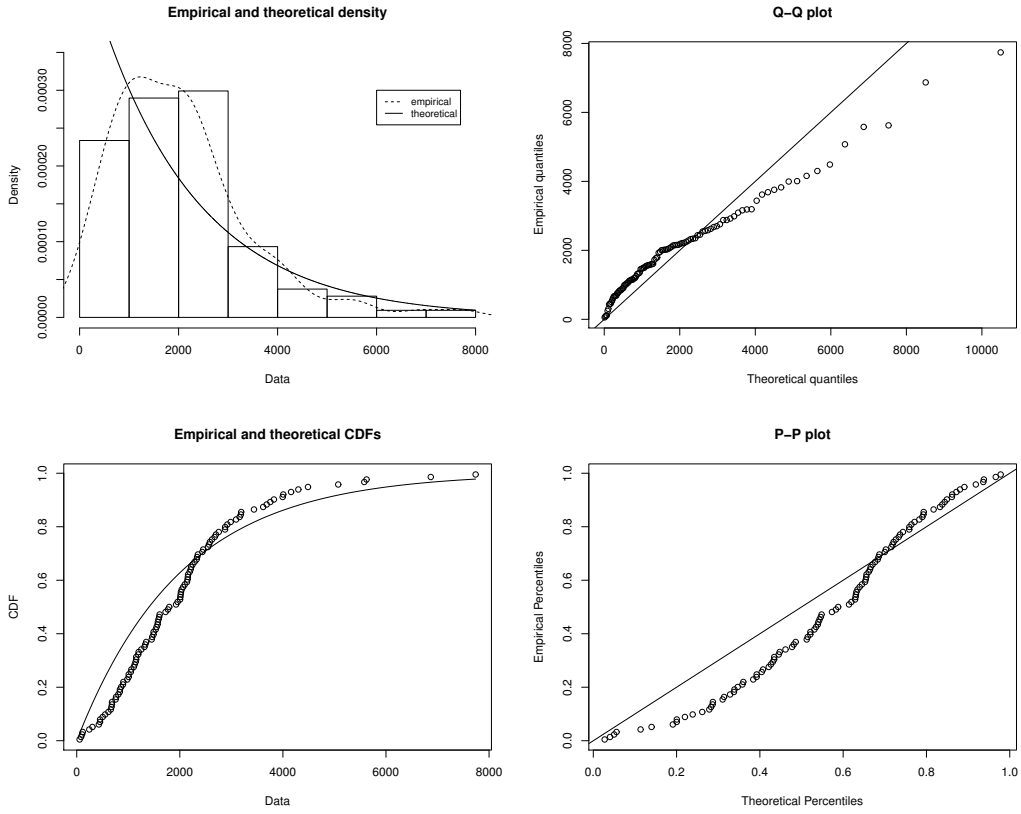

Figure 3: *Plots for dataset 2.*

6. Conclusion

In this paper we propose new consistent scale-free exponentiality tests based on the Puri-Rubin characterization. The proposed tests are shown to be very efficient in the Bahadur sense. Moreover, in the small sample case, the tests have reasonable to high empirical powers. They also outperform many recent competitor tests in terms of both efficiency and power. The quality of their performance is confirmed on two real data examples. This makes them attractive for use in practice.

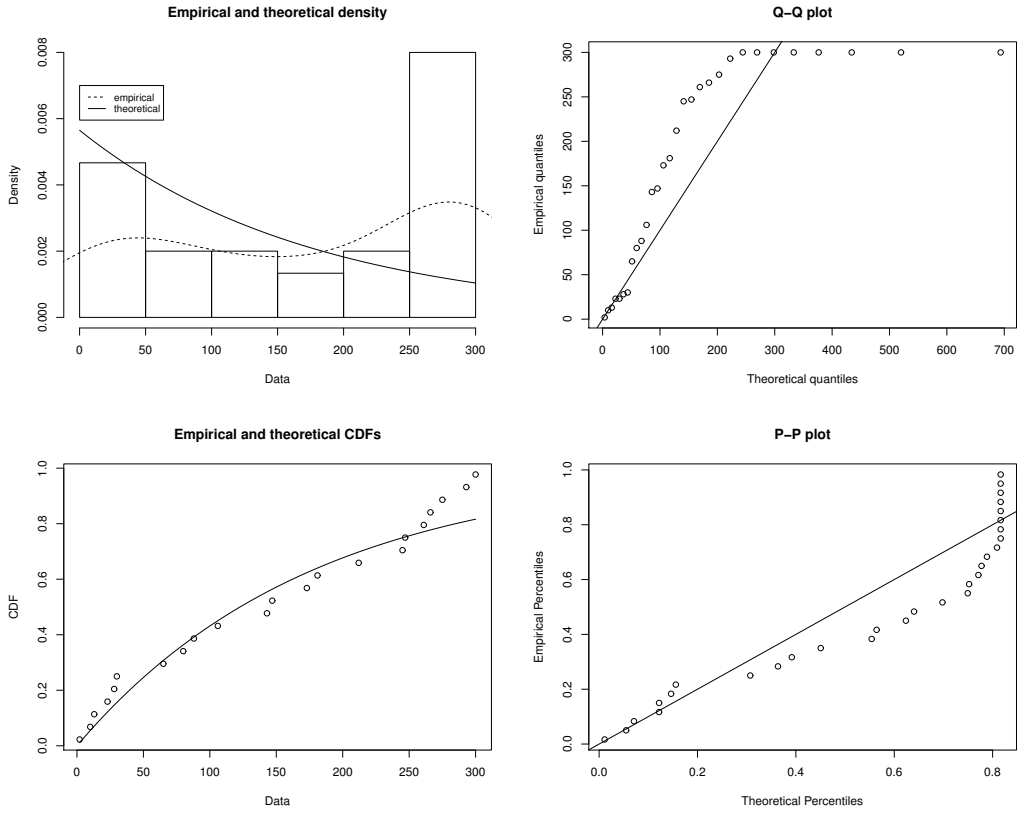

Figure 4: *Plots for dataset 3.*

Appendix A - Proofs

Proof of Theorem 2.3. Since the kernel h is non-degenerate, from the theorem for V-statistics with non-degenerate kernels (Korolyuk and Borovskikh, 1994, Theorem 4.2.5), it follows

$$\sqrt{n}(M_{n,a}(\mu)-\Delta) \xrightarrow{d} \mathcal{N}(0, 16Var(h_1(X_1,a))).$$

As the function $h(x_1,x_2,x_3,x_4,a;\gamma)$ is continuously differentiable with respect to γ at the point $\gamma=\mu$, the mean-value theorem gives

$$\sqrt{n}(M_{n,a}(\widehat{\mu})-\Delta(\mu)) = \sqrt{n}(M_{n,a}(\mu)-\Delta(\mu)) + \sqrt{n}(\widehat{\mu}-\mu)\frac{\partial M_{n,a}(\gamma)}{\partial\gamma}|_{\gamma=\mu^*},$$

for some μ^* between μ and $\widehat{\mu}$.

Using the Law of large numbers for V-statistics, the Slutsky theorem, and the fact that the limit distribution of $\sqrt{n}(M_{n,a}(\mu)-\Delta,\widehat{\mu}-\mu)$ is two dimensional normal, it fol-

lows that $\sqrt{n}(M_{n,a}(\widehat{\mu})-\Delta(\mu))$ will converge in distribution to zero mean normal random variable, with the variance equal to

$$16Var(h_1(X_1,a))+\lim_{n\to\infty}E\left(\frac{\partial M_{n,a}(\gamma)}{\partial\gamma}\right)^2 Var(\sqrt{n}\widehat{\mu})+2\lim_{n\to\infty}Cov(\sqrt{n}M_{n,a}(\mu),\sqrt{n}\widehat{\mu}).$$

Calculating the limits, we obtain (5). ∎

Proof of Lemma 3.1. Using the result of Zolotarev (1961), the logarithmic tail behaviour of limiting distribution function of $\widetilde{M}_{n,a}(\widehat{\lambda}_n)=\sqrt{nM_{n,a}(\widehat{\lambda}_n)}$ is

$$\log(1-F_{\widetilde{M}_a}(t))=-\frac{t^2}{12\delta_1}+o(t^2),\ \ t\to\infty.$$

Therefore, $a_{\widetilde{M}_a}=\frac{1}{6\delta_1}$. The limit in probability P_θ of $\widetilde{M}_{n,a}(\widehat{\lambda}_n)/\sqrt{n}$ is

$$b_{\widetilde{M}_a}=\sqrt{b_M(\theta)}.$$

Inserting this into the expression for Bahadur slope completes the proof. ∎

Proof of Lemma 3.2. For brevity, denote $\boldsymbol{x}=(x_1,x_2,x_3,x_4)$ and $\boldsymbol{G}(\boldsymbol{x};\theta)=\prod_{i=1}^4 G(x_i;\theta)$. Since $\overline{X}_n$ converges almost surely to its expected value $\mu(\theta)$, using the Law of large numbers for V-statistics with estimated parameters (see Iverson and Randles, 1989), $M_{n,a}(\widehat{\lambda}_n)$ converges to

$$\begin{aligned}b_M(\theta)&=E_\theta(h(\boldsymbol{X},a;\mu(\theta)))\\&=\int\limits_{(R^+)^4}\Big(\frac{\mu(\theta)}{x_1+x_3+a\mu(\theta)}-\frac{\mu(\theta)}{x_3+|x_1-x_2|+a\mu(\theta)}\\&\quad-\frac{\mu(\theta)}{x_1+|x_3-x_4|+a\mu(\theta)}+\frac{\mu(\theta)}{|x_1-x_2|+|x_3-x_4|+a\mu(\theta)}\Big)d\boldsymbol{G}(\boldsymbol{x};\theta).\end{aligned}$$

We may assume that $\mu(0)=1$ due to the scale freeness of the test statistic under the null hypothesis. After some calculations we get that $b'_M(0)=0$. Further,

$$b''(0)=\int\limits_{(R^+)^4}h(\boldsymbol{x},a;1)\frac{\partial^2}{\partial\theta^2}d\boldsymbol{G}(\boldsymbol{x},0)=6\int\limits_{(R^+)^2}\widetilde{h}_2(x,y)f(x)f(y)dxdy.$$

Expanding $b_M(\theta)$ into the Maclaurin series we complete the proof. ∎

Proof of Theorem 4.1. Denote $g(t) = \left(L_n^{(1)}(t) - L_n^{(2)}(t)\right)^2$. Then the test statistic can be expressed as $M_{n,a}(\hat{\lambda}_n) = \int_0^\infty g(t)e^{-at}dt$. The Maclaurin expansion of $g(t)$ is

$$g(t) = t^2\left(\frac{1}{n^2}\sum_{i,j=1}^{n}|Y_i - Y_j| - \overline{Y}_n\right)^2 + t^3\left(\frac{1}{n^2}\sum_{i,j=1}^{n}|Y_i - Y_j| - \overline{Y}_n\right)\left(\overline{Y}_n - \frac{1}{n^2}\sum_{i,j=1}^{n}(Y_i - Y_j)^2\right) + \frac{t^4}{4}\left(\overline{Y}_n - \frac{1}{n^2}\sum_{i,j=1}^{n}(Y_i - Y_j)^2\right) + o(t^4).$$

Using an Abelian theorem for the Laplace transform from (Widder, 1946, Chapter 5.2.) (see also from Baringhaus, Gürtler and Henze, 2000b, Proposition 1.1), and

$$\lim_{s\to\infty}\Gamma(4)s^3\int_0^s g(t)dt = 2\left(\frac{1}{n^2}\sum_{i,j=1}^{n}|Y_i - Y_j| - \overline{Y}_n\right)^2,$$

follows the statement of the theorem. ∎

Appendix B - Datasets

Table 8: *Dataset 1: inter-occurrence times of fatal accidents.*

20	106	14	78	94	20	21	136	56	232	89
33	181	424	14	430	155	205	117	253	86	260
213	58	276	263	246	341	1105	50	136		

Table 9: *Dataset 2: failure times for right rear breaks.*

56	83	104	116	244	305	429	452	453	503	552
614	661	673	683	685	753	763	806	834	838	862
897	904	981	1007	1008	1049	1060	1107	1125	1141	1153
1154	1193	1201	1253	1313	1329	1347	1454	1464	1490	1491
1532	1549	1568	1574	1586	1599	1608	1723	1769	1795	1927
1957	2005	2010	2016	2022	2037	2065	2096	2139	2150	2156
2160	2190	2210	2220	2248	2285	2325	2337	2351	2437	2454
2546	2565	2584	2624	2675	2701	2755	2877	2879	2922	2986
3092	3160	3185	3191	3439	3617	3685	3756	3826	3995	4007
4159	4300	4487	5074	5579	5623	6869	7739			

Table 10: *Dataset 3: failure and running times of units of an electrical system .*

275	13	147	23	181	30	65	10	300	173
106	300	300	212	300	300	300	2	261	293
88	247	28	143	300	23	300	80	245	266

Appendix C - Code

- `expTestL2puri` is a C-function which calculates the value of statistic $M_{n,a}$;
- `bootstrapStat` is an R-function which calculates statistics $M_{n,a}$ based on bootstrapped resamples from the initial sample;
- `optimal_a` is an R-function which implements the data-driven procedure from Section 4.1.

```
double expTestL2puri(NumericVector x,double a)
{
 int n = x.size();
 double n1=double(n);
 double total=0;
  for(int i=0;i<n;i++)
  {
    for(int k=0;k<n;k++)
    {
      total+=n1*n1/(a+x[i]+x[k]);
      for(int j=0;j<n;j++)
      {
        total-=2*n1/(a+x[k]+fabs(x[i]-x[j]));
        for(int l=0;l<n;l++)
        {
          total+=(1.0/(a+fabs(x[i]-x[j])+fabs(x[k]-x[l])));
        "
      "
    "
  "
 double stat=total/n1/n1/n1/n1;
 return stat;
"

bootstrapStat<-function(x,a,B=300){
  n<-length(x)
  Xs<-sample(x,B*n,replace = TRUE)
  Xs<-array(Xs,c(n,B))
  Tb<-apply(Xs/mean(Xs),2,expTestL2puri,a)
  return(Tb)
"


optimal_a<-function(y,a,B)
{
  n=length(y)
P<-rep(0,length(a))
for(k in 1:length(a)){
```

```
    ts0<-rep(0,10000)
    for(i in 1:10000){
      x<-rexp(n)
      ts0[i]<-expTestL2puri(x/mean(x),a[k])
                    "
    C<-quantile(ts0,0.95)
    Tb<-bootstrapStat(y,a[k],B)
      P[k]<-sum(Tb>=C)/B
      "


  m<-which.max(P)
  return(a[m])
"
```

Acknowledgement

We would like to thank the anonymous referees for their useful remarks that improved the paper. This work was supported by the MNTRS, Serbia under Grant No. 174012 (first and second author).

References

Alizadeh Noughabi, H. and Arghami, N. R. (2011). Testing exponentiality based on characterizations of the exponential distribution. *Journal of Statistical Computation and Simulation*, 81, 1641–1651.

Allison, J. and Santana, L. (2015). On a data-dependent choice of the tuning parameter appearing in certain goodness-of-fit tests. *Journal of Statistical Computation and Simulation*, 85, 3276–3288.

Arnold, B. C. and Villasenor, J. A. (2013). Exponential characterizations motivated by the structure of order statistics in samples of size two. *Statistics & Probability Letters*, 83, 596–601.

Bahadur, R. R. (1971). *Some Limit Theorems in Statistics*. SIAM, Philadelphia.

Baringhaus, L. and Henze, N. (2000a). Tests of fit for exponentiality based on a characterization via the mean residual life function. *Statistical Papers*, 41, 225–236.

Baringhaus, L., Gürtler, N. and Henze, N. (2000b). Theory & methods: weighted integral test statistics and components of smooth tests of fit. *Australian & New Zealand Journal of Statistics*, 42, 179–192.

Barlow, R. E. and Campo, R. (1975). Total time on test processes and applications to failure data analysis. In *Reliability and Fault Tree Analysis*, pp. 451–481. SIAM.

Božin, V., B. Milošević, Ya, Nikitin, Yu and Obradović, M. (2018). New characterization based symmetry tests. *Bulletin of the Malaysian Mathematical Sciences Society*. DOI:10.1007/s40840-018-0680-3.

Cox, D. and Oakes, D. (1984). *Analysis of Survival Data*. Chapman and Hall, New York.

D'Agostino, R. and Stephens, M. (1986). *Goodness-of-Fit-Techniques*. Marcel Dekker, Inc., New York.

Epps, T. and Pulley, L. (1986). A test of exponentiality vs. monotone-hazard alternatives derived from the empirical characteristic function. *Journal of the Royal Statistical Society. Series B (Methodological)*, 206–213.

Fortiana, J. and Grané, A. (2003). Goodness-of-fit tests based on maximum correlations and their orthogonal decompositions. *Journal of the Royal Statistical Society. Series B (Methodological)*, 65, 115–126.

Grané, A. and Fortiana, J. (2009). A location-and scale-free goodness-of-fit statistic for the exponential distribution based on maximum correlations. *Statistics*, 43, 1–12.

Grané, A. and Fortiana, J. (2011). A directional test of exponentiality based on maximum correlations. *Metrika*, 73, 255–274.

Henze, N. (1992). A new flexible class of omnibus tests for exponentiality. *Communications in Statistics-Theory and Methods*, 22, 115–133.

Henze, N. and Meintanis, S. G. (2002a). Tests of fit for exponentiality based on the empirical Laplace transform. *Statistics: A Journal of Theoretical and Applied Statistics*, 36, 147–161.

Henze, N. and Meintanis, S. G. (2002b). Goodness-of-fit tests based on a new characterization of the exponential distribution. *Communications in Statistics-Theory and Methods*, 31, 1479–1497.

Henze, N. and Meintanis, S. G. (2005). Recent and classical tests for exponentiality: a partial review with comparisons. *Metrika*, 61, 29–45.

Iverson, H. and Randles, R. (1989). The effects on convergence of substituting parameter estimates into U-statistics and other families of statistics. *Probability Theory and Related Fields*, 81, 453–471.

Jevremovic, V. (1991). A note on mixed exponential distribution with negative weights. *Statistics & Probability Letters*, 11, 259–265.

Jovanović, M., Milošević, B., Nikitin, Ya. Yu., Obradović, M. and Volkova, K. Yu. (2015). Tests of exponentiality based on Arnold–Villasenor characterization and their efficiencies. *Computational Statistics & Data Analysis*, 90, 100–113.

Klar, B. (2001). Goodness-of-fit tests for the exponential and the normal distribution based on the integrated distribution function. *Annals of the Institute of Statistical Mathematics*, 53, 338–353.

Klar, B. (2003). On a test for exponentiality against Laplace order dominance. *Statistics*, 37, 505–515.

Klar, B. (2005). Tests for exponentiality against the M and LM-Classes of life distributions. *Test*, 14, 543–565.

Korolyuk, V. S. and Borovskikh, Y. V. (1994). *Theory of U-statistics*. Kluwer, Dordrecht.

Meeker, W. Q. and Escobar, L. A. (2014). *Statistical Methods for Reliability Data*. John Wiley & Sons.

Meintanis, S. G. (2008). Tests for generalized exponential laws based on the empirical Mellin transform. *Journal of Statistical Computation and Simulation*, 78, 1077–1085.

Meintanis, S. G., Nikitin, Ya. Yu. and Tchirina, A. (2007). Testing exponentiality against a class of alternatives which includes the RNBUE distributions based on the empirical laplace transform. *Journal of Mathematical Sciences*, 145, 4871–4879.

Milošević, B. (2016). Asymptotic efficiency of new exponentiality tests based on a characterization. *Metrika*, 79, 221–236.

Milošević, B. and Obradović, M. (2016a). New class of exponentiality tests based on U-empirical Laplace transform. *Statistical Papers*, 57, 977–990.

Milošević, B. and Obradović, M. (2016b). Some characterization based exponentiality tests and their Bahadur efficiencies. *Publications de L'Institut Mathematique*, 100, 107–117.

Milošević, B. and Obradović, M. (2016c). Some characterizations of the exponential distribution based on order statistics. *Applicable Analysis and Discrete Mathematics*, 10, 394–407.

Nikitin, Ya. Yu. (1995). *Asymptotic Efficiency of Nonparametric Tests*. Cambridge University Press, New York.

Nikitin, Ya. Yu. and Peaucelle, I. (2004). Efficiency and local optimality of nonparametric tests based on U- and V-statistics. *Metron*, 62, 185–200.

Nikitin, Ya. Yu. and Volkova, K. Yu. (2010). Asymptotic efficiency of exponentiality tests based on order statistics characterization. *Georgian Mathematical Journal*, 17, 749–763.

Nikitin, Ya. Yu. and Volkova, K. Yu. (2016). Efficiency of exponentiality tests based on a special property of exponential distribution. *Mathematical Methods of Statistics*, 25, 54–66.

Obradović, M. (2015). Three characterizations of exponential distribution involving median of sample of size three. *Journal of Statistical Theory and Applications*, 14, 257–264.

Puri, P. S. and Rubin, H. (1970). A characterization based on the absolute difference of two iid random variables. *The Annals of Mathematical Statistics*, 41, 2113–2122.

Pyke, R. (1965). Spacings. *Journal of the Royal Statistical Society. Series B (Methodological)*, 27, 395–449.

Serfling, R. (2009). *Approximation Theorems of Mathematical Statistics*, Volume 162. John Wiley & Sons, New York.

Shakeel, M., Haq, M., Hussain, I., Abdulhamid, A. and Faisal, M. (2016). Comparison of two new robust parameter estimation methods for the power function distribution. *PloS one*, 11, e0160692.

Strzalkowska-Kominiak, E. and Grané, A. (2017). Goodness-of-fit test for randomly censored data based on maximum correlation. *SORT: Statistics and Operations Research Transactions*, 41, 119–138.

Torabi, H., Montazeri, N. H. and Grané, A. (2018). A wide review on exponentiality tests and two competitive proposals with application on reliability. *Journal of Statistical Computation and Simulation*, 88, 108–139.

Volkova, K. Yu. (2015). Goodness-of-fit tests for exponentiality based on Yanev-Chakraborty characterization and their efficiencies. *Proceedings of the 19th European Young Statisticians Meeting, Prague*, 156–159.

Widder, D. V. (1946). *The Laplace Transform*. Princeton university press.

Yanev, G. P. and Chakraborty, S. (2013). Characterizations of exponential distribution based on sample of size three. *Pliska Studia Mathematica Bulgarica*, 22, 237p–244p.

Zolotarev, V. M. (1961). Concerning a certain probability problem. *Theory of Probability & Its Applications*, 6, 201–204.

SORT 43 (1) January-June 2019, 51-74 DOI: 10.2436/20.8080.02.79

Bayesian joint spatio-temporal analysis of multiple diseases

Virgilio Gómez-Rubio[1], Francisco Palmí-Perales[1], Gonzalo López-Abente[2], Rebeca Ramis-Prieto[2] and Pablo Fernández-Navarro[2]

Abstract

In this paper we propose a Bayesian hierarchical spatio-temporal model for the joint analysis of multiple diseases which includes specific and shared spatial and temporal effects. Dependence on shared terms is controlled by disease-specific weights so that their posterior distribution can be used to identify diseases with similar spatial and temporal patterns.
The model proposed here has been used to study three different causes of death (oral cavity, esophagus and stomach cancer) in Spain at the province level. Shared and specific spatial and temporal effects have been estimated and mapped in order to study similarities and differences among these causes. Furthermore, estimates using Markov chain Monte Carlo and the integrated nested Laplace approximation are compared.

MSC: 62F15, 62H11, 62M10.

Keywords: Bayesian modelling, Joint modelling, Multivariate disease mapping, Shared components. Spatio-temporal epidemiology.

1. Introduction

Bayesian hierarchical models are a popular approach to analyse public health spatio-temporal data. These data often come as counts of cases of disease at different administrative levels and time periods. Hierarchical models for these data are based on a Poisson regression model that includes different types of spatial, temporal and spatio-temporal effects in the linear predictor of the model (see, for example, Lawson, 2013, for a review). Spatial effects are often modelled using a conditionally autoregressive (CAR) specification (Besag, York and Mollié, 1991). Temporal effects often rely on smooth terms, such as random walks or splines. For non-separable space-time models, Knorr-

[1] Department of Mathematics, Universidad de Castilla-La Mancha, Albacete, Spain. Corresponding author: Virgilio Gómez-Rubio (Virgilio.Gomez@uclm.es).

[2] Environmental and Cancer Epidemiology Unit, Carlos III Institute of Health, Madrid, Spain; Consortium for Biomedical Research in Epidemiology & Public Health, CIBER Epidemiología y Salud Pública - CIBERESP, Spain.

Received: August 2018
Accepted: December 2018

Held (2000) describes different interactions for spatial and temporal effects. When studying spatio-temporal trends in disease mapping, several authors have proposed different models to detect specific patterns in particular areas. For example, Abellan, Richardson and Best (2008) and Guangquan et al. (2012) propose models that can identify areas that follow a spatio-temporal trend with similar structure or that show a specific spatio-temporal pattern.

The spatial analysis of several diseases often relies on multivariate models with shared spatial effects to capture similar patterns. For example, Knorr-Held and Best (2001) use this approach to model two diseases by considering a shared spatial term in the model with a different weight for each disease. Downing et al. (2008) propose a model with several spatial effects to model six cancers jointly. Botella-Rocamora, Martínez-Beneito and Banerjee (2015) and Martínez-Beneito, Botella-Rocamora and Banerjee (2016) propose a general approach for multivariate disease mapping that can help to identify diseases with similar spatial distributions. Marí-Dell'Olmo et al. (2014) use a smoothed analysis of the variance for the analysis of several diseases in ecological models.

We have developed a novel Bayesian spatio-temporal joint model for several diseases with specific and shared spatial and temporal effects. The shared spatial and temporal terms would account for common spatial and temporal patterns. The effect of these common patterns on specific diseases is controlled by specific-weights that measure the dependence of a given disease on these patterns. By considering specific spatial and temporal patterns we allow for departures from the shared patterns for different diseases. Finally, the posterior distribution of the weights is able to capture dependence between diseases with similar spatial or temporal patterns.

Bayesian model fitting has been tackled by using Markov chain Monte Carlo (MCMC) methods (Gilks et al., 1996), which can be slow for complex spatio-temporal models. For this reason, we have also fit the models presented using the approximation provided by the integrated nested Laplace approximation (INLA) method (Rue, Martino and Chopin, 2009). INLA is able to fit the proposed models in a fraction of the time required by MCMC and provide an approximation to the posterior marginals of the model parameters. Given that INLA focuses on approximating the posterior marginals of the model parameters, multivariate posterior inference on several parameters may be difficult to do with INLA and we will still rely on MCMC for this.

The structure of this paper is as follows. First, we give an introduction to spatio-temporal disease mapping in Section 2. In Section 3 several models for the joint analysis of several diseases are described. Next, our new spatio-temporal model is fully described in Section 4. An example on three death causes in Spain is discussed in Section 5. Finally, a summary of the paper and discussion of the main results is given in Section 6.

2. Spatio-temporal disease mapping

Disease mapping (Lawson, 2013, Elliot et al., 2000, Banerjee, Carlin and Gelfand, 2014) is commonly employed in public health and epidemiology in order to describe the spatial (and temporal) variation of disease. In the analysis of public health data, we often find the number of cases at different n administrative areas and T time periods. We will denote by $O_{i,t}$ the number of cases in area i and time period t. As studying the distribution of the cases alone is misleading, expected number of cases $E_{i,t}$ are also computed using the population structure and direct or indirect standardization (Elliot et al., 2000). In addition, area-level covariates $X_{i,t}$ may be available and these can be incorporated into the models to account for socio-economic inequalities, risk exposure and other relevant risk factors.

In order to model the observed number of cases, a Poisson distribution is often used:

$$O_{i,t}|E_{i,t},\theta_{i,t} \sim Po(E_{i,t}\theta_{i,t}) \tag{1}$$

Here, $\theta_{i,t}$ is the relative risk. Values of the relative risk higher that one indicate an area of increased risk because, in that case, the mean $\mu_{i,t} = E_{i,t}\theta_{i,t}$ is higher than the expected number of cases according to the population in the area. As stated above, it is more informative to map the relative risk $\theta_{i,t}$ than the observed cases.

The relative risk can be modelled using a Poisson log-linear model. For example, if the relative risk is thought to be dependent of area-level covariates it can be modelled as:

$$\log(\theta_{i,t}) = \alpha + \beta X_{i,t}, \tag{2}$$

with α an intercept and β a vector of coefficients of covariates $X_{i,t}$. Other fixed and random effects or smooth terms can be added on the right-hand side of the previous equation, as discussed below.

Bayesian hierarchical models for disease mapping have been widely used since the seminal paper by Besag et al. (1991) was published. In this paper, the relative risk depends on area level covariates, spatially correlated random effects v_i and independent random effects u_i. This model can be extended to the spatio-temporal case as follows:

$$\log(\theta_{i,t}) = \alpha + \beta X_{i,t} + v_i + u_i + w_t \tag{3}$$

Here, v_i is a spatial random effect, u_i is an independent random effect and w_t is a temporal effect.

Independent random effects u_i are assigned a Gaussian prior with zero mean and precision τ_u. Spatially correlated random effects follow an intrinsic conditionally autoregressive (CAR) specification. In this case, the conditional distribution of v_i given all the other spatial effects v_{-i} is Gaussian with mean $\sum_{j\neq i} w_{ij}v_j / \sum_{j\neq i} w_{ij}$ and precision $\tau_v \sum_{j\neq i} w_{ij}$. In the previous expressions, w_{ij} are spatial weights and τ_v is the precision of the spatial random effect.

Spatial weights w_{ij} are often taken as 1 if areas i and j are neighbors and 0 otherwise. In this case, if by $i \sim j$ we denote that regions i and j are neighbors and by n_i the number of neighbors of region i, the conditional distribution of v_i under an intrinsic CAR specification is

$$v_i|v_{-i} \sim N\left(\sum_{j\sim i} \frac{v_j}{n_i}, \tau_v n_i\right) \tag{4}$$

When a vector of random effects $v = (v_1, \ldots, v_n)$ has a prior that is an intrinsic CAR specification with weight matrix W and precision τ_v, we will write that as $v \sim CAR(W, \tau_v)$.

Temporal effects w_t are often assigned a random walk prior with precision τ_w or a CAR prior in one dimension, with a temporal adjacency defined so that consecutive time periods are neighbors. Knorr-Held (2000) describes a number of space-time interactions that could be added to the model in Equation (3).

Regarding models that specifically try to identify differential spatial or temporal patterns, Richardson, Abellan and Best (2006) propose a joint model for two diseases with specific space and temporal terms for the second disease which allows for the identification of disease-specific patterns. Abellan et al. (2008) propose a spatio-temporal model with a spatio-temporal term that is a mixture of terms. Each term is Normally distributed with zero mean and one has a smaller variance than the other. This allows the model to classify areas according to small or large variation. Areas with large variance indicate a strong departure from the common separable spatio-temporal pattern.

Similarly, Guangquan et al. (2012) propose a Bayesian hierarchical spatio-temporal model in which the log-relative risk is modelled on a mixture of two linear predictors with different effects. The first one is the sum of an intercept, a spatial effect and a temporal effect and, the second one is the sum of an area-specific intercept and an space-time non-separable random effect.

Both Abellan et al. (2008) and Guangquan et al. (2012) propose models that include terms to highlight areas with patterns that differ from the overall spatio-temporal pattern by using a mixture of terms. These models are aimed at targeting areas which depart from the shared spatial and temporal patterns. In Section 4 we propose a new multivariate model to identify diseases with specific spatial or temporal patterns that are different from the shared spatio-temporal pattern.

3. Joint modelling of multiple diseases

The models described in the previous section can be applied to different diseases to produce space-time risk estimates that can be mapped and analysed to identify particular patterns of high risk. Diseases with similar etiologies may show similar patterns, i.e., similar spatial or temporal variation, and a multivariate analysis could be performed to

obtain better estimates of these shared patterns. At the same time, the model must allow for specific departures from the shared pattern in certain areas.

In order to build joint models for D different diseases, we will denote by $O_{i,t}^{(d)}$ and $E_{i,t}^{(d)}$ the observed and expected cases, respectively, of disease d in area i and time period t. Hence, the distribution of the number of cases $O_{i,t}^{(d)}$ is a Poisson with mean $E_{i,t}^{(d)}\theta_{i,t}^{(d)}$, where $\theta_{i,t}^{(d)}$ is the relative risk.

In a joint model, relative risks include terms that are shared by several diseases. The effect of the shared effects may be weighted, so that these weights measure the dependence of the geographic or temporal distribution of the disease on the shared pattern. For example, Knorr-Held and Best (2001) consider a model for two diseases in which the shared spatial effect has weight δ for one disease and $1/\delta$ for the second disease. δ is a parameter that is estimated and it measures the dependence of each disease on the shared pattern.

For example, this joint model for two diseases could be written down as:

$$\begin{aligned} O_i^{(d)}|E_i^{(d)},\theta_i^{(d)} &\sim Po(E_i^{(d)}\theta_i^{(d)}),\ d=1,2 \\ \log(\theta_i^{(1)}) &= \alpha^{(1)} + \delta S_i + D_i^{(1)} \\ \log(\theta_i^{(2)}) &= \alpha^{(2)} + \frac{1}{\delta} S_i + D_i^{(2)} \end{aligned} \tag{5}$$

Here, $\alpha^{(d)}$ is a disease-specific intercept, S_i is the shared spatial pattern, and $D_i^{(d)}$ are disease-specific (spatial) patterns.

The model by Knorr-Held and Best (2001) can be extended to consider more than two diseases. For instance, Downing et al. (2008) develop a joint model for six smoking related cancers in the Yorkshire region of England. They used a Bayesian model with shared effects to explore the patterns of spatial correlation and to estimate the relative weight of some covariates like smoking and other shared risk factors.

Several authors have generalized the univariate spatial models to the multivariate case in a number of ways, such as the spatial factor modelling proposed by Wang and Wall (2003) or the smoothed analysis of variance proposed by Zhang, Hodges and Banerjee (2009). Other multivariate disease mapping proposals are based on Gaussian Markov random fields (Rue and Held, 2005) and multivariate conditional autoregressive distributions.

A multivariate conditional autoregressive distribution is a generalization of the conditional autoregressive distribution (Mardia, 1988). Gelfand and Vounatsou (2003) generalized the proper conditional autoregressive distribution to the multivariate setting. In Jin, Carlin and Banerjee (2005), the authors propose a conditional approach to the multivariate problem too. MacNab (2011) proposed a multivariate generalization of spatial structures beyond conditional autoregressive distributions, where the well-known convolution prior (Besag et al., 1991) is generalized. Martínez-Beneito (2013) proposed a novel framework that encompasses most of the models already proposed by reorga-

nizing the Kronecker products of covariance matrices as simple matrix products. This allows the combination of several different spatial structures with different multivariate dependence structures and avoid computations with Kronecker products and large covariance matrices. This last work has been reformulated in order to be more efficient in computational terms (Botella-Rocamora et al., 2015). Other recent approaches for the analysis of multivariate data in disease mapping include the smoothed analysis of variance (Marí-Dell'Olmo et al., 2014) in ecological studies.

Regarding the analysis of multivariate disease mapping models with several components in the linear predictor, different authors have already tackled this problem. Corberán-Vallet (2012) apply the shared components approach to the detection of disease outbreaks proposing a multivariate model in which spatial shared components are multiplied by indicator variables to select one of the components. Carroll et al. (2016) propose a space-time mixture model that includes in the linear predictor a purely spatial term, a spatio-temporal term or a mixture of the two. Carroll et al. (2017) apply these ideas to the spatio-temporal analysis of two types of respiratory cancers and allow for the temporal variation of the coefficients of the covariates. In Carroll et al. (2017), three different types of cancer are analysed jointly and they propose mixture models to choose among different spatial, temporal and spatio-temporal terms in the linear predictor. Finally, Lawson et al. (2017) present similar mixture models with spatially and spatio-temporally varying mixture parameters.

In the next section we develop a joint spatio-temporal model for multiple diseases. This model includes two types of spatial and temporal effects, to account for the shared pattern and allow for disease-specific patterns. In addition, the weights associated to the shared spatial and temporal effects retain the associations between different diseases with similar spatial or temporal variation. It is worth noting that our model provides a simpler and more modular specification of the different spatial and temporal effects in the model than the models discussed above and it is still able to find diseases with similar spatial and temporal patterns.

Our approach differs from previous literature in a number of ways. First of all, our goal is to detect similar spatial or temporal behaviors of different diseases in a simple way. The structure of our model is different as well, as it is not based on mixture models but on spatial and temporal shared components. The application is also different, because our aim is not to detect changes at the area level in space and time but to identify shared and specific spatial and temporal patterns that can lead to the identification of diseases with a similar aetiology.

4. Spatio-temporal joint modelling of multiple diseases

When modelling spatio-temporal data our aim is to identify shared and specific patterns of disease both in space and time. For this reason, our model will combine several ideas from the models outlined in Sections 2 and 3. In particular, our model is as follows:

$$
\begin{aligned}
O_{i,t}^{(d)} | E_{i,t}^{(d)}, \theta_{i,t}^{(d)} &\sim Po(E_{i,t}^{(d)} \theta_{i,t}^{(d)}) \\
\log(\theta_{i,t}^{(d)}) &= \alpha^{(d)} + \Phi_i^{(d)} + \Psi_t^{(d)}
\end{aligned}
\tag{6}
$$

Now, $\alpha^{(d)}$ are disease-specific intercepts, and $\Phi_i^{(d)}$ and $\Psi_t^{(d)}$ are spatial and temporal effects for disease d in area i and time period t, respectively. These two effects are defined by including disease-specific and shared patterns in the following way:

$$
\begin{aligned}
\Phi_i^{(d)} &= u_i^{(d)} + \delta_d^S U_i \\
\Psi_t^{(d)} &= v_t^{(d)} + \delta_d^T V_t
\end{aligned}
\tag{7}
$$

In the previous equation we can find shared and disease specific effects. The effect of the shared spatial effect U_i on the relative risk is modulated through weights δ_d^S. Similarly, the effect of the shared temporal pattern on the relative risk is controlled via weights δ_d^T.

The vectors of disease-specific and shared effects are defined using an intrinsic CAR specification:

$$
\begin{aligned}
u^{(d)} &\sim CAR(W, \tau_d^S) \; d = 1,2,3; \quad U \sim CAR(W, \tau_0^S) \\
v^{(d)} &\sim CAR(Q, \tau_d^T) \; d = 1,2,3; \quad V \sim CAR(Q, \tau_0^T)
\end{aligned}
\tag{8}
$$

Here, W is the spatial adjacency matrix and Q defines a temporal adjacency structure. Finally, τ_d^S, τ_d^T, τ_0^S and τ_0^T are the precisions of the different effects.

Note that the previous model does not account for space-time interactions. These could be included but additional constraints would be needed (Knorr-Held, 2000, Richardson et al., 2006, Goicoa et al., 2018), making the model more complex. By adding disease-specific spatial and temporal effects we are already allowing for departures from any shared spatial and temporal trends. This means that the diseases under study may have different spatial or temporal behavior. Furthermore, uncorrelated random effects have not been considered for the same reason.

Regarding the priors for the remainder of the parameters, several options can be considered. Disease specific intercepts $\alpha^{(d)}$ are assigned improper flat priors. Spatial and temporal weights have been assigned a log-Normal prior with zero mean and precision 1/5.9 (similarly as in Downing et al., 2008).

This assumes that weights are positive, but the prior 0.25 and 0.975 quantiles are 0.0086 and 116.8319, which allows for ample variation in the values of the weights. This will also imply that the weights can take very small values. Small weights will produce a negligible effect of the shared spatial or temporal terms in the linear predictor even if the weights are not exactly zero. Hence, it is not necessary that the diseases in the model are correlated in advance as the model can produce very small weights in this case.

Constraining the weights to be positive also means that high values of the shared effects will indicate a similar higher mortality pattern for all the diseases with non-

negligible weights. This is important in order to interpret the results and the role of the shared spatial and temporal terms.

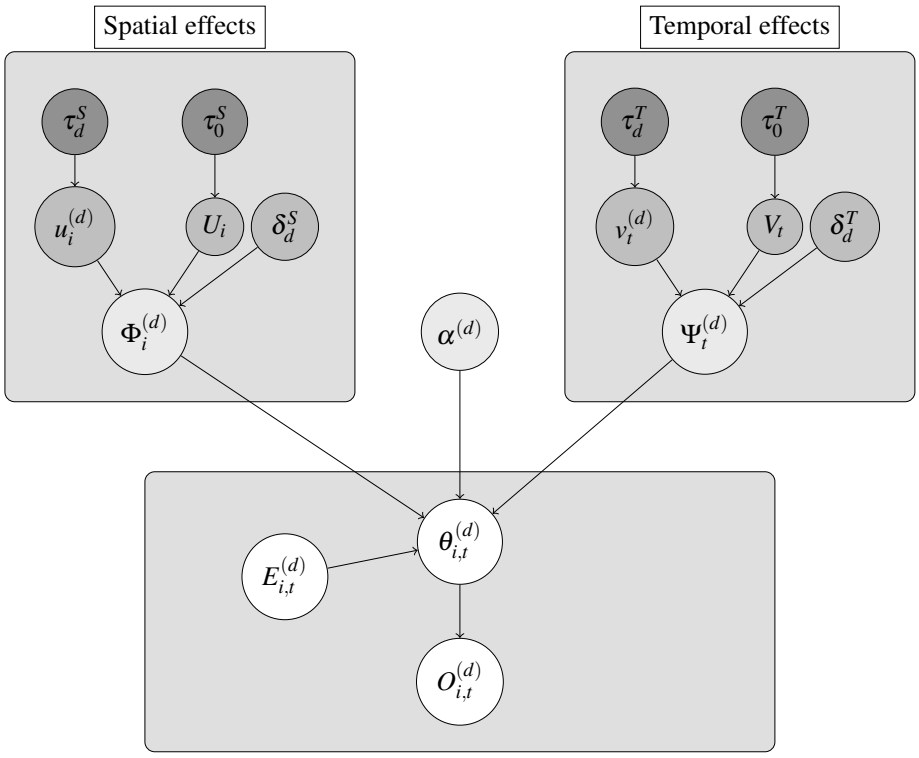

Figure 1: *Graphical representation of the joint spatio-temporal model.*

For the scale parameters of the random effects in the model we suggest trying different priors in order to conduct a sensitivity analysis on the results and investigate how different priors impact on the estimates of the relative risks and other parameters in the model. We propose fitting three different models in which all scale parameters have the same priors. First of all, we propose a uniform distribution between 0 and 10 on the standard deviations, which seems to be less informative than inverted Gammas on the precisions (Gelman, 2006). Following Gelman (2006), a half-Cauchy (with scale parameter equal to 25) as a prior for all standard deviations in the model could also be used. Finally, as an inverted Gamma is a common choice for the precision priors, a third model could be considered in which all precisions have an inverted Gamma with parameters 0.01 and 0.01 as prior.

In this model, terms U_i and V_i in the model are multiplied by disease specific weights. This may cause an identifiability problem between weights δ_d^S and δ_d^T, and the scale of the effects, i.e., precisions τ_0^S and τ_0^T. For this reason, improper priors on these parameters are not recommended. Furthermore, precisions τ_0^S and τ_0^T can be set to 1 so that the scale of spatial and temporal shared effects is incorporated into weights δ_d^S and δ_d^T.

Having said this, we have not observed any identifiability problem of effects $\Phi_i^{(d)}$ and $\Psi_t^{(d)}$ in the models fitted in the example in Section 5.

Spatial dependence between two or more diseases can be assessed by looking for correlation of weights $\{\delta_d^S\}_{d=1}^D$ in the posterior joint distribution. Similarly, temporal dependence can be assessed with the joint posterior correlation of weights $\{\delta_d^T\}_{d=1}^D$. For this reason, we will produce plots of the bivariate posterior distributions of $(\delta_k^S, \delta_l^S)_{k\neq l}$ and $(\delta_k^T, \delta_l^T)_{k\neq l}$ for all pairs of diseases to assess any posterior correlation between the weights. Furthermore, for a single disease, spatio-temporal interactions can also be inspected by considering correlations in the joint posterior distribution of (δ_d^S, δ_d^T). This analysis based on the bivariate joint posterior distributions is shown in the example developed in Section 5 using the MCMC output given that INLA focuses on marginal inference.

5. Example: Joint spatio-temporal disease mapping in Spain

In order to assess the qualities and properties of the model presented in the previous section, we develop here an example on the analysis of three causes of death in Spain. We have considered oral cavity (which includes lip, bucal cavity and pharynx), esophagus and stomach cancer. The International Classification of Disease (ICD-10) codes for the three causes that we are studying are C00-C14 for the oral cavity cancer, C15 for the esophagus cancer and C16 for the stomach cancer. All these are cancers of the upper gastrointestinal tract and are relatively frequent. Ferlay et al. (2012) has pointed out that gastric cancers were estimated to be the fourth most common cancer and the second leading cause of death in both sexes in 2008. Furthermore, oral cavity and pharyngeal cancers ranked eighth in number of new cancer cases and deaths. Also, esophageal cancer ranked sixth in terms of the number of deaths and ninth in terms of cases.

In Spain, López-Abente et al. (2007, 2014) and Aragonés et al. (2007) have studied the spatial and temporal trends of these cancers. They have provided evidence of the similarities among the spatial and temporal trends of these cancers. In particular, their analysis of oral cavity, pharynx and esophagus supported the hypothesis of shared risk factors (which could be preventable factors), such as alcohol consumption and smoking (Seoane-Mato et al., 2014). These tumors also share a South-North geographical pattern in Spain.

Population and mortality data have been obtained from the Spanish Office for National Statistics (INE). Population data contains records by age group and gender from 1996 to 2014. Mortality data comprises all deaths in Spain from 1985 to 2014, for which cause of death, age, gender and other relevant information is available.

In this analysis, the number of deaths per province in peninsular Spain in the period 1996 to 2014 has been considered. The expected number of cases per province and sex has been computed using as reference the age-specific mortality rates and the population from years 1996 to 2014. The analysis has been carried out at the province level for both

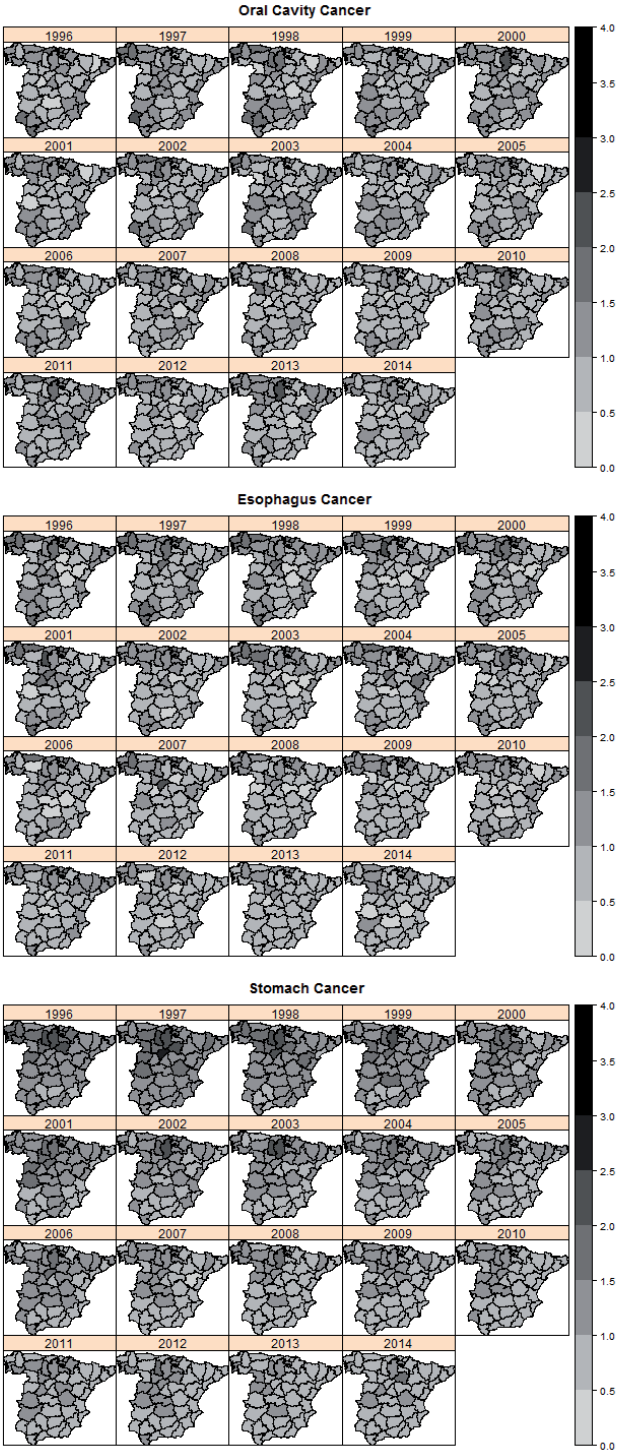

Figure 2: *Standardized mortality ratios* $O_{i,t}^{(d)}/E_{i,t}^{(d)}$.

sexes together. See López-Abente et al. (2014) for a discussion on the importance of the criteria for computing the expected number of cases in a spatio-temporal analysis.

Figure 2 shows the standardized mortality ratios for the three causes of death. Oral cavity and esophagus cancers seem to have a similar spatio-temporal pattern, whilst stomach cancer shows a different pattern. However, the three causes seem to have a region of high risk in the north of the country. These spatial patterns have already been described by Aragonés et al. (2009); López-Abente et al. (2014a,b) for stomach cancer and by Aragonés et al. (2007) for esophageal cancer for slightly different time periods to the one considered now. Furthermore, López-Abente et al. (2014); Seoane-Mato et al. (2014) also describe a decreasing temporal pattern of the risk for stomach and esophageal cancers. Finally, López-Abente et al. (2007) provide a spatial analysis of a number of types of cancer from 1989 to 1998 in Spain at the municipality level. Although our analysis has been conducted at different spatial and temporal levels, we observe a very similar pattern and we expect these patterns to show up in the analysis and to be picked up by the different effects in our model.

The model that we have fitted to the data is the one described in Section 4. The results that we show here correspond to the model with uniform priors on the standard deviations of the spatial and temporal random effects. We have also fitted the same model using half-Cauchy on the standard deviations and inverted Gamma priors on the precision parameters. A summary is provided in the sensitivity analysis in Section 5.4. Models have been fitted using the WinBUGS software (Lunn et al., 2000) using the R2WinBUGS package (Sturtz, Ligges and Gelman, 2005) for the R software (R Core Team, 2016). Regarding the MCMC simulations, we have used 4 different chains with 200,000 simulations each, of which 10% (i.e., 20,000) were used as a burn-in and we have kept one in 200 simulations to reduce autocorrelation.

In addition, INLA has been used to estimate the posterior marginals of the parameters of the models presented above. However, given the way in which INLA computes the approximations, a uniform between zero and infinity has been used instead of a uniform between 0 and 10 on the standard deviations. Details on the construction of the priors for INLA as provided in Appendix A, and computational details and R code to fit the models using MCMC and INLA are provided in the supplementary materials provided with this paper available from https://github.com/becarioprecario/joint_st_disease_mapping_INLA.

5.1. Spatial analysis

First of all, we will consider the analysis of the different spatial effects in the model. Figure 3 shows the posterior means of the total spatial effect $\Phi_i^{(d)}$ (i.e., sum of shared plus specific effects). MCMC and INLA provide very close estimates of the posterior means. Oral cavity and esophagus cancer show very similar spatial patterns, with areas of high risk in the north-west and southwest. This pattern is similar to the spatial distribution of

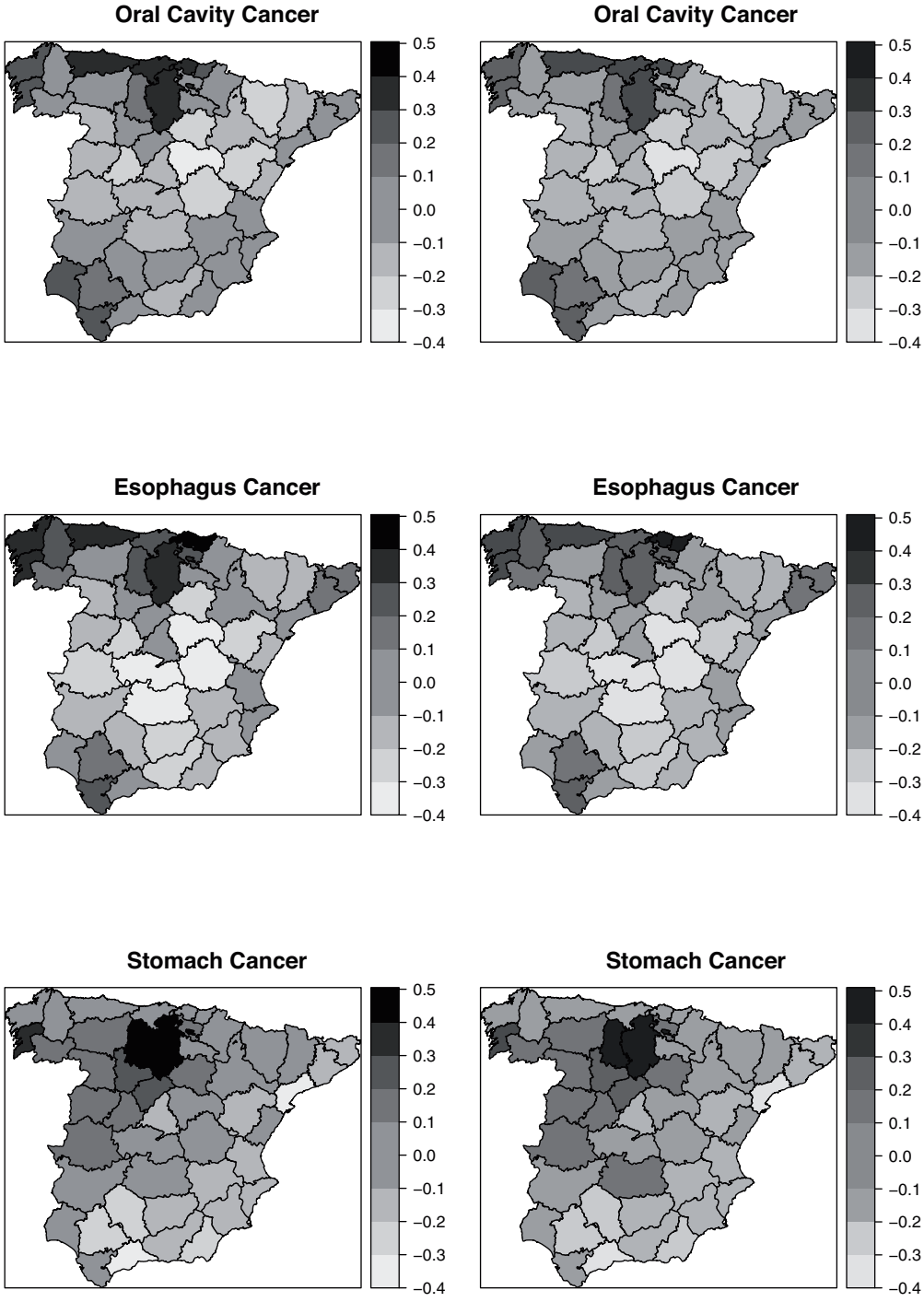

Figure 3: *Posterior means of the spatial effect* $\Phi_i^{(d)} = u_i^{(d)} + \delta_d^S U_i$ *for MCMC (left) and INLA (right).*

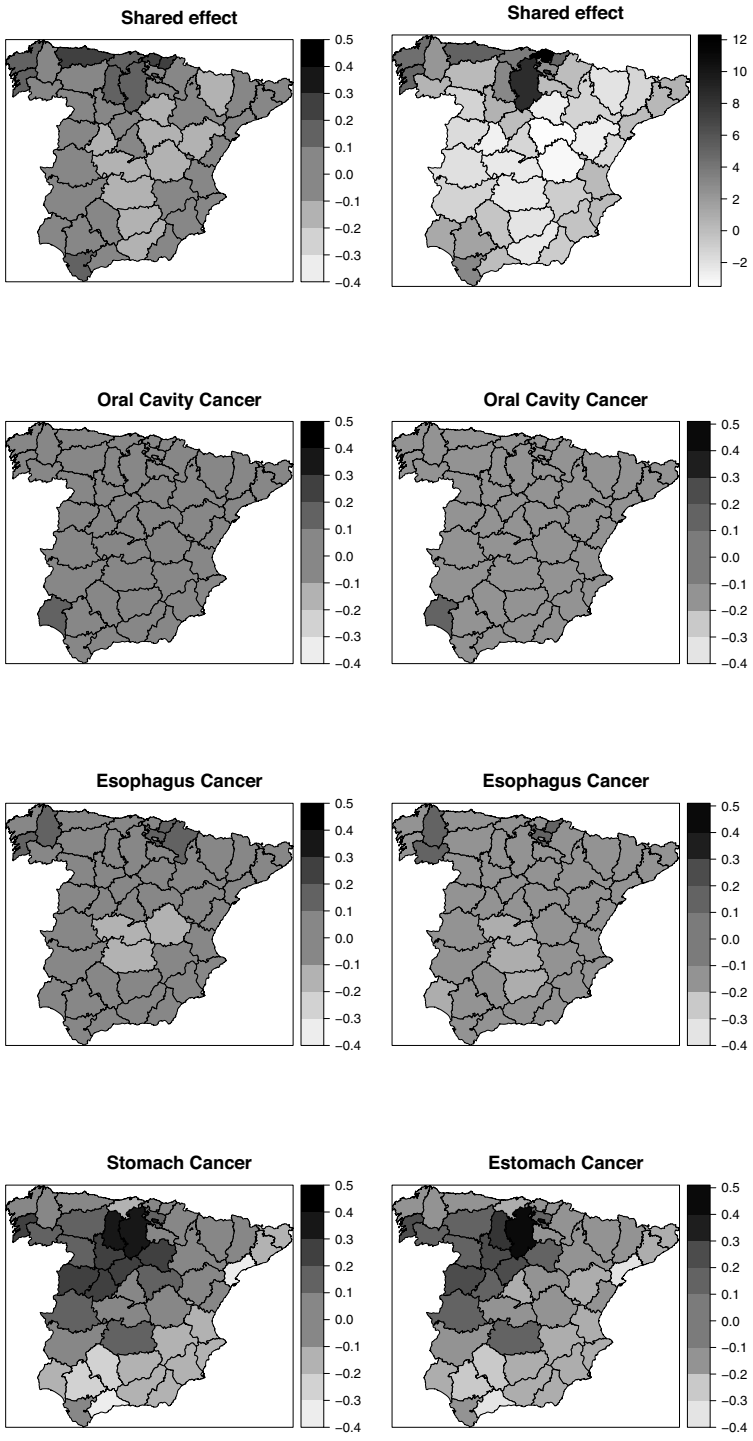

Figure 4: *Posterior means of shared spatial effect U_i (top maps) and disease specific spatial effects $u_i^{(d)}$ for MCMC (left) and INLA (right).*

Table 1: *Summary statistics of the weights for shared spatial and temporal effects for MCMC (left) and INLA (right).*

	MCMC				INLA			
Parameter	**Mean**	**Median**	**2.5% q.**	**97.5% q.**	**Mean**	**Median**	**2.5% q.**	**97.5% q.**
δ_1^S	1.455	1.425	0.854	2.263	0.716	0.371	0.022	3.501
δ_2^S	1.555	1.538	0.864	2.469	0.766	0.399	0.024	3.735
δ_3^S	0.551	0.546	0.332	0.914	0.062	0.031	0.001	0.297
δ_1^T	0.867	0.807	0.434	1.484	0.204	0.088	0.006	1.122
δ_2^T	0.943	0.892	0.515	1.483	0.270	0.109	0.007	1.530
δ_3^T	1.279	1.220	0.659	2.148	0.395	0.164	0.120	2.210

esophageal cancer between 1989 and 1998 described in Aragonés et al. (2007). Stomach cancer shows a different spatial pattern with some areas of high risk in the north. These findings are similar to the spatial patterns described by Aragonés et al. (2009) in the period 1994-2003, and López-Abente et al. (2014a,b) in the period 1989-2008.

Posterior means of the shared and disease specific spatial effects are displayed in Figure 4, and Table 1 shows summaries of the posterior distribution of the weights δ_d^S of the shared spatial effect for each disease. The estimates of the different spatial effects with MCMC and INLA are very similar but for the shared spatial term, which seems to show a very similar pattern but at different scales. This is probably due to a mild identifiability problem between the spatial weights and the precision of the shared spatial term. However, as stated above, total spatial effects are very similar between MCMC and INLA.

In all maps in Figure 4, a few areas of high risk can be found in the north part of the country. Also, the specific spatial pattern for stomach cancer seems to show more extreme values than those for oral cavity and esophagus cancer. This may be due to the lower dependence of stomach cancer on the shared spatial pattern (as seen in Table 1) which makes the specific pattern to account for most of its spatial pattern.

Table 1 shows the differences in the estimation of the weights between MCMC and INLA. This is due to the fact that INLA is not able to identify well the weights and the precision of the effects. However, as seen in Figure 3 and Figure 4 the estimates of the spatial effects are very close between MCMC and INLA. Furthermore, the results obtained with INLA also support a stronger dependence on the spatial shared term for oral cavity and esophagus cancers, and a similar dependence on the temporal shared term for all three cancers. As stated earlier, a simple way to have a better identification of the weights is by fixing the precisions of the shared terms.

Regarding the weights on the shared spatial component U_i, oral cavity and esophagus cancers seem to have a very similar weight which is significantly higher than one. Stomach cancer has a lower weight, which is significantly lower than one. This means that oral cavity and esophagus cancer have a higher dependence on the shared spatial effect, i.e., the spatial pattern is very similar to the shared pattern.

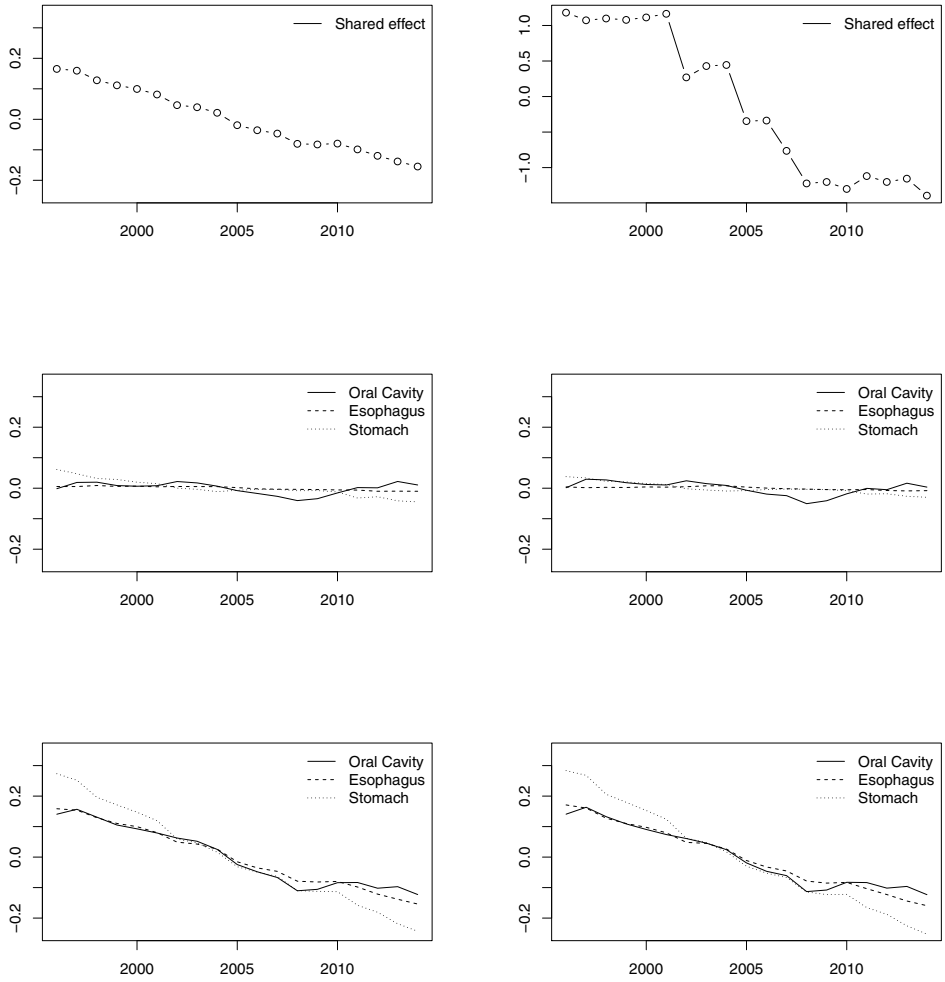

Figure 5: *Posterior means of shared temporal effect V_t (top), specific temporal effect $v_t^{(d)}$ (middle) and total temporal effect $\Psi_t^{(d)} = v_t^{(d)} + \delta_j^T V_t$ (bottom) for MCMC (left) and INLA (right).*

Finally, the dependence between oral cavity and esophagus cancers is confirmed in the analysis of weights δ_i^S on the shared spatial component shown in Section 5.3 using the MCMC output. As seen in Figure 8 (bottom row), the bivariate distribution of weights associated to oral cavity and esophagus cancers shows a strong correlation. This correlation is inexistent in the plots of each one of these causes against esophagus cancer.

5.2. Temporal analysis

Similarly, posterior means of shared and specific temporal effects are shown in Figure 5. The shared temporal effect clearly indicates a decrease in risk over time and MCMC and

INLA provide similar estimates but on different scales. Now, all three cancers show a very similar temporal pattern. The disease-specific and total temporal trends estimated by MCMC and INLA are very close.

The specific temporal effects of the three cancers do not indicate a strong departure from the shared temporal pattern and these three specific temporal patterns have an effect very close to zero for all the years. It is worth noting that the shared temporal effect captures the overall decreasing trend in time whilst the disease-specific effects are negligible, with estimates very close to zero for all years. Seoane-Mato et al. (2014) describe temporal trends for different types of tumors in the period 1952-2006. For all the causes analysed in this paper, they report a decreasing trend from 1996 to 2006, which is consistent with our findings.

Summary statistics of weights δ_d^T for the shared temporal trend are shown in Table 1. As in the spatial case, MCMC and INLA provide estimates in different scales due to the different identifiability between the temporal weights and the precision of the shared temporal term. However, the estimates of the total temporal trends are very similar between MCMC and INLA.

Oral cavity and esophagus cancers have very similar weights, with stomach cancer having a slightly higher weight. In this case, all three diseases seem to have a strong dependance on the shared temporal pattern as the weights are very close to one, which also explains the weak disease-specific temporal trends.

A joint analysis of weights δ_d^T could be done using the MCMC output to assess temporal dependence between diseases. Figure 8 (top row) shows bivariate plots of these weights. Oral cavity and esophagus cancer clearly show some correlation. Now, stomach cancer also shows a positive correlation with the other two types of cancer.

5.3. Joint spatio-temporal analysis

So far, we have analysed the results with a focus on the spatial or temporal patterns. Figure 6 shows the smoothed spatio-temporal relative risks obtained with our model. The three types of cancers considered in this study show correlation of the temporal weights. However, stomach cancer shows a different spatio-temporal pattern.

Figure 7 shows the probability of having a relative risk higher than one. Looking at the areas of high probability we can find areas of increased risk. Again, oral cavity and esophagus cancers show a very similar spatio-temporal pattern, which also seems to be persistent over time. Furthermore, the areas of high risk in our analysis are very similar to the ones reported by Aragonés et al. (2007) in the 1989-1998 period for esophageal cancer, where regions of high risk were found in the northwest and southwest of Spain.

Stomach cancer shows a persistent spatial pattern at the beginning of our study period that changes at the end, as seen in Figure 7. The areas of high risk are similar to those found by Aragonés et al. (2009) in the period from 1994 to 2003, and López-Abente et al. (2014) in the 1989-2008 period.

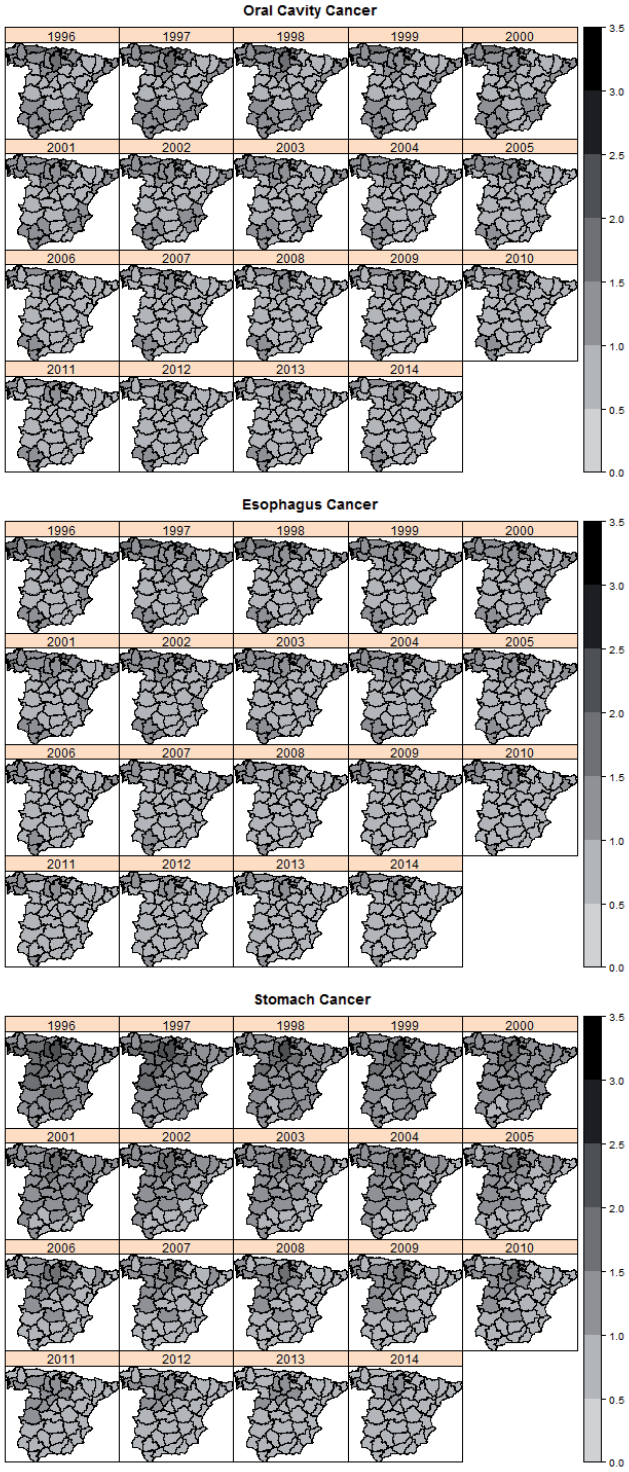

Figure 6: *Posterior means of spatio-temporal relative risks* $\theta_{i,t}^{(d)}$.

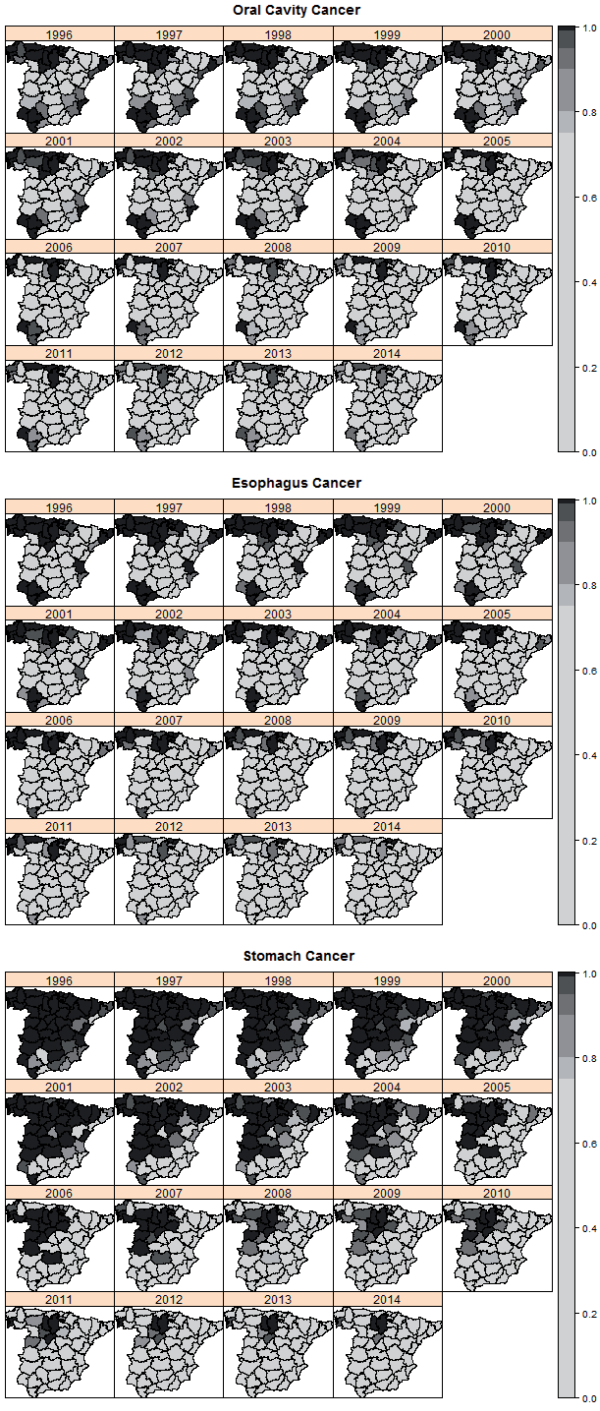

Figure 7: *Probabilities of having an estimation of the relative risk* $\theta_{i,t}^{(d)}$ *greater than 1 to identify areas of high risk.*

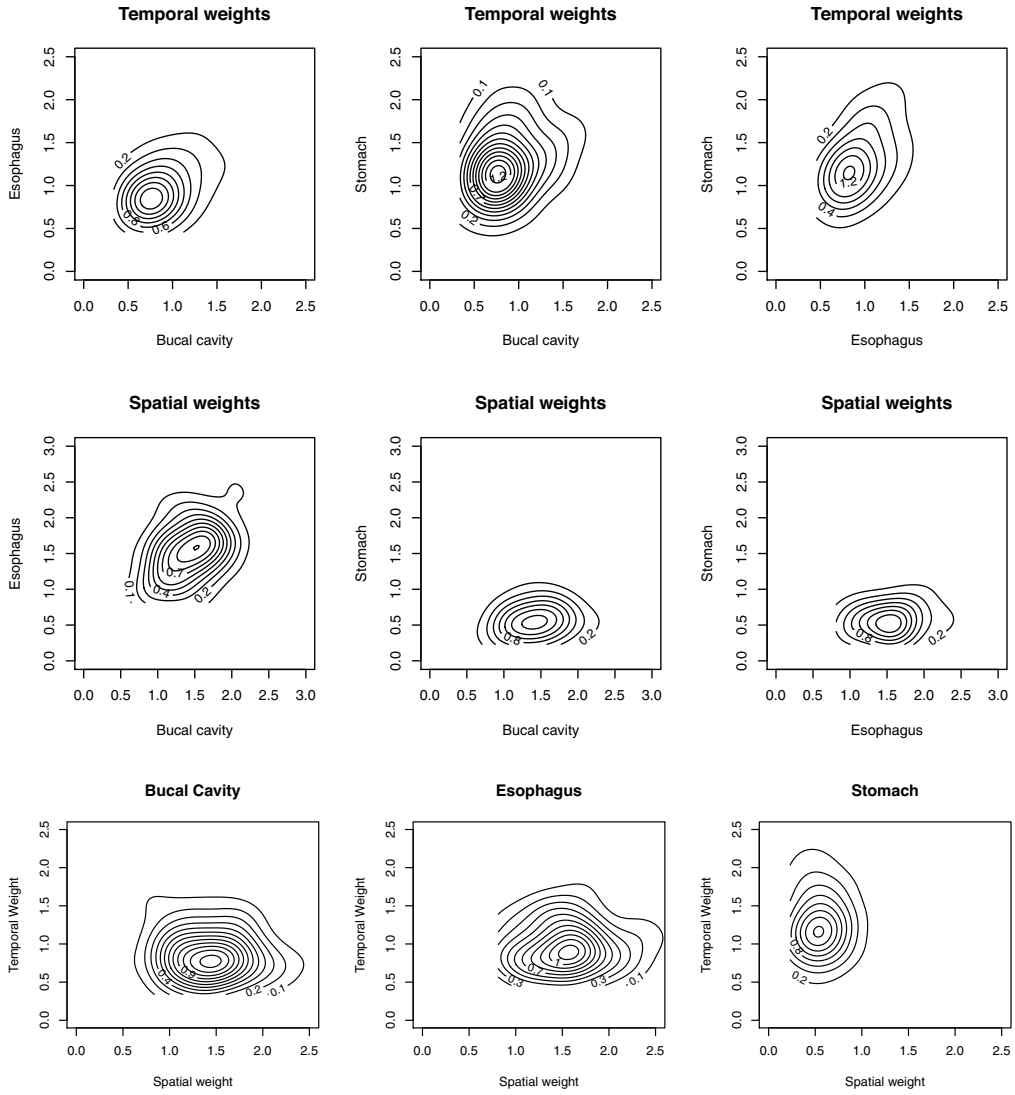

Figure 8: *Bivariate posterior distributions of weights δ_d^T (top row) and δ_d^S (middle row), and bivariate posterior distribution of the spatial and temporal weights for a given type of cancer (bottom row).*

The analysis of the posterior bivariate distribution of weights on the spatial and temporal shared effects can help to assess dependence between the different causes of death considered. Figure 8 shows the posterior bivariate distribution of each pair of weights δ_t^T (top row) and δ_i^S (middle row). In this case, spatial and temporal weights appear to be independent from each other and no correlation can be observed in the plots.

Figure 6 and Figure 7 have been produced using the MCMC output, but INLA provided similar estimates. Figure 8 has been created from the MCMC output given that it requires the bivariate joint posterior distributions of each pair of weights. These joint

distributions can be approximated with INLA, but we have preferred to use the MCMC output instead.

5.4. Sensitivity analysis

The results shown so far correspond to the model described in Section 4 with uniform priors on the standard deviations of the random effects. We have decided to use these priors because several authors (see, for example, Gelman, 2006) have questioned the use of the inverted Gamma as a prior for the precisions in the model. For this reason, we have conducted a sensitivity analysis by considering different priors for the scale parameters of the random effects in the model. We have fitted three versions of the joint spatio-temporal models where each of three options for the priors of the variances are used, as explained at the end of Section 4.

Our results show that the estimates of the relative risks do not differ when different priors for the variances of the random effects are used. Spatial and temporal effects are very similar too, as well as the estimates of the spatial and temporal weights.

6. Discussion

We have presented a Bayesian hierarchical model for the joint analysis of spatio-temporal public health data. It combines ideas from other models for spatio-temporal disease mapping (Richardson et al., 2006; Abellan et al., 2008; Guangquan et al., 2012) and the joint analysis of several diseases (Downing et al., 2008). In this way, our new model allows us to define common and specific spatial patterns of disease that are able to identify similarities and differences in the distribution of the relative risks associated to each disease. Dependence on the common spatial and temporal patterns are governed by disease-specific weights, which can help to identify diseases with shared spatial and temporal patterns. The model has been fitted using MCMC and INLA, and both methods provide similar estimates of the main effects in the model.

The analysis of the specific spatial effects can be used to detect areas with a different trend for a given disease. Similarly, by inspecting disease-specific temporal effects it is possible to highlight diseases with a different temporal variation. Furthermore, this model can help to highlight areas of high risk by looking at the posterior probabilities of the relative risk. These probabilities can also be used to detect shared patterns of high risk among several diseases.

In the example shown in this paper, we have studied oral cavity, esophagus and stomach cancers in Spain from 1996 to 2014. Our model has been able to identify a common spatial pattern between oral cavity and esophagus cancers, and a different spatial pattern for stomach cancer. It has also been able to identify that all these three types of cancer have a very similar temporal variation. All these findings are consistent with other

similar studies (Aragonés et al., 2007, Seoane-Mato et al., 2014, López-Abente et al., 2014a,b, Aragonés et al., 2009) and they support the hypothesis of a strong relationship between the spatio-temporal distribution of oral cavity and esophagus cancers.

Finding diseases with similar spatial and temporal patterns is important in public health because these patterns are often caused by similar risk factors. Hence, by identifying diseases with similar patterns it is also likely that some shared risk factors will be discovered as well. This can clearly be seen in our example as oral cavity and esophagus cancers show strong similar patterns and incidence of these cancers depends of preventable factors such as alcohol consumption and smoking (Seoane-Mato et al., 2014).

Finally, compared to other recent developments for multivariate disease mapping (see, for example, Botella-Rocamora et al., 2015, and the references therein) our model provides a simple and modular specification of different shared and specific patterns that can be explored to identify trends in the geographical and temporal distribution of disease. In the example presented in this paper we have only considered three different causes of death, but the model can be easily extended to a larger number of diseases simply by including the corresponding spatial and temporal effects.

In the future, we plan to extend this model in a number of ways. First of all, an automatic procedure could be implemented to assess for the need of the different disease-specific terms in the model. For example, in our example the disease-specific temporal trends can probably be removed given that all diseases have a very similar temporal variation. For this, being able to fit the models with INLA quickly will allow us to explore different models faster. Furthermore, model assessment criteria implemented in INLA can play an important role here to select the best model for the data.

Another way to extend this model is by clustering diseases into groups so that only diseases within the same group share spatial and temporal terms. This would involve creating a new indicator parameter for each disease to identify to which group it belongs. By computing the posterior probabilities of these indicator variables it is possible to assess what diseases have a shared spatial and temporal variation. Given that this will require exploring a large number of models, INLA will be an important asset in the implementation of this method.

A User-defined priors in INLA

INLA provides a simple way to define priors using the `muparser` library. For computational reasons, INLA works with an internal representation of the parameters and instead of dealing with the precision parameter of the random effects τ, it works with $\theta = \log(\tau)$. Hence, the prior must be specified on θ. Here, we will follow Ugarte, Adin and Goicoa (2016) to derive the two non-implemented priors on the standard deviation σ of the random effects.

First of all, note that $\sigma = (1/\tau^{1/2}) = 1/\exp(\theta/2) = \exp(-\theta/2)$. Hence, the prior on θ is defined as

$$\pi(\theta) = \pi(\sigma)|\frac{\partial\sigma}{\partial\theta}|$$

Also, note that

$$|\frac{\partial\sigma}{\partial\theta}| = \frac{1}{2}\exp(-\theta/2)$$

For the uniform prior on σ, this must be a uniform between 0 and infinity (for computational reasons), i.e., $\pi(\sigma) \propto 1$. Hence,

$$\pi(\theta) \propto 1 \cdot (\frac{1}{2}\exp(-\theta/2))$$

Similarly, the half-Cauchy prior with scale parameter γ on σ is defined as

$$\pi(\sigma|\gamma) = \frac{2}{\pi\gamma(1+(\sigma/\gamma)^2)}$$

Hence, the prior on θ is defined as

$$\pi(\theta|\gamma) = \frac{2}{\pi\gamma[1+(\exp(-\theta/2)/\gamma)^2]} \cdot (\frac{1}{2}\exp(-\theta/2))$$

Priors must be passed to INLA in the log-scale and constants can be dropped (but this will change the estimate of the marginal likelihood). Hence, the uniform prior can be set in INLA as

$$\log(\pi(\theta)) \equiv -\theta/2$$

and the half-Cauchy prior can be set using

$$\log(\pi(\theta|\gamma)) \equiv \log(1+\exp(-\theta)/\gamma^2) - \theta/2$$

Implementation details can be found at
https://github.com/becarioprecario/joint_st_disease_mapping_INLA.

Acknowledgments

This work has been supported by grants PPIC-2014-001-P and SBPLY/17/180501/000491, funded by Consejería de Educación, Cultura y Deportes (Castilla-La Mancha, Spain) and Fondo Europeo de Desarrollo Regional, and grant MTM2016-77501-P, funded by the Ministerio de Economía y Competitividad (Spain). F. Palmí-Perales was supported by a doctoral scholarship awarded by the University of Castilla-La Mancha (Spain). We also thank Prof. Håvard Rue for his help with the implementation of the model using INLA.

References

Abellan, J., Richardson, S. and Best, N. (2008). Use of space-time to investigate the stability of patterns of disease. *Enviromental Health Perspectives*, 116, 1111–1119.

Aragonés, N., Pérez-Gómez, B., Pollán, M., Ramis, R., Vidal, E., Lope, V., García-Pérez, J., Boldo, E. and López-Abente, G. (2009). The striking geographical pattern of gastric cancer mortality in Spain: environmental hypotheses revisited. *BMC cancer*, 9, 1.

Aragonés, N., Ramis, R., Pollán, M., Pérez-Gómez, B., Gómez-Barroso, D., Lope, V., Boldo, E., García-Pérez, J. and López-Abente, G. (2007). Oesophageal cancer mortality in Spain: a spatial analysis. *BMC cancer*,7, 1.

Banerjee, S., Carlin, B. and Gelfand, A. (2014). *Hierarchical Modeling and Analysis for Spatial Sata*. Crc Press.

Besag, J., York, J. and Mollié, A. (1991). Bayesian image restoration, with two applications in spatial statistics. *Annals of the Institute of Statistical Mathematics*, 43, 1–59.

Botella-Rocamora, P., Martínez-Beneito, M. and Banerjee, S. (2015). A unifying modeling framework for highly multivariate disease mapping. *Statistics in Medicine*, 34, 1548–1559.

Carroll, R., Lawson, A. B., Faes, C., Kirby, R. S., Aregay, M. and Watjou, K. (2016). Spatio-temporal bayesian model selection for disease mapping. *Environmetrics*, 27, 466–478.

Carroll, R., Lawson, A. B., Faes, C., Kirby, R. S., Aregay, M. and Watjou, K. (2017). Extensions to multivariate space time mixture modeling of small area cancer data. *International Journal of Environmental Research and Public Health*, 14, 503.

Carroll, R., Lawson, A. B., Kirby, R. S., Faes, C., Aregay, M. and Watjou, K. (2017). Space-time variation of respiratory cancers in South Carolina: a flexible multivariate mixture modeling approach to risk estimation. *Annals of Epidemiology*, 27, 42–51.

Corberán-Vallet, A. (2012). Prospective surveillance of multivariate spatial disease data. *Statistical Methods in Medical Research*, 21, 457–477.

Downing, A., Forman, D., Gilthorpe, M., Edwards, K. and Manda, S. (2008). Joint disease mapping using six cancers in the Yorkshire region of England. *International Journal of Health Geographics*, 7, 1.

Elliot, P., Wakefield, J., Best, N. and Briggs, D. (2000). *Spatial Epidemiology: Methods and Applications*. Oxford University Press.

Ferlay, J., Shin, H., Bray, F., Forman, D., Mathers, C. and Parkin, D. (2012). Cancer incidence and mortality worldwide: Iarc cancerbase no. 10 [internet]. international agency for research on cancer, Lyon, France. globocan 2008 v1. 2.

Gelfand, A. and Vounatsou, P. (2003). Proper multivariate conditional autoregressive models for spatial data analysis. *Biostatistics*, 4, 11–15.

Gelman, A. (2006). Prior distributions for variance parameters in hierarchical models. *Bayesian Analysis*, 1, 515–534.

Gilks, W., Richardson, S. and Spiegelhalter, D. (1996). *Markov Chain Monte Carlo in Practice*. Boca Raton, Florida: Chapman & Hall.

Goicoa, T., Adin, A., Ugarte, M. D. and Hodges, J. S. (2018). In spatio-temporal disease mapping models, identifiability constraints affect pql and inla results. *Stochastic Environmental Research and Risk Assessment*, 32, 749–770.

Guangquan, L., Best, N., Hansell, A., Ahmed, I. and Richardson, S. (2012). Baystdetect: detecting unusual temporal patterns in small area data via bayesian model choice. *Biostatistics*, 13, 695–710.

Jin, X., Carlin, B. and Banerjee, S. (2005). Generalized hierarchical multivariate car models for areal data. *Biometrics*, 61, 950–961.

Knorr-Held, L. (2000). Bayesian modelling of inseparable space-time variation in disease risk. *Statistics in Medicine*, 19, 2555–2567.

Knorr-Held, L. and Best, N. (2001). A shared component model for detecting joint and selective clustering of two diseases. *Journal of the Royal Statistical Society, Series A*, 1, 73–85.

Lawson, A. (2013). *Bayesian Disease Mapping: Hierarchical Modeling in Spatial Epidemiology*. CRC press.

Lawson, A. B., Carroll, R., Faes, C., Kirby, R. S., Aregay, M. and Watjou, K. (2017). Spatiotemporal multivariate mixture models for bayesian model selection in disease mapping. *Environmetrics*, 28, e2465.

López-Abente, G., Aragonés, N., García-Pérez, J. and Fernández-Navarro, P. (2014). Disease mapping and spatio-temporal analysis: importance of expected-case computation criteria. *Geospatial Health*, 9, 27–35.

López-Abente, G., Aragonés, N., Pérez-Gómez, B., Pollán, M., García-Pérez, J., Ramis, R. and Fernández-Navarro, P. (2014). Time trends in municipal distribution patterns of cancer mortality in Spain. *BMC cancer*, 14, 1.

López-Abente, G., Ramis, R., Pollán, M., Aragonés, N., Pérez-Gómez, B., Gómez-Barroso, D., Carrasco, J., Lope, V., García-Pérez, J., Boldo, E. and García-Mendizabal, M. (2007). *Atlas Municipal de Mortalidad por Cáncer en España, 1989-1998*. Madrid: Instituto de Salud Carlos III.

Lunn, D., Thomas, A., Best, N. and Spiegelhalter, D. (2000). WinBUGS – a Bayesian modelling framework: concepts, structure, and extensibility. *Statistics and Computing*, 10, 325–337.

MacNab, Y. (2011). On gaussian markov random fields and bayesian disease mapping. *Statistical Methods in Medical Research*, 20, 49–68.

Mardia, K. (1988). Multi-dimensional multivariate gaussian markov random fields with application to image processing. *Journal of Multivariate Analysis*, 24, 265–284.

Marí-Dell'Olmo, M., Martínez-Beneito, M., Gotsens, M. and Palència, L. (2014). A smoothed ANOVA model for multivariate ecological regression. *Stochastic Environmental Research and Risk Assessment*, 28, 695–706.

Martínez-Beneito, M. (2013). A general modelling framework for multivarite disease mapping. *Biometrika*, 100, 539–553.

Martínez-Beneito, M., Botella-Rocamora, P. and Banerjee, S. (2016). Towards a multidimensional approach to bayesian disease mapping. *Bayesian Analysis*, 1, 239–259.

R Core Team (2016). *R: A Language and Environment for Statistical Computing*. Vienna, Austria,: R Foundation for Statistical Computing.

Richardson, S., Abellan, J. J. and Best, N. (2006). Bayesian spatio-temporal analysis of joint patterns of male and female lung cancer risks in Yorkshire (UK). *Statistical Methods in Medical Research*, 15, 385–407. PMID: 16886738.

Rue, H. and Held, L. (2005). *Gaussian Markov Random Fields: Theory and Applications*. CRC Press.

Rue, H., Martino, S. and Chopin, N. (2009). Approximate Bayesian inference for latent Gaussian models by using integrated nested Laplace approximations. *Journal of the Royal Statistical Society, Series B*, 71 (Part 2), 319–392.

Seoane-Mato, D., Aragonés,N., Ferreras, E., García-Pérez, J., Cervantes-Amat, M., Fernández-Navarro, P., Pastor-Barriuso, R. and López-Abente, G. (2014). Trends in oral cavity, pharyngeal, oesophageal and gastric cancer mortality rates in Spain, 1952–2006: an age-period-cohort analysis. *BMC cancer*, 14, 1.

Sturtz, S., Ligges, U. and Gelman, A. (2005). R2WinBUGS: A package for running winbugs from R. *Journal of Statistical Software*, 12, 1–16.

Ugarte, M. D., Adin, A. and Goicoa, T. (2016). Two-level spatially structured models in spatio-temporal disease mapping. *Statistical Methods in Medical Research*, 25, 1080–1100. PMID: 27566767.

Wang, F. and Wall, M. (2003). Generalized common spatial factor model. *Biostatistics*, 4, 569–582.

Zhang, Y., Hodges, J. and Banerjee, S. (2009). Smoothed anova with spatial effects as a competitor to mcar in multivariate spatial smoothing. *The Annals of Applied Statistics*, 3, 1805.

SORT 43 (1) January-June 2019, 75-94 DOI: 10.2436/20.8080.02.80

Internalizing negative externalities in vehicle routing problems through green taxes and green tolls

Adrián Serrano-Hernández[1,*] and Javier Faulín[1]

Abstract

Road freight transportation includes various internal and external costs that need to be accounted for in the construction of efficient routing plans. Typically, the resulting optimization problem is formulated as a vehicle routing problem in any of its variants. While the traditional focus of the vehicle routing problem was the minimization of internal routing costs such as travel distance or duration, numerous approaches to include external factors related to environmental routing aspects have been recently discussed in the literature. However, internal and external routing costs are often treated as competing objectives. This paper discusses the internalization of external routing costs through the consideration of green taxes and green tolls. Numeric experiments with a biased-randomization savings algorithm, show benefits of combining internal and external costs in delivery route planning.

MSC: 90B06.

Keywords: Vehicle routing problem, biased randomization, green logistics, negative road externalities, internalization.

1. Introduction

Vehicle routing management is one of the most important operational activities in road freight transportation. Delivery routes are typically established by solving the NP-hard vehicle routing problem (VRP) in any of its variants (Caceres-Cruz et al., 2014; Toth and Vigo, 2014). However, the optimization of explicit operational costs is only one side of the coin. Delivery route planning has long focused on monetary aspects. Nevertheless, the negative externalities of road freight transportation related to air pollution, excessive noise levels, and traffic congestion are particularly noticeable in urban areas (European Union, 1999b; United Nations, 2016; United States Environmental Protection Agency, 2014; European Commission, 2009). In this context, different green

* Corresponding author: adrian.serrano@unavarra.es

[1] Institute of Smart Cities, Public University of Navarre, Spain.

Received: May 2018
Accepted: January 2019

logistics concepts aiming to reduce the negative impacts of road transportation have been presented (Bekta and Laporte, 2011; Gajanand and Narendran, 2013; Lin et al., 2014). Furthermore, the topic is still catching the interest of the academia as recent papers continue addressing the topic (Xiao et al., 2012; Kancharla and Ramadurai, 2018; Sawik, Faulin and Pérez-Bernabeu, 2017a, 2017b). In these papers, typically, some kind of emission estimation based on routing characteristics such as distance, load levels, vehicle type, road gradient, etc. are included in the optimization models. These estimations are then considered in the objective function in order to minimize the relevant variable.

By either focusing on monetary or environmental objectives, different factors are treated as competing variables, looking for either the cheapest solution or the least polluting option. Therefore, a way to internalize negative externalities into operational costs is of utmost interest. This paper proposes internalization through green taxes and green tolls, and evaluates the effects on company behaviours of such fiscal policies. Moreover, this paper reviews relevant literature about monetization of environmental costs and propose those values as taxation.

2. Literature review

Within the context of green logistics and road freight transportation, environmentally aware delivery route planning has received much attention in recent years (Helo and Ala-Harja, 2018). Next to new optimization problems arising from the use of new technologies such as electric vehicles (Juan et al., 2016) and the development of innovative supply chain strategies such as horizontal collaboration aimed at reducing routing related emissions (Serrano-Hernandez et al., 2017), especially the inclusion of green minimization objectives has been discussed. In this context, the green VRP (GVRP) focuses on minimizing fuel consumption instead of traditional cost- or distance based optimization targets (Erdogan and Miller-Hooks, 2012). The environmental routing impact is typically estimated with respect to the operating vehicle and some distinct criteria effecting predicted consumption/emission values. Especially travel speed, vehicle load levels, routing distances, and road gradients have been discussed (Bekta and Laporte, 2011; Demir, Bektas and Laporte, 2014; Lin et al., 2014).

Even though the GVRP is still a rather new topic, some optimization approaches have already been presented (Ubeda, Arcelus and Faulin, 2011). The energy minimizing VRP is defined by Kara, Kara and Kadri Yetis (2007), who propose a cost function for the VRP based on the product of vehicle load and travel distance. In Tavares et al. (2009), road gradient and vehicle weight is considered in optimizing fuel consumption in waste collection processes. The time dependent VRP is addressed by Kuo (2010). While the author considers different travel times and varying vehicle speed depending on the time of the day, the objective function is the minimization of fuel emissions considering vehicle loads and travel speed. The resulting model is solved with a simulated annealing metaheuristic, showing significant reductions of fuel consumption compared

to objectives based on the minimization of travel time/distance. A fuel consumption rate based on vehicle load levels (similar to the approach applied in this paper) is proposed in the work of Xiao et al. (2012). The potential benefits of applying environmentally driven models compared to traditional VRPs is also shown using a simulated annealing approach. Even though not directly related to the GVRP, the load dependent vehicle routing problem is closer examined by Zachariadis, Tarantilis and Kiranoudis (2015). The authors consider cargo weight variations in routing activities in which transported cargo accounts for a significant amount of vehicle weight. Fuel consumption is, however, not directly addressed in their work. Regarding internalization in logistics activities, it is noticeable the Abdallah et al. (2012) work who presented a novel approach to greening the supply chain. They took into account a carbon trading mechanism for pricing emissions. Later, they formulated a mixed integer program that minimizes the sum of supply chain costs and carbon trading costs.

More recently, some papers from Sawik et al. (2017a, 2017b) consider multicriteria approaches to deal with economic and environmental criteria at the same time. Nevertheless, in those works there is not an explicit internalization of environmental costs (i.e. no pricing is performed). Likewise, Xiao et al. (2012) also propose a multiobjective model for the GVRP in which speed is a relevant variable to optimize. However, they focus on their suggested algorithm and show the advantages of the hybrid quantum immune heuristic. Finally, the driving behaviour is taken into consideration in Kancharla and Ramadurai (2018) paper as they address the effect of acceleration on fuel consumption and emissions. Similarly, there is a lack of explicit internalization of external costs derived from the emissions, although they consider a richer model for estimating such emissions.

2.1. Routing externalities and internalization

Considering the definition by Laffont (2008), externalities are (...) indirect effects of consumption or production activity, that is, effects on agents other than the originator of such activity which do not work through the price system. Thus, it becomes clear that not only environmental aspects related to emission factors have to be included in routing optimization. According to Ranaiefar and Amelia (2011), negative routing externalities can be classified into four different impact areas: (*i*) economy, which include congestion, road damage and longer travel times; (*ii*) society, comprising accidents, visual intrusion and noise pollution; (*iii*) ecology, encompassing biodiversity destruction and climate change; and (*iv*) the environment, including waste, air, and water pollution. Many works have tried to physically measure such externalities. To this respect, Demir et al. (2015) give an extensive review on externalities modeling in which they accounted for several different methodologies to deal with emissions, noise, congestion and accidents. The same paper also includes a pricing section, concluding that further research should be made in that direction.

In order to incorporate such externalities in delivery route planning, monetary values have to be considered to be able to price these factors. Different approaches were carried out by Litman (2006) and Delucchi and McCubbin (2010) reports. In the extensive Litman (2006) one, it is reviewed plenty of prior works regarding transportation costs (internal and external). Noise and air pollution are visited listing various circumstances to estimate the external cost. For instance, noise costs depend on the type of vehicle, density of the area, type of road and daytime. According to their revision, the 34 tonne-truck noise costs range from USD(2007) cents 0.0088 to USD(2007) cents 0.235294 per tonne and mile whereas the Delucchi and McCubbin (2010) one estimates in USD(2006) cents 0.0-5.3. On the other hand, air pollution cost is usually analysed from the "damage function" approach described by Adamowicz (2003). It consists of valuating the relationship in welfare due to a change in the emissions, mainly divided into different types of harmful emissions: CO_2, CO, PM_{10}, CH_4, and so on. Later, a price is assigned to each based on health care costs. Then, physical emissions are calculated and translated into monetary units using the previous prices. In the report, Litman (2006) concluded the automobile air pollution costs range from USD(2007) cents 0.0032 to 0.7352 per tonne and mile similarly to Delucchi and McCubbin (2010) who estimated such costs in USD(2006) cents 0.1-18.7. Note that the high variation between these reports is due to the different characteristics in the vehicle, road and weather conditions, thus being one of the main drawbacks.

3. Internalization of green taxes and green tolls

The capacitated VRP can be formulated on a graph $G = (V,E)$. Vertex set $V = L \cup 0$ describes a subset $L = 1,2,\ldots,l$ of l customer nodes with demand $d_i \geq 0$ for all $i \in L$ and the central depot 0, at which a homogeneous fleet of vehicles with maximum capacity Q is located. Set $E = (i,j) : i,j \in V, i \neq j$ describes the connections between any two nodes i and j, whereas the travel distance $dist_{ij}$ to traverse any edge are assumed to be known. The objective of the (traditional) VRP is to minimize a distance-based costs function driven by a fleet of vehicles to serve a set of customers, subject to the following constraints: (*i*) vehicle routes start and end at the same depot, (*ii*) no customer node is visited twice, and (*iii*) vehicle capacities need to be adhered to.

Naturally, the objective of minimizing overall travel distance can be enhanced. Our approach introduces external costs $extCost_{ij}$ for each edge $(i,j) \in E$ that are made of green taxes t_{ij} and green tolls v_{ij}. Therefore, the full cost $fullCost_{ij}$ associated to each edge is described in Equation 1:

$$fullCost_{ij} = intCost_{ij} + extCost_{ij} = intCost_{ij} + t_{ij} + v_{ij} \tag{1}$$

The green taxes are charged on fuels so they will depend on fuel consumption whereas green toll costs are charged as tolls if the vehicle enters in high quality envi-

ronmental areas that may be somehow protected. Note that now we deal with a directed graph since $fullCost_{ij}$ may not be equal to $fullCost_{ji}$. A real example of a green toll is functioning in some European countries. Known as Eurovignette (European Union, 1999a), it is a road user charge for heavy vehicles to account for external costs of air and noise pollution, among other costs. Therefore, the objective function consists of two components: the traditional distance-based (internal) costs and the external costs, compounded by the green taxes and the green tolls.

1. Internal costs. These costs comprise driver wage, asset depreciation and fuel cost and can be summarized as shown in Equation 2 where C_d is a cost parameter per unit of distance for any edge.

$$intCost_{ij} = C_d\, dist_{ij} \tag{2}$$

2. External costs. Green tax costs are charged to fuel. Therefore, the amount of green tax paid is described in Equation 3, where C_t is a cost parameter per unit of fuel consumed φ_{ij}. On the other hand, the green toll is paid according to the environmental category of the area as described in Equation 4.

$$t_{ij} = C_t\, \varphi_{ij} \tag{3}$$

$$v_{ij} = \begin{cases} C_v^l, & \text{if node } j \text{ belongs to a low environmental} \\ & \text{value area and node } i \text{ does not} \\ C_v^m, & \text{if node } j \text{ belongs to a medium environmental} \\ & \text{value area and node } i \text{ does not} \\ C_v^h, & \text{if node } j \text{ belongs to a high environmental} \\ & \text{value area and node } i \text{ does not} \\ 0, & \text{otherwise} \end{cases} \tag{4}$$

Being $C_v^l \leq C_v^m \leq C_v^h$ Note that we distinguish three different quality areas in order to give more flexibility for policymaking. In this sense, consider a high quality environmental area those places that could be significantly affected by the transportation activity, i.e. national parks, biosphere reserves, world heritage sites, etc. The medium quality area is devoted for a lower level of protection such particular landscapes proposed by local/regional authorities. The rest of places could be categorized as low environmental quality area.

3.1. Measuring fuel consumption

Estimating properly the fuel consumption is of utmost interest in our work since most pollutants are released to the environment when fuel is burnt. Thus, we have used for this purpose the methodology proposed in Knörr et al. (2011) since it is updated, well documented, and takes into account upstream energy consumption (generation and dis-

tribution of energy), also known as well to tank (WTT). Note that this approach considers also the final pipeline energy consumption made in the transportation activity (the tank to wheel – TTW). As a combination of both, the WTT and the TTW, we get the well to wheel (WTW).

In such methodology, energy consumption is measured in megajoules and it depends on distance, payload, road slope, speed, and vehicle characteristics. All in all, for any given distance, the fuel consumption ϕ can be represented as a function of load weight as shown in Equation 5 where ϕ_e is the fuel consumption when empty, ϕ_f is the fuel consumption when fully loaded, P is the payload and Q is the vehicle capacity.

$$\phi = \phi_e + (\phi_f - \phi_e)P/Q \tag{5}$$

3.2. Pricing air pollution and GHG emissions- Estimating C_t

Air pollution is caused by emission of air pollutants like NOx, CO_2, non-methane volatile organic compounds ($NMVOC$), and particulate matters (PM) that affect people, vegetation, materials, and global climate. Climate change or global warming impacts of road transport are, mainly, generated by emissions of greenhouse gases (GHG): carbon dioxide (CO_2), nitrous oxide (N_2O) and methane (CH_4). Nevertheless, CO_2 is the dominant anthropogenic GHG, and the remaining GHG can be expressed as CO_2 equivalent (CO_{2e}) as described in Equation 6[1]:

$$CO_{2e} = CO_2 + 25CH_4 + 298N_2O \tag{6}$$

Table 1, based on Korzhenevych et al. (2014) shows average EU prices for 1 kg of pollutant component, in EUR(2010). On one hand, air pollution components are priced, generally, attending to the related health costs and crop losses. Later they are computed based on the average exposure. On the other hand, GHG, i.e CO_{2e}, are priced attending to prevention costs to reduce risk of climate change and the damage costs of increasing global temperature.

Table 1: *Prices for 1 kg of emitted component in EUR(2010), based on Korzhenevych et al. (2014).*

Component	Harmful effects	EUR(2010)/Kg
NOx	Smog, soil acidification	12.81
$NMVOC$	Smog, damage to health	1.89
SO_2	Soil acidification, damage to health	12.35
PM	Damage to health	47.73
CO_{2e}	Climate change	0.11

1. CO_{2e} is computed using the Global Warning Power (GWP) of the GHG relatively to the CO_2. To this respect, it is assumed that CO_2 GWP is 1, CH_4 GWP is 25 times the CO_2 GWP, and N_2O GWP is 298 times the CO_2 GWP. Further information can by found in the didactic document written by Brander (2012).

4. Solving approach

The vehicle routing problem (VRP) is one of the most studied problems in combinatorial optimization, with many real-world applications as well as logistics and transportation (Toth and Vigo, 2014). Since its appearance in 1959 by Dantzig and Ramser (1959), who made for the first time a formulation of the problem for a fuel distribution application, the study of the VRP problem has generated numerous research works and thousands of articles have been written about many variants of the classical problem (Caceres-Cruz et al., 2014). VRP is known to be a NP-hard problem and its exact solution can be only achieved for very small instances. Therefore, heuristics algorithms are widely used for solving the VRP. To this respect, the savings heuristic proposed by Clarke and Wright (1964) is still widely used because it is simple to implement and it returns relatively good and extremely fast solutions. Nevertheless, many improvements can be made to this classical heuristics in order to obtain better solutions.

A biased randomization of the classical savings heuristic is proposed in this paper following the ideas described in Grasas et al. (2017), Juan et al.(2015) and Juan et al. (2010) who showed the competitiveness of the proposed algorithm. This randomization is performed in the constructive phase using a probability distribution for selecting the nodes to merge. By doing so, every time the heuristic is executed, a different solution is returned that may outperform the best solution obtained so far. Therefore, the main difference of the randomized version of the savings heuristic is that it does not always pick the first position in the savings lists. Moreover, the biased adjective is added in such a way that the probability of selecting the nodes is not uniformly distributed but biased, contrary to greedy proposals. These biased randomized processes rely on the use of the geometric probability distribution, which is characterized by a single and bounded parameter (p). Actually, when p becomes closer to 1, the greedy behaviour of the heuristic is retrieved. Being an approach with few parameters, the algorithm does not require fine-tuning processes, which tend to be time consuming. The Figure 1 shows the flowchart of the proposed algorithm.

Given that we have to decide on the value of the aforementioned parameter (p), a learning mechanism for dynamically setting the value is implemented. Initially, we set the value at 0.2 as it is shown values belong to the (0.05, 0.25) interval provide a good performance of the algorithm (Juan et al., 2010). However, instead of using the same parameter value for all iterations we update it according to the results we are obtaining. We set the threshold for updating p at 5%. It means that if the current iteration gives a solution at least 5% worse than the best solution achieved so far, then the parameter value p is updated in the same proportion. For instance, consider the Table 2 in which we have a best solution of 100 obtained with parameter value of 0.2 and a current solution of 110 at iteration k. As our new solution is 10% worse than the best one, we will change the parameter value to 0.22 and 0.18 ($\pm$ 10%) for our next two iterations ($k+1$ and $k+2$). We now look into those two new solutions and three different outcomes are possible.

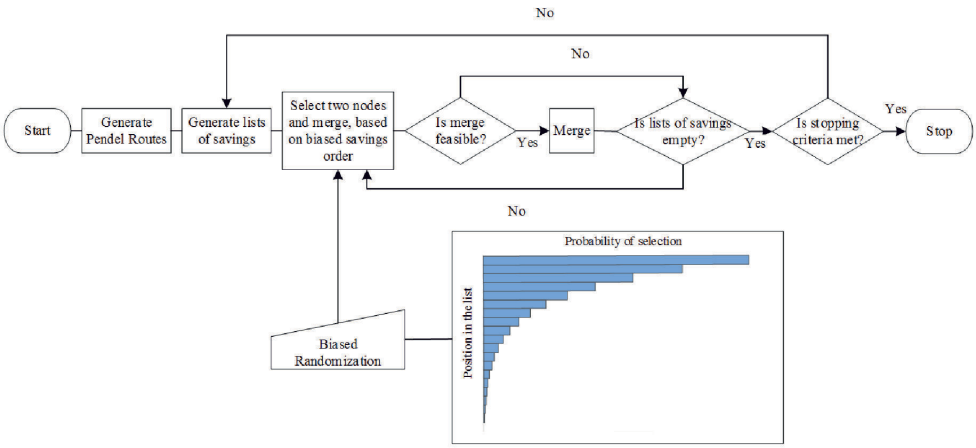

Figure 1: *Biased-randomized savings algorithm.*

Table 2: *Numerical example on the application of the learning mechanism.*

	Before iteration k Best solution= 100 $p = 0.2$	
	Iteration k Current solution= 110 $p = 0.2$	
Case A	**Case B**	**Case C**
Iteration $k+1$ Current solution= 115 $p = 0.22$	Iteration $k+1$ Current solution= 102 $p = 0.22$	Iteration $k+1$ Current solution= 115 $p = 0.22$
Iteration $k+2$ Current solution= 98 $p = 0.18$	Iteration $k+2$ Current solution= 104 $p = 0.18$	Iteration k+2 Current solution= 120 $p = 0.18$
Before Iteration k+3 Best solution= 98 $p = 0.18$	Before iteration k+3 Best solution= 100 $p = 0.2$	Before iteration k+3 Best solution= 100 $p = 0.253 \rightarrow p = 0.25$
		Before iteration $k+4$ Best solution= 100 $p = 0.187$

- Case A: a new best solution is achieved from one or both of those two iterations. Then for the next iteration it is considered the parameter value associated to the best solution obtained so far.
- Case B: no improvements are made and threshold is not exceeded. Then consider the previous solution and the initial parameter value.

- Case C: no improvements are made and threshold is exceeded. Then take the solution closest to the best solution (i.e. 150) and update the parameter value properly ($\pm$ 15%). Additionally, if the value of the parameter lays out of the previous interval (0.05, 0.25), then it is used the closest value in the interval. Later, the process continues.

5. Experimental results

5.1. Parameter setting

Augerat et al. (1995) set A instances are used as database because its wide implementation in which coordinates are random points in a [100, 100] grid and demands are generated from a uniform distribution $U(1,30)$ (Uchoa et al., 2017; Faulin et al., 2011). Vehicles are defined as a standard EURO V 26-40 truck, i.e. $Q = 26$ and curb weight = 14; for parameter setting, based on Ecotransit estimations (Knörr et al., 2011). Since upstream energy consumption is taken into account, conversion factors referring to WTW are used as shown in Table 3. A standard desktop with an Intel® Core™ i5- 3570 CPU @ 3.40 GHz and 8GB RAM was used to run all the experiments with a time limit set at 120 seconds.

Table 3: *Conversion factors for tank to wheel (TTW) and considering upstream energy consumption- well to wheel (WTW).*

	TTW	WTW
$MJ/l\,diesel$	35.86	42.68
$gr\,NOx/l\,diesel$	6.79	8.25
$gr\,NMVCO/l\,diesel$	0.12	0.93
$gr\,SO_2/l\,diesel$	0.01	1.08
$gr\,PM/l\,diesel$	0.11	0.16
$kg\,CO_{2e}/l\,diesel$	2.67	3.24

With the following estimated diesel fuel (liters) consumption function per kilometer based on payload, where parameters ϕ_e and ϕ_f have been replaced by their real values according to the aforementioned vehicle.

$$\phi = 0.2364 + 0.15P/26; 0 \leq P \leq 26 \tag{7}$$

The green tax is set through the economic valuation of air pollution and GHG described in the Table 1 of Section 3. The computation is shown in Table 4.

Table 4: *Details of computation of parameter C_t.*

Pollutant	kg emitted per liter	Price per kg (EUR)	Total
NOx	0.00825	12.61	0.1040
$NMVCO$	0.00093	1.73	0.0016
SO_2	0.00108	12.03	0.0130
PM	0.00016	47.43	0.0076
CO_{2e}	3.24000	0.11	0.3564
Total (C_t)			**0.4826**

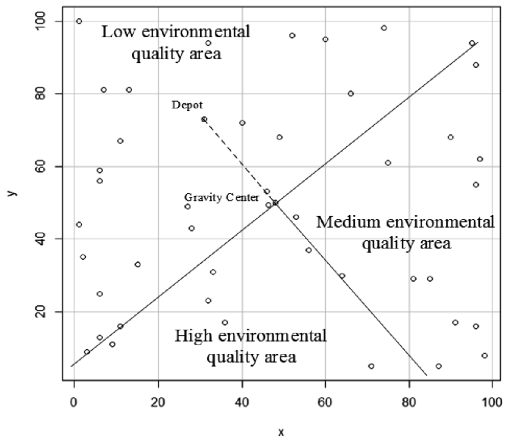

Figure 2: *Example of area allocation corresponding to the instance A-n45-k6.*

With respect to the cost parameter related to the internal costs, (C_d), it corresponds to the traditional distance-based VRP in which a cost parameter of 1.15 EUR/km has been applied. This value is considered appropriate for an average articulated truck that operates in Spain (Spanish Ministry of Transportation, 2016). Green tolls are set at 0, 10 and 30 for C_v^l, C_v^m, and C_v^h respectively. We consider those values appropriate in order to significantly influence driver behaviours. Nevertheless they are in line to those proposed in the EU for the Eurovignette (European Union, 1999a). Moreover, for our experiments, the nodes have to be assigned to one of the proposed environmental area: low, medium, and high. That process is executed for all instances in such a way that it guarantees that (i) the depot is always in the low environmental quality area, (ii) low environmental quality area represents 50% of the total area, (iii) medium environmental quality area represents 25% of the total area and, (iv) high environmental quality area represents 25% of the total area. The detailed description of the process is as follows. Firstly, the centre of gravity is computed with all the customers. Secondly, the perpendicular line at centre of gravity resulting from linking the depot to the centre of gravity is set as the border for the low environmental quality area that the depot belongs to. Thirdly, the other region is also divided into two subregions, following the line from linking the depot to the centre of gravity. Finally, the region with fewer customers is set as high environmental quality area and the other is set as medium environmental qual-

ity area. If there is a tie in customers, areas are randomly assigned. As an illustrative example, the Figure 2 shows the area allocation corresponding to the instance A-n45-k6.

5.2. Results

Detailed results are depicted in the Tables 5-8 considering the implementation of the green taxes (Table 5), green tolls (Tables 6 and 7) and both at the same time (Table 8). The structure of the instances is A-nX-kY where X is the number of nodes and Y is the number of vehicles available, i.e. maximum routes (Augerat et al., 1995). All tables have same structure. The first block contains the values corresponding to the traditional approach, i.e. the objective function is minimizing the internal costs (IC). Information about external costs (EC) was also saved when solving and it is shown in that approach. Finally, FC accounts for the full costs of operation; that is, including internal and external costs. The second block corresponds to the approach which includes EC; that is, objective function is minimizing the FC. Finally, a difference block is reported to compare the approaches.

Table 5 details the results when EC are included as green taxes. On average, including green taxes would lead to a reduction of 26.34% of external costs paid. That fact is achieved by increasing 1.57% the internal costs invoice. All in all, a reduction of 1.62% in FC is reached. Reasons behind such a reduction have to do with a much better utilization of vehicle load as well as a smarter way to do the deliveries. This is achieved by delivering high loads sooner in order to drive higher distances with a lighter vehicle. Particularly interesting is the case of instance A-n54-k7 where a huge reduction in EC is achieved by slightly increasing the IC. That suggest that in some cases there exist strong possibilities of reducing EC with simply taking them into account when optimizing. In general, those opportunities arise in bigger instances.

Table 6 depicts the results when implementing EC as green tolls. In that case a reduction of 14.38% in EC can be achieved, again slightly increasing the IC. Nevertheless, the effect on FC is lower than in the case of green taxes. Highly interesting is the information referred in the Table 7 in which H, M, L state for the fuel consumed on the areas of high, medium and low environmental quality. A last column (T) is the total fuel consumption within the three areas. Those results suggest the application of green tolls would lead to a reduction in the fuel consumed, i.e. emissions, in the high environmental quality area and an increase in the other two areas. On average, it is obtained a fuel consumption reduction of 2.84% in the high quality area and 0.37% in the medium quality area against an increase of 17.99% in the low environmental quality area. However, that also means that an increase in the fuel consumption is requested. Note that the behaviour of the medium quality area is irregular and it is not guaranteed a reduction in fuel consumption in that area as a consequence of implementing green tolls.

Finally, Table 8 combines the result of applying green taxes and green tolls as EC. As can be observed, an increase in IC of 1.23% is borne for reducing a 17.56% and a 7.52% the green taxes and green tolls costs, respectively. This finally led to a reduction of

Table 5: *Detailed results when green taxes are implemented.*

	Traditional Approach			Green Taxes					
Instance	IC	EC	FC	IC	EC	FC	Dif IC	Dif EC	Dif FC
A-n32-k5	905.05	118.77	1023.82	924.70	95.90	1020.60	2.17%	−19.26%	−0.31%
A-n33-k5	761.30	96.08	857.38	779.50	72.29	851.79	2.39%	−24.75%	−0.65%
A-n33-k6	853.30	109.11	962.41	872.25	87.24	959.49	2.22%	−20.05%	−0.30%
A-n34-k5	898.15	115.87	1014.02	916.36	87.64	1004.00	2.03%	−24.36%	−0.99%
A-n36-k5	922.30	120.21	1042.51	940.86	83.29	1024.16	2.01%	−30.71%	−1.76%
A-n37-k5	772.80	95.59	868.39	787.47	68.16	855.63	1.90%	−28.70%	−1.47%
A-n37-k6	1092.50	140.49	1232.99	1116.90	90.98	1207.89	2.23%	−35.24%	−2.04%
A-n38-k5	841.80	110.08	951.88	861.33	72.25	933.58	2.32%	−34.36%	−1.92%
A-n39-k5	955.65	122.63	1078.28	973.35	89.56	1062.91	1.85%	−26.97%	−1.43%
A-n39-k6	957.95	126.49	1084.44	970.61	94.75	1065.36	1.32%	−25.09%	−1.76%
A-n44-k7	1089.05	141.94	1230.99	1104.89	94.54	1199.43	1.45%	−33.40%	−2.56%
A-n45-k6	1097.10	140.97	1238.07	1114.84	105.63	1220.48	1.62%	−25.07%	−1.42%
A-n45-k7	1320.20	169.46	1489.66	1338.24	137.21	1475.45	1.37%	−19.03%	−0.95%
A-n46-k7	1054.55	137.60	1192.15	1069.46	91.78	1161.25	1.41%	−33.29%	−2.59%
A-n48-k7	1290.30	162.70	1453.00	1300.66	130.06	1430.72	0.80%	−20.06%	−1.53%
A-n53-k7	1173.00	150.63	1323.63	1185.15	118.21	1303.36	1.04%	−21.52%	−1.53%
A-n54-k7	1346.65	176.70	1523.35	1357.27	118.73	1476.00	0.79%	−32.81%	−3.11%
A-n55-k9	1239.70	159.80	1399.50	1249.74	104.87	1354.61	0.81%	−34.37%	−3.21%
A-n61-k9	1197.15	155.94	1353.09	1210.09	127.24	1337.33	1.08%	−18.40%	−1.16%
A-n65-k9	1373.10	177.67	1550.77	1382.27	143.37	1525.64	0.67%	−19.30%	−1.62%
Average	**1057.08**	**136.44**	**1193.52**	**1072.80**	**100.69**	**1173.48**	**1.57%**	**–26.34%**	**–1.62%**

Table 6: *Detailed results when green tolls are implemented.*

	Traditional Approach			Green Tolls					
Instance	IC	EC	FC	IC	EC	FC	Dif IC	Dif EC	Dif FC
A-n32-k5	905.05	60.00	965.05	905.05	60.00	965.05	0.00%	0.00%	0.00%
A-n33-k5	761.30	60.00	821.30	761.30	60.00	821.30	0.00%	0.00%	0.00%
A-n33-k6	853.30	70.00	923.30	861.38	60.00	921.38	0.95%	−14.29%	−0.21%
A-n34-k5	898.15	60.00	958.15	898.15	60.00	958.15	0.00%	0.00%	0.00%
A-n36-k5	922.30	60.00	982.30	922.30	60.00	982.30	0.00%	0.00%	0.00%
A-n37-k5	772.80	60.00	832.80	772.80	60.00	832.80	0.00%	0.00%	0.00%
A-n37-k6	1092.50	60.00	1152.50	1092.50	60.00	1152.50	0.00%	0.00%	0.00%
A-n38-k5	841.80	80.00	921.80	857.20	60.00	917.20	1.83%	−25.00%	−0.50%
A-n39-k5	955.65	60.00	1015.65	955.65	60.00	1015.65	0.00%	0.00%	0.00%
A-n39-k6	957.95	80.00	1037.95	959.02	60.00	1019.02	0.11%	−25.00%	−1.82%
A-n44-k7	1089.05	110.00	1199.05	1101.19	80.00	1181.19	1.11%	−27.27%	−1.49%
A-n45-k6	1097.10	90.00	1187.10	1113.83	60.00	1173.83	1.52%	−33.33%	−1.12%
A-n45-k7	1320.20	100.00	1420.20	1333.64	80.00	1413.64	1.02%	−20.00%	−0.46%
A-n46-k7	1054.55	120.00	1174.55	1063.81	90.00	1153.81	0.88%	−25.00%	−1.77%
A-n48-k7	1290.30	100.00	1390.30	1293.42	90.00	1383.42	0.24%	−10.00%	−0.50%
A-n53-k7	1173.00	110.00	1283.00	1185.64	90.00	1275.64	1.08%	−18.18%	−0.57%
A-n54-k7	1346.65	110.00	1456.65	1352.35	90.00	1442.35	0.42%	−18.18%	−0.98%
A-n55-k9	1239.70	140.00	1379.70	1250.93	110.00	1360.93	0.91%	−21.43%	−1.36%
A-n61-k9	1197.15	160.00	1357.15	1210.53	120.00	1330.53	1.12%	−25.00%	−1.96%
A-n65-k9	1373.10	160.00	1533.10	1388.13	120.00	1508.13	1.09%	−25.00%	−1.63%
Average	**1057.08**	**92.50**	**1149.58**	**1063.94**	**76.50**	**1140.44**	**0.61%**	**–14.38%**	**–0.72%**

Table 7: *Fuel consumption allocation within the three areas when green tolls are implemented.*

	Traditional Approach				Green Tolls							
Instance	H	M	L	T	H	M	L	T	Dif H	Dif M	Dif L	Dif T
A-n32-k5	62.90	71.50	111.72	246.12	62.03	71.48	135.65	269.16	−1.40%	−0.02%	21.43%	9.36%
A-n33-k5	56.23	57.71	85.27	199.20	53.62	56.58	111.61	221.82	−4.63%	−1.95%	30.90%	11.36%
A-n33-k6	22.92	66.18	137.04	226.14	22.13	64.94	166.11	253.18	−3.45%	−1.88%	21.21%	11.96%
A-n34-k5	46.33	60.09	134.26	240.68	45.72	59.05	149.92	254.69	−1.32%	−1.74%	11.67%	5.82%
A-n36-k5	51.59	61.24	137.08	249.91	49.79	60.71	155.80	266.30	−3.49%	−0.86%	13.65%	6.56%
A-n37-k5	55.12	50.60	92.63	198.36	53.94	50.97	108.72	213.63	−2.14%	0.72%	17.36%	7.70%
A-n37-k6	93.24	54.74	143.13	291.12	91.49	55.45	165.07	312.01	−1.88%	1.30%	15.32%	7.18%
A-n38-k5	53.32	59.96	115.24	228.52	52.66	59.84	138.29	250.78	−1.25%	−0.20%	20.00%	9.74%
A-n39-k5	76.84	51.15	126.40	254.39	73.75	50.52	145.14	269.41	−4.01%	−1.23%	14.82%	5.91%
A-n39-k6	78.89	64.09	119.33	262.31	77.16	63.40	137.93	278.49	−2.19%	−1.08%	15.59%	6.17%
A-n44-k7	92.37	79.68	122.20	294.25	88.78	80.65	150.02	319.44	−3.89%	1.22%	22.76%	8.56%
A-n45-k6	82.01	60.87	149.28	292.16	80.65	61.24	174.06	315.94	−1.67%	0.61%	16.60%	8.14%
A-n45-k7	106.29	87.68	157.41	351.37	101.85	88.70	175.05	365.60	−4.17%	1.16%	11.21%	4.05%
A-n46-k7	63.26	74.75	147.76	285.77	60.38	75.02	165.54	300.95	−4.54%	0.36%	12.03%	5.31%
A-n48-k7	127.47	68.63	141.09	337.19	124.75	68.46	180.44	373.64	−2.14%	−0.26%	27.89%	10.81%
A-n53-k7	48.96	99.92	163.28	312.16	47.33	101.87	184.50	333.71	−3.33%	1.96%	13.00%	6.90%
A-n54-k7	113.87	54.26	198.38	366.51	109.53	53.19	240.14	402.86	−3.81%	−1.97%	21.05%	9.92%
A-n55-k9	69.38	97.97	163.68	331.03	68.40	96.31	196.34	361.06	−1.41%	−1.69%	19.96%	9.07%
A-n61-k9	100.69	52.82	169.91	323.43	96.31	52.52	189.42	338.25	−4.35%	−0.57%	11.48%	4.58%
A-n65-k9	89.22	86.45	193.17	368.84	87.70	85.38	235.60	408.68	−1.70%	−1.24%	21.96%	10.80%
Average	**74.55**	**68.01**	**140.41**	**282.97**	**72.40**	**67.81**	**165.27**	**305.48**	**–2.84%**	**–0.37%**	**17.99%**	**7.95%**

Table 8: *Detailed results when green taxes and green tolls are implemented.*

	Traditional Approach				Green Taxes and Green Tolls							
Instance	IC	Tax	Toll	FC	IC	Tax	Toll	FC	Dif IC	Dif Tax	Dif Toll	Dif FC
A-n32-k5	905.05	118.77	60.00	1083.82	906.72	103.56	60.00	1070.28	0.18%	−12.81%	0.00%	−1.25%
A-n33-k5	761.30	96.08	60.00	917.38	766.91	82.04	60.00	908.95	0.74%	−14.61%	0.00%	−0.92%
A-n33-k6	853.30	109.11	70.00	1032.41	860.07	91.19	70.00	1021.25	0.79%	−16.43%	0.00%	−1.08%
A-n34-k5	898.15	115.87	60.00	1074.02	915.00	91.70	60.00	1066.70	1.88%	−20.86%	0.00%	−0.68%
A-n36-k5	922.30	120.21	60.00	1102.51	934.22	96.10	60.00	1090.32	1.29%	−20.05%	0.00%	−1.11%
A-n37-k5	772.80	95.59	60.00	928.39	781.03	78.49	60.00	919.52	1.06%	−17.89%	0.00%	−0.96%
A-n37-k6	1092.50	140.49	60.00	1292.99	1108.09	115.40	60.00	1283.49	1.43%	−17.86%	0.00%	−0.73%
A-n38-k5	841.80	110.08	80.00	1031.88	853.42	93.54	60.00	1006.96	1.38%	−15.03%	−25.00%	−2.42%
A-n39-k5	955.65	122.63	60.00	1138.28	973.14	97.84	60.00	1130.97	1.83%	−20.22%	0.00%	−0.64%
A-n39-k6	957.95	126.49	80.00	1164.44	960.86	102.88	70.00	1133.75	0.30%	−18.66%	−12.50%	−2.64%
A-n44-k7	1089.05	141.94	110.00	1340.99	1103.08	116.75	90.00	1309.83	1.29%	−17.75%	−18.18%	−2.32%
A-n45-k6	1097.10	140.97	90.00	1328.07	1115.89	113.17	90.00	1319.06	1.71%	−19.72%	0.00%	−0.68%
A-n45-k7	1320.20	169.46	100.00	1589.66	1339.97	133.07	90.00	1563.04	1.50%	−21.47%	−10.00%	−1.67%
A-n46-k7	1054.55	137.60	120.00	1312.15	1064.80	110.98	100.00	1275.78	0.97%	−19.34%	−16.67%	−2.77%
A-n48-k7	1290.30	162.70	100.00	1553.00	1310.75	133.01	100.00	1543.76	1.58%	−18.25%	0.00%	−0.60%
A-n53-k7	1173.00	150.63	110.00	1433.63	1191.74	122.81	100.00	1414.55	1.60%	−18.47%	−9.09%	−1.33%
A-n54-k7	1346.65	176.70	110.00	1633.35	1369.31	146.61	110.00	1625.92	1.68%	−17.03%	0.00%	−0.45%
A-n55-k9	1239.70	159.80	140.00	1539.50	1251.76	137.62	110.00	1499.38	0.97%	−13.88%	−21.43%	−2.61%
A-n61-k9	1197.15	155.94	160.00	1513.09	1209.60	133.47	130.00	1473.07	1.04%	−14.41%	−18.75%	−2.64%
A-n65-k9	1373.10	177.67	160.00	1710.77	1392.19	148.37	130.00	1670.56	1.39%	−16.49%	−18.75%	−2.35%
Average	**1057.08**	**136.44**	**92.50**	**1286.02**	**1070.43**	**112.43**	**83.50**	**1266.36**	**1.23%**	**–17.56%**	**–7.52%**	**–1.49%**

1.49% in the FC. Note that those figures are intermediate values to the one obtained when individually implemented the green taxes and the tolls. However the effect on FC is not so penalized and a reduction on fuel consumption (i.e. emissions) is obtained, contrarily to the implementation of just green tolls. At the same time, given the reduction of the green tolls, it is also gained a redistribution of fuel consumption from the highest environmental quality area to poorer ones.

6. Conclusions and future research

The consideration of external cost of routing is of utmost interest in present-day society that is increasingly suffering from air pollution, among other externalities. In this sense, literature about transportation externalities has mainly focused on achieving the greenest solution, usually omitting the economic implications of those approaches. However, they are both sides of the same coin and the treatment of environmental and economic objectives as competing variables would lead to a myopic solutions. For that reason, this article considers the internalization of external costs within the economic structure of the company. Thus, not only the traditional approach of distance-based internal costs of routing is taken into account but also the external costs are used as the objective function: that is, minimization of the full costs. Two protocols of internalizing are further analysed and discussed: green taxes and green tolls.

The effect of implementing green taxes is doubtless. In one hand, behaviour of companies when internalize their external costs through a green taxes significantly changes. That means that they plan a different route in order to minimize their full costs. On the other hand, this change allows for a noticeable reduction on fuel consumption, i.e. emissions. Green tolls effects are rather limited. Even though it also contributes to a change in the behaviour of the companies, it is not achievable a reduction in emissions. Instead, an increase and a redistribution of emissions within different environmental areas are obtained. However, those insights are pretty interesting from the policy maker's point of view since it is possible to transfer emissions from cherished environmental areas to a valueless ones. This is particularly applicable to protected areas such as national parks or high value landscapes. Through combining both mechanisms, an intermediate point is reached. That is, it is possible to change the delivery planning routes in order to make them greener, in the sense that a reduction of fuel consumption is achieved. Moreover, it is possible to obtain fairer scenarios, in the sense that emissions are transferred from high quality environmental areas to poorer ones; and economically supported, in the sense that a real cost function is minimized.

Many limitations arise as a consequence of the assumptions made, though. Firstly, the way fuel consumption is calculated can be fairly enriched with many other factors such as speed, road gradient, and so on. Secondly, parameters for the green taxes and green tolls can be also enchanted and plenty of sensitivity analysis can be performed in that direction. Finally, our results and conclusions are structured within a capacitated

vehicle routing problem and may be not valid in any other variant. Therefore, those limitations make the base for the future research lines: richer variants of the VRP, more exhaustive fuel consumption estimation and deeper analysis in the parametrization.

Acknowledgements

This work has been partially supported by the Spanish Ministry of Economy and Competitiveness (TRA2013-48180-C3-P and TRA2015-71883-REDT), FEDER, and the Ibero-American Program for Science and Technology for Development (CYTED2014-515RT0489). Moreover, we appreciate the financial support of the Erasmus+ Program (2016-1-ES01-KA108-023465) and the CAN Foundation in Navarre, Spain (Grant CAN2017-6101). Likewise, we want to acknowledge the financial support received by Spanish Ministry of Education (Grant FPU 2014-0024)

References

Abdallah, T., Farhat, A., Diabat, A. and Kennedy, S. (2012). Green supply chains with carbon trading and environmental sourcing: Formulation and life cycle assessment. *Applied Mathematical Modelling*, 36, 4271–4285.

Adamowicz, W. (2003). Valuation of environmental externalities. Handbook of Transport and the Environment. Emerald Group Publishing Limited.

Augerat, P., Belenger, M., Benavent, E., Corberan, A., Naddef, D. and Rinaldi, G. (1995). Computational results with a branch and cut code for the capacitated vehicle routing problem. Technical Report RR 949-M, University Joseph Fourier, Grenoble, France.

Bekta, T. and Laporte, G. (2011). The pollution-routing problem. *Transportation Research Part B: Methodological*, 45, 1232–1250.

Brander, M. (2012). Greenhouse gases, co2, co2e, and carbon: What do all these terms mean? report from econometrica. URL: https://ecometrica.com/assets/GHGs-CO2-CO2e-and-Carbon-What-Do-These-Mean-v2.1.pdf (accessed 22.03.2019).

Caceres-Cruz, J., Arias, P., Guimarans, D., Riera, D. and Juan, A. (2014). Rich vehicle routing problem: Survey. *ACM Computing Surveys*, 47.

Clarke, G. and Wright, J.W. (1964). Scheduling of vehicles from a central depot to a number of delivery points. *Operations Research*, 12, 568–581.

Dantzig, G.B. and Ramser, J.H. (1959). The truck dispatching problem. *Management Science*, 6, 80–91.

Delucchi, M. and McCubbin, D. (2010). External costs of transport in the u.s. technical report, university of california. URL: http://escholarship.org/uc/item/ 13n8v8gq (accessed 22.03.2019).

Demir, E., Bektas, T. and Laporte, G. (2014). A review of recent research on green road freight transportation. *European Journal of Operational Research*, 237, 775–793.

Demir, E., Huang, Y., Scholts, S. and Van Woensel, T. (2015). A selected review on the negative externalities of the freight transportation: Modeling and pricing. *Transportation Research Part E: Logistics and Transportation Review*, 77, 95–114.

Erdogan, S. and Miller-Hooks, E. (2012). A green vehicle routing problem. *Transportation Research Part E: Logistics and Transportation Review*, 48, 100–114.

European Commission (2009). Environmentally harmful subsidies (ehs): Identification and assessment, 2009. URL: http://ec.europa.eu/environment/enveco/taxation/pdf/Annex%205%20-%20Calculations%20from%20the%20case%20studies.pdf (accessed 22.03.2019).

European Union (1999a). Directive 1999/62/ec of the european parliament and of the council of 17 june 1999 on the charging of heavy goods vehicles for the use of certain infrastructures. URL: http://eur-lex.europa.eu/legal-content/EN/TXT/HTML/?uri=LEGISSUM:l24045b&from=EN (accessed 22.03. 2019).

European Union (1999b). Eu transport ghg: Routes to 2050 ii. the role of ghg emissions from infrastructure construction, vehicle manufacturing, and elvs in overall transport sector emissions, 2012. URL: http://www.eutransportghg2050.eu/cms/assets/Uploads/Reports/EU-Transport-GHG-2050-II-Task-2-FINAL-30Apr12. pdf (accessed 22.03.2019).

Faulin, J., Juan, A., Lera, F. and Grasman, S. (2011). Solving the capacitated vehicle routing problem with environmental criteria based on real estimations in road transportation: A case study. (pp. 323–334). volume 20.

Gajanand, M. and Narendran, T. (2013). Green route planning to reduce the environmental impact of distribution. *International Journal of Logistics Research and Applications*, 16, 410–432.

Grasas, A., Juan, A., Faulin, J., de Armas, J. and Ramalhinho, H. (2017). Biased randomization of heuristics using skewed probability distributions: A survey and some applications. *Computers and Industrial Engineering*, 110, 216–228.

Helo, P. and Ala-Harja, H. (2018). Green logistics in food distributiona case study. *International Journal of Logistics Research and Applications*, 21, 464–479.

Juan, A., Faulin, J., Ruiz, R., Barrios, B. and Caball, S. (2010). The sr-gcws hybrid algorithm for solving the capacitated vehicle routing problem. *Applied Soft Computing Journal*, 10, 215–224.

Juan, A., Mendez, C., Faulin, J., De Armas, J. and Grasman, S. (2016). Electric vehicles in logistics and transportation: A survey on emerging environmental, strategic, and operational challenges. *Energies*, 9 , 1–21.

Juan, A., Pascual, I., Guimarans, D. and Barrios, B. (2015). Combining biased randomization with iterated local search for solving the multidepot vehicle routing problem. *International Transactions in Operational Research*, 22, 647–667.

Kancharla, S. and Ramadurai, G. (2018). Incorporating driving cycle based fuel consumption estimation in green vehicle routing problems. *Sustainable Cities and Society*, 40, 214–221.

Kara, I., Kara, B. and Kadri Yetis, M. (2007). Energy minimizing vehicle routing problem. *Lecture Notes in Computer Science*, 4616 , 62–71.

Knörr, W., Seum, S., Schmied, M., Kutzner, F. and Anthes, R. (2011). Ecological transport information tool for worldwide transports-methodology and data update. DB Schenker Germany and International Union of Railways (UIC), Berlin, Hannover, Heidelberg.

Korzhenevych, A., Dehnen, N., Brocker, J., Holtkamp, M., Meier, H., Gibson, G., Varma, A. and Cox, V. (2014). Update of the handbook on external costs of transport. Technical Report, European Commission DG MOVE.

Kuo, Y. (2010). Using simulated annealing to minimize fuel consumption for the time-dependent vehicle routing problem. *Computers and Industrial Engineering*, 59, 157–165.

Laffont, J. (2008). Externalities. In The New Palgrave Dictionary of Economics, 2nd edition. Palgrave Macmillan, Basingstoke.

Lin, C., Choy, K., Ho, G., Chung, S. and Lam, H. (2014). Survey of green vehicle routing problem: Past and future trends. *Expert Systems with Applications*, 41, 1118–1138.

Litman, T. (2006). Transportation cost and benefit analysis, techniques, estimates and implications. victoria transport policy institute, second edition. URL: http: //www.vtpi.org/tca/ (accessed 22.03.2019).

Ranaiefar, F. and Amelia, R. (2011). Freight-transportation externalities. In Logistics Operations and Management. Elsevier, London.

Sawik, B., Faulin, J. and Pérez-Bernabeu, E. (2017a). Multi-criteria optimization for fleet size with environmental aspects. (pp. 61–68). volume 27.

Sawik, B., Faulin, J. and Pérez-Bernabeu, E. (2017b). A multicriteria analysis for the green vrp: A case discussion for the distribution problem of a spanish retailer. (pp. 305–313). volume 22.

Serrano-Hernandez, A., Juan, A., Faulin, J. and Pérez-Bernabeu, E. (2017). Horizontal collaboration in freight transport: Concepts, benefits, and environmental challenges. *SORT*, 41 , 1–22.

Spanish Ministry of Transportation (2016). Encuesta permanente de transporte de mercancias por carretera, technical report. URL: https://www. fomento.gob.es/NR/rdonlyres/B9FD898B-B888-4F99-8404-03537369CCC8/ 141950/EPTMC2016Texto.pdf in Spanish (accessed 22.03.2019).

Tavares, G., Zsigraiova, Z., Semiao, V. and Carvalho, M. (2009). Optimisation of msw collection routes for minimum fuel consumption using 3d gis modelling. *Waste Management*, 29 , 1176–1185.

Toth, P. and Vigo, D. (2014). *Vehicle routing: Problems, methods, and applications volume 18 of MOS-SIAM series on optimization*. (2nd ed.). Philadelphia, PA, USA: SIAM.

Ubeda, S., Arcelus, F. and Faulin, J. (2011). Green logistics at eroski: A case study. *International Journal of Production Economics*, 131 , 44–51.

Uchoa, E., Pecin, D., Pessoa, A., Poggi, M., Vidal, T. and Subramanian, A. (2017). New benchmark instances for the capacitated vehicle routing problem. *European Journal of Operational Research*, 257, 845–858. United Nations (2016). Statistical yearbook for asia and the pacific. URL: http://www. unescap.org/sites/default/files/ESCAP_SYB2016_SDG_baseline_report.pdf (accessed 22.03.2019).

United States Environmental Protection Agency (2014). Greenhouse gas emissions 1990- 2014. URL: https://www.epa.gov/sites/production/files/2017-04/documents/us-ghg-inventory-2016-main-text.pdf (accessed 22.03.2019).

Xiao, Y., Zhao, Q., Kaku, I. and Xu, Y. (2012). Development of a fuel consumption optimization model for the capacitated vehicle routing problem. *Computers and Operations Research*, 39, 1419–1431.

Zachariadis, E., Tarantilis, C. and Kiranoudis, C. (2015). The load-dependent vehicle routing problem and its pick-up and delivery extension. *Transportation Research Part B: Methodological*, 71, 158–181.

SORT 43 (1) January-June 2019, 95-112 DOI: 10.2436/20.8080.02.81

A probabilistic model for explaining the points achieved by a team in football competition. Forecasting and regression with applications to the Spanish league

Emilio Gómez-Déniz[1], Nancy Dávila-Cárdenes[1]
and José María Pérez-Sánchez[2]

Abstract

In the last decades, a lot of research papers applying statistical methods for analysing sports data have been published. Football, also called soccer, is one of the most popular sports all over the world organised in national championships in a round robin format in which the team reaching the most points at the end of the tournament wins the competition. The aim of this work is to develop a suitable probability model for studying the points achieved by a team in a football match. For this purpose, we built a discrete probability distribution taking values, zero for losing, one for a draw and three for a victory. We test its performance using data from the Spanish Football League (First division) during the 2013-14 season. Furthermore, the model provides an attractive framework for predicting points and incorporating covariates in order to study the factors affecting the points achieved by the teams.

MSC: 62J02, 62J20, 62F15.

Keywords: Covariate, football data, forecasting, regression, sport statistics, truncated distribution, weighted distribution.

1. Introduction

Football or soccer sparks interest not only among its supporters or fans, but has also become one of the most profitable industries, with a significant economic impact in infrastructure development, TV rights, sponsorships and transfers of players. According to Marian Otamendi, director of the World Football Summit, the international event of the football industry, gathering the most influential professionals, football could become the 17th largest world economy. Beyond the game, the growth in revenues and

[1] Department of Quantitative Methods and T*i*DES Institute. University of Las Palmas de Gran Canaria, Spain.
[2] Department of Applied Economic Analysis. University of Las Palmas de Gran Canaria, Spain.
Received: July 2018
Accepted: December 2018

the worldwide interest in football prove a successful and lucrative industry in which the aggregate revenue for the top 20 Money League clubs rose 6 percent to 7.9 billion € in 2016/17 (from Deloitte Football Money League 2018). Therefore, football and money go hand in hand and it is also interesting to see, as a simple example, how the emergence of the Chinese Super League and its financially and politically powerful clubs impact on the established European football business order.

Focusing on the game itself, a football competition is played under two basic types of tournaments around the world, the round robin and the knock-out. In the first one, each team plays against each opponent twice in home and away. The possible outcomes are win, draw or loss and the teams receive three, one or none points respectively depending on the result. At the end of a season, the team with the largest number of points wins the championship. This sport has become a multi-billion dollar business, where tactics are basic to the game and with many styles and playing formations available (see for example, (Brillinger, 2008)). Statisticians started to create models to analyse the several aspects involved in a football match, from predicting the outcome of soccer games to determine the best playing strategies, see Díaz and Núñez (2010) and Louzada, Suzuki and Salasar (2014), among others. According to Karlis and Ntzoufras (2000), research in soccer statistics can be divided into three main categories. The first one models the outcome of a game what can be used for ranking soccer teams and it may be extended to quantify the home effect. The second one investigates models for predicting about the number of goals scored by each team, and the third one concentrates in modelling other characteristics of the game. As pointed out by Rue and Salvesen (2006), the outcome of a soccer match depends on many factors, among these are: the home-away ground effect, the effect of injured players, psychological effects, etc. A good knowledge about these factors only determines the result up to significant, but not too dominant, random components. Other papers have focused on modelling football outcomes through the number of goals scored as Karlis and Ntzoufras (2003) who made use of the correlation of the goals scored by the two teams. Also, Rue and Salvesen (2006) predicted the outcome using a Bayesian methodology, whose predictive accuracy is better than other techniques. Finally, Baio and Blangiado (2010) predicted football results making use of a Bayesian hierarchical model.

The method for assigning three points for a win, no points awarded to the losing team and one point assigned to each team if the game ends with a draw, is a standard scoring system used in many sports leagues and tournaments, especially in football, field hockey, the rugby union, ice hockey, among others. However, the scoring system has changed over time. Many leagues and competitions originally awarded two points for a win and one point for a draw, before switching to the three points for a win system. The increase in rewards for a win from two to three points was adopted in 1995. Hon and Parinduri (2016), using regression discontinuity design as the empirical strategy, did not find evidence that the three-point rule makes games more decisive, increases the number of goals, or decreases goal differences, they found some evidence that the three-point rule increases the second-half goals of the losing first-half team. In this paper, far from pre-

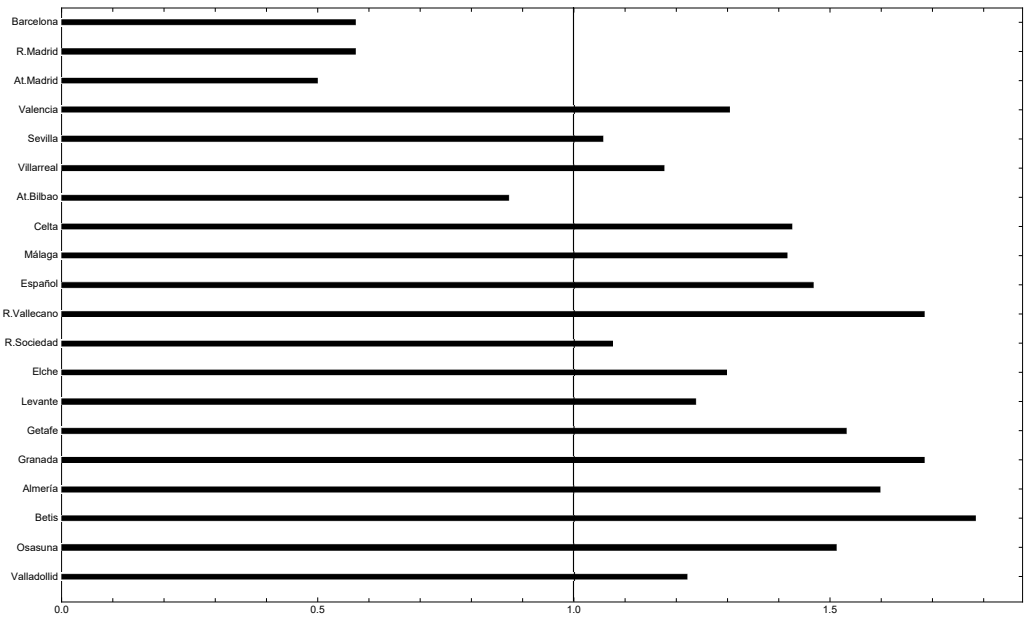

Figure 1: *Index of dispersion for the different teams in the Spanish League.*

dicting football results or analysing the effect of the scoring system in the results, we consider soccer matches played in a league in which the teams play against each other twice (home and away) where many explanatory variables may influence the result of a forthcoming soccer match. In this context, we analyse the factors that could affect the points achieved by a football team using data from the Spanish League during the 2013-2014 season. A similar analysis could be done to other leagues and sports for which a data base were available.

Empirical analysis shows that the sequence of points for teams with a lot of points, and therefore fighting for the title of the competition, is characterized for being under-dispersed (variance lower than the mean) while the teams with less points at the end of the competition show over-dispersion (variance larger than the mean). Let X be the random variable which gives us the sequence of points achieved by a team in a competition. The index of dispersion is defined as $\mathrm{ID} = \mathrm{var}(X)/\mathrm{E}(X)$. This value is represented in Figure 1 for the twenty teams of the Spanish Football League at the end of the competition in 2013-14 season. As we can see, this index is lower than 1 for the five best teams of the competition while is larger than 1 for the worst teams.

In this work, we present a probability model to analyse the points achieved by a team in a football match competition. That is, we propose a probability model which takes values in the set $\{0,1,2,3\}$ and with zero mass probability in $x = 2$. Furthermore, the model accommodates for over-dispersion and under-dispersion and it is suitable for incorporating covariates. The proposed model is simple and the estimation of the

parameters is easily obtained. Therefore, it is a candidate for fitting data sets of points in football match competitions.

The rest of this paper is organised as follows. The main model together with some of its most important properties are developed in Section 2. In Section 3, an application to the Spanish Football League in 2013-14 season is given. Finally, summary and discussion of the results are shown in the last Section.

2. Probabilistic model for points

The Poisson distribution represents a simple model as a starting point to construct a probability mass function (pmf) in the scenario we are considering. In football sport the number of goals scored by each team in a match has been assumed to follow a Poisson distribution by numerous authors. Some examples in which the Poisson distribution has been used to predict football results are Karlis and Ntzoufras (2000), Greenhough et al. (2002) and Saraivaa et al. (2016). However, to our knowledge, the distribution of the number of points, which is a discrete variable, has not been formally treated. Let us to start with the classical Poisson distribution whose pmf is given by,

$$f_\theta(x) = \frac{\theta^x \exp(-\theta)}{x!}, \quad x = 0, 1, \ldots, \ \theta > 0. \tag{1}$$

We need a random variable X which takes only 4 values, to say 0,1,2 and 3 and with the constraint that for $x = 2$ the mass of probability should be zero. Therefore, it has a two-parameter pmf of the form: $P(X = 0) = 1 - p - q$, $P(X = 1) = q$, $P(X = 2) = 0$ and $P(X = 3) = p$, with $0 < p < 1$, $0 < q < 1$, $p + q < 1$. The "probability generating function (pgf)" is $g(t) = 1 - p - q + qt + pt^3$ and $E(X) = q + 3p$. In order to simplify the model, we attend to the particular case $p = \theta^3\kappa(\theta)$ and $q = \theta\kappa(\theta)$, where

$$\kappa(\theta) = \frac{6}{24 + \theta(6 + \theta^2)}. \tag{2}$$

Thus, the expression

$$g_\theta(x) = \kappa(\theta)(x-2)^2\frac{\theta^x}{x!}, \quad x = 0, 1, 3 \tag{3}$$

defines a genuine pmf with support in $\mathcal{X} = \{0, 1, 3\}$. Recall that for a distribution with pmf $f_\theta(x)$, X with support in $\mathcal{X}$, depending on a vector of parameteres $\theta \in \Theta$, we can construct a new distribution with pmf (see for instance Fisher, 1934, Patil and Rao, 1978 and Harandi and Alamtsaz, 2013) using a weighted function, $w(x) > 0$,

$$g_\theta(x) = \frac{w(x)}{E_{f_\theta(X)}(w(X))} f_\theta(x), \tag{4}$$

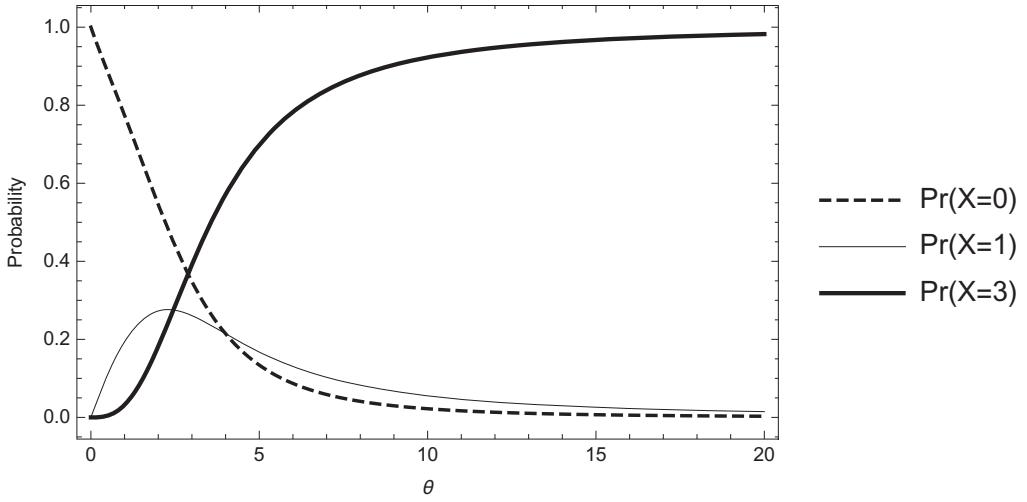

Figure 2: *Probabilities of victory, draw and defeat depending on θ.*

where it is assumed that $E_{f_\theta(X)}(w(X)) < \infty$, and w is a weighted function depending on X. Now, it is easy to see that the pmf given in (3) is a weighted version of the pmf given in (1) by taking $w(x) = (x-2)^2$ and restricting (truncating) its support to take only the values 0, 1 and 3. Therefore we are using truncation and weighting, where the latter can be viewed as a particular case of the first (see Johnson, Kemp and Kotz, 2005, p. 63 for details).

Figure 2 shows the graph of the values of p, q and $1-p-q$, i.e. the values of the probability of victory, draw and defeat, in the definition domain of θ parameter.

It can be easily proved that the following chains of inequalities are satisfied among the probabilities of the three events that are intended to be modelled through the pmf given in (3):

$$\begin{aligned}
&0 < \theta < 2.45: && \Pr(X=0) > \Pr(X=1) > \Pr(X=3),\\
&2.45 < \theta < 2.88: && \Pr(X=0) > \Pr(X=3) > \Pr(X=1),\\
&2.88 < \theta < 4: && \Pr(X=3) > \Pr(X=0) > \Pr(X=1),\\
&\theta > 4: && \Pr(X=3) > \Pr(X=1) > \Pr(X=0).
\end{aligned}$$

Therefore, the teams that have the expectation of playing Champions League will be characterized by the achievement of points that make the θ parameter greater than 4. In contrast, teams that only aspire to maintain the category are characterized by θ values less than 2.45. Hence, the θ parameter can be interpreted as the value that will position a team in the four areas in which a football competition can be divided: Champions, Euroleague, no-relegation and relegation zones.

2.1. Statistical properties

The moments can be obtained from the pgf. In particular, the mean and second order moment about zero are given by

$$E(X) = \frac{\kappa(\theta)}{2}\theta(2+\theta^2), \tag{5}$$

$$E(X^2) = \frac{\kappa(\theta)}{2}\theta(2+3\theta^2). \tag{6}$$

Using (5) and (6) we get the variance, given by

$$var(X) = \frac{\kappa(\theta)^2}{3}2\theta\left[6+\theta^2(9+\theta)\right] \tag{7}$$

and some computations provide the index of dispersion, which is

$$ID = \frac{var(X)}{E(X)} = \frac{4\kappa(\theta)\left[6+\theta^2(9+\theta)\right]}{3(2+\theta^2)}. \tag{8}$$

Figure 3 shows the ID given in (8) for some values of the support of the parameter θ.

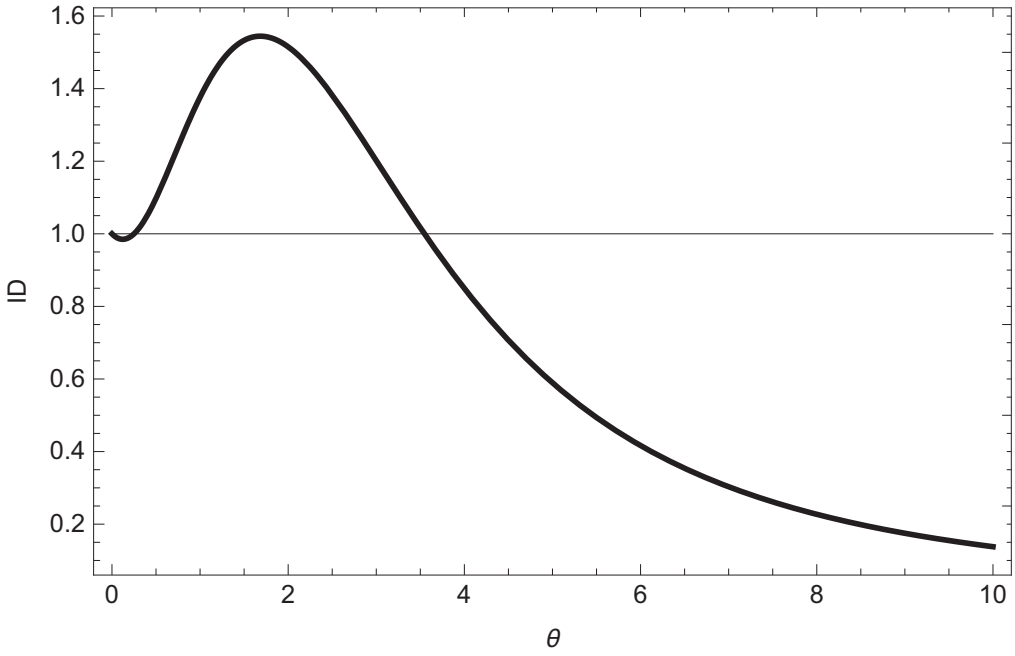

Figure 3: *Index of dispersion of the probability model depending on θ.*

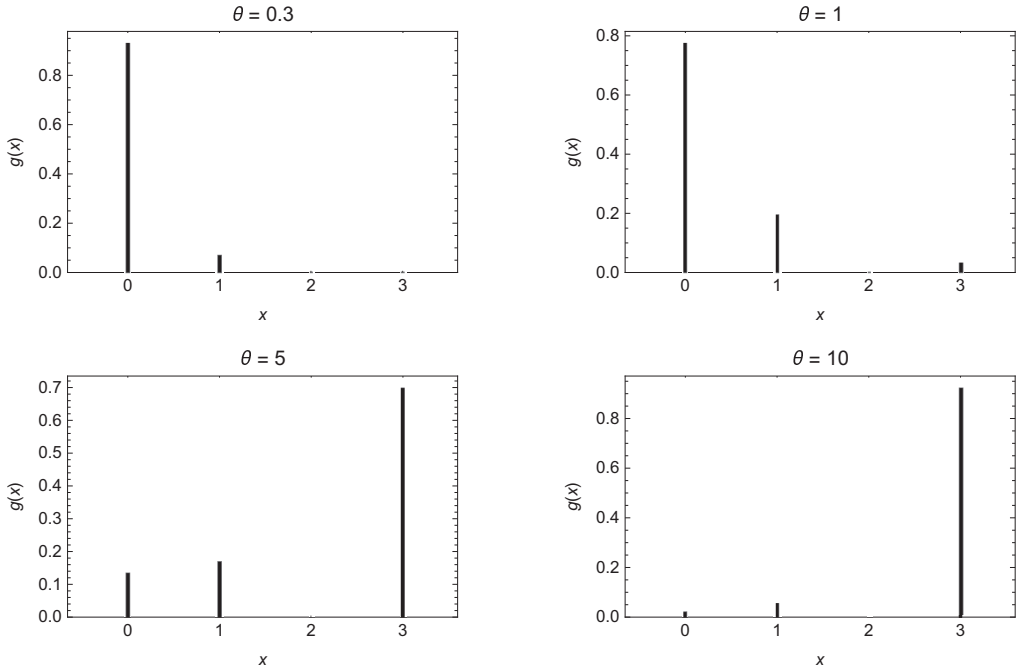

Figure 4: *Plot of the pmf in (3) for selected values of the parameter θ.*

It is simple to verify that the pmf accommodates over-dispersion (variance larger than the mean) when $0.250081 < \theta < 3.54676$ and under-dispersion when $0 < \theta < 0.250081$ and when $\theta > 3.54676$. Furthermore, the maximum value of the ID is reached for $\theta = 1.68365$, taking the value of 1.544.

Furthermore, the relation connecting the cumulants $k_{[r]}$ and the moments about the origin μ_r can be obtained using expression (8) in Noack (1950). Relations between factorial-cumulants and cumulants can also be given using results in Khatri (1959). See also Johnson et al. (2005, p. 77).

Figure 4 shows the probability mass function of the proposed model for different parameter values.

In view of this figure, a large value of the parameter θ gives more mass of probability to the value $x = 3$, and then to the victory, which is consistent with the values that give rise to an index of dispersion lower than one. For the teams that finally remain in the leaderboard in the highest positions, the dispersion index is lower than one, as shown in Figure 1. Additionally, for values of the parameter between 0.25 and 3.5 (such as $\theta = 0.3$ and $\theta = 1$) the distribution assigns more weight to the values $x = 0$ and $x = 1$, therefore it represents teams which have obtained few victories and, in consequence, these teams will remain in the lagging positions at the end of the season.

The cumulative distribution function can be written in terms of the exponential integral function given by $E_n(z) = \int_1^\infty \exp(-zt)/t^n\, dt$, and it results

$$\Pr(X \leq x) = \frac{\kappa(\theta)}{x!}\left[\theta^{x+1}(3-x-\theta+(4+\theta(\theta-3))\exp(\theta)E_{\theta}(-x)\right].$$

2.2. Parameter estimates

In this subsection, two estimation methods for estimating the parameter of the distribution are analysed. First, the method of moments for which let $\tilde{x} = (x_1, x_2, \ldots, x_n)$ be a random sample obtained from model (3). Then, using (5) it is simple to see that the estimator of θ is the real solution of the equation

$$\theta^3(3-\bar{x}) + 6\theta(1-\bar{x}) - 24\bar{x} = 0, \tag{9}$$

where $\bar{x}$ is the sample mean.

Second, the maximum likelihood estimation that it will be used here and where the θ estimator is easy to derive. The log-likelihood function is proportional to

$$\ell(\tilde{x};\theta) \propto n\log\kappa(\theta) + n\bar{x}\log\theta. \tag{10}$$

The likelihood equation obtained from (10) results

$$\theta\kappa'(\theta) + \bar{x}\kappa(\theta) = 0,$$

and provides the unique maximum likelihood estimator of θ, which is the same solution of the equation given in (9). Thus, the moment and the maximum likelihood estimators of the parameter θ are the same.

A little algebra provides the Fisher's information matrix, given by

$$\mathcal{I}(\widehat{\theta}) = E\left[-\frac{d^2\ell(\theta;\tilde{x})}{d\theta^2}\right]_{\theta=\widehat{\theta}} = \frac{2n\kappa(\widehat{\theta})^2}{3\widehat{\theta}}\left[6+\widehat{\theta}^2(9+\widehat{\theta})\right],$$

where $\text{var}(\widehat{\theta}) = \left[\mathcal{I}(\widehat{\theta})\right]^{-1/2}$. The discrete distribution proposed in this work satisfies the regularity conditions (see Lehmann and Casella, 1998, p. 449) under which the unique maximum likelihood estimator $\hat{\theta}$ of θ is consistent and asymptotically normal. They are simply verified in the following way. Firstly, the parameter space $\{0,1,3\}$ is a subset of the real line and the range of x is independent of θ. Additionally, the parameter θ is identifiable, that is, if $\theta_1 \neq \theta_2$ then $\exists x \in \mathcal{X}$ such that $g_{\theta_1}(x) \neq g_{\theta_2}(x)$. By using expression (10) it is easy to show that $E(\frac{\partial \log g_{\theta}(x)}{\partial\theta}) = 0$. Now, because, $\left.\frac{\partial^2\ell(\tilde{x};\theta)}{\partial\theta^2}\right|_{\theta=\widehat{\theta}} < 0$, the Fisher's information is positive. Finally, by taking $M(x) = \frac{\partial^3 \log g_{\theta}(x)}{\partial\theta^3} + 1$, a function which may depend on θ, we have that $\left|\frac{\partial^3 \log g_{\theta}(x)}{\partial\theta^3}\right| \leq M(x)$ and $E(M(x))$ is finite. Therefore the maximum likelihood estimator $\widehat{\theta}$ of θ is consistent and asymptotically normal and

$$\sqrt{n}(\widehat{\theta}-\theta) \xrightarrow{d} N(0,\mathcal{I}^{-1}(\widehat{\theta})),$$

where $N(\cdot,\cdot)$ represents the normal distribution. For details about this assert, the reader can consult Corollary 3.11 in Lehmann and Casella (1998). Due to this, we conclude that the maximum likelihood estimator of θ is asymptotically efficient.

2.3. Including covariates

In this section, we investigate the covariates that may affect the number of points achieved by the teams playing in home (and later away). Let X be a response variable, and let $\boldsymbol{y}$ be an associated $k\times 1$ vector of covariates. For the sake of convenience, we rewrite (3) in another form, so that covariates may be introduced into the model. By equating (5) to μ we get the same equation as the one given in (9). Now, by using Cardano's method of solution of the cubic polynomial equation we get $\theta=\sum_{i=1}^{2} R_i$, where

$$R_i=\sqrt[3]{(-1)^i\sqrt{4\left(\frac{\mu}{\mu-3}\right)^2+\left[\frac{1-\mu}{3(3-\mu)}\right]^3}-\frac{2\mu}{\mu-3}}.$$

The solution for the $\theta\equiv\theta(\mu)$ parameter given above can also be written in another way.[1] A common specification for the mean parameter μ is in terms of exponential functions, ensuring the non-negativity of this parameter. That is,

$$\mu_i=\frac{3\exp\left(\boldsymbol{\beta}^\top\boldsymbol{y}\right)}{1+\exp\left(\boldsymbol{\beta}^\top\boldsymbol{y}\right)}, \tag{12}$$

where $\boldsymbol{y}$ is the vector of covariates and $\boldsymbol{\beta}=(\beta_1,\ldots,\beta_q)^\top$ is an unknown vector of regression coefficients. Expression (12) ensures that the mean is a positive-valued function with support in $[0,3]$. Now, (3) is written as

$$g_{\theta_i}(x_i)=\kappa(\theta(\mu_i))(x_i-2)^2\frac{\theta(\mu_i)^{x_i}}{y_i!},\quad i=1,2,\ldots,n,$$

1. The closed expression for the θ parameter results

$$\theta\equiv\theta(\mu)=\frac{\sqrt[3]{2}\left[\sqrt[3]{2}(3+\mu(\mu-4))-\psi(\mu)^{2/3}\right]}{(\mu-3)\psi(\mu_i)^{1/3}},$$

where

$$\psi(\mu)=6\mu(\mu-3)^2+\sqrt{2(\mu-3)^3(\mu(3+19\mu(\mu-3))-1)}. \tag{11}$$

where again $\kappa(\theta(\mu_i))$ is as in (2). The log-likelihood of the model with covariates is proportional to

$$\ell(\tilde{x};\boldsymbol{\beta}) \propto \sum_{i=1}^{n} \left[\log(\kappa(\theta(\mu_i))) + x_i \log\theta(\mu_i)\right].$$

The normal equations which provide the maximum likelihood estimates of the parameters β_j, $j = 1,\ldots,q$, are

$$\frac{\partial \ell(\tilde{x};\boldsymbol{\beta})}{\partial \beta_j} = \sum_{i=1}^{n} \frac{1}{\kappa(\theta(\mu_{ij}))} \frac{\partial}{\partial \beta_j} \kappa(\theta(\mu_{ij})) + \sum_{i=1}^{n} \frac{x_{ij}}{\theta(\mu_{ij})} \frac{\partial}{\partial \beta_j} \theta(\mu_{ij}) = 0, \tag{13}$$

for $j = 1,2,\ldots,q$. The second partial derivatives can be seen in the Appendix Section.

Maximising the log-likelihood function (13) with respect to β_j $(j = 1,\ldots,q)$ is simple via the scoring algorithm or Newton-Raphson iteration. The solutions of the nonlinear equations shown in the Appendix provide the maximum likelihood estimates of these parameters. However, these equations cannot be explicitly solved and the solutions may be obtained either by maximising the log-likelihood function or by numerical methods. Different initial values of the parametric space can be considered as a seed points. In this study, the `FindMaximum` function of Mathematica software package v.11.0 (see for instance, Wolfram, 2003 and Ruskeepaa, 2009) was used, although the same results can be obtained by other methods, such as Newton, PrincipalAxis or QuasiNewton (all of which are available in this package), or by other packages such as R, Matlab or WinRats. Finally, the standard errors of the parameter estimates were obtained by inverting the Hessian matrix.

2.4. Marginal effects

The marginal effect reflects the variation of the conditional mean of X due to a one-unit change in the j-th covariate, and is calculated as

$$\frac{\partial \mu_i}{\partial \beta_j} = y_j \mu_i \left(1 - \frac{\mu_i}{3}\right),$$

for $i = 1,\ldots,n$ and $j = 1,\ldots,q$. Thus, the marginal effect indicates that a one-unit change in the j-th regressor increases or decreases the expectation of the points, pointing out that it depends on the sign, positive or negative, of the regressor for each mean. For indicator variables such as y_k, which takes only the value 0 or 1, the marginal effect in term of the odds-ratio is $\exp(\beta_j)$. Therefore, the conditional mean is $\exp(\beta_j)$ times larger if the indicator variable is one rather than zero.

3. Numerical application

In this section, we consider the data corresponding to the points obtained by the 20 teams participating in the First Division of the Spanish Football League in the 2013-14 season. This section is divided into two parts. First, we analyse the predictive capacity of the proposed model without including covariates. So, we study the expected points of the whole season and the expected points and positions based on the first 19 matches of the season (the middle of the competition). Second, we try to identify the significant factors which can explain the expected number of points of the home team by including covariates in the analysis.

3.1. Number of points without covariates

1. Prediction of the final points for the home teams. Figure 5 shows the observed and fitted accumulated points for home teams. The estimated value of the θ parameter is 3.370 and the standard error is 0.131.

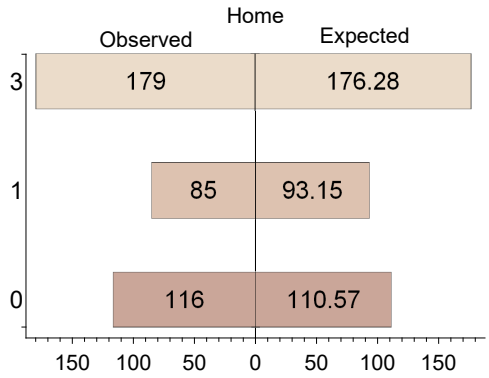

Figure 5: *Observed (left) and fitted (right) home points.*

2. Prediction of the final points based on the first 19 match-days (190 matches). Figure 6 shows the accumulated observed and expected points based on the first 19 match-days.

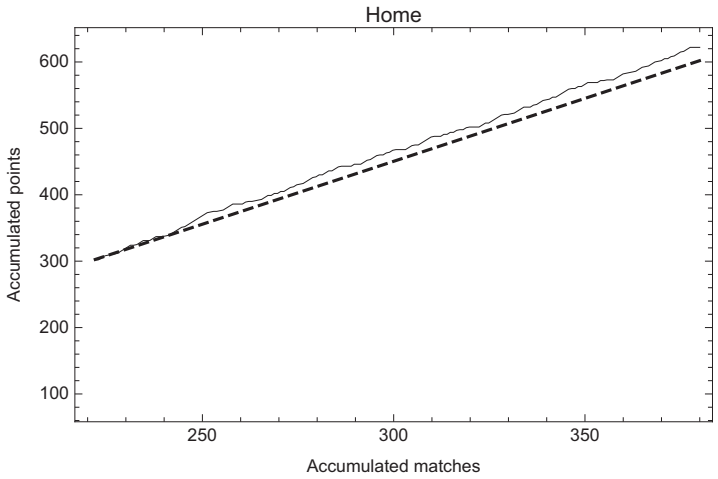

Figure 6: *Accumulated observed points (thin line) and expected (dashed line) based on the first 190 matches given the pmf (3) in the Spanish League.*

3. Prediction of the position of the teams at the end of the competition based on the first 19 match-days of the competition. Table 1 shows the estimated value of θ, the standard error (SE), the value of the maximum of the log-likelihood and the estimated μ parameter. Figure 7 illustrates the prediction of the positions of the teams at the end of the competition. The maximum likelihood estimated value of the θ parameter and the index of dispersion appears between parenthesis.

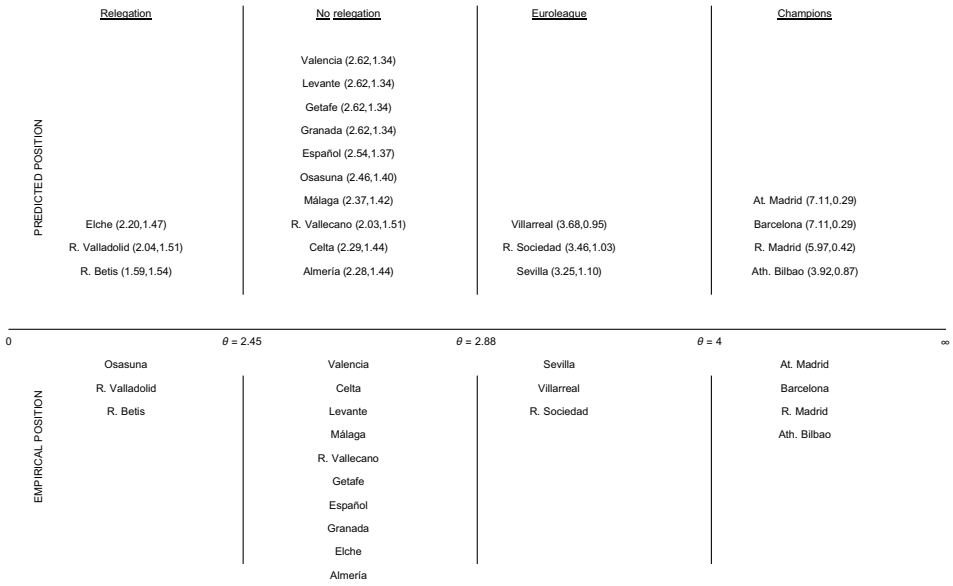

Figure 7: *Prediction based on the first 19 match-days and real final position of the teams at the end of the competition.*

Table 1: *Estimations based on first 19 match-days.*

$\widehat{\theta}$	S.E.	$\ell_{\max}$	$\widehat{\mu}$
3.269	0.179	−199.706	1.584

3.2. Number of points including covariates

First, we briefly describe all the variables that have been considered in the study in order to analyse the factors involved in the total points achieved by a team in a competition, we consider four groups of variables. Those related to the statistics of the game, one group of variables directly associated to the match, non-sport variables, and finally those related to the referee. Among all the considered variables in the different groups, the following were chosen for the econometric models. In the game statistics category, the shots on target, for both home and away teams were labeled as "HST" and "AST", respectively. It seems to be reasonable that the number of shots on goal are involved in the result of a match. The number of fouls for both teams were "HF" and "AF". Finally, the yellow and red cards labelled as "HYR" and "AYR" for the home and away team, were also considered. One match variable was introduced and was introduced and defined as "DERBY", which represents a match played between teams from the same city or region, or between the strongest teams of the competition. This variable takes the value 1 if the match respond to a derby and zero, otherwise.

Variables considered as non-sport were those concerning the team's budgets, defined as the logarithm value of the home team budget, "BUDH", and "BUDA" the logarithm of the away team budget. Finally, variables related to the referee were the international referee experience, "INTERNATIONAL", which was scored as 1 if the referee had such experience, and 0 otherwise, and the logarithm of the number of years of experience in the Spanish first division, namely as "AGEXP". The logarithm of the referee's age is denoted by "AGEREF". A brief description of these variables is shown in Table 2.

In order to check the goodness of the fitting, we have calculated the following information criterium and statistics. The Akaike information criterium (AIC), the mean absolute error (MAE) and the root mean square error (RMSE) statistics are obtaining by

$$\text{AIC} = 2k - 2\ell_{\max},$$

$$\text{MAE} = \frac{1}{n}\sum_{i=1}^{n}|y_i - \widehat{y}_i|,$$

$$\text{RMSE} = \left(\frac{1}{n}\sum_{i=1}^{n}(y_i - \widehat{y}_i)^2\right)^{1/2},$$

$$\text{Raw residuals} = y_i - \widehat{y}_i,$$

where k is the number of parameters of the model and $\ell_{\max}$ is the maximum value of the log-likelihood function.

Table 2: *Description of the variables.*

Variable	Description
Game statistics	
HST	Home team shots on target
AST	Away team shots on target
HF	Number of home team fouls.
AF	Number of away team fouls.
HYR	Home team yellow and red cards.
AYR	Away team yellow and red cards.
Match variable	
DERBY	Match played between teams from the same city or region or between the strongest teams in the league.
Extra games	
BUDH	Logarithm of home team budget
BUDA	Logarithm of away team budget
Referee	
INTERNATIONAL	Scored as 0 if the referee has no international experience and 1 if he does.
AGEXP	Logarithm of years of experience in the first division
AGEREF	Logarithm of referee's age

The results both under the standard linear regression model and under the proposed regression model are shown in Table 3. As we expected, the home and away shots on target are significant factors with the expected signs and at the 1% level of significance. Furthermore, the OLS model only detects another significant factor, namely, the home team's budget at the 5% significance level. The AIC is equal to 1194.69 and the MAE and RMSE statistics are 1.008 and 1.182, respectively. The estimations of the proposed model, in addition to finding the same results as the previous one, detect an important new factor concerning the referee subject: the fact that a referee is international reduces the expected points of the home team at the 10% significance level. In this sense, we can see that the "home effect" is lower in those matches in which there is an international referee. The AIC for the proposed model is 691.218 and the MAE and RMSE statistics are 0.921 and 1.115, respectively, i.e, these values are notably lower than the ones obtained for the standard linear model.

Figure 8 shows the raw residuals of the OLS and the proposed models (left plot) and box-and-whisker chart of the raw residuals (right plot). Both plots remark a greater dispersion of the OLS residuals.

Table 3: *Estimation results for the OLS and the proposed regression models.*

	OLS			Proposed model		
Variables	$\hat{\beta}$	Standard Error	p-value	$\hat{\beta}$	Standard Error	p-value
Intercept	2.286^{**}	1.156	0.049	2.153	1.822	0.238
DERBY	0.139	0.164	0.397	0.203	0.292	0.487
HST	0.130^{***}	0.024	0.000	0.249^{***}	0.047	0.000
AST	-0.175^{***}	0.028	0.000	-0.307^{***}	0.052	0.000
HF	0.004	0.016	0.816	-0.012	0.028	0.657
AF	0.014	0.015	0.371	0.015	0.027	0.565
HYR	-0.0652	0.045	0.151	-0.115	0.077	0.139
AYR	-0.039	0.042	0.345	-0.059	0.072	0.409
BUDH	0.129^{**}	0.072	0.075	0.235^{*}	0.138	0.089
BUDA	-0.111	0.069	0.109	-0.166	0.117	0.156
INTERNATIONAL	-0.220	0.159	0.165	-0.519^{*}	0.281	0.065
ACIENT	0.068	0.177	0.702	0.059	0.050	0.238
AGEREF	-0.017	0.031	0.593	-0.047	0.043	0.276
AIC		1194.69			691.218	
MAE		1.008			0.921	
RMSE		1.182			1.115	

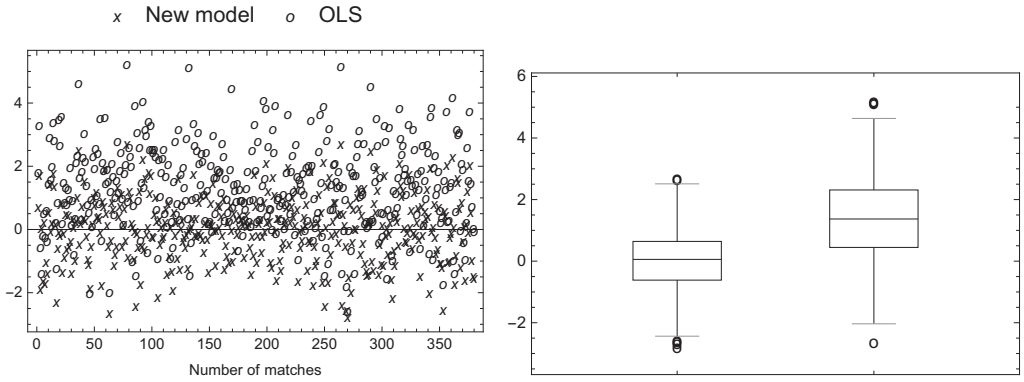

Figure 8: *Raw residuals and the box-and-whisker chart of the OLS (right) and proposed (left) raw residuals.*

Figure 9 illustrates the normal probability plot of the OLS residuals. As we can observe, the residuals plot is approximately linear supporting the condition that the error terms are normally distributed.

4. Discussion of results

In this study, we propose a new pmf for modeling the number of points achieved by a home or visitor team in a football match. In this context, we have analysed the number of points, firstly, without including covariates and, secondly, including this information.

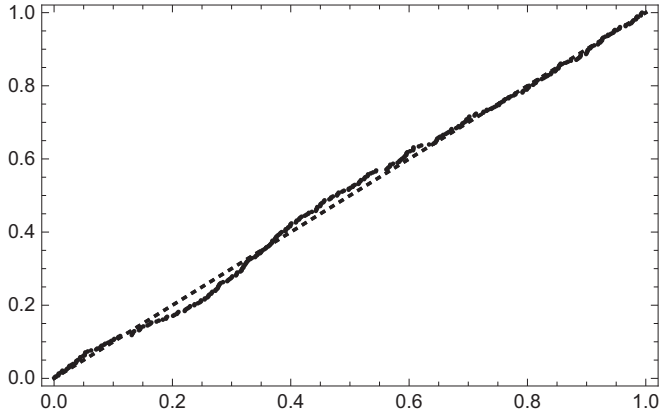

Figure 9: *Probability plot of the OLS residuals.*

The first part of the study includes estimation and prediction of the points achieved by the teams without using covariates. We can observe that this model provides good results except for some of the worst teams, i.e., the model fails only for two teams, Elche and Osasuna. While Elche finally remained in the First Division, Osasuna relegated. The second part focuses on the introduction of covariates. Several variables are considered from the Spanish Football League (First division) during the 2013-14 season and two sets of models are analysed. First, the home linear (standard) regression model. And second, the home regression model proposed in this paper. The results obtained indicate that the latter model produces better fits than the other standard model. In view of the good results obtained in this case and in the estimation without covariates previously studied, we believe the distribution given in (3) is appropriate for this data set.

Several factors, proposed in earlier studies, were considered relevant to the expected number of points. Karlis and Ntzoufras (2000) considered the number of goals as an indicator for the strength of a team and it can be used to determine the performance of a team. Rue and Salvesen (2006) ignored data as number of near goals, corners or free kicks and focused on the defending and attacking skills of each team. With the proposed model, home and away team shots on target, which are in some way the attacking strength, are the most significant factors considering the game statistics variables. With respect to the coefficients of the budgets, the large budgets home teams have more expected points. Finally, a significant factor appears regarding the referee variable which has not been significant in the previous models, namely, the international issue. International referees have a negative (positive) relationship with the home (away) teams indicating that this kind of referee is not influenced by the "home effect" of the match. Quite the opposite, if there is an international referee in the match, the expected number of points increases (decreases) for the away (home) team. These findings support those obtained in Pérez-Sánchez, Gómez-Déniz and Dávila-Cárdenes (2018) in which the authors proposed a skewed logistic model for estimating the probability of an away victory.

To conclude, in this work, significant variables are obtained not only related to the game itself, but also to the referees or even the economic potential of the teams. This fact may be used by others actors around the sport of football as coaches or even bookmakers, who analyse all the available information as part of their bets.

Appendix

Second partial derivatives to get the Fisher's information matrix are:

$$\frac{\partial^2 \ell(\tilde{x};\boldsymbol{\beta})}{\partial \beta_j^2} = \sum_{i=1}^{n} \frac{\partial^2}{\partial \beta_j^2} \kappa(\theta(\mu_{ij})) + \sum_{i=1}^{n} \frac{x_{ij}}{\theta(\mu_{ij})} \left[\frac{\partial^2}{\partial \beta_j^2} \theta(\mu_{ij}) - \left(\frac{1}{\theta(\mu_{ij})} \frac{\partial}{\partial \beta_j} \theta(\mu_{ij}) \right)^2 \right],$$

$$\frac{\partial^2 \ell(\tilde{x};\boldsymbol{\beta})}{\partial \beta_j \partial \beta_l} = \sum_{i=1}^{n} \frac{\partial^2}{\partial \beta_j \beta_l} \kappa(\theta(\mu_{ij})) + \sum_{i=1}^{n} \frac{x_{ij}}{\theta(\mu_{ij})} \left[\frac{\partial^2}{\partial \beta_j \beta_l} \theta(\mu_{ij}) - \left(\frac{1}{\theta(\mu_{ij})} \frac{\partial}{\partial \beta_j} \theta(\mu_{ij}) \right)^2 \right],$$

for $j = 1,2,\ldots,q$, $l = 1,2,\ldots,q$ and $j \neq l$ and the derivatives needed are the followings,

$$\frac{d\kappa(\varphi(\mu))}{d\varphi(\mu)} = -\frac{36 + 18\varphi(\mu)^2}{24 + \varphi(\mu)(6 + \varphi(\mu)^2)},$$

$$\frac{\partial \mu_i}{\partial \beta_j} = \frac{1}{3} x_j \mu_i \exp\left(\beta^\top \boldsymbol{x}\right),$$

$$\frac{d\varphi(\mu_i)}{d\mu_i} = \varphi(\mu_i) \left[\frac{\sqrt[3]{2}\left(4 - 2\mu_i - 2/3\psi(\mu_i)^{-1/3}\psi'(\mu_i)\right)}{\sqrt[3]{2}\left(3 - \mu_i(\mu_i - 4) - \psi(\mu_i)^{2/3}\right)} - \frac{\psi'(\mu_i)}{3\psi(\mu)} - \frac{1}{\mu_i - 3} \right],$$

$$\frac{d\psi(\mu_i)}{d\mu_i} = \mu_i \left[2(\mu_i - 3) + 4\mu_i + \frac{\sqrt{2(\mu_i - 3)}(\mu_i - 1)(2 + 19\mu_i(\mu_i - 3))}{\sqrt{\mu_i\left(3 + 19\mu_i(\mu_i - 3) - 1\right)}} \right].$$

Acknowledgement

EGD and JMPS work was partially funded by grant ECO2013–47092 (Ministerio de Economía y Competitividad, Spain and ECO2017–85577–P (Ministerio de Economía, Industria y Competitividad. Agencia Estatal de Investigación)).

References

Baio, G. and Blangiado, M. (2010). Bayesian hierarchical model for the prediction of football result. *Journal of Applied Statistics*, 37, 253–264.

Brillinger, D. (2008). Modelling game outcome of the Brazilian 2006 series a championship as ordinal-valued. *Brazilian Journal of Probability and Statistics*, 22, 89–104.

Díaz, I. and Núñez, V. (2010). On the use of simulation methods to compute probabilities: application to the first division Spanish soccer league. *SORT*, 34, 181–200.

Fisher, R. (1934). The effects of methods of ascertainment upon the estimation of frequencies. *Annals of Eugenics*, 6, 13–25.

Greenhough, J., Birch, P., Chapman, S. and Rowlands, G. (2002). Football goal distributions and extremal statistics. *Physica A*, 316, 615–624.

Harandi, S.S. and Alamtsaz, M. (2013). Discrete alpha-skew-Laplace distribution. *SORT*, 39, 71–84.

Hon, L. and Parinduri, R. (2016). Does the three-point rule make soccer more exciting? evidence from a regression discontinuity design. *Journal of Sports Economics*, 17, 377–395.

Johnson, N., Kemp, A. and Kotz, S. (2005). *Univariate Discrete Distributions* John Wiley, INC.

Karlis, D. and Ntzoufras, I. (2000). On modelling soccer data. *Student*, 3, 229–244.

Karlis, D. and Ntzoufras, I. (2003). Analysis of sports data by using bivariate Poisson models. *Journal of the Royal Statistical Society. Series D, The Statistician*, 52, 133–145.

Khatri, C. (1959). On certain properties of power-series distributions. *Biometrika*, 46, 486–490.

Lehmann, E. and G. Casella, G. (1998). *Theory of Point Estimation* Springer, New York.

Louzada, F., Suzuki, A. and Salasar, L.B. (2014). Predicting match outcomes in the English premier league: Which will be the final rank? *Journal of Data Science*, 12, 235–254.

Noack, A. (1950). A class of random variables with discrete distributions. *The Annals of Mathematical Statistics*, 21, 127–132.

Patil, G. and Rao, C. (1978). Weighted distributions and size biased sampling with applications to wildlife populations and human families. *Biometrics*, 34, 179–184.

Pérez-Sánchez, J.M., Gómez-Déniz, E. and Dávila-Cárdenes, N. (2018). A comparative study of logistic models using an asymmetric link: Modelling the away victories in football. *Symmetry*, 10, 1–12.

Rue, H. and Salvesen, O. (2006). Prediction and retrospective analysis of soccer matches in a league. *Journal of the Royal Statistical Society. Series D. The Statistician*, 49, 399–418.

Ruskeepaa, H. (2009). *Mathematica Navigator. Mathematics, Statistics, and Graphics. Third Edition* Academic Press. USA.

Saraivaa, E., Suzuki, A., Ciro, A. and Luzadab, F. (2016). Predicting football scores via Poisson regression model: applications to the National Football League. *Communications for Statistical Applications and Methods*, 23, 297–319.

Wolfram, S. (2003). *The Mathematica Book* Wolfram Media, Inc.

SORT 43 (1) January-June 2019, 113-142 DOI: 10.2436/20.8080.02.83

Automatic regrouping of strata in the goodness-of-fit chi-square test

Vicente Núñez-Antón[1], Juan Manuel Pérez-Salamero González[2], Marta Regúlez-Castillo[1], Manuel Ventura-Marco[2] and Carlos Vidal-Meliá[3]

Abstract

Pearson's chi-square test is widely employed in social and health sciences to analyse categorical data and contingency tables. For the test to be valid, the sample size must be large enough to provide a minimum number of expected elements per category. This paper develops functions for regrouping strata automatically, thus enabling the goodness-of-fit test to be performed within an iterative procedure. The usefulness and performance of these functions is illustrated by means of a simulation study and the application to different datasets. Finally, the iterative use of the functions is applied to the Continuous Sample of Working Lives, a dataset that has been used in a considerable number of studies, especially on labour economics and the Spanish public pension system.

MSC: 62G10, 62P25.

Keywords: Goodness-of-fit chi-square test, statistical software, Visual Basic for Applications, Mathematica, Continuous Sample of Working Lives.

1. Introduction

Empirical studies require data samples to be representative of the target population with respect to the principal characteristics. There are many papers on the issue of selecting representative samples, including Ramsey and Hewitt (2005), Grafstörm and Schelin (2014), Kruskal and Mosteller (1979a), Kruskal and Mosteller (1979b), Kruskal and Mosteller (1979c), Kruskal and Mosteller (1980), Omair (2014). One way of determin-

[1] (Corresponding author) Department of Applied Economics III (Econometrics and Statistics), Faculty of Economics and Business, University of the Basque Country UPV/EHU. Avda. Lehendakari Aguirre 83, 48015 Bilbao. (Spain). vicente.nunezanton@ehu.eus, marta.regulez@ehu.eus.

[2] Department of Financial Economics and Actuarial Science. Faculty of Economics. University of Valencia. Avenida de los Naranjos s.n., 46022 Valencia. (Spain). juan.perez-salamero@uv.es, manuel.ventura@uv.es

[3] Department of Financial Economics and Actuarial Science. Faculty of Economics. University of Valencia. Avenida de los Naranjos s.n., 46022 Valencia. (Spain) and research affiliation with the Instituto Complutense de Análisis Económico (ICAE), Complutense University of Madrid (Spain), and the Centre of Excellence in Population Ageing Research (CEPAR), UNSW (Australia). carlos.vidal@uv.es

Received: May 2018

Accepted: January 2019

ing whether a sample is representative of a population is to use a goodness-of-fit test to check whether the data fits the population distribution. The goal is to test whether the sample data fits a distribution from a certain population. One procedure commonly used is Pearson's χ^2 goodness-of-fit test. When the variables under study are grouped in given categories or strata in the population, the data in the sample are organized in the same way in order to apply this test. The strata are constructed so that the population is divided into major categories that are relevant to the research interest. In each category the test statistic compares the observed frequency in the sample with the expected frequency in the theoretical or known population.

Pearson's χ^2 and the likelihood ratio test statistic G^2 are arguably the two most widely used statistics in contingency table analysis (see Cai et al. 2006). Both can be used to test independence between categorical variables in contingency tables and to test homogeneity to determine whether frequency counts are distributed identically across different populations. These statistics may also be used to assess goodness-of-fit in multivariate statistics such as in logistic regression (Hosmer et al. 1997, Hosmer and Lemeshow 2000), log-linear modelling (Bishop, Fienberg and Holland, 1975, Fienberg 2006) and Latent Class Analysis (LCA) (Lazarsfeld and Henry 1968, Goodman 1974). Under some conditions, these statistics have an asymptotic chi-square distribution, where the validity of the test results depends on a minimum size of expected cell frequencies. As a rule of thumb, that number is established in practice as 5. It is well known (Cochran 1952) that when some expected cell frequencies or probabilities are small, their reference asymptotic distribution is not suitable for assessing p-values or the size of the test. This problem arises frequently in social sciences, biomedical and health sciences and psychometrics applications (Cai et al. 2006, Bartholomew and Tzamourani 1999) with sparse contingency tables (Agresti 2002).

Delucchi (1983) reviewed the research conducted after the paper by Lewis and Burke (1949) in an attempt to address the problems listed by them and to form recommendations regarding the use and misuse of the chi-square test. The various papers examined by Delucchi (1983) regarding the problem of working with excessively small expected frequencies recommend different minimum sizes depending on the type of test for all the strata or for a percentage of them, with fixed values or values depending on the number of categories, etc. Along the same lines, Moore (1986) and Wickens (1989) established some criteria for the selection of the minimum size. García Pérez and Nuñez-Antón (2009) found, via simulation, that Pearson's χ^2 was sufficiently accurate and only showed minor misbehaviour when table density was less than two observations per cell for testing independence or homogeneity in two-way contingency tables. To solve these limitations, various alternative approaches have been proposed in the literature. One of them is to use resampling methods such as the parametric bootstrap to obtain an empirical p-value (Lin, Chang and Pal, 2015, Bartholomew, Knott and Moustaki, 2011, Bartholomew and Tzamourani 1999, Collins et al. 1993). The use of resampling methods has become increasingly popular given the power of today's computers. Cai et al. (2006) pointed out that resampling methods are not very practical from a compu-

tational perspective given that in comparing the fit of different models the resampling procedure must be repeated for each model. Moreover, Tollenaar and Mooijaart (2003) showed that the validity of a bootstrap-based test depends critically on what statistic is being bootstrapped. In particular, bootstrapping Pearson's χ^2 or the likelihood ratio test statistic G^2 does not provide immediate Type I error rate control under sparseness.

Other alternatives call for Yate's continuity correction[1] to be used (Yates 1934), applying exact tests such as Fisher's exact test (Fisher 1935, Mehta and Patel 1983) to test independence[2], or trying to estimate the cumulative distribution function (CDF) of the statistics (Tsang and Cheng 2006). One last proposal, which has proved very popular in practice, is to pool or regroup cells to reach the desired minimum number of expected frequencies. If the test is to be conducted just once and regrouping is the option chosen (in spite of its limitations[3]), it could be carried out exogenously before the statistic is computed.

However, tests can often be used repeatedly in successive studies, or more importantly there may be techniques that use a test in an iterative process. An example of the latter would be to carry out sampling or subsampling (Pérez-Salamero González, Regúlez-Castillo and Vidal-Meliá, 2017), including the goodness-of-fit test in mathematical programming problems. Similar examples could be found (Marsaglia 2003) in the analysis of random number generation processes, where tests have to be performed a number of times or in the sequential analysis of goodness-of-fit for different models using contingency tables. Therefore, if researchers choose to regroup the strata in order to solve the failure on the minimum size requirement in the goodness-of-fit chi-square test, automatic re-grouping procedures in statistical software would be very useful, especially when tests are applied sequentially.

The paper is organized as follows. Section 2 presents an example to motivate the problem to be solved, and extensively analyse the software that carries out the Pearson's χ^2 goodness-of-fit test in order to check whether there is any automatic regrouping in the strata to satisfy the desired requirement of a minimum size. We conclude that, in general, there is not. Section 3 shows the flowchart that inspired the development of the proposed functions for regrouping the strata to satisfy the desired minimum requirement, independently of whether they are in the tails or in the middle. Section 4 shows some simulation results to illustrate the performance of the procedure in terms of nominal significance levels under different settings. Section 5 presents three more examples: one to illustrate the utility of the functions and to analyse the behaviour of the test in different software packages, a second to illustrate the use of the regrouping functions

1. This correction reduces the numerical value of the test statistic, and hence weakens the power and significance level of the test, making it overly conservative (Haviland 1990, Hirji 2006, Agresti 2002, Lydersen, Fagerland and Laake, 2009).

2. Campbell (2007) and Kroonenberg and Verbeek (2018) compare and discuss the problem of selection from these alternatives.

3. See for example Bosgiraud (2006) and Bartholomew and Tzamourani (1999) for an excellent discussion on this issue.

when it is necessary to estimate parameters of the distribution and finally, an example that shows the iterative use of the regrouping functions in a mixed integer programming framework. This is a real problem based on the Continuous Sample of Working Lives (CSWL), a dataset widely used in numerous studies, especially on labour economics and the Spanish public pension system. The paper ends with some concluding remarks and further research proposals. In addition, we provide three appendices in the supplementary material. The first appendix provides a summarized review of selected software packages as regards whether they include Pearson's χ^2 goodness-of-fit test, or at least functions that enable that test to be conducted. The second includes the mathematical approach to the real problem explained in Section 5, i.e. the selection of the larger subsample that verifies the goodness-of-fit χ^2 test. The authors can be contacted to supply the codes developed in Microsoft Excel 2016 and Microsoft Excel VBA (Visual Basic for Applications 7.1) and Mathematica[4] that make automatic regrouping and the correct application of the χ^2 test possible.

2. Illustration of the problem and software review

The χ^2 goodness-of-fit test approach can be found in any basic manual of statistical inference. It is due to the pioneering work of Pearson (1900). It is a nonparametric test which can be applied to categorical, discrete, and continuous random variables. The statistic for the test is given by the following expression:

$$\chi^2 = \sum_{i=1}^{k} \frac{(O_i - E_i)^2}{E_i}, \tag{1}$$

with O_i being the observed values and E_i the expected or theoretical values. For large samples it is proved that this statistic is distributed under the null hypothesis as a χ^2 with $v = k - r - 1$ degrees of freedom, where k is the number of categories or strata, depending on how the population and the sample are organized, and r is the number of parameters estimated using the observed data in the sample. The χ^2 goodness-of-fit test is carried out by comparing the sample value of the statistic with the corresponding critical value obtained from the χ^2 distribution with v degrees of freedom and a level α of significance. If the test statistic is less than the critical value, then the null hypothesis that the sample (observed values) has the same distribution as the population (expected values) is not rejected. The test can also be used based on the p-value obtained from the sample value of the statistic.

To illustrate the problem that we seek to address with our procedure, we propose the following example that we call "No Moore rules." In this example, the dataset does not

4. Mathematica is a registered trademark of Wolfram Research Inc. version 11.

meet the rules indicated by Moore (1986) for the minimum size required to carry out the χ^2 goodness-of-fit test. Moore established a general minimum size of 1, but it should be 5 in 80% of the categories. As shown in Table 1, in this example the size of the expected values is below 5 in 5 of the 10 categories, and below 1 in 3 of them. Moreover, there are intermediate categories that do not satisfy the minimum size requirement, i.e. bins 6 and 7 with values lower than 5. The population distribution used is a multinomial with probabilities as shown in the second column of Table 1.

Table 1: *Example featuring "No Moore rules" conditions. Values for the goodness-of-fit χ^2 test statistic, degrees of freedom (df) and p-values are also reported.*

Category	Pop. prob.	Original		Regrouped	
		Obs.	Exp.	Obs.	Exp.
1	0.161926968	9	8.0963	9	8.0963
2	0.168545644	3	8.4273	3	8.4273
3	0.037262021	5	1.8631		
4	0.162660577	10	8.1330	15	9.9961
5	0.015025858	1	0.7513		
6	0.017927913	4	0.8964		
7	0.109949741	3	5.4975	8	7.1452
8	0.099373226	5	4.9687		
9	0.037554998	3	1.8777	8	6.8464
10	0.189773053	7	9.4887	7	9.4887
Total	1	50	50	50	50
	χ^2	22.5925		7.0503	
	df	9		6	
	p-value	0.007		0.217	

There are problems in conducting the test in software packages in general, because there is no automatic regrouping of the small size categories. The ways in which this issue is treated in some programs are outlined in Appendix A in the supplementary material so as to illustrate the response a potential user would have when carrying out this test with this kind of data. Applying the automatic regrouping of strata with the procedure developed in this paper as introduced in the next section and the custom functions in Excel and Mathematica that we present in the supplementary material in Appendix C, the data are regrouped into 6 categories. The last two columns of Table 1 show how the categories are regrouped. Considering the 6 categories after regrouping, the sample value obtained for the χ^2 statistic with 5 degrees of freedom gives a p-value equal to 0.217. It can be seen that without regrouping the categories the null hypothesis is rejected, but when the custom functions regroup to meet the minimum size requirement it is not rejected. If the minimum size requirement for validating the test is not

taken into account, the results could be wrong and, in this case, opposite to the case of regrouping.

After a comprehensive review of the software that can carry out this test, Table A1 in Appendix A in the supplementary material summarizes whether selected software packages can be used for statistical purposes to check whether Pearson's χ^2 goodness-of-fit test, or at least whether specific functions that enable it to be implemented are available in them. It also reports whether automatic re-grouping of strata is possible if the test statistic (1) is computed. Many computer programs have the option of filtering and/or grouping data before the test is run, but they do not offer automatic regrouping in the internal instructions for computing the test. There are only two programs that offer the possibility of automatic regrouping of strata when the required or desired minimum size is not reached:

a. MATLAB, which allows users to choose the minimum size so as to regroup giving a positive integer as the value for the argument because the number zero indicates that there is no regrouping of strata in terms of the size of the expected values. The **chi2gof** function in MATLAB regroups only the strata at the extreme end of either tail, but it does not combine the interior bins.

b. SSJ 3.2.0 Stochastic Simulation written in Java. This tool allows regrouping but not in a single step. To use this facility, one must first construct an **OutcomeCategoriesChi2** object by entering the expected number of observations for each original category into the constructor. By calling up the method **regroupCategories** the program will then regroup categories in such a way that the expected number of observations in each category reaches a given threshold **minExp**. The procedure starts by analysing the size of the expected value in the first category. If it finds a category that does not reach the minimum size required, **minExp**, then it will be added to the next category. It follows the same regrouping criterion down to the end, where if the last category does not have the minimum size it will be added to the nearest one where the condition holds. The method then counts the number of elements in each category and calls up **chi2** to compute the chi-square test statistic value.

Therefore, there is consistent evidence to suggest that there are very few computer tools and statistical packages that have the possibility of automatic regrouping, not only at the extreme end of either tail but also in the interior bins. Hence, it is worth developing an automatic regrouping method that could be easily adapted to different software environments without having to perform the regrouping exogenously to the procedure each time the minimum size for the expected values is not met.

3. Automatic regrouping of strata: the procedure

The automatic regrouping of categories or strata is a sequential procedure that starts with an individual analysis of the size of each stratum. Before the procedure is applied, one must know the observed and expected values to be compared in the test. The expected values can either come from a fully specified population distribution or from a theoretical distribution with unknown parameters to be estimated from the observed sample values. The second step is to regroup the categories that do not meet the minimum size requirement, if necessary, together with the adjacent ones, such that the resultants reach the desired minimum value. It might be of interest to regroup not only the strata at the extreme ends of the tails but also those in intermediate categories. Prime examples are, for example, geographical grouping to follow economic variables, the population at risk from certain diseases, the distribution of passengers on a track between important cities (for hours or cities with shutdown), visitor flows to shopping centres, and online submissions of tax return forms within the deadline. In particular, the automatic strata regrouping procedure proposed analyses their size in increasing order from the first strata to the last. The ordering is determined by the variable that is at the origin of the stratification procedure. The regrouping starts from the first category and goes down to the last one. If a category does not reach the minimum size it is added to the smallest adjacent category. If there are adjacent categories of the same size the proposed procedure will add it to the next one, the one with a larger numbering index. A flowchart of the algorithm is given in Figure 1. Three enlargements of parts of this flowchart are given in Figures 2, 3 and 4, showing the steps involved in the regrouping process on which the subsequent computation procedure is based. The main elements and the dynamics of the chart displayed in the aforementioned figures are as follows:

1. The observed and expected values needed to calculate the goodness-of-fit test, together with the required minimum size value for the strata, **min**, are introduced.

2. Check whether the number of observed values in the strata, k, is equal to the number of expected values, m. If not, the data entry stage must be revised. If the two dimensions coincide, continue.

3. The variable i, representing the index of a specific observed and expected value, is given an initial value of 1 within the corresponding vector of values. The variable **last** is given an initial value of 0, and represents the indicator for the last group with a regrouped size equal to or greater than the minimum.

4. Check whether the expected value for the first category reaches the minimum size, **min**.

5. If the expected value for the first category does not reach the minimum value and given that it does not have a previous category, its elements will be added to the second category.

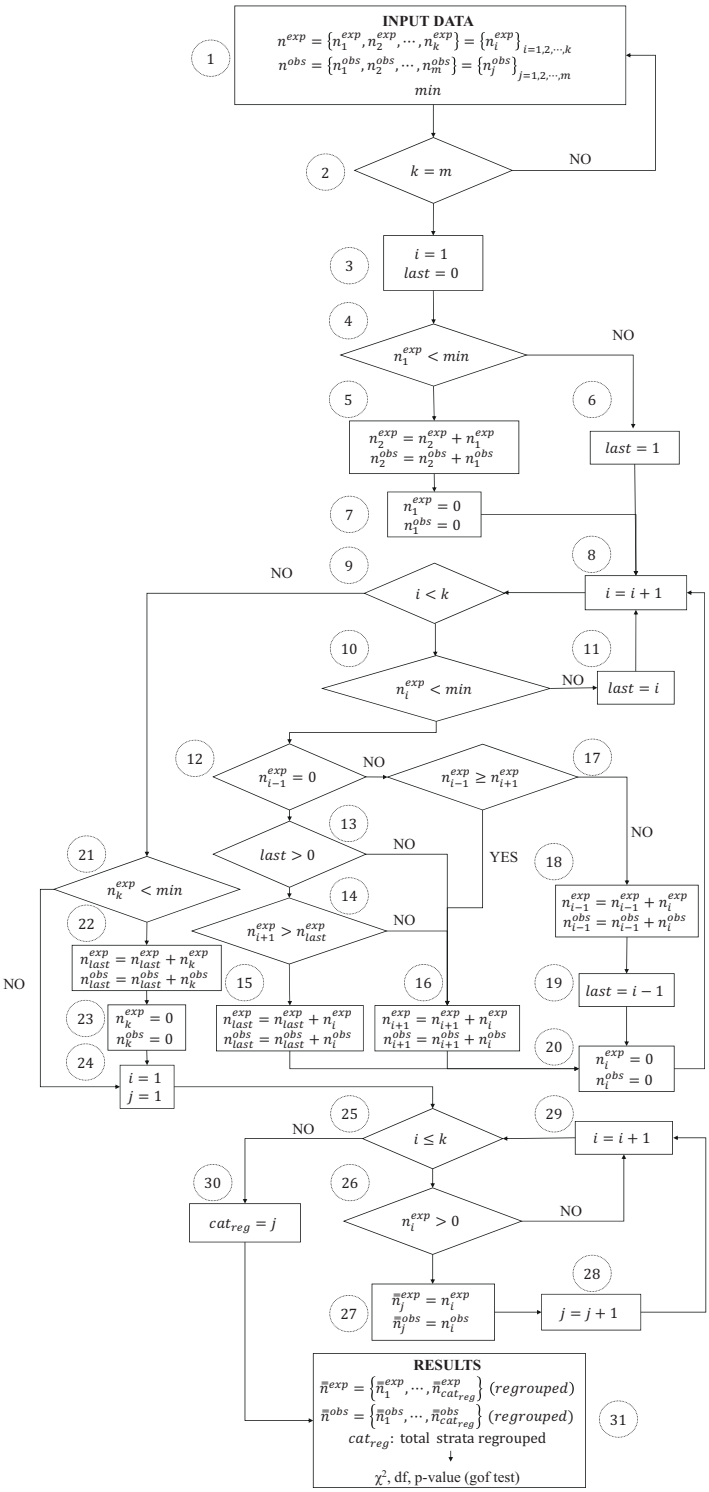

Figure 1: *Flowchart. Automatic regrouping of strata.*

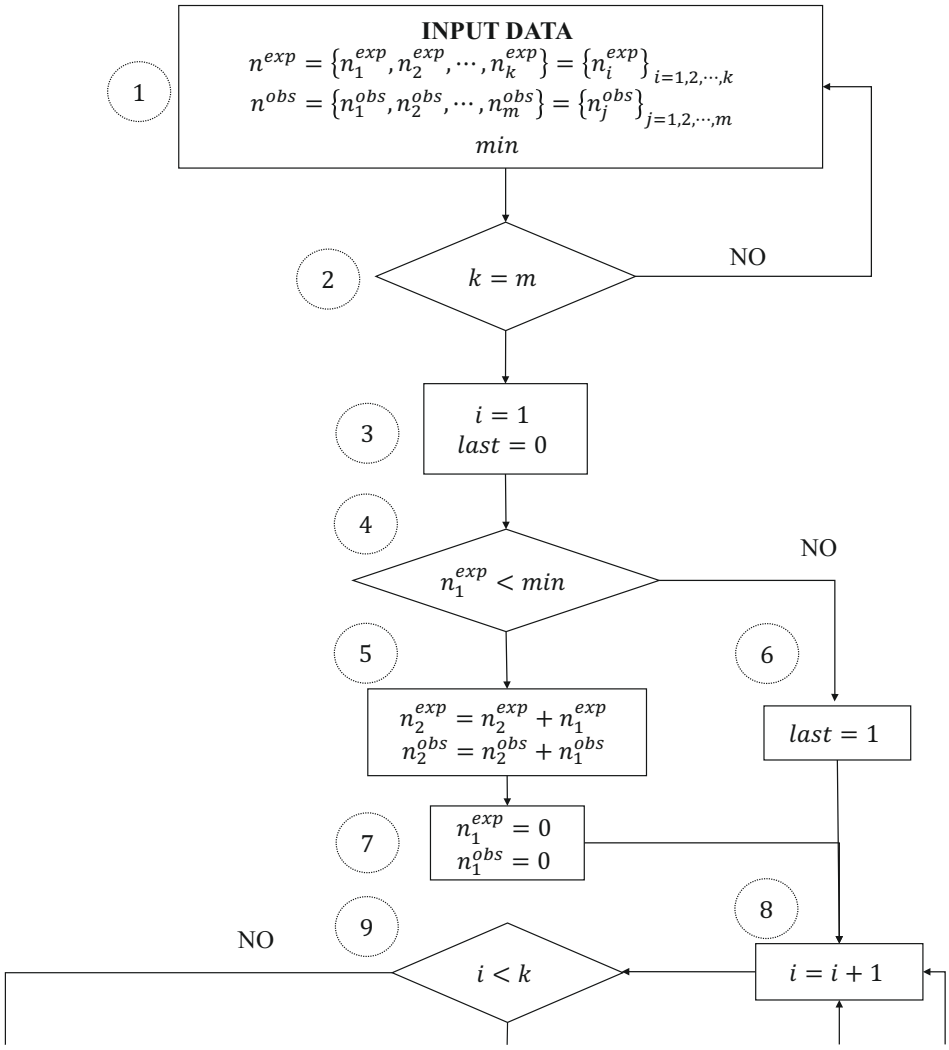

Figure 2: *Flowchart: Steps 1 to 9. Automatic regrouping of strata.*

6. If the expected value for the first category reaches the minimum size, **min**, it will be stored in the variable **last**, to be, initially, the last category to reach this minimum.

7. If the expected values for the first category have been added to the second one, then the values of the first category will be initialized to zero.

8. The index *i* will increase to proceed with the analysis of the subsequent categories.

9. Check whether the last stratum or category has been reached by comparing the stratum index, *i*, with the total number of strata, *k*. If the last stratum has not yet

been reached, continue with the next step. If the last stratum is reached, $i = k$, go to step 21 (see Figure 3).

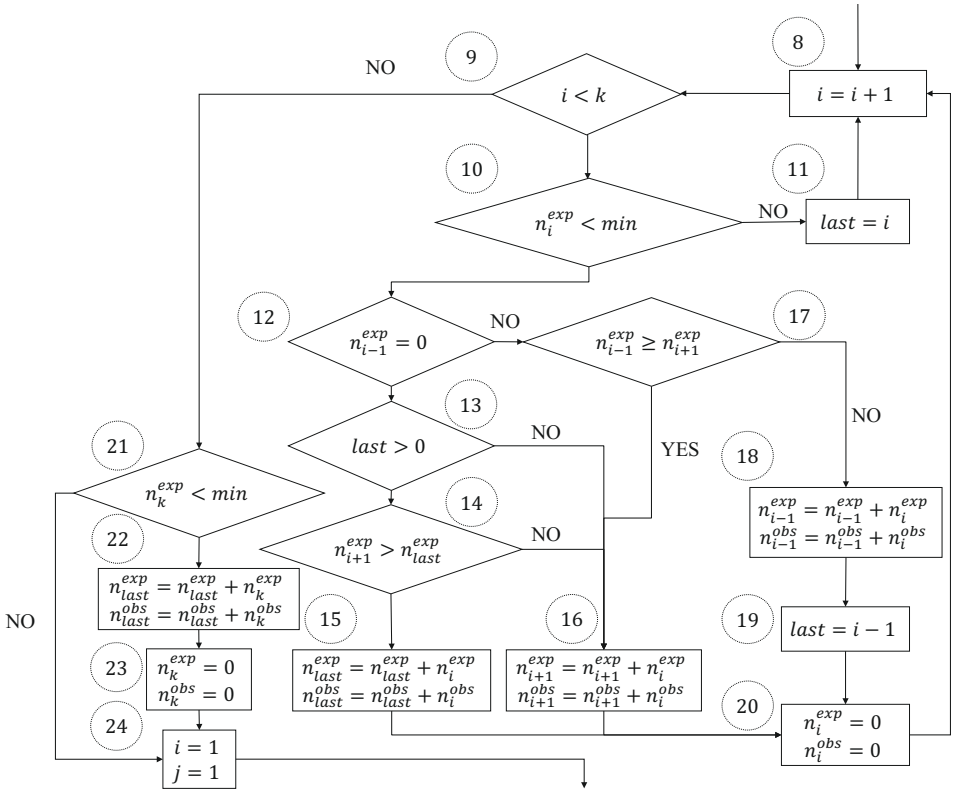

Figure 3: *Flowchart: Steps 9 to 24. Automatic regrouping of strata.*

10. The expected value in stratum i, n_i^{exp}, is compared with the minimum size established at the beginning, **min**. It is worth mentioning that, except for the first category or stratum, the size of the expected value in a category to be compared with the minimum is that obtained after the loop 9-8-4-9 is performed, where step 4 is only performed for $i = 1$. In other words, it might be the result of the sum of the original value for this category and previous ones which have failed to reach the required minimum size.

11. If the expected value of a category reaches the minimum size, **min**, it is stored in the variable **last**, to be the last category to reach this minimum. Then proceed to check the next one (i.e. steps 8-9).

12. If the size of the expected value in a category does not reach the minimum, check whether the previous one is empty (i.e. it takes a value of zero).

13. If the value of a category i does not reach the minimum and the immediately previous category $i-1$ is empty, check whether there is a previous non-empty category, that has a size greater than the minimum, **last**> 0.

14. If the value of a category i does not reach the minimum, the previous one, $i-1$, is empty and there is a previous category that is not empty, **last**> 0, then compare the expected value of the next adjacent category, $i+1$ with the one of the previous non-empty category that reaches the minimum value; that is, the category with the index of **last**.

15. If the value of a category i does not reach the minimum, the previous one, $i-1$, is empty, there is a previous category that is not empty, **last**> 0, and the expected value of the next adjacent category is greater than the previous non-empty one that reaches the minimum value, then the values of the category analysed, i, are added to the nearest previous non-empty category, **last**.

$$n_{last}^{exp} = n_{last}^{exp} + n_i^{exp}$$

$$n_{last}^{obs} = n_{last}^{obs} + n_i^{obs}$$

After that, the values of the category analysed are reset (i.e. step 20), and the next one is then analysed (i.e. steps 8-9).

16. From the second category, the values of the category analysed are added to the following one, $n_{i+1}^{exp} = n_{i+1}^{exp} + n_i^{exp}$, $n_{i+1}^{obs} = n_{i+1}^{obs} + n_i^{obs}$ when the expected value does not reach the minimum, **min**, and some of the following conditions are met:

    - The immediately previous category, already analysed, is not empty because it reached the minimum size required, but its expected value is greater than or equal to the value of the next category, $n_{i-1}^{exp} \geq n_{i+1}^{exp}$;
    - There is no previous category already analysed that meets the minimum size requirement (i.e. all are empty), so that **last** $= 0$;
    - The immediately previous category, already analysed, is empty. That is, there is a one previous category that reached an expected value equal to or greater than the minimum, but at the same time is not minor than the next category to be analysed, $n_{i+1}^{exp} \leq n_{last}^{exp}$.

17. If the expected value of the category analysed does not reach the minimum, **min**, and the previous category is not empty, compare the size of the previous category with that of the subsequent one, $n_{i-1}^{exp} \geq n_{i+1}^{exp}$.

18. If the expected value of the category analysed does not reach the minimum, **min**, and the previous category is smaller than the subsequent one, $n_{i-1}^{exp} < n_{i+1}^{exp}$ but not

empty, the values of the category analysed are added to the previous category because it is the smallest size adjacent category.

$$n_{i-1}^{exp} = n_{i-1}^{exp} + n_i^{exp}$$

$$n_{i-1}^{obs} = n_{i-1}^{obs} + n_i^{obs}$$

19. Once the values of the category analysed have been added to the previous one (in step 18) the index of that category is stored in the variable **last**$= i-1$ because it is the last one to reach the minimum value.

20. Once the values of the category analysed have been added to the previous one (in step 18), the subsequent one (in step 16) or to the one with the index **last** (in step 15), the category analysed is initialized, $n_i^{exp} = 0$, $n_i^{obs} = 0$, and the next category is then analysed.

21. Once the last category of expected values is finally reached, its accumulated expected value, n_k^{exp}, is compared with the minimum, **min**.

22. If the accumulated expected value for the last category, n_k^{exp}, does not reach the minimum, **min**, the relevant value is added to the last one which did reach the minimum size, $n_{last}^{exp} = n_{last}^{exp} + n_i^{exp}$, and the same is done with the observed value of the original last one, $n_{last}^{obs} = n_{last}^{obs} + n_i^{obs}$. If the accumulated expected value for the last group reaches the minimum, then it remains unchanged.

23. After the expected and observed values of the last category, k, are added to the category **last** (in step 22), reset them all to zero.

24. The indexes for the categories (original and regrouped) are initialized, $i = 1$, $j = 1$.

25. Start a new loop (steps 25-29) to put together the vector of regrouped expected and observed values obtained in the previous steps. This loop is performed for all the expected values of the different strata, from the first to the last, k, i.e. for all $i \leq k$.

26. Check whether the accumulated expected value is greater than 0, $n_i^{exp} > 0$, which means, given what is mentioned in step 20, that it will be greater than the minimum.

27. If after regrouping the accumulated expected value of the i-th category is greater than 0 and, therefore, greater than the minimum, that value is assigned as the j-th component of a new vector of regrouped expected values, $\overline{\overline{n}}_j^{exp} = n_i^{exp}$, and the i-th updated observed value is assigned to the j-th component of the new vector of regrouped observed values $\overline{\overline{n}}_j^{obs} = n_i^{obs}$.

28. Count the number of regrouped strata put together up to this point, adding 1 to the index variable of regrouped strata in the new vectors (i.e., $j = j+1$).

29. Increment the index i for the original categories of the expected values: $i = i+1$, up to the maximum, k.

30. Once the loop in steps 25-29 ends, the final number of regrouped categories in the new vector of expected values, $cat_{reg} = j$, is obtained.

31. The information that enables Pearson's chi-square goodness-of-fit test (χ^2, df, p-value) to be carried out after the regrouping of strata is now available: $\{\overline{\overline{n}}_1^{exp}, \overline{\overline{n}}_2^{exp}, \ldots, \overline{\overline{n}}_{cat_{reg}}^{exp}\} = \{\overline{\overline{n}}_1^{obs}, \overline{\overline{n}}_2^{obs}, \ldots, \overline{\overline{n}}_{cat_{reg}}^{obs}\}$: total strata regrouped.

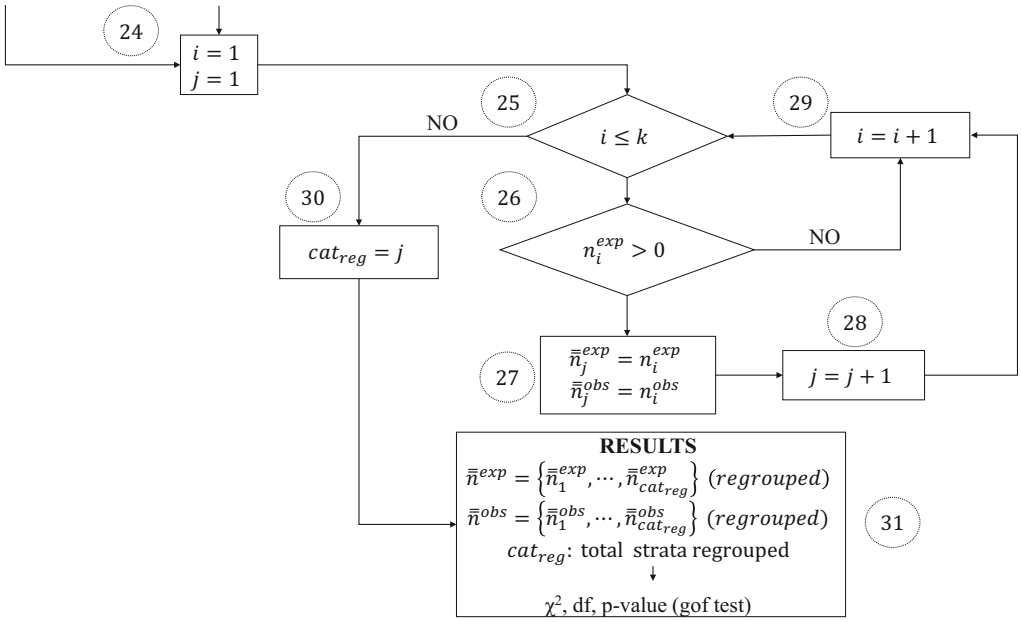

Figure 4: *Flowchart: Steps 25 to 31. Automatic regrouping of strata.*

The procedure for the regrouping of strata or categories given a minimum size is written in Excel VBA. As reported by McCullough (2008), it is well known that there are quite a few shortcomings in this statistical package; however he also pointed out, as Wilkinson (1994) and Ripley (2002) claimed, that it is the most commonly used software in basic statistical calculations. This is one of the main reasons for analysing its precision (Keeling and Pavur 2011), and to provide functions that can be incorporated into the Microsoft Excel Function Library to help other users, as other authors have already done (e.g., Okeniyi and Okeniyi 2012) or, for example, to improve Excel as a useful tool for teaching (Quintela-del-Río and Francisco-Fernández 2017). In the specialized literature there is an example of using Visual Basic (Khan 2003) and its relation to Fisher's exact test (FET). This test calculates the probability value for the relationship between two dichotomous variables in a 2×2 contingency table. FET is

used when a chi-square test is to be conducted but at least one of the cells has an expected frequency of five or less. FET can be used regardless of how small the expected frequency is. Khan (2003) emphasizes the potential utility of Visual Basic because of the user friendliness of the program, its object-oriented feature and the fact that most users are familiar with a Microsoft Windows environment, especially in biomedical applications. Furthermore, the procedure is written in Mathematica to illustrate that the proposed functions can be generalized to other software. As for example McCullough (2000) pointed out, Mathematica cannot be really categorized as a statistical package, but it has complements for carrying out statistical analysis with more precision than other statistical packages. The functions are inspired by the work of Ross (2015) and Pérez-Salamero González (2015), the latter being written in VBA. More specifically, the programming adopts functions defined by the user which yield the values for the elements needed to calculate the χ^2 test. In other words, the programming relies on the functions already available which are related to the test.

Listing 1 and Listing 2 (the latter for Mathematica) in the supplementary material in Appendix C include the code of the functions that yield the value of the χ^2 statistic after automatic regrouping starting from a minimum value set by the user. The length of the code can be attributed more to explanatory purposes than to an effort to keep it short. There is a difference between the functions that yield the observed and expected values in VBA and Mathematica. In the former we choose to define a matrix function such that the result appears in many cells because the user does not know exactly when the function will need to be used or how many regrouped categories will result. The function is written in such a way that it selects two columns and as many rows as there were original categories, so that the user can see the regrouped categories as well as those with zero values. In the case of Mathematica, the function that returns the vectors of observed and expected values is designed to put together the categories, showing only those regrouped with values above the minimum (i.e. those with non-zero values are eliminated) as indicated in the flowchart loop (steps 25-29). Listing 3 in the supplementary material in Appendix C includes the code for the functions written in VBA. These functions give the number of regrouped strata in order to determine the degrees of freedom for the test. Likewise, Listing 4 shows the code for a matrix function in Excel which yields the output of the observed and expected values of the regrouped categories. Finally, for the case of Mathematica we incorporate the number of categories (see Listing 5 in the supplementary material in Appendix C), the p-value for the test (Listing 6). Finally, Listing 7 shows the relevant information resulting from the regrouping procedure, such as the value of the χ^2 statistic, the p-value, and the regrouped strata (observed and expected).

4. Simulation study

The purpose of this simulation study is to illustrate the performance of the proposed regrouping procedure on the goodness-of-fit chi-square test. The simulation study will focus on showing whether or not the proposed regrouping procedure attains the nominal significant level. We consider two different settings:

S1. The null hypothesis includes a fully specified model, so there are no parameters to be estimated.
S2. The null hypothesis includes a partially specified model in which parameters need to be estimated to compute the theoretical expected frequencies under the null hypothesis before the value of the goodness-of-fit chi-square test statistic is computed.

4.1. Fully Specified Population Distribution

Simulation 1. The complete simulation steps are described below:

1. Six different combinations of the number of observations available, N, and the number of categories, k, are considered: A ($N = 50$, $k = 10$) , B ($N = 75$, $k = 15$), C ($N = 100$, $k = 20$), D ($N = 1000$, $k = 20$), E ($N = 500$, $k = 20$) and F ($N = 250$, $k = 20$).

2. For each combination, 5000 samples are generated from 100 different, fully specified multinomial populations under the null hypothesis, covering a wide range of possible multinomial probabilities distributions.

3. Once the 5000 samples have been generated for each combination and under each different multinomial population, we use the goodness-of-fit chi-square test statistic to test whether the data fits the theoretical distribution without regrouping. Under the null hypothesis, the chi-square statistic follows a chi-square distribution with $(k-1)$ degrees of freedom. We use three different nominal significance levels, (α=0.10, 0.05 and 0.01). Hence, the significance levels attained are computed, corresponding to the number of times that the null hypothesis is rejected for each of the 5000 samples.

4. To assess the behaviour of the procedure proposed the same thing is done, but in this case, the categories are regrouped in those samples where the procedure proposed suggests that regrouping of some of the adjacent categories is necessary. In this case, the chi-square statistic follows a chi-square distribution with $(k-1)$ degrees of freedom under the null if it is not necessary to regroup, and with (k^*-1) degrees of freedom if it is, where k^* is the number of classes remaining after regrouping. Three different nominal significance levels are used, (α=0.10, 0.05 and 0.01), and the significance levels attained are computed as before.

5. Finally, the significance levels attained for the three nominal significance levels under study are compared, without no regrouping procedure and with the regrouping procedure proposed here.

Table 2 summarizes the results of the simulation study described above. Because it is realized that the different settings mean that these results cannot really be combined, the table includes the mean and standard deviation of the significance levels attained for the 5000 simulations in each of the six (N,k) combinations considered for the 100 different multinomial populations in the null hypothesis. The results shown in the table lead us to conclude that the regrouping procedure proposed provides mean attained significance levels closer to the nominal ones than those obtained by not regrouping. Moreover, standard deviations for the attained nominal significance levels are smaller when the regrouping procedure proposed is used.

Table 2: *Simulation 1. Mean attained and standard deviations from nominal significance levels for the 5000 simulations in each of the six (N,k) combinations considered for the 100 different multinomial populations in the null hypothesis of a fully specified population distribution for the chi-square goodness-of-fit test.*

		nominal significance level					
populations		α **= 10%**		α **= 5%**		α **= 1%**	
		do not reg	**reg**	**do not reg**	**reg**	**do not reg**	**reg**
A	mean	0.1019	0.0974	0.0558	0.0484	0.0168	0.0099
	st. dev.	*0.0097*	*0.0037*	*0.0103*	*0.0031*	*0.0105*	*0.0013*
B	mean	0.1049	0.0980	0.0585	0.0489	0.0175	0.0101
	st. dev.	*0.0092*	*0.0045*	*0.0097*	*0.0031*	*0.0077*	*0.0013*
C	mean	0.1073	0.0985	0.0613	0.0491	0.0200	0.0101
	st. dev.	*0.0093*	*0.0042*	*0.0088*	*0.003*	*0.0079*	*0.0014*
D	mean	0.1021	0.1011	0.0527	0.0508	0.0119	0.0104
	st. dev.	*0.0968*	*0.0044*	*0.0041*	*0.0035*	*0.0024*	*0.0015*
E	mean	0.1020	0.0998	0.0532	0.0506	0.0127	0.0106
	st. dev.	*0.1048*	*0.0036*	*0.0044*	*0.0029*	*0.0028*	*0.0016*
F	mean	0.1027	0.0996	0.0540	0.0501	0.0137	0.0103
	st. dev.	*0.1018*	*0.0043*	*0.0052*	*0.0031*	*0.0040*	*0.0015*
ALL	mean	**0.1036**	**0.0989**	**0.0562**	**0.0495**	**0.0157**	**0.0102**

For the sake of brevity, Tables A2 to A7 in the supplementary material show results for only 10 selected different multinomial populations out of the 100 considered in this simulation study, where the theoretical probabilities under the null hypothesis are described at the top of the tables for the different sample sizes N and numbers of categories

k considered in the simulation study. As indicated above, 5000 simulations from each of these populations were simulated for different N and k, and three different nominal significance levels were considered. Significance levels attained by using the procedure without regrouping and those obtained using the regrouping procedure proposed here are reported at the bottom of the tables for each setting. From the results reported in Tables A2 to A7 in the supplementary material, and given that the significance levels attained are very close to the nominal significance levels considered here for all the different combinations of sample sizes, population distributions, and nominal significance levels considered in the study, it can be concluded that the regrouping procedure proposed performs reasonably well compared to the results obtained without regrouping in the case of a chi-square goodness-of-fit test to a fully specified distribution.

4.2. Partially Specified Population Distribution

Simulation 2. The complete simulation steps are described below:

1. 5000 samples are generated from a known distribution, with no loss of generality: a N(0,1) distribution, for 6 different combinations of the number of observations available, N, and the number of categories, k: A ($N = 50$, $k = 10$) , B ($N = 75$, $k = 15$), C ($N = 100$, $k = 20$), D ($N = 1000$, $k = 20$), E ($N = 500$, $k = 20$) and F ($N = 250$, $k = 20$).

2. For each sample and each setting, the mean μ and the standard deviation σ of the normal distribution are estimated using the maximum likelihood method.

3. For the 6 different combinations of N and k, each of the 100 different multinomial probability combinations is assigned to each of the k categories.

4. The different k categories (i.e. the interval limits for each class or category) in the estimated distribution $N(\hat{\mu}, \hat{\sigma}^2)$ are built up so that these intervals match the probability of belonging to this class in the estimated distribution $N(\hat{\mu}, \hat{\sigma}^2)$ with that in the corresponding multinomial population considered.

5. Once the 5000 samples have been generated for each combination and under each different multinomial populations, we use the goodness-of-fit chi-square test statistic to test wether the data fits the theoretical distribution without regrouping. Under the null hypothesis, the chi-square statistic follows a chi-square distribution with $(k-r-1) = (k-2-1) = (k-3)$ degrees of freedom. Three different nominal significance levels are used: (α=0.10, 0.05 and 0.01). Hence, the significance levels attained are computed, corresponding to the number of times that the null hypothesis is rejected for each of the 5000 samples.

6. To assess the behaviour of the proposed procedure, the same is done, but in this case, the categories are regrouped in those samples where the procedure proposed

suggests that regrouping of some of the adjacent categories is necessary. In this case, the chi-square statistic follows a chi-square distribution with $(k-3)$ degrees of freedom under the null if it is not necessary to regroup, and with (k^*-3) degrees of freedom if it is, where k^* is the number of remaining classes after regrouping. Three different nominal significance levels are used: (α=0.10, 0.05 and 0.01), and the significance levels attained are computed as before.

7. Finally, the significance levels attained are compared for the three nominal significance levels under study without and then with the regrouping procedure proposed.

Table 3 summarizes the results obtained of the simulation study described above. Because it is realized that the different settings mean that these results cannot really be combined, the table includes the mean and standard deviation of the significance levels attained for the 5000 simulations in each of the six (N,k) combinations considered for the 100 different multinomial population distributions for a partially specified goodness-of-fit test of the null hypothesis of a normal distribution. The results shown in the table lead us to conclude that the regrouping procedure proposed provides mean nominal significance levels closer to the nominal ones than those obtained by not regrouping, with the exceptions of the combinations A, for $\alpha = 10\%$ and 5%, and B, for $\alpha = 10\%$. Moreover, standard deviations for the attained nominal significance levels are smaller when the regrouping procedure proposed is used.

For the sake of brevity, Tables A8 to A13 in the supplementary material show results for only 10 selected different multinomial probability distributions out of the 100 considered in this simulation study for the null hypothesis of a normal population distribution, where the theoretical probabilities assigned to each of the classes under the null hypothesis are described in the top part of the tables for the different sample sizes N and numbers of categories k considered in the simulation study. As indicated above, 5000 simulations from a standard normal population were simulated for different N and k, and three different nominal significance levels were considered. Significance levels attained by using the procedure without and then with the regrouping procedure proposed here are reported at the bottom of the tables for each setting. From the results reported in Tables A8 to A13 in the supplementary material, and given that the significance levels attained are very close to the nominal significance levels considered here for all of the different combinations of sample sizes, population distributions, and nominal significance levels considered in the study, it can concluded that the regrouping procedure proposed performs reasonably well compared to the results obtained without regrouping in the case of a chi-square goodness-of-fit test to a partially specified distribution where parameters needed to be estimated.

Table 3: *Simulation 2. Mean attained and standard deviations from nominal significance levels for the 5000 simulations in each of the six (N,k) combinations considered for the 100 different multinomial populations in the null hypothesis of a partially specified normal population distribution for the chi-square goodness-of-fit test.*

		nominal significance level					
populations		α **= 10%**		α **= 5%**		α **= 1%**	
		do not reg	**reg**	**do not reg**	**reg**	**do not reg**	**reg**
A	mean	0.1134	0.1378	0.0617	0.0689	0.0180	0.0135
	st. dev.	*0.0097*	*0.0183*	*0.0107*	*0.0101*	*0.0114*	*0.0020*
B	mean	0.1375	0.1422	0.0890	0.0862	0.0461	0.0404
	st. dev.	*0.0099*	*0.0049*	*0.0110*	*0.0032*	*0.0084*	*0.0013*
C	mean	0.1107	0.1087	0.0624	0.0539	0.0202	0.0106
	st. dev.	*0.0087*	*0.0047*	*0.0092*	*0.0030*	*0.0087*	*0.0013*
D	mean	0.1063	0.1056	0.0554	0.0536	0.0129	0.0113
	st. dev.	*0.1128*	*0.0041*	*0.0053*	*0.0032*	*0.0032*	*0.0014*
E	mean	0.1080	0.1063	0.0566	0.0545	0.0137	0.0116
	st. dev.	*0.1080*	*0.0035*	*0.0045*	*0.0028*	*0.0031*	*0.0015*
F	mean	0.1059	0.1036	0.0563	0.0526	0.0142	0.0110
	st. dev.	*0.1150*	*0.0036*	*0.0054*	*0.0025*	*0.0042*	*0.0013*
ALL	mean	**0.1143**	**0.1185**	**0.0643**	**0.0624**	**0.0216**	**0.0169**

5. Further illustrative examples

We use three additional examples and datasets to illustrate the use of the customized functions defined in Excel and Mathematica, where the regrouping of strata or categories could arise. In the first, the functions proposed in this paper are compared with some of the software tools described in Appendix A in the supplementary material. Some of them do not automatically regroup and others, e.g. MATLAB, do so but only at the extreme ends of the tails. The second example illustrates the use of the regrouping functions when it is necessary to estimate parameters in the theoretical distribution. The third shows the iterative use of the regrouping functions with application to analyse the Continuous Sample of Working Lives (CSWL) survey from Spain.

5.1. Case 1. Pearson's Illustration V

The data labeled "*Illustration V*" comes from the paper by Pearson (1900). Table 4 shows that 6 of the 17 categories considered in the example have positive expected values lower than 5, with 4 of them being values smaller than 1. Those strata are all located

in the bins at the extreme ends. The null hypothesis is the fully specified population distribution with probabilities described in Pearson (1900).

Table 4: *Case 1. Illustration V example. Observed and expected values are reported, as well as results for the goodness-of-fit chi-square test for fully specified distributions with no regrouping of categories and with the regrouping procedure proposed here.*

Category	Original		Regrouped	
	Observed	Expected	Observed	Expected
1	0	0.18		
2	3	0.68		
3	7	13.48	10	14.34
4	35	45.19	35	45.19
5	101	79.36	101	79.36
6	89	96.10	89	96.10
7	94	90.90	94	90.90
8	70	71.41	70	71.41
9	46	48.25	46	48.25
10	30	28.53	30	28.53
11	15	14.94	15	14.94
12	4	6.96	10	11.34
13	5	2.88		
14	1	1.06		
15	0	0.34		
16	0	0.10		
17	0	0.00		
Total	500	500.36	500	500.36
χ^2	11.75		10.51	
df	16		9	
p-value	0.101		0.31083538	
Source: Own work based on Pearson (1900)				

Pearson (1900) considered there to be 17 categories, though the expected value of the last one is zero. Taking into account all the strata and with no regrouping, the value of the χ^2 test statistic compared to a chi-square distribution with 16 degrees of freedom results in a p-value of 0.101. Moreover, the functions defined in Excel and Mathematica, presented in the supplementary material included in Appendix 2, regroup them into 10 categories. The last two columns of Table 4 show how the proposed functions regroup

Table 5: *Case 2. Observed and expected values are reported, as well as results for the goodness-of-fit chi-square test for partially specified distributions with no regrouping of categories and with the regrouping procedure proposed here. The null hypothesis states that the population follows a partially specified normal distribution.*

Categ.	pexp	expected	ac prob exp	levels	Obs	Obs. Reg.	Exp. reg.
1	0.161926968	8.09634839	0.161926968	−0.7747845	9	9	8.09634839
2	0.168545644	8.42728221	0.330472612	−0.31307327	8	8	8.42728221
3	0.037262021	1.86310107	0.367734633	−0.22818199	0		
4	0.162660577	8.13302885	0.530395211	0.12075745	10	10	9.99612992
5	0.015025858	0.75129289	0.545421068	0.152639283	1		
6	0.017927913	0.89639567	0.563348982	0.190863633	4		
7	0.109949741	5.49748705	0.673298723	0.434859108	3	8	7.14517561
8	0.099373226	4.96866129	0.772671949	0.68648864	5		
9	0.037554998	1.8777499	0.810226947	0.796917803	3	8	6.84641119
10	0.189773053	9.48865267	1	0.796917803	7	7	9.48865267
				p-value do not reg.	0.028	p-value reg.	0.7839

the original categories. Considering the 10 categories resulting after regrouping, the value of the χ^2 test statistic, when compared to a chi-square distribution with 9 degrees of freedom results in a p-value of 0.311. The problems a potential user would have when using the different software tools available for the analysis of this dataset are outlined in Appendix A in the supplementary material.

5.2. Case 2. Example of a partially specified population distribution

This example illustrates the use of the regrouping functions once the parameters of a partially specified theoretical distribution have been estimated by the maximum likelihood method using the sample data provided in Table A14 in the supplementary material. The example is based on the second simulation study described in Section 4. The null hypothesis states that the population follows a partially specified normal distribution and its parameters, its mean and standard deviation, are unknown and must therefore be estimated from the values reported in Table A14 in the supplementary material. Parameters are estimated by maximum likelihood, using the **fitdistrib** function in the MASS library in R. Therefore, the null hypothesis states that the data follows a $N(\widehat{\mu},\widehat{\sigma}) = N(0.056497994, 0.842599379)$ distribution. To test this hypothesis and obtain the goodness-of-fit chi-square test statistic for partially specified distributions, there are originally $k = 10$ categories and $(k-3)$ degrees of freedom for test statistic chi-square distribution in the case of not regrouping. In the case of regrouping, the degrees of freedom are (k^*-3), where k^* is the number of remaining categories after the regrouping procedure proposed is applied. In order to force the necessity for regrouping, different probabilities are randomly assigned to the $k = 10$ categories used for this test. Given the estimated parameters and the probabilities assigned to each category, we obtain the interval limits for these categories by using the procedure previously described in the Simulation 2 settings. Table 5 reports the information required to perform the test and the resulting p-values obtained with and without regrouping. Under the regrouping procedure proposed the null hypothesis is not rejected, but it is clearly rejected if there is no regrouping, at least at the 10% and 5% significance levels.

5.3. Case 3. Example with the Continuous Sample of Working Lives dataset

This example illustrates the iterative use of the proposed regrouping functions. The χ^2 test statistic value is included as a constraint that requires that the null hypothesis not be rejected in an optimization problem written in Excel. This example is taken from Pérez-Salamero González et al. (2017). The sample data used is the Continuous Sample of Working Lives (CSWL) survey from Spain for calendar year 2013 (DGOSS 2014). A comprehensive overview of this dataset can be found in Pérez-Salamero González, Regúlez-Castillo and Vidal-Meliá (2016, 2017) and MESS (2017). The Continuous

Sample of Working Lives (CSWL) is a simple random sample of around 4% of the reference population defined as individuals who have had some connection (through contributions, pensions or unemployment benefits) with the Social Security System at some time during the year of reference. It contains administrative data on working lives, which provide the basis for this sample taken from Spanish Social Security records, and comprises anonymized microdata with detailed information on individuals. Using a post-stratification process, Pérez-Salamero González et al. (2017) obtain from the CSWL for the calendar year 2013, the data corresponding to the number of male pensioners classified as permanently disabled, organized by age in 18 categories or strata. The population distribution is known as of December 31st (INSS 2014), which means that the relative expected frequencies are also known, and hence so are the expected values (i.e. this is a fully specified population distribution test setting). Table 6 reports the observed values from the CSWL and the expected values from the theoretical population under the null hypothesis, along with the corresponding fully specified chi-square goodness-of-fit test results with and without regrouping. From the results reported in Table 6, we conclude that the null hypothesis is clearly rejected whether regrouping is performed or not. That is, the null hypothesis is clearly rejected in the case of automatic regrouping and also in the case of no regrouping of strata. The **chisq.test** function written in Excel is used for the regrouping procedure proposed. Moreover, the fit of the sample to the population could be improved, since the null hypothesis is rejected, and given that the p-value is very small. If a subsample from the CSWL is selected such that its distribution does not reject the null hypothesis for a given significance level, this would provide a more representative subsample of the permanently disabled male pensioner population by age than the original sample, which is one of the main objectives for practitioners in the area.

To further show the utility of the customized functions used iteratively which enable the χ^2 test to be conducted with automatic regrouping of strata that violate the minimum size requirement, we propose an optimization problem with constraints. The aim is to find the largest subsample contained in the CSWL subject to the non rejection of the null hypothesis of the assumed theoretical distribution for the population. The search for the largest subsample is justified by an attempt to ensure that as few pension records as possible are missed out, so as not to overlook diversity in pensioners' working lives. The mathematical development of the problem is shown in Appendix B in the supplementary material. It is implemented in Excel by using the functions defined in the supplementary material in Appendix C, which allows for an automatic regrouping procedure. The problem is solved by using the **Solver** by *Frontline Systems*. Given its non-linearity, the method for solving the problem is GRG *Nonlinear*. Moreover, we omit the integer constraint (6) on the variables (see Appendix B).

Table 6: *CSWL 2013. Permanent Disability: Males. Observed and expected values are reported, as well as results for the goodness-of-fit chi-square test for completely specified distributions without regrouping categories and with the regrouping procedure proposed here.*

Age Category	Original		Regrouped	
	Observed	Expected	Observed	Expected
15-19	0	0.04		
20-24	29	30.04	29	30.08
25-29	198	195.33	198	195.33
30-34	606	581.48	606	581.48
35-39	1,201	1,203.73	1,201	1,203.73
40-44	2,014	1,982.02	2,014	1,982.02
45-49	3,106	3,050.46	3,106	3,050.46
50-54	4,281	4,230.30	4,281	4,230.30
55-59	5,710	5,706.36	5,710	5,706.36
60-64	7,151	7,269.83	7,151	7,269.83
65-69	3	58.48	3	58.48
70-74	6	3.28		
75-79	7	4.28	13	7.56
80-84	14	10.88	14	10.88
≥ 85	17	16.48	17	16.48
Total	24,343	24,343	24,343	24,343
χ^2	62.76		62.66	
df	14		12	
p-value	p-value$<$0.0001		p-value$<$0.0001	
Source: Own work based on Pérez-Salamero González et al. (2017)				

Accuracy in compliance with constraints is set to 0.0000001. We select the option "Multistart" to use the multistart method for global optimization with a population size of $100,000$ and a random seed value of $100,000$, using "Central" to estimate derivatives through central differencing. After $100,000$ subproblems are solved, a non-integer solution is reached ("*Solver found a probability of reaching a global solution*"). The solution is then rounded and it is finally checked that the one obtained is contained in the original sample. Constraint **[2.]** in Appendix B, related to the improvement of the goodness-of-fit, is not satisfied by a small error of 0.000000722, the difference between the sample value of the test and the critical value at the 5% significance level, with a reported p-value of 0.0499993. The emergence of this solution, with no attention paid to the minimum size requirement for the strata, is due to the functions defined in the sup-

plementary material in Appendix C. These functions regroup the original 15 strata into 12, with the regrouping being carried out at different times during the iterative process. This highlights the need for an automatic regrouping process because it is completely impossible to regroup exogenously in the procedure within each iteration.

Table 7: *Subsample from the CSWL 2013. Permanent disability: Males. Observed and expected values are reported, as well as results for the goodness-of-fit chi-square test for completely specified distributions without regrouping categories and with the regrouping procedure proposed here. In addition, results for the subsample obtained with the proposed algorithm are also reported.*

Age Category	Original sample CSWL		Subsample (before rounding)			
	Observed	Observed (regrouped)	Observed	Expected	Observed (regrouped)	Expected (regrouped)
15-19	0		0	0.02		
20-24	29	29	13.03	12.98	13.03	13.00
25-29	198	198	84.59	84.41	84.59	84.41
30-34	606	606	251.80	251.27	251.80	251.27
35-39	1,201	1,201	521.25	520.15	521.25	520.15
40-44	2,014	2,014	858.27	856.46	858.27	856.46
45-49	3,106	3,106	1,320.94	1,318.14	1,320.94	1,318.14
50-54	4,281	4,281	1,831.85	1,827.97	1,831.85	1,827.97
55-59	5,710	5,710	2,471.03	2,465.80	2,471.03	2,465.80
60-64	7,151	7,151	3,148.06	3,141.39	3,148.06	3,141.39
65-69	3	3	3	25.27	3	25.27
70-74	6		2.25	1.42		
75-79	7	13	0.25	1.85		
80-84	14	14	5.48	4.70	7.99	7.97
≥ 85	17	17	7.14	7.12	7.14	7.12
Total	24,343	24,343	10,518.94	10,518.94	10,518.94	10,518.94
χ^2	62.76	62.66	21.69		19.68	
df	14	12	14		11	
p-value	$p < 0.0001$	$p < 0.0001$	0.0851783		0.0499993	
Source: Own work based on Pérez-Salamero González et al. (2017)						

The results of the optimization process and the size of the strata associated with the solution obtained are presented in Table 7. The first two columns in Table 7 correspond to the first and third columns of Table 6, and we report them back in order to improve the comparison between the original sample and the subsample obtained. The last four columns in Table 7 have the same structure as the ones shown in Tables 1, 4, 5 and 6.

Table 7 shows that the p-value of 0.085 obtained for the χ^2 goodness-of-fit test in the subsample with no regrouping of strata results in no rejection of the null hypothesis, whereas the p-value of 0.04999928 obtained after regrouping is at the limit of rejection of the null hypothesis, both at the 5% significance level.

In relation to this example, Pérez-Salamero González et al. (2017) conduct a similar analysis for the CSWL for 2010. They simultaneously consider five types of pension and both genders and obtain the largest representative subsample contained in the original sample with 146 strata, reaching the last iteration and regrouping them into 115 categories to carry out the corresponding goodness-of-fit test. This illustrates the importance of having automatic regrouping when a large-scale iterative procedure is used.

6. Summary, conclusions and further research

In empirical studies where Pearson's goodness-of-fit χ^2 test is conducted, it is a common practice to regroup strata to attain a minimum size of expected frequencies for the test to be valid and its conclusions reliable. In general, after a comprehensive review of the software that can carry out this test, we conclude that there is no automatic regrouping of strata to meet this requirement, although it would be very useful if such a feature were available. Having such automatic regrouping available in other packages would be of great help to researchers in many areas, such as social sciences, biomedical and health sciences, and others where this test is usually required in empirical research. This paper proposes some functions that enable automatic regrouping to take place. This process is not only applied at the extreme ends of the tail strata, as in the case of MATLAB, but also when intermediate categories do not meet the minimum size requirement, as in SSJ (a Java library for stochastic simulation).

A simulation study shows that the regrouping functions proposed in this paper work reasonably well compared to the test without regrouping. We find that the nominal significance levels attained with regrouping are suitable and slightly better than those obtained without regrouping. They guarantee that the hypotheses of the minimum size are satisfied, reducing the risk of a wrong conclusion on the goodness-of-fit chi-square test. The customized functions developed here have the advantage of being easier to implement than SSJ in an iterative process, where the test statistic must be calculated and the regrouping carried out in each iteration. Moreover, they offer an alternative way of regrouping that solves the asymmetry problem in the test results. This type of process is illustrated with a real case example in the resolution of mathematical optimization problems. MATLAB also has this advantage, but it does not allow regrouping in intermediate categories. Therefore, those functions enable Pearson's goodness-of-fit chi-square test to be carried out with the possibility of regrouping categories, which we believe is quite a major improvement on the current software available for basic statistical analysis, both in the case of the most widely used program, Excel, and other more precise packages

such as Mathematica. We also believe that these proposals could be very useful to make the automatic regrouping of categories or strata available in the iterative use of the test statistics used in Big Data and Data Mining (Larose and Larose, 2014), for example, at the instance selection and association analysis stages, among others.

Finally, based on the proposals included and results reported in this paper, one possible direction for future research would be to adapt the code of the proposed functions to other languages and optimization environments such as AMPL, GAMS, LINGO, R, etc, in order to be able to integrate them into the numerical resolution of problems of this type. It would also be interesting to make the regrouping process automatic, but based on other, more general criteria, such as, for example, sample size or number of categories, and to explore alternative ways of regrouping. This would require analysing the effect of the different regrouping proposals on the goodness-of-fit chi-square test results for different sample sizes, number of categories and theoretical distributions under study. This is out of the current scope of this paper, but could be the objective of future research.

Acknowledgements

The authors gratefully acknowledge financial support from Ministerio de Economía y Competitividad (Spain), Agencia Estatal de Investigación (AEI), and the European Regional Development Fund (ERDF), under research grants ECO2015-65826-P (AEI/ERDF, EU) and MTM2016-74931-P (AEI/ERDF, EU) and from the Department of Education of the Basque Government (UPV/EHU MacLab Research Group and UPV/EHU Econometrics Research Group) under research grants IT 793-13 and IT-642-13, respectively. The authors wish to thank the editor and two anonymous referees for providing thoughtful comments and suggestions which have led to substantial improvement in the presentation of the material in this paper. They also would like to thank Jose M. Pavía, Miguel Angel García Pérez and Fernando Tusell for their comments and suggestions, and Christopher G. Pellow for his help with the English. Any errors are entirely due to the authors.

References

Agresti, A. (2002). *Categorical Data Analysis* (2nd edition). Wiley, New York.

Bartholomew, D.J. and Tzamourani, P. (1999). The goodness-of-fit of latent trait models in attitude measurement. *Sociological Methods and Research*, 27, 525–546.

Bartholomew, D.J., Knott, M. and Moustaki, I. (2011). *Latent Variable Models and Factor Analysis* (3rd edition). Wiley, New York.

Bishop, Y.M.M., Fienberg, S.E. and Holland, P.W. (1975). *Discrete Multivariate Analysis: Theory and Practice*. MIT Press, Cambridge.

Bosgiraud, J. (2006). Sur le regroupement des classes dans le test du Khi-2. *Revue Romaine de Mathématiques Pures et Appliquées*, 51, 167–172.

Cai, L., Maydeu-Olivares, A., Coffman, D.L. and Thissen, D. (2006). Limited-information goodness-of-fit testing of item response theory models for sparse 2p tables. *British Journal of Mathematical and Statistical Psychology*, 59, 173–194.

Campbell, I. (2007). Chi-squared and Fisher-Irwin tests of two-by-two tables with small sample recommendations. *Statistics in Medicine*, 26, 3661–3675.

Cochran, W.G. (1952). The χ^2 test of goodness-of-fit. *The Annals of Mathematical Statistics*, 23, 315–345.

Collins, L.M., Fidler, P.L., Wugalter, S.E. and Long, J. (1993). Goodness-of-fit testing for latent class models. *Multivariate Behavioral Research*, 28, 375–389.

Delucchi, K.L. (1983). The use and misuse of chi-square: Lewis and Burke revisited. *Psychological Bulletin*, 94, 166–176.

DGOSS (2014). Muestra Continua de Vidas Laborales 2013. Secretaría de Estado de la Seguridad Social. Dirección General de Ordenación (DGOSS). Ministerio de Trabajo e Inmigración. Madrid, Spain.

Fienberg, S.E. (2006). Log-linear models in contingency tables. In *Encyclopedia of Statistical Sciences*. Wiley, New York.

Fisher, R.A. (1935). The logic of inductive inference. *Journal of the Royal Statistical Society*, 98, 39–54.

García Pérez, M.A. and Nuñez-Antón, V. (2009). Accuracy of power-divergence statistics for testing independence and homogeneity in two-way contingency tables. *Communications in Statistics - Simulation and Computation*, 38, 503–512.

Goodman, L.A. (1974). Exploratory latent structures analysis using both identifiable and unidentifiable models. *Biometrika*, 61, 215–231.

Grafstörm, A. and Schelin, L. (2014). How to select representative samples. *Scandinavian Journal of Statistics*, 41, 277–290.

Haviland, M.G. (1990). Yates´ s correction for continuity and the analysis of 2×2 contingency-tables. *Statistics in Medicine*, 9, 363–367.

Hirji, K.F. (2006). *Exact Analysis of Discrete Data*. Chapman and Hall, Boca Raton.

Hosmer, D.W., Hosmer, T., Le Cessie, S. and Lemeshow, S. (1997). A comparison of goodness-of-fit tests for the logistic regression model. *Statistics in Medicine*, 16, 965–980.

Hosmer, D.W. and Lemeshow, S. (2000). *Applied Logistic Regression*. Wiley, New York.

INSS (2014). Informe Estadístico 2013. Secretaría de Estado de Seguridad Social. Ministerio de Empleo y Seguridad Social, MESS. Madrid, Spain.

Keeling, K.B. and Pavur, R.J. (2011). Statistical accuracy of spreadsheet software. *The American Statistician*, 65, 265–273.

Khan, H.A. (2003). A visual basic software for computing Fisher´s exact probability. *Journal of Statistical Software*, 8, 1–7.

Kroonenberg, P.M. and Verbeek, A. (2018). The tale of Cochran´s rule: my contingency table has so many expected values smaller than 5, what am I to do? *The American Statistician*, 72, 175–183.

Kruskal, W. and Mosteller, F. (1979a). Representative sampling, I. *International Statistical Review*, 47, 13–24.

Kruskal, W. and Mosteller, F. (1979b). Representative sampling, II: scientific literature, excludind statistics. *International Statistical Review*, 47, 111–127.

Kruskal, W. and Mosteller, F. (1979c). Representative sampling, III: the current statistical literature. *International Statistical Review*, 47, 245–265.

Kruskal, W. and Mosteller, F. (1980). Representative sampling, IV: The History of the Concept in Statistics, 1895-1939. *International Statistical Review*, 48, 169–195.

Larose, D.T. and Larose, C.D. (2014). *Discovering Knowledge in Data: An Introduction to Data Mining*. Wiley, New York.

Lazarsfeld, P.F. and Henry, N.W. (1968). *Latent Structure Analysis*. Houghton Mifflin, Boston.

Lewis, D. and Burke, C.J. (1949). The use and misuse of chi-square. *Psychological Bulletin*, 46, 433–489.

Lin, J.J., Chang, C.H. and Pal, N. (2015). A revisit to contingency table and tests of Independence: bootstrap is preferred to chi-square approximations as well as Fisher's exact test. *Journal of Biopharmaceutical Statistics*, 25, 438–458.

Lydersen, S., Fagerland, M.W. and Laake, P. (2009). Tutorial in biostatistics. Recommended tests for association in 2x2 tables. *Statistics in Medicine*, 28, 1159–1175.

Marsaglia, G. (2003). Random number generators. *Journal of Modern Applied Statistical Methods*, 2, 2–13.

McCullough, B.D. (2000). The accuracy of Mathematica 4 as a statistical package. *Computational Statistics*, 15, 279–299.

McCullough, B.D. (2008). Special section on Microsoft Excel 2007. *Computational Statistics and Data Analysis*, 52, 4568–4569.

Mehta, C.R. and Patel, N.R. (1983). A network algorithm for performing Fisher's exact test in r×c contingency tables. *Journal of the American Statistical Association*, 78, 427–434.

MESS (2017). La Muestra Continua de Vidas Laborales. Guía del contenido. Estadísticas, Presupuestos y Estudios. Estadísticas. Secretaría de Estado de Seguridad Social. Ministerio de Empleo y Seguridad Social, MESS. Madrid, Spain.

Moore, D.S. (1986). Tests of chi-squared type. In *Goodness-of-fit Techniques* (R. D'Agostino and M. Stephens, eds.). Marcel Dekker, New York, 63–95.

Okeniyi, J.O. and Okeniyi, E.T. (2012). Implementation of Kolmogorov Smirnov p-value computation in Visual Basic: implication for Microsoft Excel library function. *Journal of Statistical Computation and Simulation*, 82, 1727–1741.

Omair, A. (2014). Sample size estimation and sampling techniques for selecting a representative sample. *Journal of Health Specialties*, 2, 142–147.

Pearson, K. (1900). On the criterion that a given system of deviations from the probable in the case of a correlated system of variables is such that it can be reasonably supposed to have arisen from random sampling. *Philosophical Magazine*, 50, 157–175.

Pérez-Salamero González, J.M. (2015). La Muestra Continua de Vidas Laborales (MCVL) como fuente generadora de datos para el estudio del sistema de pensiones. Unpublished Ph.D. Thesis. Universitat de Valéncia, Spain.

Pérez-Salamero González, J.M., Regúlez-Castillo, M. and Vidal-Meliá, C. (2016). Análisis de la representatividad de la MCVL: el caso de las prestaciones del sistema público de pensiones. *Hacienda Pública Española (Review of Public Economics)*, 217, 67–130

Pérez-Salamero González, J.M., Regúlez-Castillo, M. and Vidal-Meliá, C. (2017). The continuous sample of working lives: improving its representativeness. *SERIEs. Journal of the Spanish Economic Association*, 8, 43–95.

Quintela-del-Río, A. and Francisco-Fernández, M. (2017). Excel templates: a helpful tool for teaching statistics. *The American Statistician*, 71, 317–325.

Ramsey, C.A. and Hewitt, A.D. (2005). A methodology for assessing sample representativeness. *Environmental Forensics*, 6, 71–75.

Ripley, B.D. (2002). Statistical methods need software: a view of statistical computing. *Opening lecture - Royal Statistical Society*, Plymouth.

Ross, A. (2015). Probability or statistics-permorming a chi-square goodness-of-fit test. *Mathematical Stack Exchange*.

Tollenaar, N. and Mooijaart, A. (2003). Type I errors and power of the parametric bootstrap goodness-of-fit test: Full and limited information. *British Journal of Mathematical and Statistical Psychology*, 56, 271–288.

Tsang, W.W. and Cheng, K.H. (2006). The chi-square test when the expected frequencies are less than 5. In *COMPSTAT 2006 - Proceedings in Computational Statistics* (A. Rizzi and M. Vichi, eds.). Physica Verlag - Springer, Heidelberg, 1583–1589.

Wickens, T.D. (1989). *Multiway Contingency Tables Analysis for the Social Sciences*. Hillsdale, NJ: Erlbaum.

Wilkinson, L. (1994). Practical guidelines for testing statistical software. In *Computational Statistics: Papers Collected on the Occasion of the 25th Conference on Statistical Computing at Schloss Reisensburg* (P. Dirschedl and R. Ostermann, eds.). Physica Verlag - Springer, Heidelberg, 1–16.

Yates, F. (1934). Contingency tables involving small numbers and the χ^2 test. *Supplement to the Journal of the Royal Statistical Society*, 1, 217–235.

SORT 43 (1) January-June 2019, 145-162 DOI: 10.2436/20.8080.02.82

On the optimism correction of the area under the receiver operating characteristic curve in logistic prediction models

Amaia Iparragirre*,[1], Irantzu Barrio[1,3] and María Xosé Rodríguez-Álvarez[2,4]

Abstract

When the same data are used to fit a model and estimate its predictive performance, this estimate may be optimistic, and its correction is required. The aim of this work is to compare the behaviour of different methods proposed in the literature when correcting for the optimism of the estimated area under the receiver operating characteristic curve in logistic regression models. A simulation study (where the theoretical model is known) is conducted considering different number of covariates, sample size, prevalence and correlation among covariates. The results suggest the use of k-fold cross-validation with replication and bootstrap.

MSC: 62J99.

Keywords: Prediction models, logistic regression, area under the receiver operating characteristic curve, validation, bootstrap.

1. Introduction

Prediction models play an important role in daily clinical practice. They provide clinicians with a tool to identify individuals at higher risk, and thus help in the decision making process. The development of risk prediction models for patients with diseases such as breast cancer (Wishart et al., 2012), chronic obstructive pulmonary disease (Quintana et al., 2014), or heart failure (Garcia-Gutierrez et al., 2017), among others, has increased during the last years. Once a model is developed, the aim is generally to apply it on new patients. Thus, a good but accurate predictive (or generalisation)

* Corresponding author: amaia.iparragirre@ehu.eus. Address: Departamento de Matemática Aplicada, Estadística e Investigación Operativa. Facultad de Ciencia y Tecnología. Universidad del País Vasco UPV/EHU. Barrio Sarriena s/n. 48940 Leioa.

[1] Departamento de Matemática Aplicada, Estadística e Investigación Operativa. Universidad del País Vasco UPV/EHU.

[2] BCAM-Basque Center for Applied Mathematics, Bilbao, Spain.

[3] Red de Investigación en Servicios de Salud en Enfermedades Crónicas (REDISSEC).

[4] IKERBASQUE, Basque Foundation for Science, Bilbao, Spain.

Received: February 2018
Accepted: January 2019

model performance is required. This work focuses on logistic regression models. In this setting, there are different ways to evaluate the performance, including calibration and discrimination measures (Steyerberg, 2009). Calibration refers to the agreement between observed outcomes or responses and predictions, while discrimination is concerned with the ability of the model to discriminate between individuals with and without the characteristic of interest. The area under the receiver operating characteristic (ROC) curve (Bamber, 1975; Hanley and McNeil, 1982; Swets, 1988), on which this work is focused, is a measure of discrimination.

It is well known that if in the development process of a prediction model, the same data is used to, first, fit the model and, then, evaluate its performance, this estimate, usually referred to as apparent or re-substituted performance, could be optimistic (see, e.g., Efron, 1986; Copas and Corbett, 2002). This is a consequence of the fact that most model fitting strategies rely on optimality criteria for the data used. Thus, in order to guarantee the model's usefulness when applied to new patients, the validation or correction of this optimism is required. Arguably, the best strategy to estimate the generalisation model performance is to apply it to new data. That is to say, the performance of the model is estimated based on individuals (observations) that have not been used in the model derivation/development process. This strategy is called external validation. Unfortunately, in practice this is usually not feasible. Most of the times it is not possible to obtain new data for that purpose due to difficulty or expense in their collection. To overcome the problem, different approaches have been proposed in the literature with the aim of estimating the performance of a model internally, i.e., re-using the data where the model has been derived/fitted. Split-sample validation (Picard and Berk, 1990; Snee, 1977) is possibly the most commonly used method in medical research. However, especially for small sample sizes, it has shown to provide pessimistic (over-corrected) estimates of the performance with a large variance (see, e.g., Steyerberg et al., 2001; Austin and Steyerberg, 2017). Therefore, alternative approaches to split-sample validation, such as k-fold cross-validation or bootstrap techniques, have been suggested (Stone, 1974; Efron, 1983; Harrell, Lee and Mark, 1996).

For the specific case of binary outcomes (as is the case of this paper), the literature contains several papers comparing different methods for correcting the optimism of the apparent area under the ROC curve (AUC). Important references are Harrell (2001); Steyerberg et al. (2001, 2003); Airola et al. (2011); Smith et al. (2014); Austin and Steyerberg (2017). For instance, Airola et al. (2011) compare different cross-validation techniques for estimating the AUC and propose the leave-pair-out cross-validation as the preferred method for optimism correction. To a similar conclusion comes Smith et al. (2014), who focus on small data sets. Yet, other authors recommend the use of bootstrapping (e.g., Smith et al., 2014; Steyerberg et al., 2001; Austin and Steyerberg, 2017). The papers by Steyerberg et al. (2001, 2003); Smith et al. (2014) and Austin and Steyerberg (2017) all focus on logistic regression models. In particular, all these papers study the impact of different values of events per variable (EPV) on the performance of several correction methods by means of simulations based on a large real data set.

EPV is defined by the ratio of the number of events (i.e., the number of observations in the smaller of the two groups of the binary outcome), relative to the number of regression coefficients in the model (see e.g., van Smeden et al., 2018). In most of the above-mentioned papers, simulations are done with a fixed number of covariates. Nevertheless, in practice other factors beyond the EPV may impact the performance of the methods, such as a) the number of covariates in the model, b) the available sample size, c) the prevalence; and/or d) the correlation among covariates. The number of covariates, sample size and prevalence are all together related to the EPV, but the last two are imposed by the available data. It has been reported that the bias of the apparent model performance estimate increases as the number of covariates increases (Hastie, Tibshirani and Friedman, 2001; Copas and Corbett, 2002). However, to the best of our knowledge there is a lack of studies comparing different correction methods in terms of the number of covariates. Hence, the primary aim of this study is to empirically evaluate the effect that the increase of the number of covariates may have on the performance of different methods (including split-sample, cross-validation and bootstrap) for the correction of the apparent AUC. In addition, we study the impact of the correlation among covariates as well as the prevalence of the disease and the sample size. Finally, in contrast to the above-mentioned studies, we conduct a simulation study in a situation where the theoretical logistic regression model is known.

The rest of the paper is organised as follows. Section 2 outlines the optimism correction methods that have been considered in this work. In Section 3 the simulation study conducted to analyse the performance of the optimism correction methods is described. Additionally, the results obtained are reported. Finally, the paper closes with a discussion in Section 4.

2. Methods

This section introduces the needed notation and background and describes the different methods that have been considered throughout this study to correct for the optimism of the apparent AUC. Recall that we denote as apparent AUC that which is obtained when all the available data are used to, first, fit the model and then, estimate the AUC.

2.1. Notation and preliminaries

Consider a collection of p covariates denoted by the vector $\boldsymbol{X} = (1, X_1, X_2, \ldots, X_p)^\intercal$, and let D be the random variable denoting the presence ($D = 1$) or absence ($D = 0$) of the characteristic of interest (e.g., a certain disease). Let $p(\boldsymbol{x}) = P(D = 1|\boldsymbol{X} = \boldsymbol{x})$ denote the conditional probability of being diseased for a patient with a vector of covariate values $\boldsymbol{x} = (1, x_1, x_2, \ldots, x_p)^\intercal$ in the domain of $\boldsymbol{X}$. It is assumed that $D|\boldsymbol{X} = \boldsymbol{x} \sim Bernoulli(p(\boldsymbol{x}))$.

The specific form of the logistic regression model is:

$$p(\boldsymbol{x}) = \frac{e^{\beta_0+\beta_1 x_1+\ldots+\beta_p x_p}}{1+e^{\beta_0+\beta_1 x_1+\ldots+\beta_p x_p}} = \frac{e^{\boldsymbol{\beta}^{\mathsf{T}}\boldsymbol{x}}}{1+e^{\boldsymbol{\beta}^{\mathsf{T}}\boldsymbol{x}}} \in (0,1), \tag{1}$$

where $\boldsymbol{\beta} = (\beta_0,\ldots,\beta_p)^{\mathsf{T}}$ is the vector of (unknown) regression coefficients. Let us assume that we have a sample of independent and identically distributed (i.i.d.) observations $\{(\boldsymbol{x}_i,d_i)\}_{i=1}^n$ from population $(\boldsymbol{X},D)$, and denote as $\hat{\boldsymbol{\beta}} = (\hat{\beta}_0,\ldots,\hat{\beta}_p)^{\mathsf{T}}$ the maximum likelihood estimator of $\boldsymbol{\beta}$ (Hosmer and Lemeshow, 2000; McCullagh and Nelder, 1989). The estimated probabilities of being diseased for each individual in the sample can be thus calculated as follows (see (1)):

$$\hat{p}(\boldsymbol{x}_i) = \frac{e^{\hat{\boldsymbol{\beta}}^{\mathsf{T}}\boldsymbol{x}_i}}{1+e^{\hat{\boldsymbol{\beta}}^{\mathsf{T}}\boldsymbol{x}_i}} \quad (i=1,\ldots,n). \tag{2}$$

2.2. Discriminative ability

As said in the Introduction, this paper focuses on the AUC. The AUC ranges from 0.5 (in the case of an uninformative model) to 1 (a perfect model), and it is frequently estimated by the Mann-Whitney U-statistic (Bamber, 1975; Hanley and McNeil, 1982; Pepe, 2003). More precisely, for the specific case of the logistic regression model, we have

$$\widehat{AUC} = \frac{1}{n_0 \cdot n_1} \sum_{j\in D_0} \sum_{k\in D_1} \left[I\left(\hat{p}(\boldsymbol{x}_j) < \hat{p}(\boldsymbol{x}_k)\right) + 0.5 I\left(\hat{p}(\boldsymbol{x}_j) = \hat{p}(\boldsymbol{x}_k)\right)\right], \tag{3}$$

where D_0 and D_1 are the index sets for $D=0$ and $D=1$, respectively and n_0 and n_1 their respective sizes. Note that expression (3) corresponds to the so-called apparent AUC, since all data are used for its calculation.

2.3. Optimism correction methods

2.3.1. Split-sample validation

In split-sample validation, the available sample $\{(\boldsymbol{x}_i,d_i)\}_{i=1}^n$ is randomly divided into two subsamples, a derivation sample $\left(\{\boldsymbol{x}_l^{der},d_l^{der}\}_{l=1}^{n_{der}}\right)$ and a validation sample $\left(\{\boldsymbol{x}_m^{val}, d_m^{val}\}_{m=1}^{n_{val}}\right)$, with $n = n_{der}+n_{val}$. Typically, the sample is split into two subsamples of the same size $(1/2:1/2)$ (Snee, 1977). Split-sample validation proceeds as follows. A logistic regression model is fitted to the derivation sample and the regression coefficients are estimated. These regression coefficients are used to estimate the predicted probabilities for the individuals in the validation sample following expression (2), which then are further used to calculate the corrected AUC by means of equation (3).

2.3.2. K-fold cross-validation

This method consists in splitting the available sample into k subsamples of (approximately) the same size. In pretty much the same way as split-sample validation, $k-1$ subsamples are considered as the derivation sample, and the remainder is used as validation sample to estimate the AUC. In contrast, however, to split-sample, the process is repeated k times, leaving-out one different subsample every time as validation sample. Finally, the corrected AUC is the average of these k estimated AUCs.

K-fold cross-validation with replication is another variant of this method (see, e.g., Smith et al., 2014). The process explained above is repeated r times, with a different k-split of the sample each time. Finally, the corrected AUC is the average of $r \times k$ estimated AUCs.

We would like to note that the described k-fold cross-validation method is usually referred in the literature, for obvious reasons, as the averaging strategy in contrast to the pooling strategy (see, e.g., Bradley, 1997). In the later, predicted probabilities are calculated in each validation sample, which are then pooled and used to estimate the corrected AUC. This work focuses on the averaging strategy, as it has shown a better performance in previous studies (Parker, Günter and Bedo, 2007; Airola et al., 2011). In particular, the averaging strategy does not suffer from the pessimism that occurs when pooling, and it is not affected by the so-called stratification bias. These results have also been corroborated in our setting (results not shown). However, averaging presents a problem that pooling does not have. If the number of diseased (or healthy) individuals is low (or the sample size small), it may happen that some folds will have few individuals (or even none) of the underrepresented group. This will impact the estimate of the AUC when these folds are used as the validation samples, which in turn can lead to a high variance in the estimates of the corrected AUC (Airola et al., 2011).

2.3.3. Leave-one-out cross-validation

In leave-one-out cross-validation, a single observation is omitted from the original sample. The logistic regression model is fitted to the remaining observations (derivation sample). Then, the fitted model is applied on the omitted observation and its predicted probability is estimated (see equation (2)). The process is repeated n times (where n is the size of the original sample), leaving-out one different observation every time. Finally, the AUC corrected by leave-one-out cross-validation method is calculated based on the estimated predicted probabilities of all individuals (see, e.g., Airola et al., 2011; Lachenbruch and Mickey, 1968).

2.3.4. Bootstrap validation

Another possibility to correct for the optimism of the AUC is to use bootstrap techniques (Efron and Tibshirani, 1993). This method can be summarised as follows:

Step 1. Fit the logistic regression model to the original sample $\{(\boldsymbol{x}_i, d_i)\}_{i=1}^{n}$ and estimate the apparent AUC, say $\widehat{AUC}_{app}$.

For $b = 1, 2, \ldots, B$ (where B is the number of bootstrap resamples):

Step 2. Generate a bootstrap resample $\left(\left\{\boldsymbol{x}_i^b, d_i^b\right\}_{i=1}^{n}\right)$, of the same size as the original sample, by resampling with replacement from the original sample.

Step 3. Fit a logistic regression model to the bootstrap resample, and estimate its apparent AUC, say $\widehat{AUC}_{boot}^{b}$.

Step 4. Apply the fitted logistic regression model in **Step 3.** on the original sample, calculate the predicted probabilities for each observation and estimate the AUC. Let $\widehat{AUC}_{o}^{b}$ be this estimate.

The optimism is estimated as follows:

$$\widehat{O} = \frac{1}{B}\sum_{b=1}^{B}(\widehat{AUC}_{boot}^{b} - \widehat{AUC}_{o}^{b}),$$

and the corrected AUC is: $\widehat{AUC}_{bootstrap} = \widehat{AUC}_{app} - \widehat{O}$.

3. Simulation study

This section describes and presents the results of the simulation study conducted to evaluate the behaviour of the correction methods discussed in Section 2.3.. Specifically, the aim of the study was to compare the AUC estimates provided by the different methods (including the apparent AUC) against the "true" out-of-sample AUC associated with the derived logistic regression model. The "true" out-of-sample AUC refers to the true discriminatory capacity of the derived/fitted model when applied to new data or subjects. A variety of factors that could impact the performance of the methods were considered in this study, such as, the number of covariates in the model, the available sample size, the prevalence of the disease (i.e., $prev = P(D = 1)$) and the correlation among covariates. The steps of the simulation study are described in detail in next section.

3.1. Scenarios and set-up

For a given number of covariates, say, p, the steps of the simulation study can be summarised as follows:

Step 1. Generate two independent samples $\left\{\boldsymbol{x}_i^{(p)*}, d_i^*\right\}_{i=1}^{n}$ and $\left\{\boldsymbol{x}_l^{(p)**}, d_l^{**}\right\}_{l=1}^{N}$ of respectively size n and N (the superscript (p) is used to emphasise the covariate vector length) as follows:

Step 1.1 Generate $\eta_i \sim Bernoulli(prev)$, and generate the covariate vector value $\boldsymbol{x}_i^{(p)*}$

$$\begin{cases} \boldsymbol{x}_i^{(p)*} \sim N\left(\boldsymbol{\mu}_{D_0}^{(p)}, \boldsymbol{\Sigma}^{(p)}\right) & \text{if } \eta_i = 0, \\ \boldsymbol{x}_i^{(p)*} \sim N\left(\boldsymbol{\mu}_{D_1}^{(p)}, \boldsymbol{\Sigma}^{(p)}\right) & \text{if } \eta_i = 1. \end{cases} \tag{4}$$

By simulating the covariates in this way, the logistic regression model holds, and the true value of the regression coefficient vector $\boldsymbol{\beta}^{(p)}$ is known (see Appendix A). This vector is used in **Step 1.2** below.

Step 1.2 Calculate $p(\boldsymbol{x}_i^{(p)*})$ using equation (1).

Step 1.3 Generate $d_i^* \sim Bernoulli(p(\boldsymbol{x}_i^{(p)*}))$.

(To generate $\left\{\boldsymbol{x}_l^{(p)**}, d_l^{**}\right\}_{l=1}^{N}$ we followed the same steps. We note that this sample is used in **Step 3.** to estimate the out-of-sample AUC.)

Step 2. Fit a logistic regression model to the first sample, $\left\{\boldsymbol{x}_i^{(p)*}, d_i^*\right\}_{i=1}^{n}$, and estimate the apparent and corrected AUCs (by means of any method discussed in Section 2.3).

Step 3. Apply the fitted logistic regression model in **Step 2.** on sample $\left\{\boldsymbol{x}_l^{(p)**}, d_l^{**}\right\}_{l=1}^{N}$, calculate the predicted probabilities for each observation and estimate the "true" out-of-sample AUC ($\widehat{AUC}_{oos}$).

Note that to generate the covariate vector in **Step 1.1**, the parameters of the multivariate normal distribution (see equation (4)) need to be specified. In particular, in this study we considered:

$$\begin{cases} \boldsymbol{\mu}_{D_0}^{(10)} &= (0,\ldots,0)^\intercal, \\ \boldsymbol{\mu}_{D_1}^{(10)} &= (0.6, 0.55, 0.5, 0.45, 0.4, 0.3, 0.25, 0.2, 0.15, 0.1)^\intercal. \end{cases}$$

Thus, for example, for two covariates we have $\boldsymbol{\mu}_{D_0}^{(2)} = (0,0)^\intercal$ and $\boldsymbol{\mu}_{D_1}^{(2)} = (0.6, 0.55)^\intercal$. Note that the covariates are sorted (and thus included in the simulation) from the most explicative to the weakest. With respect to the variance-covariance matrix, we assumed

$$\boldsymbol{\Sigma}^{(p)} = (1-\gamma)\cdot I_{p\times p} + \gamma \cdot J_{p\times p},$$

where $I_{p\times p}$ is the identity matrix of dimension $p \times p$ and $J_{p\times p}$ is the matrix of ones of the same dimension. Here γ controls the correlation among covariates (when $\gamma = 0$ the covariates are independent). For a given number of covariates p ($p \in \{1,\ldots,10\}$), different sample sizes ($n \in \{500, 1000, 2000\}$), prevalences ($prev \in \{0.1, 0.2, 0.5\}$) and correlations ($\gamma \in \{0, 0.15, 0.60\}$) were considered, yielding a total of 27 different spec-

ifications per number of covariates. In all results shown below, the out-of-sample AUC (see **Step 3.**) was estimated on the basis of a sample of size $N = 50000$, and a total of $R = 500$ replicates were performed. Split-sample validation was used with half of the sample for derivation and the other half for validation ($1/2 : 1/2$). For k-fold cross-validation we considered $k = 10$ folds (which is the one most commonly used in the literature), without replicates (the procedure is performed only once) and with $r = 20$ replicates. Bootstrap validation was performed with $B = 100$ and $B = 500$ bootstrap resamples. Recall that in addition to those methods, we also evaluated the performance of the apparent AUC, and the leave-one-out cross-validation procedure. We note that for split-sample validation, the logistic regression model in **Step 2.** was fitted on half of the available data, and this fitted model was the one used in **Step 3.** to calculate the "true" out-of-sample AUC. Thus, neither the fitted model nor the "true" out-of-sample AUC is the same as for the other methods. We proceeded in this way since, in our experience, the reported model is, in general, the one developed in the derivation sample and not using the whole sample. Finally, the performance of the methods was measured in terms of bias and mean squared error (MSE), that were calculated over the $R = 500$ runs

$$\text{Bias} = \frac{1}{R}\sum_{r=1}^{R}\left(\widehat{AUC}^{r}_{cor} - \widehat{AUC}^{r}_{oos}\right),$$

$$\text{MSE} = \frac{1}{R}\sum_{r=1}^{R}\left(\widehat{AUC}^{r}_{cor} - \widehat{AUC}^{r}_{oos}\right)^2,$$

where $\widehat{AUC}_{cor}$ denotes the estimated AUC obtained by means of any of the methods considered in this work (including the apparent), and $\widehat{AUC}_{oos}$ is the estimated out-of-sample AUC (computed, based on a sample of size N=50000, as explained in **Step 3.**).

It is important to note that all methods considered in this work (except leave-one-out cross-validation) are based on either splitting the data or resampling it. One may argue that, for a particular sample, different splits or resamples can lead to different corrected AUCs. Thus, in addition to the previous simulation, a smaller study was performed with the aim of evaluating the variability of the corrected AUC estimates for a particular sample. For simplicity, in this case we restricted our attention to the most extreme parameter specification ($n = 500$, $prev = 0.1$, $\gamma = 0.60$) and an intermediate one ($n = 1000$, $prev = 0.2$, $\gamma = 0.15$).

3.2. Results

Given the large number of proposed parameter specifications (a total of 270), we begin by summarising the main findings. As could have been expected, the bias of the apparent AUC increases as the number and correlation among covariates increase, and as the prevalence and sample size decrease. With respect to the other methods considered in the study, except for the leave-one-out cross-validation all seem to correct for the opti-

mism of the apparent AUC (small bias) and there is not a clear method that performs the best across all specifications. However, in terms of variability in the estimates, the 10-fold cross-validation without replication and the split-sample validation are the methods that present the largest variability, and this is especially remarkable for split-sample validation. For split-sample, the large variability can come from two different sources. First, the model is fitted to half of the data and therefore there is more uncertainty, and second, the corrected AUC is estimated with also half of the data. This issue has also been discussed by Smith et al. (2014). For 10-fold cross-validation without replication a similar explanation as in split-sample can be given (Smith et al., 2014), but in addition, an extra problem can arise, especially for small sample sizes and low prevalences. As noted in Section 2.3.2, the random split of the full sample into 10 folds may yield folds with very few events, which affects the estimation of the corrected AUC when using these folds. However, this effect might be mitigated if the 10-fold cross-validation with replication is used, as the corrected AUC is the average of a large number of values. In our simulations we ensured that at least there is one event in each fold, but we are aware that it might not be enough. To finish this part we would like to mention that, in contrast to other studies (see, e.g., Austin and Steyerberg, 2017), in this work we compared the corrected AUCs provided by the split-sample method with the out-of-sample AUCs obtained based on the model fitted to the derivation sample. This may explain why we do not observe a pessimistic behaviour (negative bias) of this method.

We now present some numerical and graphical results. Since the mayor differences among the methods have been observed for the most extreme specifications, these are the results shown here.

Table 1 shows the numerical results obtained for a correlation of 0.60 ($\gamma = 0.60$), sample sizes of 500 and 2000 ($n \in \{500, 2000\}$), prevalences of 0.1, 0.2 and 0.5 ($prev \in \{0.1, 0.2, 0.5\}$) and 2, 5 and 8 number of covariates ($p \in \{2, 5, 8\}$). Specifically, the average and standard deviation of the estimated AUCs are reported jointly with the bias and MSE. Note that except for a small number of covariates and a large sample size, the apparent AUC is optimistic (positive bias). Split-sample is the method presenting the largest variability and therefore MSE. Note also that, the average of the estimated corrected AUCs given by split-sample validation is in general the lowest. This is especially remarkable for large number of covariates and small sample sizes, and is a consequence of fitting the model using only half of the data. If we compare cross-validation with and without replication, we observe that the presence of replicates reduces the variability and therefore the MSE. Curiously, at least in our simulations, we do not observe a large difference between $B = 100$ and $B = 500$ in the bootstrap method. In all the results shown in Table 1, the largest MSE is obtained for split-sample (coming from the largest variability). For the remaining methods, as the sample size increases, all perform almost indistinguishably. The largest differences among the methods are observed for a sample size of $n = 500$ and a prevalence of 0.1. This can also be observed in Figure 1. The figure depicts the bias associated to each method across the 500 runs, for 1 to 10 number of covariates ($p \in \{1, 2, \ldots, 10\}$), a prevalence of 0.1 ($prev = 0.1$), a correlation

Table 1: *Average of the estimated AUCs (mean), standard deviation (sd), bias and mean squared error (MSE) for all the methods considered. The reults shown are for correlation of 0.60 among covariates ($\gamma = 0.60$), different sample sizes ($n \in \{500, 2000\}$), prevalences (Prev.) ($prev \in \{0.1, 0.2, 0.5\}$) and number of covariates (2, 5 and 8).*

Sample Size	Prev.	Method	2 covariates			5 covariates			8 covariates		
			Mean (sd)	Bias	MSE	Mean (sd)	Bias	MSE	Mean (sd)	Bias	MSE
500	0.1	Apparent	0.6824(0.0423)	0.0105	0.0019	0.6948(0.0364)	0.0352	0.0025	0.7375(0.0369)	0.0544	0.0043
		Split	0.6652(0.0582)	−0.0011	0.0032	0.6451(0.0609)	0.0015	0.0030	0.6679(0.0657)	0.0030	0.0037
		CV	0.6855(0.0404)	0.0136	0.0018	0.6736(0.0418)	0.0140	0.0019	0.7022(0.0432)	0.0191	0.0022
		CV Replication	0.6864(0.0346)	0.0145	0.0014	0.6752(0.0347)	0.0156	0.0014	0.6990(0.0372)	0.0159	0.0016
		Leave-1-out	0.6576(0.0499)	−0.0143	0.0027	0.6445(0.0489)	−0.0151	0.0024	0.6776(0.0489)	−0.0055	0.0023
		Boot (B=100)	0.6730(0.0459)	0.0010	0.0021	0.6630(0.0434)	0.0034	0.0017	0.6951(0.0447)	0.0120	0.0020
		Boot (B=500)	0.6726(0.0457)	0.0007	0.0021	0.6621(0.0438)	0.0025	0.0018	0.6945(0.0447)	0.0114	0.0020
	0.2	Apparent	0.6808(0.0299)	0.0059	0.0009	0.6858(0.0285)	0.0186	0.0011	0.7276(0.0267)	0.0312	0.0016
		Split	0.6715(0.0430)	−0.0010	0.0018	0.6572(0.0461)	−0.0007	0.0019	0.6848(0.0458)	0.0004	0.0018
		CV	0.6756(0.0321)	0.0007	0.0010	0.6640(0.0355)	−0.0031	0.0012	0.6980(0.0324)	0.0016	0.0010
		CV Replication	0.6760(0.0296)	0.0011	0.0009	0.6659(0.0299)	−0.0013	0.0009	0.6977(0.0299)	0.0013	0.0008
		Leave-1-out	0.6670(0.0325)	−0.0079	0.0011	0.6565(0.0339)	−0.0106	0.0012	0.6924(0.0317)	−0.0041	0.0009
		Boot (B=100)	0.6755(0.0312)	0.0005	0.0010	0.6660(0.0321)	−0.0011	0.0010	0.7012(0.0303)	0.0047	0.0009
		Boot (B=500)	0.6751(0.0311)	0.0002	0.0010	0.6657(0.0321)	−0.0014	0.0010	0.7008(0.0303)	0.0043	0.0009
	0.5	Apparent	0.6782(0.0234)	0.0049	0.0006	0.7923(0.0191)	0.0026	0.0004	0.8100(0.0195)	0.0089	0.0005
		Split	0.6708(0.0325)	−0.0007	0.0010	0.7812(0.0303)	−0.0047	0.0009	0.7902(0.0296)	−0.0044	0.0008
		CV	0.6732(0.0257)	−0.0001	0.0007	0.7841(0.0207)	−0.0055	0.0005	0.7975(0.0218)	−0.0036	0.0005
		CV Replication	0.6731(0.0241)	−0.0002	0.0006	0.7841(0.0200)	−0.0056	0.0004	0.7967(0.0209)	−0.0043	0.0005
		Leave-1-out	0.6692(0.0246)	−0.0041	0.0006	0.7814(0.0200)	−0.0083	0.0005	0.7946(0.0209)	−0.0065	0.0005
		Boot (B=100)	0.6746(0.0241)	0.0013	0.0006	0.7847(0.0200)	−0.0050	0.0004	0.7979(0.0208)	−0.0032	0.0004
		Boot (B=500)	0.6745(0.0241)	0.0012	0.0006	0.7846(0.0199)	−0.0051	0.0004	0.7979(0.0207)	−0.0032	0.0004
2000	0.1	Apparent	0.6763(0.0188)	0.0002	0.0004	0.6833(0.0190)	0.0109	0.0005	0.7157(0.0200)	0.0159	0.0006
		Split	0.6715(0.0278)	−0.0032	0.0008	0.6695(0.0312)	0.0013	0.0009	0.6977(0.0281)	0.0036	0.0008
		CV	0.6737(0.0201)	−0.0024	0.0004	0.6735(0.0212)	0.0010	0.0004	0.7018(0.0224)	0.0020	0.0005
		CV Replication	0.6731(0.0195)	−0.0030	0.0004	0.6733(0.0205)	0.0009	0.0004	0.7021(0.0218)	0.0023	0.0005
		Leave-1-out	0.6703(0.0194)	−0.0058	0.0004	0.6709(0.0205)	−0.0015	0.0004	0.7001(0.0218)	0.0003	0.0005
		Boot (B=100)	0.6741(0.0192)	−0.0020	0.0004	0.6748(0.0202)	0.0024	0.0004	0.7037(0.0215)	0.0039	0.0005
		Boot (B=500)	0.6740(0.0191)	−0.0021	0.0004	0.6747(0.0201)	0.0023	0.0004	0.7035(0.0215)	0.0037	0.0005
	0.2	Apparent	0.6757(0.0140)	−0.0009	0.0002	0.6817(0.0144)	0.0074	0.0003	0.7146(0.0151)	0.0074	0.0003
		Split	0.6738(0.0219)	−0.0021	0.0005	0.6747(0.0221)	0.0028	0.0005	0.7041(0.0209)	0.0005	0.0004
		CV	0.6743(0.0144)	−0.0024	0.0002	0.6761(0.0153)	0.0018	0.0002	0.7066(0.0155)	−0.0006	0.0002
		CV Replication	0.6741(0.0143)	−0.0026	0.0002	0.6761(0.0151)	0.0018	0.0002	0.7068(0.0159)	−0.0004	0.0002
		Leave-1-out	0.6723(0.0143)	−0.0044	0.0002	0.6745(0.0151)	0.0002	0.0002	0.7055(0.0159)	−0.0017	0.0003
		Boot (B=100)	0.6745(0.0141)	−0.0022	0.0002	0.6768(0.0150)	0.0025	0.0002	0.7075(0.0158)	0.0003	0.0002
		Boot (B=500)	0.6744(0.0141)	−0.0023	0.0002	0.6766(0.0149)	0.0023	0.0002	0.7073(0.0158)	0.0002	0.0002
	0.5	Apparent	0.6769(0.0112)	0.0023	0.0001	0.6812(0.0117)	0.0024	0.0001	0.7145(0.0117)	0.0051	0.0002
		Split	0.6769(0.0167)	0.0027	0.0003	0.6768(0.0164)	−0.0002	0.0003	0.7073(0.0167)	0.0003	0.0003
		CV	0.6761(0.0113)	0.0015	0.0001	0.6775(0.0121)	−0.0013	0.0001	0.7092(0.0122)	−0.0002	0.0001
		CV Replication	0.6760(0.0113)	0.0013	0.0001	0.6776(0.0120)	−0.0012	0.0001	0.7093(0.0120)	−0.0001	0.0001
		Leave-1-out	0.6747(0.0114)	0.0001	0.0001	0.6765(0.0120)	−0.0023	0.0001	0.7084(0.0120)	−0.0009	0.0001
		Boot (B=100)	0.6761(0.0113)	0.0014	0.0001	0.6779(0.0120)	−0.0009	0.0001	0.7097(0.0121)	0.0003	0.0001
		Boot (B=500)	0.6760(0.0112)	0.0014	0.0001	0.6778(0.0120)	−0.0010	0.0001	0.7095(0.0120)	0.0002	0.0001

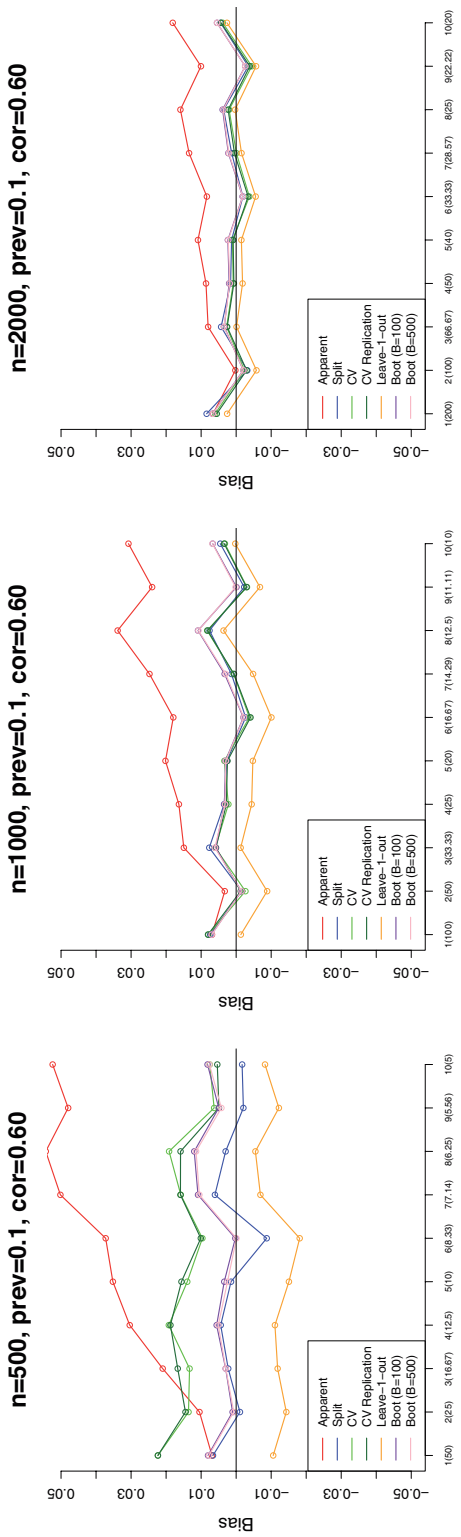

(a) (b) (c)

Figure 1: *Bias associated with each correction method according to the number of covariates in the logistic regression model ($p \in \{1, 2, \ldots, 10\}$). The results shown are for a prevalence of 0.1, a correlation of 0.60 and a sample size of (a) $n = 500$, (b) $n = 1000$ and (c) $n = 2000$.*

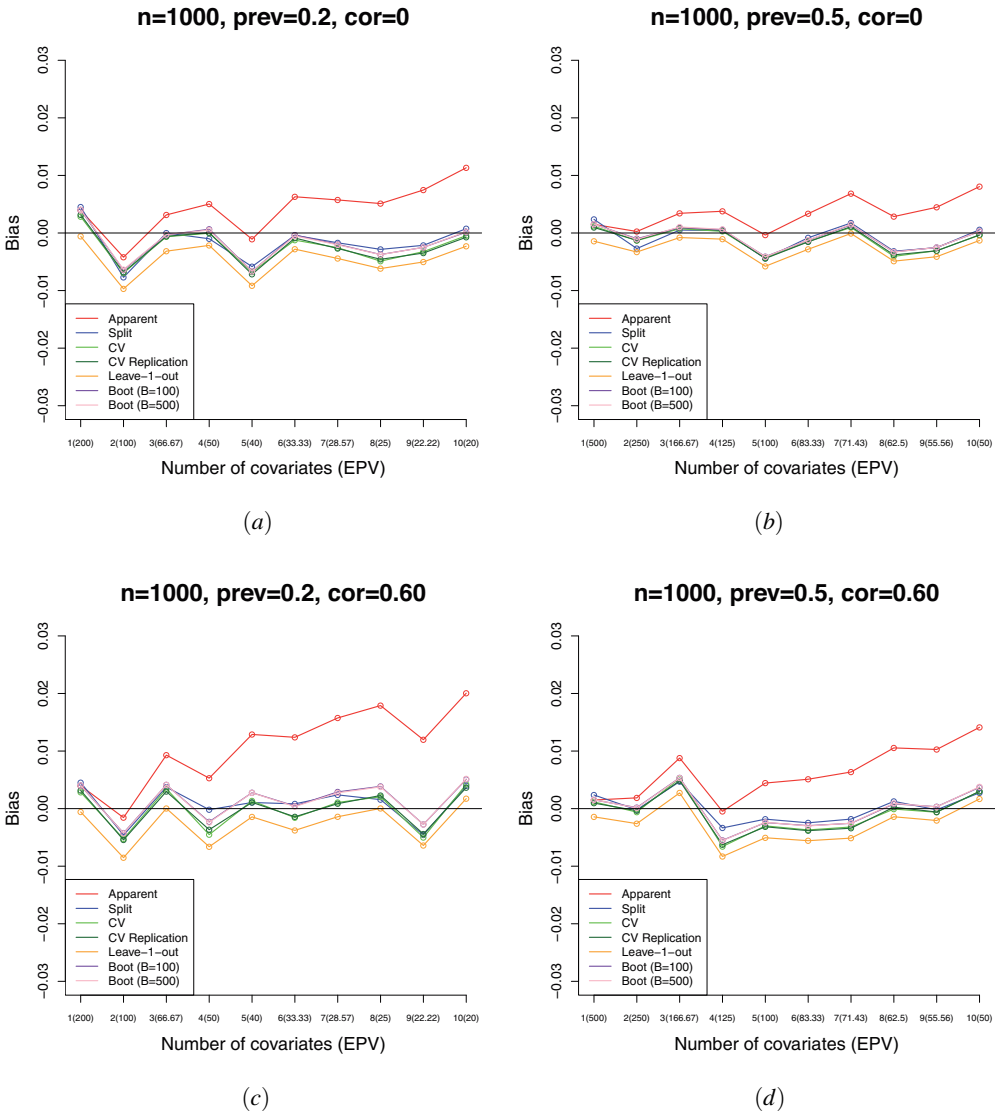

Figure 2: *Bias associated to each correction method according to the number of covariates included in the logistic regression model ($p \in \{1,2,\ldots,10\}$). The results shown are for a sample size of $n = 1000$ and different prevalences and correlations: (a) $prev = 0.2$ and $\gamma = 0$, (b) $prev = 0.5$ and $\gamma = 0$, (c) $prev = 0.2$ and $\gamma = 0.60$, and (d) $prev = 0.5$ and $\gamma = 0.60$.*

of 0.60 ($\gamma = 0.60$) and different sample sizes ($n \in \{500, 1000, 2000\}$). Note that for a sample size of $n = 500$ the bias of 10-fold cross-validation with and without replication and the leave-one-out cross-validation is very large, but the bias decreases as the sample size increases. Thus, with a low prevalence, larger sample sizes are required for those methods to perform well.

Figure 2 shows also the bias associated to each method, but for other parameter specifications. In particular, we present the results for a sample size of $n = 1000$, but different prevalences and correlations. Figure 2(a) depicts the bias for $n = 1000$, $prev = 0.2$ and $\gamma = 0$, Figure 2(b) for $n = 1000$, $prev = 0.5$ and $\gamma = 0$, Figure 2(c) for $n = 1000$, $prev = 0.5$ and $\gamma = 0.60$, and Figure 2(d) for $n = 1000$, $prev = 0.5$ and $\gamma = 0.60$. These results corroborate that the bias of the apparent AUC increases as the correlation increases and/or the prevalence decreases. In all cases, leave-one-out cross-validation is the method presenting the most pessimistic behaviour (negative bias), and, as noted before, in terms of bias, split-sample validation seems to perform similarly to 10-fold cross-validation (with and without replication) and bootstrap (with $B = 100$ and $B = 500$). These results also show that, on average, the corrected AUCs provided by bootstrap are larger than those provided by 10-fold cross-validation (the difference between the corrected AUCs and the out-of-sample AUC is larger), and this pattern is maintained across all specifications.

To finish with the presentation of results we show in Figure 3 the variability of the estimated corrected AUCs when the methods were applied to 500 different random splits or resamples of a particular sample. Recall that for these results we considered the most extreme parameter specification ($n = 500$, $prev = 0.1$, $\gamma = 0.60$) and an intermediate one ($n = 1000$, $prev = 0.2$, $\gamma = 0.15$), both including 5 covariates. For both situations, it is remarkable the large variability of the split-sample validation and the 10-fold cross-validation without replication, with the other three methods (i.e., 10-fold cross-validation with replication and, bootstrap with $B = 100$ and $B = 500$ resamples), presenting a rather low variability (note that the scale of the y-axes is different in both graphics). These results emphasise the above-discussed conclusions.

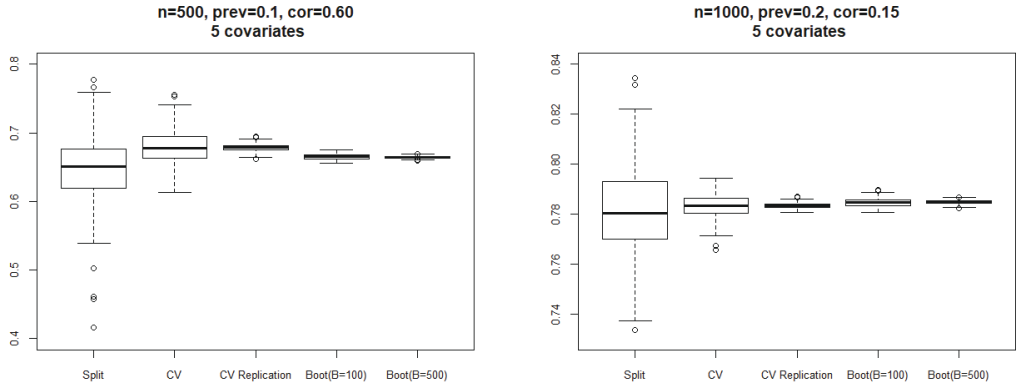

(*a*) (*b*)

Figure 3: *Box-plot of the estimated corrected AUCs by means of the different correction methods when applied to 500 different splits or resamples of the same sample. This figure illustrates the variability of the different correction methods.* (*a*) *Most extreme parameter specification* ($n = 500$, $prev = 0.1$, $\gamma = 0.60$, *5 covariates).* (*b*) *Intermediate specification* ($n = 1000$, $prev = 0.2$, $\gamma = 0.15$, *5 covariates). Note that the scale of the y-axes is different in both graphics.*

4. Discussion

In this work we compared the behaviour of different methods when correcting for the optimism of the apparent AUC in logistic regression models. A large simulation study was conducted in which different scenarios were considered regarding the number of covariates, sample size, prevalence and correlation among covariates. The predictor variables were simulated following a multivariate normal distribution in such a way that the theoretical logistic regression model is known. We now summarise the main conclusions that we have drawn throughout the study.

If enough data are available, all methods seem to properly correct for the optimism of the apparent AUC, except for the leave-one-out cross-validation, which gives the most pessimistic results. Moreover, in terms of bias the behaviour of all remaining correction methods is similar (there is not a clear method that performs the best) and the bias is, in general, low. In contrast, the problems appear when the available data is insufficient and/or imbalanced. For example, when working with a low prevalence and correlated covariates, larger sample sizes will be needed to ensure a good performance of the optimism correction methods.

The results of the simulation study suggest the use of either k-fold cross-validation with replication or bootstrap (we note that, for cross-validation, we only examined the case of $k = 10$ number of folds). In particular, in the most extreme cases, the bootstrap method should be used according to these results. Even though k-fold cross-validation with replication and bootstrap are the most computationally demanding methods, for the sample sizes considered in this study, the computing time was affordable (in general, less than 10 seconds).

The results obtained in this work are in line with those obtained in previous studies (Austin and Steyerberg, 2017; Airola et al., 2011; Steyerberg et al., 2001; Smith et al., 2014). Nevertheless, we have also observed some differences.

On the one hand, we should note the differences in the results of the split-sample validation. In previous studies, split-sample has given pessimistic results. In contrast, in this study, the bias of the estimated AUC corrected by split-sample is very low. The reason is the following. Some researchers have claimed that despite using split-sample for the validation of the model, the final model should be based on the full sample (see, e.g., Harrell et al., 1996; Steyerberg et al., 2001). For this reason, in previous studies, the AUC corrected with split-sample was compared to the "true" out-of-sample AUC of the full model (see, e.g., Austin and Steyerberg, 2017). Nevertheless, at least in our experience, in practice, the model reported when split-sample validation is used is, in general, the one developed in the derivation sample and not derived using the whole sample (see, e.g., Quintana et al., 2014; Wada et al., 2017). Thus, in this study, we compared the AUC corrected by split-sample validation to the "true" out-of-sample AUC of the model fitted to the derivation sample. Our results suggest that, in terms of the bias, split-sample validation properly corrects the apparent AUC of the model fitted to the derivation sample. However, similarly to the results obtained in the above-

mentioned studies, the variability of the split-sample validation is very large compared to the other available methods. Furthermore, as only half of the data is used to derive the model, model's performance is in general worse than when the full sample is used, and the "true" AUC of the model fitted to the derivation sample is also lower, unless enough data is available. We conclude that we do not recommend the use of the split-sample validation, because of its large variability and the worse performance of the final model.

On the other hand, for the same EPV values, very different results were obtained in this study. For instance, for an EPV=10, for some parameter specifications the optimism of the apparent AUC was successfully corrected, but for other parameter specifications, the methods presented some bias. Thus, in addition to the EPV, the factors that were analysed in this study (the number of covariates in the model, the available sample size, the prevalence of the disease and the correlation among covariates) should also be regarded when correcting for the optimism of the apparent AUC.

We would like to conclude commenting on the limitations of our study. In the first place, we only studied the impact from 1 to 10 covariates in the model. In our daily practice, it is not common to fit models with more than 10 covariates. Nevertheless, in some cases, it could be interesting to study the impact of a larger number of covariates in the behaviour of different correction methods (see, e.g., Airola et al., 2011). Secondly, in our simulation study, we only considered the case of multivariate normally distributed covariates. However, the results we obtained are in concordance with a similar simulation study we conducted based on categorical covariates (results not shown), as well as with the results other authors obtained in previous studies (Austin and Steyerberg, 2017; Steyerberg et al., 2001; Smith et al., 2014). Also, for cross-validation we only examined the case of $k = 10$. For small sample sizes and unbalanced data, this value may be too large as it may yield into folds with very few events, thus affecting the behaviour of the method. Further research is therefore guaranteed to study the impact of the number of folds. Another limitation of this study is that we did not focus on important aspects in the development of a prediction model, such as variable selection and model derivation, but we went directly to the evaluation of the performance (and its optimism correction) of a "pre-defined" model. Moreover, as noted in the introduction, we focused on the discrimination of the model (measured by the AUC) rather than on its calibration (e.g. goodness-of-fit), which should also be considered when developing prediction models. An interesting area of research would be the study of the behaviour of the methods considered in this work when applied to measures of calibration. Finally, we did not study the behaviour of the leave-pair-out cross-validation, which has shown good behaviour in previous studies (see, e.g., Airola et al., 2011; Smith et al., 2014). We focused the simulation study on the most commonly used correction methods in the literature.

A Appendix

Let us assume that the vector of p covariates $\boldsymbol{X}$ is distributed according to a multivariate normal distribution in both healthy and diseased populations. That is to say, $\boldsymbol{X}_{D_0} \equiv \boldsymbol{X}|D=0 \sim N(\boldsymbol{\mu}_{D_0}, \boldsymbol{\Sigma})$ and $\boldsymbol{X}_{D_1} \equiv \boldsymbol{X}|D=1 \sim N(\boldsymbol{\mu}_{D_1}, \boldsymbol{\Sigma})$, where the variance-covariance matrix $\boldsymbol{\Sigma}$ is assumed to be the same for both distributions. Given that $\boldsymbol{\Sigma}$ is a symmetric matrix, it can be shown that $\boldsymbol{\Sigma}^{-1} = \frac{1}{|\boldsymbol{\Sigma}|}\boldsymbol{A}$, where $|\boldsymbol{\Sigma}|$ denotes the determinant of $\boldsymbol{\Sigma}$ and $\boldsymbol{A}$ is the adjoint matrix of $\boldsymbol{\Sigma}$. Under these assumptions, it is easy to show that the logistic regression model (see eqn. (1)) holds and that the true values of the regression coefficients are

$$\begin{cases} \beta_0 = ln\left(\frac{P(D=1)}{P(D=0)}\right) - \frac{1}{2\,|\boldsymbol{\Sigma}|}\sum_{k=1}^{p}\sum_{j=1}^{p} A_{jk}(\mu_{D_1 j}\mu_{D_1 k} - \mu_{D_0 j}\mu_{D_0 k}), \\ \beta_k = \frac{1}{|\boldsymbol{\Sigma}|}\sum_{j=1}^{p} A_{jk}(\mu_{D_1 j} - \mu_{D_0 j}), \quad (k = 1, \ldots, p). \end{cases}$$

Funding

This study was partially supported by grants Severo Ochoa Program SEV-2013-0323, Basque Government BERC Program 2018-2021, IT620-13 from the Departamento de Educación, Política Lingüística y Cultura del Gobierno Vasco and through project MTM2017-82379-R funded by (AEI/FEDER, UE) and acronym "AFTERAM", and projects MTM2014-55966-P and MTM2016-74931-P from the Ministerio de Economía y Competitividad and FEDER. Amaia Iparragirre was partially supported by an Intership Position at BCAM - Basque Centre for Applied Mathematics.

Conflict of interest

The authors declare that there are no conflicts of interest.

References

Airola, A., Pahikkala, T., Waegeman, W., De Baets, B., and Salakoski, T. (2011). An experimental comparison of cross-validation techniques for estimating the area under the ROC curve. *Computational Statistics & Data Analysis*, 55, 1828–1844.

Austin, P.C. and Steyerberg, E.W. (2017). Events per variable (EPV) and the relative performance of different strategies for estimating the out-of-sample validity of logistic regression models. *Statistical Methods in Medical Research*, 26, 796–808.

Bamber, D. (1975). The area above the ordinal dominance graph and the area below the receiver operating characteristic graph. *Journal of Mathematical Psychology*, 12, 387–415.

Bradley, A.P. (1997). The use of the area under the ROC curve in the evaluation of machine learning algorithms. *Pattern Recognition*, 30, 1145–1159.

Copas, J. and Corbett, P. (2002). Overestimation of the receiver operating characteristic curve for logistic regression. *Biometrika*, 89, 315–331.

Efron, B. (1983). Estimating the error rate of a prediction rule: improvement on cross-validation. *Journal of the American Statistical Association*, 78, 316–331.

Efron, B. (1986). How biased is the apparent error rate of a prediction rule? *Journal of the American Statistical Association*, 81, 461–470.

Efron, B. and Tibshirani, R.J. (1993). *An Introduction to the Bootstrap*. New York: Chapman & Hall/CRC.

Garcia-Gutierrez, S., Quintana, J.M., Antón-Ladislao, A., Gallardo, M.S., Pulido, E., Rilo, I., Zubillaga, E., Morillas, M., Onaindia, J.J., Murga, N., et al. (2017). Creation and validation of the acute heart failure risk score: AHFRS. *Internal and Emergency Medicine*, 12, 1197–1206.

Hanley, J.A. and McNeil, B.J. (1982). The meaning and use of the area under a receiver operating characteristic (ROC) curve. *Radiology*, 143, 29–36.

Harrell, F.E. (2001). *Regression Modeling Strategies: With Applications to Linear Models, Logistic and Ordinal Regression, and Survival Analysis*. New York: Springer.

Harrell, F.E., Lee, K.L. and Mark, D.B. (1996). Multivariable prognostic models: issues in developing models, evaluating assumptions and adequacy, and measuring and reducing errors. *Statistics in Medicine*, 15, 361–387.

Hastie, T., Tibshirani, R. and Friedman, J. (2001). *The Elements of Statistical Learning*. Springer Series in Statistics. Springer New York Inc., New York, NY, USA.

Hosmer, D.W. and Lemeshow, S. (2000). *Applied Logistic Regression*. New York, N.Y.: Wiley.

Lachenbruch, P.A. and Mickey, M.R. (1968). Estimation of error rates in discriminant analysis. *Technometrics*, 10, 1–11.

McCullagh, P. and Nelder, J.A. (1989). *Generalized Linear Models, 2nd ed*. London: Chapman & Hall/CRC.

Parker, B.J., Günter, S. and Bedo, J. (2007). Stratification bias in low signal microarray studies. *BMC Bioinformatics*, 8, 326.

Pepe, M. (2003). *The Statistical Evaluation of Medical Tests for Classification and Prediction*. Oxford Statistical Science Series. Oxford University Press.

Picard, R.R. and Berk, K.N. (1990). Data splitting. *The American Statistician*, 44, 140–147.

Quintana, J., Esteban, C., Unzurrunzaga, A., Garcia-Gutierrez, S., Gonzalez, N., Lafuente, I., Bare, M., de Larrea, N.F., Vidal, S., et al. (2014). Prognostic severity scores for patients with COPD exacerbations attending emergency departments. *The International Journal of Tuberculosis and Lung Disease*, 18, 1415–1420.

Smith, G. C.S., Seaman, S.R., Wood, A.M., Royston, P. and White, I.R. (2014). Correcting for optimistic prediction in small data sets. *American Journal of Epidemiology*, 180, 318–324.

Snee, R.D. (1977). Validation of regression models: methods and examples. *Technometrics*, 19, 415–428.

Steyerberg, E. (2009). *Clinical Prediction Models: A Practical Approach to Development, Validation, and Updating*. Springer Science & Business Media.

Steyerberg, E.W., Bleeker, S.E., Moll, H.A., Grobbee, D.E. and Moons, K.G. (2003). Internal and external validation of predictive models: a simulation study of bias and precision in small samples. *Journal of Clinical Epidemiology*, 56, 441–447.

Steyerberg, E.W., Harrell, F.E., Borsboom, G.J., Eijkemans, M., Vergouwe, Y. and Habbema, J.F. (2001). Internal validation of predictive models. *Journal of Clinical Epidemiology*, 54, 774–781.

Stone, M. (1974). Cross-validatory choice and assessment of statistical predictions. *Journal of the Royal Statistical Society. Series B (Methodological)*, 36, 111–147.

Swets, J.A. (1988). Measuring the accuracy of diagnostic systems. *Science*, 240, 1285–1293.

van Smeden, M., Moons, K.G., de Groot, J.A., Collins, G.S., Altman, D.G., Eijkemans, M.J. and Reitsma, J.B. (2018). Sample size for binary logistic prediction models: Beyond events per variable criteria. *Statistical Methods in Medical Research*, in press.

Wada, T., Yasunaga, H., Yamana, H., Matsui, H., Fushimi, K. and Morimura, N. (2017). Development and validation of an ICD-10-based disability predictive index for patients admitted to hospitals with trauma. *Injury*, in press.

Wishart, G., Bajdik, C., Dicks, E., Provenzano, E., Schmidt, M., Sherman, M., Greenberg, D., Green, A., Gelmon, K., Kosma, V., et al. (2012). PREDICT Plus: development and validation of a prognostic model for early breast cancer that includes HER2. *British Journal of Cancer*, 107, 800–807.

SORT 43 (1) January-June 2019, 163-190 DOI: 10.2436/20.8080.02.84

Efficient algorithms for constructing D- and I-optimal exact designs for linear and non-linear models in mixture experiments

Raúl Martín Martín[1], Irene García-Camacha Gutiérrez[1] and Bernard Torsney[2]

Abstract

The problem of finding optimal exact designs is more challenging than that of approximate optimal designs. In the present paper, we develop two efficient algorithms to numerically construct exact designs for mixture experiments. The first is a novel approach to the well-known multiplicative algorithm based on sets of permutation points, while the second uses genetic algorithms. Using (i) linear and non-linear models, (ii) D- and I-optimality criteria, and (iii) constraints on the ingredients, both approaches are explored through several practical problems arising in the chemical, pharmaceutical and oil industry.

MSC: 62-K05.

Keywords: Optimal experimental design, D-optimality, I-optimality, mixture experiments, multiplicative algorithm, genetic algorithm, exact designs.

1. Introduction

Applications of mixture problems can be found in several areas including the chemical, pharmaceutical and oil industries. Their main purpose is to identify the composition of different blends which optimally describe the characteristic-response of their products. Standard choice designs and models are typically applied in the literature. However, due to the benefits of the optimal experimental design (OED) theory, more attention is receiving the development of this theory for mixture experiments nowadays (Coetzer and Haines, 2017; García-Camacha Gutiérrez, 2017; Goos, Jones and Syafitri, 2016; Wong et al., 2015; Brown, Donev and Bissett, 2015). Many authors have worked on developing efficient algorithms for designing exact optimal experimental design. The limited number of theoretical results focuses on approximate optimal designs to precise parameter estimation (Cornell, 2002; Atkinson, Donev and Tobias, 2007). Kiefer (1961) analyt-

[1] Department of Mathematics, University of Castilla–La Mancha, Spain. Author for correspondence: Irene.GarciaCamacha@uclm.es, Avda. Carlos III s/n, Ed. 21 (21.1.04), 45071, Toledo, Spain

[2] School of Mathematics & Statistics, University of Glasgow, United Kingdom.

Received: February 2018
Accepted: February 2019

ically determined D-optimal designs for quadratic models. Galil and Kiefer (1977) extended these results for ϕ_p-optimization, while Mikaeili and Lim's works focused on cubic polynomials (Mikaeili, 1989; Lim, 1990). Nevertheless, no remarkable result exists for general-degree polynomials. Chan (1992) and Chan and Guan (1998) computed optimal designs for other classes of models such as log-contrast ones, with inverse terms or additive ones and Chan and Guan (2001) gave an extensive review about this topic. The book *Optimal Mixture Experiments* is an updated guide about both analytical and numerical results (Sinha et al., 2014). On the other hand, less attention has been paid in the statistical literature to seek I-optimal designs. Goos et al. (2016) provided a recent literature review on I-optimal designs and Coetzer and Haines (2017) introduced a new approach to the construction of D- and I- optimal designs when the mixture components are linearly constrained. Thus there is some space for exploiting the problem to develop more efficient numerical algorithms than the traditional ones.

The aim of this paper is to propose two novel design constructions algorithms for identifying exact D- and I-optimal designs in mixture experiments. The first one is based on a multiplicative algorithm (MA). This is a well known algorithm in OED (Torsney, 1977; Silvey, Titterington and Torsney, 1978). It consists of an update rule of probability measures and its convergence has been extensively studied for approximate design theory (Yu (2010)). However, the application of this methodology is not straightforward in exact mixture problems. In this work, we provide a new approach of the MA using a special class of designs known as exchangeable designs (Draper and Pukelsheim, 1999). The idea of these designs is to generate candidate points in the mixture designs using permutations of a fixed set of component values. In this paper, this class of designs are called *permutation mixture experimental designs* (PMEDs), where the use of MA takes advantage of exploiting the general equivalence theorem. On the other hand, an efficient genetic algorithm (GA) is provided as an heuristic alternative which is also valid in constrained mixture problems. Borkowski (2003) was a pioneer applying this numerical optimization tool to OED field and motivated its use for irregularly-shaped design regions. The nature of mixture experiments requires special conditions on the operators and even more if there are experimental limitations on the proportions. For that reason, although the basis of our algorithm is standard, adaptations of the operators have been carried out. GAs have been tested in a wide variety of contexts, in particular, they have been used as alternatives to exchange algorithms. Several modifications have already been developed to accelerate the convergence of these algorithms. Most of them are focused on the operators. Two new improvements are proposed in this paper. The first one based on the selection of the initial population and the second one is a new strategy based on a clusterization process around optimal points. Mixing laws for fluid viscosity, drug delivery systems, drug formulation and improvement of crude quality are some real examples suitable for computing optimal designs and for checking the goodness of the proposed algorithms.

The paper is organized as follows. Section 2 recalls the basis of mixture experimental design. We describe the existing designs for mixture experiments and an introduction

of the OED theory is presented. The proposed multiplicative and genetic algorithms for computing exact D- and I-optimal designs in mixture experiments are described in Section 3. Examples of applications to real problems are shown in Section 4. Finally, Section 5 provides a brief discussion and some future lines of research.

2. Background

2.1. Models and designs for mixture experiments

Controlled variables in a standard mixture problem are nonnegative, belonging to $[0,1]$ and dependent through the relationship $\mathbf{1}_q^\intercal p = 1$ where $\mathbf{1}_q = (1,\ldots,1)^\intercal \in \mathbb{R}^q$ and $p = (p_1,\ldots,p_q)^\intercal$ is the vector of relative proportions in a q-component mixture. These constraints define the design region χ as a $(q-1)$-dimensional simplex $\mathcal{S} = \{p \in [0,1]^q : \mathbf{1}_q^\intercal p = 1\}$. In addition, many real mixture problems are often constrained by lower and upper bounds on their proportions, $0 \leq L_i \leq p_i \leq U_i \leq 1$, $i = 1,\ldots,q$. This is mainly due to experimental limitations or ingredient availability considerations.

A suitable model must be selected a priori describing the composition-response relationship. Let $y = \boldsymbol{\eta}^\intercal(p)\boldsymbol{\theta} + \varepsilon(p)$ be the observed response, where $\boldsymbol{\eta}^\intercal(p) = (\eta_1(p),\ldots,\eta_k(p))$ is a vector of k linearly independent functions, $\boldsymbol{\theta} = (\theta_1,\ldots,\theta_k)^\intercal$ is the unknown parameter vector and $\varepsilon(p)$ is the error term. Additive uncorrelated random errors with common variance will be assumed. Because of the ordinary polynomials do not allow estimation of parameters due to collinearity between proportions, canonical polynomials introduced by Scheffé (1958) are the most commonly used for a large of practical situations. To illustrate, a third-order Scheffé polynomial (the full cubic model) is

$$E[y] = \sum_{i=1}^{q} \theta_i p_i + \sum_{i=1}^{q-1} \sum_{j=i+1}^{q} \theta_{ij} p_i p_j + \sum_{i=1}^{q-1} \sum_{j=i+1}^{q} \delta_{ij} p_i p_j (p_i - p_j) + \sum_{i=1}^{q-2} \sum_{j=i+1}^{q-1} \sum_{k=j+1}^{q} \theta_{ijk} p_i p_j p_k,$$

where δ_{ij} are reparametrizations of the parameters of an ordinary full third-order polynomial. In spite of being the most popular, other models have been proposed in the literature for data from mixture experiments with particular properties. Darroch and Waller's additive polynomials (Darroch and Waller, 1985), models with homogeneous functions (Becker, 1968), models with inverse terms (Draper and John, 1977), log-contrast models (Aitchison and Bacon-Shone, 1984) or Draper and Pukelsheim's *K-polynomials* (Draper and Pukelsheim, 1997) are some of them.

Although many aspects differ between experiments from different areas, standard designs are often used by practitioners in mixture problems. In general, standard mixture designs are adopted in the literature for fitting standard mixture models. If $m \geq 1$ is

an integer, the $\{q,m\}$-simplex lattice in $\mathcal{S}$ is defined as the collection of points whose coordinates are integer multiples of $1/m$, that is the set of points $\{p \in \mathcal{S},\ p_i = \frac{j}{m}, 0 \leq j \leq m,\ 1 \leq i \leq q\}$ (Scheffé, 1958). Thus a $\{q,m\}$-*simplex lattice* design describes a design that takes observations at the above set of points, the $\{q,m\}$-lattice. On the other hand, a $\{q,m\}$-*simplex centroid* ($1 \leq m \leq q$) is defined as a collection of points in $\mathcal{S}$ with $q-j$ coordinates equal to zero and j coordinates equal to $\frac{1}{j}$, $j = 1,\ldots,m$ (Scheffé, 1963). However, if interest is focused on exploring within the simplex, another class of designs named *axial designs* were suggested by Cornell (2002). Snee and McLean and Anderson (Snee, 1979; McLean and Anderson, 1966) proposed extreme-vertex designs for constrained mixture problems.

In summary, the analysis of mixture experiments has been developed using canonical polynomials models and other alternative linear models under standard designs. However, there are situations where models that are nonlinear in the parameters would be preferable and standard designs are not appropiated. The application of mixture experiments to nonlinear models appears to be a very interesing question which has been little explored (Coetzer and Focke, 2010; Brown et al., 2015). On the other hand, even considering linear models, if the design region is constrained, standard designs are not suitable 6 (Piepel, Cooley and Jones, 2005). In this paper we apply the OED theory to obtain optimal designs using both linear and nonlinear models and considering unconstrained and constrained regions. In the next subsection, we introduce the OED basis, which is used in what follows.

2.2. Optimal experimental design background

Let a linear model $y = \boldsymbol{\eta}^{\mathrm{T}}(p)\boldsymbol{\theta} + \varepsilon(p)$ as defined above. A set of experimental conditions, p, must be determined in order to observe the outcome in an optimal manner (mainly to attain precise estimations of the parameters or to obtain accurate response predictions). An *exact design* will be a sequence of experimental conditions (mixture settings) $\xi_N = \{p^1, p^2, \ldots, p^N\}$ from a compact set (the $(q-1)$-dimensional simplex $\mathcal{S}$) which are not necessarily distinct. Assuming that only J of the points are different the design may be represented by a probability measure. Thus, if the point p^j appears n_j times in the design, $\omega_j = n_j/N$ will be the probability of p^j within the sample. Then the exact design problem can be viewed as one of determining these proportions optimally subject to them being rational. Using this idea Kiefer (1961) relaxed this condition, defining *an approximate design* as any probability measure ξ on χ with a finite support,

$$\xi = \begin{Bmatrix} p^1 & p^2 & \cdots & p^J \\ \omega_1 & \omega_2 & \cdots & \omega_J \end{Bmatrix},$$

where the ω_j values satisfy $0 \leq \omega_j \leq 1$ and $\sum_{j=1}^{J} \omega_j = 1,\ j = 1,\ldots,J$. From the Carathéodory theorem, an upper bound for the number of support points can be derived as $\frac{k(k+1)}{2} + 1$ (Chapter 8, Pukelsheim, 2006). For moderate and large numbers of runs,

the number of replicates of design points can be determined by integer appr oximation to the optimal measure.

The most important element for describing the quality of statistical inference that can be drawn from data collected with a design is the Fisher information matrix.

For an N-point exact design ξ_N we can assume $J = N$ and $\omega_j = 1/N$; so

$$M(\xi_N) = \sum_{j=1}^{N} \boldsymbol{\eta}(p^j)\boldsymbol{\eta}^{\intercal}(p^j)\omega_j = \frac{1}{N} VV^{\intercal} \propto VV^{\intercal},$$

where the i^{th} column of the matrix V is $\boldsymbol{\eta}(p^i)$ denoted by $v_i = v(p^i)$. The set of information matrices, $\mathcal{M}$, is convex and compact. The inverse of the information matrix is proportional to the covariance matrix of the least squares estimates. Thus, an experimental designing "optimizing", in some sense, the information matrix, should be found. Following convention, the ranking of alternative designs is based on a scalar-valued criterion function, $\psi[M(\xi_N)]$, so that, the problem becomes one of function optimization. A function ψ defined on the set of information matrices defines an optimality criterion if it is non decreasing in the Loewner sense ($\psi(M_1) \leq \psi(M_2)$ whenever $M_1 - M_2$ is non-negative definite). For notational issues, let us define two functions $\psi[\cdot]$ and $\phi(\cdot)$, both relative the criterion function whose use will depend on its argument, in particular $\psi[M(\xi_N)] = \phi(\xi_N)$. In this paper, we consider two optimality criteria: D- and I-optimality. The goal of D-optimality is connected to parameter estimation. This criterion seeks to minimize the volume of the confidence ellipsoid of the parameters and is formulated as $\phi_D(\xi_N) = \det[M(\xi_N)]^{-1/k}$. On the other hand, due to the importance of predictive capability of many mixture experiments, I-optimal designs were considered in this work too. This criterion focuses on precise prediction, and is defined by the following function: $\phi_I(\xi_N) = \frac{\int_{\mathcal{S}} \eta(p)^{\intercal} M^{-1}(\xi_N)\eta(p)dp}{\int_{\mathcal{S}} dp} = \Gamma(q) \cdot \text{trace}[M^{-1}(\xi_N)B]$, where B is the moment matrix given by $B = \int_{\mathcal{S}} \eta(p)\eta^{\intercal}(p)dp$ and $\int_{\mathcal{S}} dp = \frac{1}{\Gamma(q)}$ when the domain of the mixture settings is the simplex. Thus, I-optimal designs seek to minimize the average prediction variance over the design region.

A design optimizing the criterion function in the class Ξ_N of all exact designs of size N is referred to as an exact ϕ-optimal design, ξ_N^*. Thus we can compare the quality of two designs of the same size (N) through the ratio of the criterion values. When the optimal exact design is known, ξ_N^*, the efficiency of a design $\xi \in \Xi_N$ is defined as $\text{Eff}_\phi(\xi_N) = (\phi(\xi_N)/\phi(\xi_N^*))$.

However, finding an exact optimal design is not an easy task because it is a discrete optimization problem and there is no general analytical tool for confirming whether an exact design is optimal or not. On the contrary, approximate designs are easier to find. The most important advantage of searching approximate designs is the concavity (convexity) of the criterion functions. Under these conditions, an excellent tool to check whether a particular approximate design is optimal (especially for differentiable criteria) is the Equivalence Theorem. Even though finding approximate optimal design is

easier because of the above results, in practical settings, only exact designs can be implemented. So, when an optimal approximate design has been found, then it has to be rounded to obtain an exact design (Pukelsheim and Rieder, 1992). A weakness of this approach is that the final exact design obtained by rounding off an approximate design for implementation is not unique. In addition, a large sample size is needed to obtain a design close to the optimal exact design.

It is worth mentioning that in many real situations, mixing laws do not linearly respond as composition varies. For the linear case, optimal designs are independent of the value of θ. In the case where non-linear models are appropriate, the most common method for analyzing them is based on the use of the linear Taylor series approximation of the model. Under these conditions, the covariance matrix of the least squares estimator of $\boldsymbol{\theta}$ is asymptotically approximated by the inverse of the information matrix induced by the design

$$M(\xi_N, \boldsymbol{\theta}^0) = \frac{1}{N} \sum_{j=1}^{N} v(p^j, \boldsymbol{\theta}^0) v^{\mathsf{T}}(p^j, \boldsymbol{\theta}^0),$$

where $v(p^j, \boldsymbol{\theta}^0) = (\frac{\partial \eta(p^j, \boldsymbol{\theta})}{\partial \theta_1}, \ldots, \frac{\partial \eta(p^j, \boldsymbol{\theta})}{\partial \theta_k})^{\mathsf{T}}\big|_{\boldsymbol{\theta}=\boldsymbol{\theta}^0}$ and $\boldsymbol{\theta}^0$ is a prior guess of $\boldsymbol{\theta}$ (Chernoff, 1953). In this sense, the computed designs are locally optimum.

3. Algorithms for solving mixture exact design problems

As it was defined in the previous section, finding a ϕ-optimal exact N-point design is a combinatorial problem, and it has been considered an NP-hard problem (Welch, 1982). Globally optimal exact designs usually cannot be established and, in most cases, we need to resort to heuristic algorithms to find good designs. Several algorithms are available in the literature, most of which can be only used to compute approximate designs. They can be categorised into two broad groups: *greedy algorithms* such as those based on Fedorov-type exchanges, candidate-free coordinate exchange and multiplicative updating of the weights, and *nature inspired algorithms* which include simulated annealing, genetic algorithms and swarm intelligence between others (Dean et al., 2015).

The first algorithms developed for dealing with exact designs are based on exchange methods and were proposed for the D-optimality criterion (Fedorov, 1972; Wynn, 1970). Some modifications of these procedures were suggested in order to speed up the original algorithms (DETMAX algorithm (Mitchell, 1974); KL-exchange algorithm (Atkinson and Donev, 1989); coordinate-exchange algorithm (Meyer and Nachtsheim, 1995). McLean and Anderson's method (McLean and Anderson, 1966), XVERT (Snee and Marquardt, 1974) and CONSIM (Snee, 1979) were specifically developed for obtaining designs on irregularly shaped experimental regions. The resulting designs are called *the extreme-vertex designs*. Most of these algorithms were later directly applied to mixture settings. Neither of the algorithms are guaranteed to find the globally optimum design

because the support points are chosen from a pre-specified grid points. This requirement implies an exhaustive search over all candidate points, which is time-consuming and inefficient. During the last few years, algorithms have been improved to avoid this drawbacks. In particular, for constructing approximate designs, hybrid algorithms have been developed for improving computational efficiency (Martín-Martín and García-Camacha Gutiérrez, 2015) for D-optimality, Saleh and Pan (2016) for G-optimality, and Coetzer and Haines (2017) for D- and I-optimality for mixture experiments with linear constraints). They are based on suitably adjusting the strategies followed by the standard algorithms so that the new proprieties were able to solve the arisen problems using these methods in an isolated way. Another class of algorithms, inside of the first group of algorithms, which has received much attention for finding optimal approximate designs is the class of multiplicative algorithms (Torsney, 1977; Silvey et al., 1978). In spite of the several improvements to this class of algorithms, only Torsney and Martín-Martín (2009) adapted the multiplicative algorithm to cope with exact designs. In the present paper, this numerical method will be adapted to the special nature of mixture design.

The second group of optimization techniques used in OED to compute optimal designs are the meta-heuristic optimization algorithms. Due to their flexibility and potential, they have become a common tool in computational statistics as alternatives to standard algorithms. One of the most popular ones is the GA. Borkowski (2003) was a pioneer applying this numerical optimization tool to OED field and motivated its use for irregularly-shaped design regions. Heredia-Langer et al. (2003) and Limmuun, Borkowski and Chomtee (2013) gave a substantial discussion about the relative merits of GAs for design of experiments and some of the potential pitfalls of the implementation. On the other hand, in a recent paper, Wong et al. (2015) proposed a modified particle swarm optimization (PSO) technique for computing D-optimal approximate designs for mixture linear models. It is important to highlight that these algorithms take the mixture proportions to be continuous over the design region. Variable-Neighbourhood Search (VNS) is also a metaheuristic strategy commonly used to escape from local optima. Several variants of VNS have been proposed in the literature (Vazquez, Goos and Schoen, 2018). In this work, two new improvements have been incorporated to the proposed GA. The first one is based on the selection of the initial population and the second one is a new strategy based on a clustering process around presumed optimal design points.

3.1. A novel approach of the MA to determining exact optimal design for mixture experiments

Symmetry and balancedness have always been a prime attribute of good experimental designs (Draper and Pukelsheim, 1999). Nevertheless, in the case of mixture experiments, symmetry cannot be conducted in the general geometrical sense since the simplex is not itself a symmetric region. The natural structure of symmetry in the simplex deals with the invariance under permutation of its coordinates, it means symmetry through

the centroid of the simplex. Following this idea and since the support points of most the optimal mixture designs obtained in the literature are permutations of proportions, we consider the use of permutations of fixed sets of q component values or proportions, say $p = (p_1, \ldots, p_q)$ where $\mathbf{1}_q^{\intercal} p = 1$, to generate candidate points for mixture designs. In this paper, this class of designs is called *Permutation Mixture Experimental Designs* (PMEDs).

Let $p = (p_1, \ldots, p_q)$ be a single mixture point in the $(q-1)$-dimensional simplex $\mathcal{S}$ and let

$$\mathcal{P}(p) = \{a = (a_1, \ldots, a_q) = \sigma(p_1, \ldots, p_q),\ \sum_{i=1}^{q} p_i = 1,\ p_i \geq 0, i = 1, \ldots, q\}$$

be the set of all possible permutations of its proportions, $\#\mathcal{P}(p) = q!$. A PMED of $p \in \mathcal{S}$ mixtures is an exact $N = q!$-design generated by one set of components $\xi_{\mathcal{P}(p)} = \{\mathcal{P}(p)\}$. From this definition, it is worth mentioning that the set of the permutation points of any point belonging to a linearly-constrained region into the simplex may not be entirely included in this region. Consequently, this new approach cannot be applied for solving constrained mixture problems. In this regard, new approaches are being explored for overcoming this situation.

Let us denote the PMED design $\xi_{\mathcal{P}(p)} \underset{Not}{\equiv} \mathbb{P}$. The corresponding information matrix will be written as

$$M(\mathbb{P}) = \frac{1}{q!} \sum_{j=1}^{q!} v(p^j) v^{\intercal}(p^j). \tag{1}$$

We are interested in finding $p^* = (p_1^*, \ldots, p_q^*)$ optimally to maximize a chosen design criterion, $\psi[M(\mathbb{P}^*)] = \phi(p^*) = \max_{p \in \mathcal{S}} \phi(p)$. This problem can be considered as special case of the general class optimization problem discussed by Torsney and Martín-Martín (2009). One advantage of this approach is that we can use calculus to determine first-order conditions of optimality for exact designs.

The first-order conditions for a local maximum (minimum) are:

$$F_i^* = F_\phi(p^*, e_i) = \begin{cases} = 0, & \text{for } p_i^* > 0 \\ \leq (\geq) 0 & \text{for } p_i^* = 0, \end{cases} \quad i = 1, \ldots, q \tag{2}$$

where $F_i = F_\phi(p, e_i)$ is the directional derivative of $\phi()$ at p in the direction of the extreme vertex $e_i \in \mathbb{R}^q$. It is noteworthy that the elements of the information matrix (1) in the mixture experiment context are not linear functions of p even for simple models such as higher first-order polynomials. Therefore, the criterion function $\phi(p) = \psi[M(\mathbb{P})]$ is probably a non-concave (non-convex) function, in which case (2) are necessary but not sufficient conditions for local maxima (minima). For illustrative purposes, directional derivatives for *D*-optimality are computed following the above considerations (see supplementary material A). The expression of the directional derivative in the case of non-

linear arguments is

$$F_\phi(p,e_i) = F_\psi\left[M(\mathbb{P}),\ M(\mathbb{P}) + \frac{\partial M(\mathbb{P})}{\partial p_i} - \sum_{l=1}^{q} p_l \frac{\partial M(\mathbb{P})}{\partial p_l}\right].$$

The directional derivatives for the D- and I-optimality criteria derived from these are

$$F_{\phi_D}(p,e_i) = \mathrm{Tr}\left[M^{-1}(\mathbb{P})\frac{\partial M(\mathbb{P})}{\partial p_i}\right] - \sum_{l=1}^{q} p_l \mathrm{Tr}\left[M^{-1}(\mathbb{P})\frac{\partial M(\mathbb{P})}{\partial p_l}\right], \tag{3}$$

and

$$F_{\phi_I}(p,e_i) = \mathrm{Tr}\left[LM^{-1}(\mathbb{P})\frac{\partial M(\mathbb{P})}{\partial p_i}M^{-1}(\mathbb{P})L^{\mathrm{T}}\right] - \sum_{l=1}^{q} p_l \mathrm{Tr}\left[LM^{-1}(\mathbb{P})\frac{\partial M(\mathbb{P})}{\partial p_l}M^{-1}(\mathbb{P})L^{\mathrm{T}}\right], \tag{4}$$

where L is the Cholesky factor of the moment matrix B.

To satisfy the constrains of this problem of maximizing a criterion function of proportions $p_1,\ldots,p_q$, we will use an iterative multiplicative algorithm. Thus, the n-th update corresponding to the i-th component of p is

$$p_i^{(n)} = \frac{p_i^{(n-1)} f(x_i^{(n-1)},\delta)}{\sum_{l=1}^{q} p_l^{(n-1)} f(x_l^{(n-1)},\delta)},\ \ i = 1,\ldots,q,$$

where $x_i^{(n-1)} = F_\phi(p^{(n-1)},e_i)$, $f(x_i^{(n-1)},\delta)$ is positive, $\partial f(x,\delta)/\partial x > 0$ and, if $\delta = 0$, $f(x,\delta)$ is constant; $n = 1,2,\ldots$ is the iteration number and $p^{(0)} = (p_1^0,\ldots,p_q^0)$ a starting point such that $M(\mathbb{P}^{(0)})$ is not a singular matrix. The choice of f plays an important role in the convergence of the algorithm. δ is a small positive constant whose choice must be suitably made for the monotoniciy of the algorithm. Since the criterion function can have negative derivatives, two appropriate choices of $f(x,\delta)$ are $f(x,\delta) = \Phi(\delta x)$, where Φ is the c.d.f. of the standard normal distribution, and $f(x,\delta) = \exp(\delta x)/(1+\exp(\delta x))$, i.e., the logistic c.d.f. evaluated at δx. An iteration of the algorithm will be completed when all components have been updated. It is important to note that the application of the standard version of the MA for computing the optimal approximate design with $q!$ points, will imply $q!\cdot q$ updates in each iteration, while it will be only q in the case of considering a permutation design due to only one set of proportions needs to be computed. The stopping rule will comprise checking if the first-order conditions (4) are satisfied up to a certain tolerance.

One of the limitations of considering one set of permutations is that, in many mixture systems, it is not sufficient to estimate all model parameters. This is mainly due to singularity occurring in the information matrix by the repetition of its elements (permutations

of blends with repeated coordinates) or simply because the number of design-points ($q!$) is lower than the number of parameters. In order to solve these problems, we provide a natural extension of the algorithm presented above. This approach consists of the simultaneous calculation of more than one set of permutations, say t sets,

$$p_{(h)} = (p_{h1}, \ldots, p_{hq}),\ h = 1, \ldots, t,$$

where

$$\sum_{i=1}^{q} p_{hi} = 1 \ \ \forall h = 1, \ldots, t \ \text{ and } \ p_{hi} \geq 0, \forall h = 1, \ldots, t,\ i = 1, \ldots, q.$$

Thus, a greater variety of designs points can be included in the designs,

$$\begin{aligned} \mathcal{P}(p_{(1)}, \ldots p_{(t)}) = \Bigg\{ & a_{(h)} = (a_{h1}, \ldots, a_{hq}) = \sigma(p_{h1}, \ldots, p_{hq}) : \\ & \sum_{i=1}^{q} p_{hi} = 1, p_{hi} \geq 0, h = 1, \ldots, t,\ i = 1, \ldots, q \Bigg\} \\ & = \mathcal{P}(p_{(1)}) \cup \ldots \cup \mathcal{P}(p_{(t)}). \end{aligned}$$

A PMED of $p_{(1)}, \ldots, p_{(t)} \in \mathcal{S}$ mixtures is an exact $N = t \cdot q!$ - design,

$$\xi_{\mathcal{P}(p_{(1)}, \ldots, p_{(t)})} = \Big\{ \mathcal{P}(p_{(1)}), \quad \mathcal{P}(p_{(2)}), \quad \ldots, \quad \mathcal{P}(p_{(t)}) \Big\}$$

consisting of all possible points formed by permutation of the coordinates of $(p_{(1)}, \ldots, p_{(t)}) \in \mathcal{S}$. Then, according to (1), the information matrix is

$$M(\mathbb{P}_{(1)}, \ldots, \mathbb{P}_{(t)}) = \sum_{h=1}^{t} M(\mathbb{P}_{(h)}) = \frac{1}{t \cdot q!} \sum_{h=1}^{t} \sum_{j=1}^{q!} v(p_{(h)}^{j}) v^{\intercal}(p_{(h)}^{j}).$$

Thus we are facing to the following optimization problem: optimize $\phi(p_{(1)}, \ldots, p_{(t)})$ over $p_{(1)}, \ldots, p_{(t)} \in \mathcal{S}$. Then the following ($h$-sets) simultaneous approaches are used

$$p_{hi}^{(n)} = \frac{p_{hi}^{(n-1)} f_h(x_{hi}^{(n-1)}, \delta_h)}{\sum_{l=1}^{q} p_{hl}^{(n-1)} f_h(x_{hl}^{(n-1)}, \delta_h)}, h = 1, \ldots, t, i = 1, \ldots, q$$

where n is the iteration number, $f_h(x_{hi}^{(n-1)}, \delta_h)$ are positive increasing functions and $x_{hi}^{(n-1)} = F_\phi(p_{(h)}^{(n)}, e_i) \underset{Not}{\equiv} F_{hi}$ are the directional derivatives defined as above. There are necessary optimality conditions equivalent to those in Eq. (2). Therefore, the algorithm stops when the following conditions

$$F^*_{hi} = F_\phi(p^*_{(h)}, e_i) = \begin{cases} = 0, & \text{for } p^*_{hi} > 0 \\ \leq (\geq) 0 & \text{for } p^*_{hi} = 0, \end{cases} \quad i = 1,\ldots,q, \;\; h = 1,\ldots,t \qquad (5)$$

are simultaneously satisfied.

Multiplicative algorithm for ϕ-optimal mixture design

Step 0. Input q, $p^{(0)}_{(1)}$, $\xi^{(0)}_{\mathcal{P}} = \xi_{\mathcal{P}(p^{(0)}_{(1)})}$, $\boldsymbol{\delta}_1$, tol. Set $n = 1, t = 1$.

Step 1. Update the proportions for each mixture point generator,$(p^{(0)}_{(1)},\ldots,p^{(0)}_{(t)})$

For $h = 1,\ldots,t$, do,

- For $i = 1,\ldots,q$, do $p^{(n+1)}_{hi} = \frac{p^{(n)}_{hi} f_h(x^{(n)}_{hi},\delta_h)}{\sum_{l=1}^{q} p^{(n)}_{hl} f_h(x^{(n)}_{hl},\delta_h)}$

with $x^{(n)}_{hi} = F_\phi(p^{(n)}_{(h)}, e_i)$ calculated as in (3), (4).

Step 2. Construct the design $\xi^{(n+1)}_{\mathcal{P}} = \xi_{\mathcal{P}(p^{(n+1)}_{(1)},\ldots,p^{(n+1)}_{(t)})}$.

Step 3. If $|M(\mathbb{P}^{(n+1)}_{(1)},\ldots,\mathbb{P}^{(n+1)}_{(t)})| \approx 0$, then repeat from step 1 to step 3 adding a new group of permutation, $\xi^{(0)}_{\mathcal{P}} = \xi_{\mathcal{P}(p^{(0)}_{(1)},\ldots,p^{(0)}_{(t)},p^{(0)}_{(t+1)})}$, $t = t+1$. Otherwise, go to step 4.

Step 4. Stopping rule: If

$$\min_{\substack{h=1,\ldots,t \\ i=1,\ldots,q}} \{F_\phi(p^{(1)}_{(hi)}, e_i)\} \leq 10^{-tol}$$

where tol is a number specified by the user, then STOP.
Else update $\xi^{(n)}_{\mathcal{P}}$ by $\xi^{(n+1)}_{\mathcal{P}}$, $n = n+1$, and return to Step 1.

In the next section we explore the potential of this method in a variety of examples encompassing both linear and non-linear models for D-optimality and I-optimality.

3.2. Genetic algorithm

When the design space is regular and conventional mathematics can be applied the NP-hard combinatorial optimization problem of finding a ϕ-optimal exact N-point design can be solved using traditional optimization techniques. However many difficulties such as the irregular structure of the design spaces, the non-linear and non-differentiable objective functions, etc. make that optimization techniques break down in many optimization problems. For this reason, metaheuristic strategies have been developed to solve these difficulties. The goal is to explore the design space in a smart way to get near-optimal solutions.

One of these algorithms is the genetic algorithm (GA). GAs are population based stochastic search algorithms inspired by Darwin's Theory of Evolution and the survival-of the fittest. The weakest individuals will disappear while the best ones will survive and be able to reproduce themselves for generating the next population. Although there is no metaheuristic algorithm that will be universally the winner, it should be pointed out that GAs are robust, flexible and easy to implement. As other metaheuristics strategies, the two main features of the algorithm are the locally and intensively exploring/searching around the best solutions (intensification) and the generation of diverse solutions to make sure the algorithm explores the design space globally (diversification).

It is common to find in the literature related to this class of algorithms a specific terminology based on Genetics. P denotes the population of M initial N-point exact designs. Potential solutions of the problem (designs) are named chromosomes, whereas support points (blends) are labelled genes.

GAs start to search from an initial population. The information provided for each exact design is measured in terms of the criterion function value relative to the population. This value is a probability measure of the design goodness known as the fitness function. At each iteration a number of operators is applied to the designs of the current population to generate the designs of the population of the next generation (iteration). The most popular genetic operators are (1) selection (certain elitism is used to ensure the monotonicity of the algorithm. Also, designs with higher fitness have higher probabilities of being selected for successive processes); (2) crossover, also called the recombination operator (new designs, called offspring, are generated from two designs, called parents with a crossover probability, P_C); (3) mutation (to avoid premature convergence toward local optimal, with a mutation probability, P_M). Applying this process iteratively, new generations of designs are created until some stopping rule is reached. In this work, the algorithm stops after performing a prefixed maximum number of consecutive iterations (N_{max}) without improvement of the best fitness function value.

In the first step of a GA an initial population of designs, which are created from a set of points, is needed. As in Heredia-Langer et al. (2003) we use a population size of $M = 40$ exact designs. It is reasonable to believe that if the set contains *good* points to create designs, then we will have more possibilities to find the near-optimal design. Thus, if some information about the optimal solutions is available it will be convenient to use. On the other hand, if no information about the solution is available, it would be expected that the more diverse the initial population is, the greater the possibility to find a solution (Diaz-Gomez and Hougen, 2007). With this in mind, several scenarios were considered in this work. Basically they are distinguished by the fact that they include just randomly points or also contain vertices, the overall centroid and the centroid of all lower dimensional simplices of a $(q-1)$-simplex. A detailed explanation of different frameworks can be found in the supplementary material B. Through numerical examples we study the effect of the initial populations in the convergence of the algorithm.

The choice of the algorithm operators and parameters is a hard problem that will determine whether the algorithm will find a near-optimum solution and whether it will

find such a solution efficiently (Eiben, Hinterding and Michalewicz, 1999). Although the proposed algorithm is based on the presented one in Limmuun et al. (2013), new modifications was needed to avoid infeasible solutions. In particular, solutions out of the feasible region were penalized during the recombination, whereas suitable replacements were carried out during mutation.

Finally, a new intensification strategy to improve the fitness of designs was applied when the fitness function was based on D-optimality. Due to exact D-optimal designs for Scheffé mixture models are $\{q,m\}$ simplex-lattice designs, $\{q,m\}$ simplex-centroid designs, and replications of points of them, that points can be viewed as consisting of *clusters* of points. It suggests that if the points of the designs are near of this *cluster* points (points in the open balls centred at cluster points with radius tol_{clu}), they will be reached in some iterations so an appropriate strategy consists of moving nearby points to them with certain frequency (n_{it}^{clu} iterations).

The step-by-step implementation of GA is explained as follows:

Genetic algorithm for D- and I-optimal mixture design

Step 0. Input M, N_{elite}, P_{elite}, P_C, P_M, N_{max}, tol, n_{it}^{clu}, tol_{clu}.

Step 1. Initialize $counter = 1$ and select an scenario to generate $\mathcal{P}^{(1)} = \{\xi_1^{(1)}, \xi_2^{(1)}, \ldots, \xi_M^{(1)}\}$:

- Unrestricted mixture experiments: RD, RUD or VD.
- Restricted mixture experiments: RRD, EVD or SEVD.

Step 2. For each $j = 1, \ldots, M$, calculate the fitness

$$fit_j^D = \frac{\Phi_D(\xi_j)}{\sum_{i=1}^{M} \Phi_D(\xi_i)} \text{ or } fit_j^I = \frac{1}{\sqrt{i_j} \cdot \sum_{j=k}^{M} \left(\frac{1}{\sqrt{i_k}}\right)},$$

according to the chosen optimality criterion. The subscripts $i_1, \ldots, i_M$ are refereed to the position of $\xi_1, \ldots, \xi_M$ increasingly sorted according to their criterion function values.

Step 3. Selection:

(i) *Selection with elitism.* Select the $N_{elite} = P_{elite} \cdot M$ designs with the highest fitness values.

(ii) *Probabilistic selection.* Select the i_1^*-th and i_2^*-th parent designs, being

$$i_1^* = min\{i : \sum_{s=1}^{i} fit_s^{\phi} \geq \gamma_1\} \quad \text{and} \quad i_2^* = min\{i : \sum_{s=1}^{i} fit_s^{\phi} \geq \gamma_2\},$$

where $\gamma_1, \gamma_2 \sim U(0,1)$. The superscript ϕ is taken to be ϕ_D or ϕ_I to denote D- or I-optimality respectively

Step 4. Crossover:

(i) *Arithmetic blending*. For each $p_j^{i_1^*} \in \xi_{i_1^*}$, $j = 1,\ldots,n$, generate $\gamma \sim U(0,1)$. If $\gamma < P_C$, then

$$p_{\text{off}_j} = \lambda p_j^{i_1^*} + (1-\lambda) p_j^{i_2^*} \quad \text{and} \quad p_{\text{off}_j} = (1-\lambda) p_j^{i_1^*} + \lambda p_j^{i_2^*}$$

where $\lambda \sim U(0,1)$. Otherwise, remain unchanged. ξ_{off_1} and ξ_{off_2} denote the new created offsprings.

(ii) *Single-crossover point*. Let $p_j = (p_1,\ldots,p_q)$ be the j-th gen of ξ_{off_1} from (i). Thus, p_j can be written as

$$p_j = (0.abc_1^j \mid def_1^j, ..., 0.abc_q^j \mid def_q^j),$$

being abc_k^j and def_k^j are the the decimal figures corresponding to the head and tail respectively. Let us consider third decimal position to divide for illustrating. For each $j = 1,\ldots,n$, if $\gamma < P_C$, then keep $abc_k^j \ \forall k = 1,\ldots,q$ and replace the tails by a random permutation $\sigma(def_1^j,\ldots,def_q^j)$. Otherwise, remain unchanged. Repeat the same operation with ξ_{off_2} genes. If there are constrains over the ingredients, remain unchanged cross points out of the feasible region.

Step 5. Mutation: Let ζ be a randomly selected $U(0,1)$. For each p_j, $j = 1,\ldots,n$, of ξ_{off_1} from (ii), if $\zeta < P_M$, then replace p_j by other randomly selected gen in the feasible region. Otherwise, remain unchanged. Repeat the same operation with ξ_{off_2} genes.

Step 6. Repeat step 3(ii)-5 until having obtained a new generation $\mathsf{P}^{(2)}$ of M new designs.

Step 7. Let ξ_1^{best} and ξ_2^{best} be the designs with highest (lowest) D- (I-)criterion function value in $\mathsf{P}^{(1)}$ and $\mathsf{P}^{(2)}$ respectively. If

$$\frac{\Phi_D(\xi_{best}^{(2)}) - \Phi_D(\xi_{best}^{(1)})}{\Phi_D(\xi_{best}^{(2)})} \leq 10^{-tol} \text{ or } \frac{\Phi_I(\xi_{best}^{(1)}) - \Phi_I(\xi_{best}^{(2)})}{\Phi_I(\xi_{best}^{(2)})} \leq 10^{-tol} \tag{6}$$

is satisfied, where tol is a number specified by the user, then $counter++$. Otherwise, $counter = 1$.

Step 8. If $\phi = \phi_D$ and $counter \equiv 0 \pmod{n_{it}^{clu}}$, then clusterize:

(i) Construct a distance matrix D, where $d_{ij} = \| p_i - p_j \|_2$, $p_j \in \xi_{best}^{(k+1)}$, $j = 1,\ldots,n$, $p_i \in C$ or V, $i = 1,\ldots,\#(C)$ or $\#(V)$, depending on whether it is a unrestricted or restricted mixture problem, respectively.

(ii) Define a new design ξ_{clu} to store the clusterized version of $\xi_{best}^{(k+1)}$ and initialize $\xi_{clu} = \xi_{best}^{(k+1)}$. Let

$$i_j^* = \underset{1 \le i \le \#(C) \text{ or } \#(V)}{arg\,\min} \; d_{ij}$$

be the position of the i_j^*-th point belonging to C or V nearest the j-th point of $\xi_{best}^{(k+1)}$. For each $p_j \in \xi_{clu}$, $j = 1, ...n$, if $d_{i_j^* j} < tol_{clu}$, then $p_j = p_i$.

iii) Replace $\xi_{worst}^{(k+1)}$ by ξ_{clu}, where $\xi_{worst}^{(k+1)}$ is the design with lowest D-criterion function value in $\mathcal{P}^{(k)}$.

(iv) If $\Phi_D(\xi_{clu}) > \Phi_D(\xi_{best}^{(k+1)})$, then $counter = 1$.

Step 9. Stopping rule: If $counter = N_{max}$, then STOP. Else update $\mathsf{P}^{(1)}$ by $\mathsf{P}^{(2)}$ and repeat from step 2.

4. Numerical Examples

Several real problems in the chemical, pharmaceutical and oil industry were used to demonstrate the effectiveness of the proposed algorithms. The selected models were set for three or four-ingredient blends since they were the most commonly used in the literature for data from mixture experiments. For illustrative purposes, D- and I-exact optimal designs were also computed for more ingredients and different numbers of points.

Both algorithms were developed in *R 3.6.0* software (R Core Team, 2018). The tolerance level considered with GA was 10^{-10} whereas it was 10^{-5} with MA since it has a more stringent stopping rule. It was established $N_{max} = 200$ in the stopping rule of the GA and the cumulative distribution function (CDF) of the standard normal distribution or logistic distribution were taken as the $f(x, \delta)$ function with $\delta = 1$ in the MA.

In all examples, we compared results from MA and GA with one of the most popular algorithm in the literature to compute exact designs, the KL-exchange algorithm (KLA), implemented in the R package OptimalDesign. As usual, it is recommended to verify the quality of the designs obtained by other heuristic methods. The application of this method is not direct since it is necessary to provide a set of candidate points. The type of initial mesh strongly affects the finding of the optimal designs. In this work, we propose several procedures for generating sets of candidate points (see supplementary material B) in order to improve its yield. On the other hand, we used the coordinate-exchange algorithm (CEA) of Piepel et al. (2005), which does not require specification of a candidate set. Other comparisons were made with other algorithms such as the cocktail algorithm, but they were not include in this paper for space considerations. A brief discussion of these algorithms will be provided in the last section.

In order to compute I-optimal exact designs with KLA, we found some computational problems considering the IV-optimality criterion provided in OptimalDesign package. Then, the corresponding problem of A-optimality was set such as imple-

menters suggest. The entries of the moment matrix for calculating I-optimal designs, $\mathbf{B}$, were obtained directly from the moments of a Dirichlet distribution (DeGroot, 1970, p. 51) when the experimental region was the $(q-1)$-dimensional simplex and linear models were considered (Goos and Syafitri, 2014). In other cases, that is, when the experimental region was a constrained space or the model was non-linear, the moment matrix was obtained by numerical calculations generating a large candidate set o points uniformly on the region. This was very important because a poor approximation could lead to suboptimal designs (Goos et al., 2016).

4.1. Real applications of the proposed algorithms

4.1.1. Tramadol matrix tablets formulation

Polynomial models have been widely used in pharmacology, particularly in optimizing drug delivery systems. The following example is motivated by a real problem in which the aim was to determine the release-modifying effect of carboxymethyl xyloglucan for oral drug delivery (Madgulkar et al., 2013). A special cubic polynomial (7) was used to explain the percentage of drug release after a few hours in terms of the drug formulation. The mixture comprised three ingredients: p_1 =carboxymethyl xyloglucan, p_2 =gelling agent (HPMC K100M) and p_3 =dicalcium phosphate (DCP).

$$E[y(p)] = \theta_1 p_1 + \theta_2 p_2 + \theta_3 p_3 + \theta_{12} p_1 p_2 + \theta_{13} p_1 p_3 + \theta_{23} p_2 p_3 + \theta_{123} p_1 p_2 p_3. \quad (7)$$

Various softwares are often employed by practitioners to obtain designs on which must be carried out by experimenters. Classical designs such as simplex-lattice or simplex centroid are the most common choice suggested by these programs. In this simple case, there are analytical results about the D-optimal design. Uranisi (1964) showed that the $\{3,3\}$-simplex centroid was the D-optimal exact design of size 7. Indeed, when the size of the exact design N is proportional to the number of parameters, m, then the D-optimal exact design is the continuous one replicating N/m times each point. In other case, the design points should be as equireplicated as possible regardless which points are replicated most frequently (Goos et al., 2016). Our algorithms produced the same optimal designs for many common models. So, the validation of both techniques is especially interesting for our purposes.

We computed D-optimal designs with $N = 7, 14$ and 18 runs for $q = 3$, and $N = 25$ and 50 for $q = 5$ ingredients. MA was used considering three groups of permutations and GA algorithm was applied under the different scenarios (see supplementary material B). In order to compare our results with the KLA, the exact optimal designs were calculated taking into account that the initial candidate set of points were obtained through the same scenarios than GA. CEA was also run for the same study cases.

Table 1 (supplementary material C) collects the D-efficiencies of the obtained designs with regard to the optimal designs available in the literature or, otherwise, the best design achieved from the algorithms used in this work. They will be named as relative efficiencies. It is noteworthy the robustness of GA under different approaches we considered to construct the initial population in the case of three ingredients. Although this behaviour did not hold for five-ingredient mixtures, the optimum was always achieved under VD scenario (supplementary material B). Regarding the performance of the KLA, it is remarkable to say that this algorithm found difficulties to obtain the optimal design when a random grid of initial points was considered. This situation got worse when a bigger number of ingredients was considered. As it could be expected, the CEA achieved the optimum in all frameworks since it is not based on a set of candidate designs points and it was specially designed to tackle problems with large number of mixture components. On the other hand, when the optimum was a permutation design, such was the case of $N = 18$ runs, the MA quickly achieved the optimum. The convergence speed of the GA is shown in the Figure 1 (a). Despite the fact that the optimum was obtained in all scenarios, the initial population constructed from VD led to the solution faster than the others because it started from designs nearer optimum. Owing to space considerations, these figures are only presented for one case in each example.

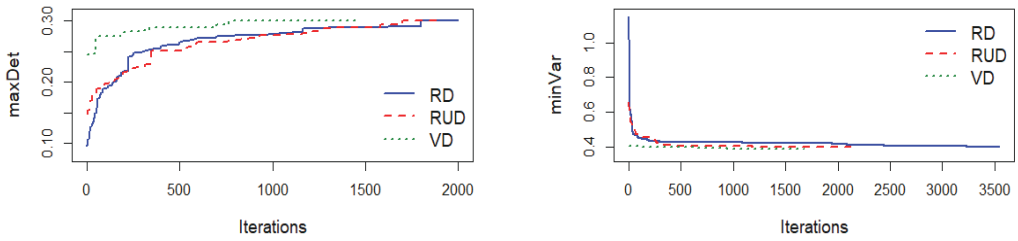

(a) (b)

Figure 1: *Values of the D- and I-optimality criteria for GA applied to example 4.1.1 with three ingredients and $N = 18$ runs under different scenarios (RD, RUD and VD), (a) and (b) respectively.*

Regarding I-optimality, exact designs were computed for the second-order Scheffé model in order to compare our results with the presented ones in Goos et al. (2016). I-optimal designs with $N = 6,7,8,18$ and 30 runs for $q = 3$, $N = 15,16$ and 17 for $q = 4$, and $N = 15$ and 30 runs for $q = 5$ ingredients were calculated. From Table 2 (supplementary material C) it is deduced that, differently from D-optimality, there is no a strong dependence of the initial scenario for achieving the optimum regardless the number of ingredients considered in the problem. Designs achieved with GA are highly efficient in all study cases. This behaviour is also observed in the Figure 1 (b) in which it is shown that the optimum is practically obtained in 500 iterations for all scenarios. Optimal designs were obtained in all samples using the CEA. Again, when MA could be used, the optimal design was nimbly achieved. As in Goos et al. (2016) for

$q = 3$-ingredient mixtures, the $\{3,2\}$-simplex-lattice was found for $N = 6$ runs, whereas the $\{3,3\}$-simplex-centroid was obtained for $N = 7$. Nevertheless, some interior points appear in the optimum in many cases for I-optimality (Goos et al., 2016). These points cannot be obtained with the KLA unless they are included in the initial set of points. The higher the number of ingredients is, the lower the probability of being contained in the initial grid is. In spite of providing a thin grid, poorly efficient designs were obtained.

4.1.2. Mixing laws for fluid viscosity

Another usual application of mixture models is found in chemistry and chemical engineering. When the purpose of the study is to analyse the kinematic viscosity of a fluid blend, optimal design tools are used to achieve the best parameter estimation in mixing laws. Most fluid viscosities do not linearly change as formulation varies. Therefore, researchers have developed complex mixture models for their prediction. The selected model in this example is a popular mixing law (8) provided by Grunberg and Nissan (1949). It is a particular case of a wide class of models named *power-mean-mixture models* (Focke, Sandrock and Kok, 2007). They used (8) to explain the viscosity as a function of the three components namely p_1 =acetone, p_2 =methanol and p_3 =water. We assume $\theta_{ij} = \theta_{ji}$ and the nominal values as in Focke et al. (2007),

$$E[y(p,\boldsymbol{\theta})] = \boldsymbol{\eta}(p,\boldsymbol{\theta}) = Exp\left(\sum_{i=1}^{3}\sum_{j=1}^{3} Ln(\theta_{ij})p_i p_j\right). \tag{8}$$

Coetzer and Focke (2010) computed a six-point D-optimal design for this model using a non-linear constrained optimization technique. Variations in the location of the design points caused a significant increase in the criterion function value. The design provided in Coetzer and Focke (2010) is 86.69% efficient relative to the six-point optimal design obtained with the GA and KLA as we can observe from Table 3 (supplementary material D). One set of permutations provided three different support points (permutations of $(1,0,0)$) which was not enough to estimate the model parameters with MA. Therefore, new groups of permutations were considered in the problem, although this involved adding $q!$ new design points for each group. We will compute the optimal designs with $N = 6, 12$, and 18 runs for ternary blends, and $N = 15$ and 30 for five-ingredient samples for both D- and I-optimality criteria.

Similar performances of the algorithms were found to those observed in the previous example (see Table 3, supplementary material D). The I-optimal designs obtained with GA and KLA for five ingredients and $N = 15$ runs are shown in Table 4 (supplementary material D). This table illustrates the GA searchability when optimal design points are located in the interior of the design region. This situation is frequently found when response is not linear in the parameters. Figure 2 shows that the speed of convergence is less dependent on the initial scenario for I-optimality than it is for D-optimality. The CEA cannot be directly applied on non-linear mixture models so that it is not imple-

mented in the most popular commercial softwares. Designs cannot be calculated using this method since a new adaptation is necessary to tackle the non-linearity of the model at the same time that mixture coordinates cannot be independently exchanged without violating the constraint that proportions must sum to one.

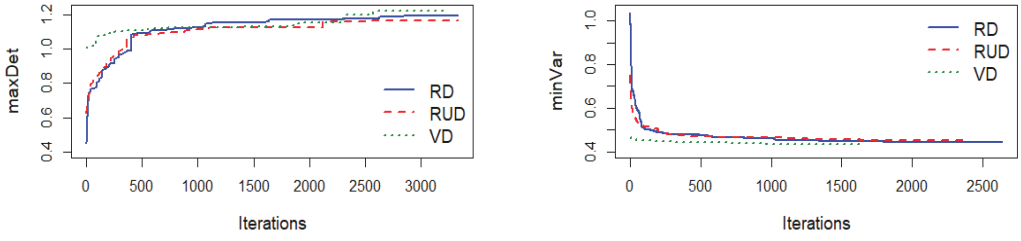

(a) (b)

Figure 2: *Values of the D- and I-optimality criteria for GA applied to example 4.1.2 with three ingredients and $N = 18$ runs under different scenarios (RD, RUD and VD), (a) and (b) respectively.*

The following examples are constrained mixture problems. As we mentioned in section 3.1, the extension of the MA proposed in this work does not allow to tackle such kind of problems. New approaches are being investigated for overcoming this situation. Nevertheless, if the initial population of designs is randomly generated over the constrained region, new solutions will remain in this region by construction of the operators proposed in the GA.

4.1.3. Size control of amphiphilic cyclodextrin nanoparticles

Natural or modified cyclodextrins are important excipients used in the pharmaceutical industry to reduce toxicity while improving stability, solubility and bioavailability of hydrophobic drugs (Choisnard et al., 2005). The nanoparticle capacity associated with a drug is expected to be partially influenced by nanoparticle size. This study was focused on controlling the size of amphiphilic β-cyclodextrin (βCDa) nanoparticles using a nano-precipitaciton procedure which strongly depends on solvent formulation. The influence of p_1 =water, p_2 =acetone and p_3 =ethanol proportions involved in this technique was investigated through an experimental design methodology using the full second-degree polynomial to estimate the nanoparticle size. Due to difficulties found in preliminary studies, the experimental region was limited to $0.4 \leq p_1 \leq 0.7$ and $0 \leq p_2, p_3 \leq 0.6$. These limitations are necessary to control the high solubility of βCDa in organic solvent and to avoid the low limit of scattering intensity.

The model chosen in Choisnard et al. (2005) is not an appropriate model for this kind of settings. It is not a canonical polynomial so that the parameters associated with its terms are not unique. Consequently, the design used by the experimenters with that model led to a singular determinant of the information matrix. Thus, a reparametrization

of the full second-degree polynomial was used in this work

$$E[y(p)] = \theta_1 p_1 + \theta_2 p_2 + \theta_3 p_3 + \theta_{12} p_1 p_2 + \theta_{13} p_1 p_3 + \theta_{23} p_2 p_3. \quad (9)$$

It does not only avoid the singularity of the information matrix but also it involves a reduction in the number of model parameters. Thus, fewer runs are needed to estimate the parameters.

Table 5 (supplementary material E) collects the D-efficiencies obtained with GA, KLA and CEA with $N = 6$ and 12 runs in the case of ternary blends, and $N = 15$ runs for five-ingredient mixtures. Both samples in this latter case have different complexity. In the first case $^{(\star)}$, fourth and fifth ingredient can be freely allocated into the simplex, whereas all ingredients are constrained in the second case $^{(\star\star)}$. D-optimal designs achieved with GA and CEA were quite robust, while KLA showed difficulty to find the optimum for RRD and SEVD scenarios for ternary blends and it was unable to achieve them for five ingredients.

Problems of numerical accuracy were found with KLA in the calculus of the I-optimal exact designs despite being recommended in the literature to verify the quality of the designs obtained by other heuristic methods (Harman, Bachrata and Filová, 2016). I-optimal designs cannot be calculated by using this algorithm. Table 6 (supplementary material E) contains the I-efficiencies obtained with GA and CEA in several examples. The CEA applicable for constrained mixture experiments was designed to D-optimally select design points without candidate points (Piepel et al., 2005). In view of the results, this strategy does not seem adequate to achieve I-optimal constrained mixture designs. On the contrary, GA results seem quite robust. It is noteworthy from Figure 3 that both D- and I-optimal design are quickly achieved in a few iterations which reveals the good GA performance in constrained problems.

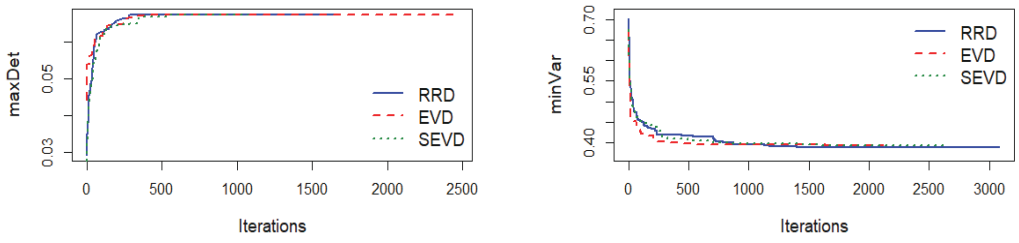

(a) (b)

Figure 3: *Values of the D- and I-optimality criteria for GA applied to example 4.1.3 with three ingredients and $N = 12$ runs under different scenarios (RRD, EVD and SEVD), (a) and (b) respectively.*

4.1.4. Aqueous phase composition of a microemulsion

Enhanced oil recovery process is obtained determining the optimal formulation of a microemulsion system. Water and oil are not miscible substances at ambient temperatures. The mixture needs to be made under critical conditions due to the existing incompatibility between these fluids. However, a small amount of surfactant, co-surfactant, brine and water may render them compatible to form a structure called microemulsion. This desirable effect is produced due to the properties of these substances. Jerirani et al. (2012) modeled this behaviour using the special cubic polynomial (10) for predicting IFT (interfacial tension) as a measure of energy at the interface of two immiscible fluids. Lower IFT is expected to produce a more effective microemulsion system. Providing a suitable model is essential to finding the formulation which yields its minimum value. Four components are involved in this experiment: p_1 =isopropyl alcohol (IPA), p_2 =sodium chloride (NaCl), p_3 =polysorbate 80 (Tween80) and p_4 =water. A relevant issue arises in the construction of valid formulations under which a microemulsion system is effective. A large amount of water is involved in this process and the rest of the components are practically negligible in spite of their significant positive effect. Particularly, the constraints are $0.01 \leq p_1 \leq 0.04,\ 0 \leq p_2 \leq 0.03,\ 0.002 \leq p_3 \leq 0.02$, and $0.91 \leq p_4 \leq 0.98998$. This fact implies an extreme difficulty in the search for the optimum.

$$E[y(p)] = \theta_1 p_1 + \theta_2 p_2 + \theta_3 p_3 + \theta_4 p_4 + \theta_{12} p_1 p_2 + \theta_{13} p_1 p_3 + \theta_{14} p_1 p_4 + \theta_{23} p_2 p_3 + \\ + \theta_{24} p_2 p_4 + \theta_{34} p_3 p_4 + \theta_{123} p_1 p_2 p_3 + \theta_{124} p_1 p_2 p_4 + \theta_{134} p_1 p_3 p_4 + \theta_{234} p_2 p_3 p_4 \tag{10}$$

Table 7 (supplementary material F) shows the GA power to seek a D-optimum over a severely constrained region, whereas the KLA is even less D-efficient than in the previous case. Unlike 4.1.3 example, CEA was unable to achieve the D-optimum. Figure 4 shows that a random or "semi-random" scenario is preferable to any other for D-optimality. This matter demonstrates that KLA and CEA are inefficient in samples where the optimum is not allocated on extreme-vertex points.

The same drawback than in the previous example was found considering KLA for I-optimality, so that we can only compare with the designs provided by the experimenters and the CEA for this criterion. A 20-point I-optimal design was selected in Jerirani et al. (2012) for IFT modelization. In view of the I-efficiencies shown in Table 8 (supplementary material F), we have that the design obtained by the experimenters is 4.51% efficient in comparison with the design obtained with GA. This fact implies the methodology used by them to carry the optimization out is not adequate. The robustness of the GA for I-optimality can be observed in Figure 4, whereas the CEA inefficiently performs again.

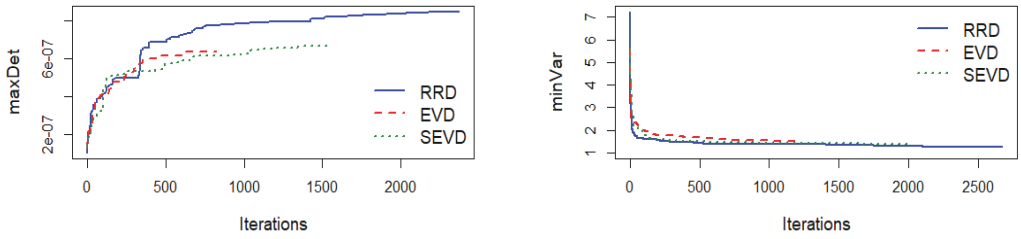

(a) (b)

Figure 4: *Values of the D- and I-optimality criteria for GA applied to example 4.1.4 with four ingredients and $N = 20$ runs under different scenarios (RRD, EVD and SEVD), (a) and (b) respectively.*

5. Discussion

This paper presents two new optimization tools for constructing D- and I-optimal exact designs, when the variables controlled by the experimenter are proportions, and then discusses their properties.

The MA is well known in OED and its convergence has been extensively studied in approximate design theory. However, its application to the solution of exact mixture problems is not straightforward and a new approach based on a class of permutation designs is proposed in this paper. Since symmetry and balancedness have always been a prime attribute of good experimental designs (Draper and Pukelsheim, 1999), and in view of the results obtained, considering PMED seems to be a suitable strategy to generate candidate points for mixture design. The new definition of the multiplicative iteration has a substantial advantage over the other algorithms: first order conditions can be obtained by exploiting the equivalence theorems, whereas stopping rules in the other methods are based on the idea of not finding a better exchange or a better solution. Another advantage the MA offers is that it does not need to anticipate the number of design points, unlike the other methods. The optimal number of permutation groups is automatically determined by the algorithm. However, disadvantages include the fact that it cannot be used when the design space has constraints beyond the natural one and the fact that the sample size has to be a multiple of q!. While this may not be too restrictive in a small q, in other cases it can become a difficulty.

GAs are a class of stochastic optimization methods, easy to implement and computationally powerful. We provided an efficient GA as a heuristic alternative when additional constraints over the experimental region appeared in real problems. One common feature of the GAs is that their computational time is relative. This situation has led to the development of a number of modifications to accelerate their convergence. Most of them focus mainly on the operators. Nevertheless, another interesting but much less studied option relates to initial populations. Several scenarios were proposed in this paper and substantial differences were observed in the speed of convergence rather than

the quality of final solution. A new strategy based on a clustering process around optimal points was also incorporated into the algorithm for this purpose. The number of iterations required to achieve the optimum is much lower than when clustering is not considered. This approach helps operators to explore and quickly reach potential solutions. Moreover, it prevents suboptimal designs from being obtained, in the sense of generating near-optimal points. Many algorithms have the disadvantage of achieving support points close to the vertices, the overall centroid and the centroid of all lower dimensional simplices of a $(q-1)$-dimensional simplex. This intensification strategy gives further guarantees of reaching the optimum. It is also noteworthy that if the optimum does not lie on the extreme vertex points, this new mechanism does not force their inclusion in the optimal design considering all possible cases. On the other hand, changes in the operators were made in order to hold the solutions within the feasible regions.

Genetic algorithms were seen as robust problem solvers that exhibit approximately the same accuracy over the different scenarios considered for constructing the initial populations (supplementary material B) in a wide range of problems. This property is even more evident when I-optimal designs are sought. In this regard, the MA and the CEA do not depend on an initial set of candidate points. However, the strong dependency of KLA on the initial set of points means it is a good choice when the interest is in selecting rather than finding solutions. As may be deduced from the examples, a GA does not offer significant benefits over exchange algorithms when the designs spaces are regular in the case of D-optimality. Unlike point-exchange algorithms, the CEA performs successfully when the optimal design points are located in the interior of the design region (I-optimality) in unrestricted regions. In spite of these advantages, this algorithm cannot be directly applied to non-linear mixture models. Due to the CEA efficiency, it could be interesting to explore a new approach to this algorithm in this kind of situation. On the other hand, when there is no evidence of potential candidate points as, for instance, in severely constrained design regions, the designs generated by exchange algorithms are not frequently optimal under any scenario. On the other hand, the GA and the MA (when possible) converged in all examples and showed excellent searchability.

Other algorithms were also used in this paper apart from KLA and CEA for comparison purposes. In the examples where the cocktail algorithm could be applied, the efficiencies of the designs obtained were the lowest due to rounding effects. Rounding methods take neither the model nor the criteria into account. As a consequence, they are guaranteed to produce efficient results only if the number of trials is high compared to the dimension of the unknown parameter (Harman and Filová, 2014). Results could not be obtained for a predetermined number of runs N since the approximation rule will depend on the weight assigned to each point of the discretized space. These results were omitted due to their poor performance and for considerations of space.

Particular attention is drawn to the successful performance of the proposed algorithms when non-linear mixture models are considered. We can recommend to practi-

tioners more efficient designs than those used in their experiments. They provided better results than general optimization solvers and the algorithms implemented in commercial software.

Finally, although at this stage the use of the multiplicative method seems to be limited, this approach offers the advantages previously noted. In regard to limitations, we are exploring other alternatives as a line of future research. In particular, we are looking at a partition of the simplex into symmetrical regions to simplify the research as the number of proportions increases, and we are working on imposing order constraints on the proportions so the sample size need not be a multiple of q!. In addition, it would be interesting to use the MA proposed here to construct *D*- and *I*-optimal designs for mixture experiments in which linear constraints are imposed on the components. A new adaptation of MA for tackling this kind of practical situation is also being explored. Moreover, we expect that these algorithms can be applied to find optimal designs for a much broader class of optimality criteria. All these studies will be aimed at solving real situations in other fields of study where OED with mixtures plays an essential role.

Acknowledgements

The authors have been sponsored by Ministerio de Economía, Industria y Competitividad, Agencia Estatal de Investigación (MTM2016-80539-C2-1-R), Consejería de Educación, Cultura y Deportes de la Junta de Comunidades de Castilla-La Mancha (SBPLY/17/180501/000380) and Fondo Europeo de Desarrollo Regional (FEDER).

References

Aitchison, J. and Bacon-Shone, J. (1984). Log contrast models for experiments with mixtures. *Biometrika*, 2, 323–330.

Atkinson, A. and Donev, A. (1989). The construction of exact D-optimum experimental designs with application to blocking response suface designs. *Biometrika*, 3, 515–526.

Atkinson, A., Donev, A. and Tobias, R. (2007). *Optimum Experimental Designs with SAS*. Oxford Statistical Science Series. United Kingdom: Oxford University Press.

Becker, N. (1968). Models for the response of a mixture. *Journal of the Royal Statistical Society*, 1, 107–112.

Borkowski, J. (2003). Using genetic algorithm to generate small exact response surface designs. *Journal of Probability and Statistical Science*, 1, 65–88.

Brown, L., Donev, A. and Bissett, A.C. (2015). General blending models for data from mixtures experiments. *Technometrics*, 4, 449–456.

Chan, L. (1992). D-optimal design for a quadratic log contrast model for experiments with mixtures. *Communications in Statistics. Theory and Methods*, 10, 2909–2930.

Chan, L. and Guan, Y. (1998). Design in mixture models with inverse terms for two components. *Private comunication*.

Chan, L. and Guan, Y. (2001). A- and D-optimal designs for a log contrast model for experiments with mixtures. *Journal of Applied Statistics*, 28, 537–546.

Chernoff, H. (1953). Locally optimal designs for estimating parameters. *The Annals of Mathematical Statistics*, 24, 582–602.

Choisnard, L., Géze, A., Bigan, M., Putaux, J. and Wouessidjewe, D. (2005). Efficient size control of amphiphilic cyclodextrin nanoparticles through a statistical mixture design methodology. *Journal of Pharmacetical Sciences*, 3, 593–600.

Coetzer, R. and Focke, W. (2010). Optimal designs for estimating the parameters in weighted power-mean-mixture models. *Chemometrics*, 24, 34–42.

Coetzer, R. and Haines, L. (2017). The construction of D- and I-optimal designs for mixture experiments with linear constraints on the components. *Chemometrics and Intelligent Laboratory Systems*, 171, 112–124.

Cornell, J. (2002). In *Experiments with Mixtures*, New York. Wiley.

Darroch, J. and Waller, J. (1985). Additivity and interaction in three component experiments with mixtures. *Biometrika*, 1, 153–163.

Dean, A., Morris, M., Stufken, J. and Binghman (2015). *Handbook of Design and Analysis of Experiments*.

DeGroot, M. (1970). *Optimal Statistical Decisions*. New York: McGraw Hill.

Diaz-Gomez, P. A. and Hougen, D.F. (2007). Initial population for genetic algorithms: A metric approach. In H.R. Arabnia, J.Y. Yang, and M.Q. Yang (Eds.), *GEM*, pp. 43–49. CSREA Press.

Draper, N. and John, R. (1977). A mixtures models with inverse term. *Technometrics*, 1B, 37–46.

Draper, N. and Pukelsheim, F. (1997). Mixture models based on homogeneous polynomials. *Journal of Statististical Planing and Inference*, 71, 303–311.

Draper, N. and Pukelsheim, F. (1999). Kiefer ordering of simplex designs for first- and second-degree mixture models. *Journal of Statistical Planning and Inference*, 79, 325–348.

Eiben, A., Hinterding, R. and Michalewicz, Z. (1999). Parameter control in evolutionary algorithms. *IEEE Transactions on Evolutionary Computation*, 3, 124–141.

Fedorov, V. (1972). In *Theory of optimal experiments*, New York. Academic Press.

Focke, W., Sandrock, C. and Kok, S. (2007). Weighted-power-mean mixture model: Empirical mixing laws for liquid viscosity. *Industrial and Engineering Chemistry Research*, 46, 4660–4666.

Galil, Z. and Kiefer, J. (1977). Comparison of simplex designs for quadratic mixture models. *Technometrics*, 4, 445–453.

García-Camacha Gutiérrez, I. (2017). *Diseño óptimo de experimentos para modelos de mezclas aplicados en la ingeniería y las ciencias experimentales*. Ph. D. thesis, Departamento de Matemáticas. Área de Estadística e Investigación Operativa. Universidad de Castilla-La Mancha.

Goos, P., Jones, B. and Syafitri, U. (2016). I-optimal design of mixture experiments. *Journal of the American Statistical Association*, 111, 899–911.

Goos, P. and Syafitri, U. (2014). V-optimal mixture designs for the qth degree model. *Chemometrics and Intellingent Laboratory Systems*, 136, 173–178.

Grunberg, L. and Nissan, A. (1949). Mixing law for viscosity. *Nature*, 164, 799.

Harman, R., Bachrata, A. and Filová, L. (2016). Heuristic construction of exact experimental designs under multiple resource constraints. *Applied Stochastic Models in Business and Industry*, 32, 3–17.

Harman, R. and Filová, L. (2014). Computing efficient exact designs of experiments using integer quadratic programming. *Computational Statistics and Data Analysis*, 71, 1159–1167.

Heredia-Langer, A., Carlyle, W., Montgomery, D., Borror, C. and Runger, G. (2003). Genetic algorithms for the construction of D-optimal designs. *Journal of Quality Technology*, 35, 28–46.

Jerirani, Z., Jan, B., Ali, B., Noor, I., Hwa, S. and Saphanuchart, W. (2012). The optimal mixture design of experiments: Alternative method in optimizing the aqueous phase composition of a microemulsion. *Chemometrics*, 112, 1–7.

Kiefer, J. (1961). Optimal design in regression problems. *The Annals of Mathematical Statististics*, 2, 298–325.

Lim, Y. (1990). D-optimal design for cubic polynomial regression on the q-simplex. *Journal of Statistical Planning and Inference*, 25, 141–152.

Limmuun, W., Borkowski, J. and Chomtee, B. (2013). Using a genetic algorithm to generate D-optimal design for mixture experiments. *Quality and Reliability Engineering International*, 29, 1055–1068.

Madgulkar, A., Bhalekar, M., Padalkar, R. and Shaikh, M. (2013). Optimization of carboxymethyl-xyloglucan-based tramadol matrix tablets using simplex centroid mixture design. *Journal of Pharmaceutics*.

Martín-Martín, R. and García-Camacha Gutiérrez, I. (2015). Combined algorithm to compute D-optimal designs. *Journal of Computational and Applied Mathematics*, 278, 248–257.

McLean, R. and Anderson, V. (1966). Extreme vertices design of mixture experiments. *Technometric*, 3, 447–454.

Meyer, R. and Nachtsheim, C. (1995). The coordinate-exchange algorithm for constriction exact optimal experimental designs. *Technometrics*, 37, 60–69.

Mikaeili, F. (1989). D-optimal design for cubic without 3-way effect on the simplex. *Journal of Statistical Planning and Inference*, 21, 107–115.

Mitchell, T. (1974). An algorithm for construction of D-optimal experimental designs. *Technometrics*, 16, 203–210.

Piepel, G., Cooley, S.K. and Jones, B. (2005). Construction of a 21-component layered mixture experiment design using a new mixture coordinate-exchange algorithm. *Quality Engeniering*, 17, 579–594.

Pukelsheim, F. (2006). *Optimal Design of Experiments*. Classics in Applied Mathematics. Society for Industrial and Applied Mathematics.

Pukelsheim, F. and Rieder, F. (1992). Efficient rounding of approximate designs. *Biometrika*, 79, 763 – 770.

R Core Team (2018). *R: A Language and Environment for Statistical Computing*. Vienna, Austria: R Foundation for Statistical Computing.

Saleh, M. and Pan, R. (2016). A clustering-based coordinate exchange algorithm for generating g-optimal experimental designs. *Journal of Statistical Computation and Simulation*, 86, 1582–1604.

Scheffé, H. (1958). Experiments with mixtures. *Journal of the Royal Statistical Society*, B, 344–369.

Scheffé, H. (1963). The simplex-centroid design for experiments with mixtures. *Journal of the Royal Statistical Society*, 2B, 235–263.

Silvey, S., Titterington, D. and Torsney, B. (1978). An algorithm for optimal designs on a finite design space. *Communications in Statistic*, A, 1379–1389.

Sinha, B., Mandal, N., Manisha, P. and Das, P. (2014). In *Optimal mixture experiments*, Lecture Notes in Statistics. Springer.

Snee, R. (1979). Experimental designs for mixture systems with multicomponent constrains. *Communications in Statictics. Theory and Methods*, 4, 306–326.

Snee, R. and Marquardt, D. (1974). Extreme vertices designs for linear mixture models. *Technometrics*, 16, 399–408.

Torsney, B. (1977). Contribution to discussion of "maximum likelihood estimation via the em algorithm" by dempster et al. *Journal of Royal Statistical Society*, B, 26–27.

Torsney, B. and Martín-Martín, R. (2009). Multiplicative algorithms for computing optimum designs. *Journal of Statistical Planning and Inference*, 139, 3947–3961.

Uranisi, H. (1964). *Optimal Design for the Special Cubic Regression Model on the q-simplex*. Mathematical Report 1, Kyushu University, General Education Department.

Vazquez, A.R., Goos, P. and Schoen, E.D. (2018). Constructing two-level designs by concatenation of strength-3 orthogonal arrays. *Technometrics*.

Welch, W.J. (1982). Three NP-hard problems in computational statistics. *Journal of Computation and Simulation*, 1, 41–48.

Wong, W., Chen, R.-B., Huang, C.-C. and Wang, W. (2015). A modified particle swarm optimization technique for finding optimal designs for mixture models. *PLoS ONE 10, e0124720*, 6.

Wynn, H. (1970). The sequential generation of D-optimum experimental designs. *The Annals of Statistics*, 6, 1273–1285.

Yu, Y. (2010). Monotonic convergence of a general algorithm for computing optimal designs. *The Annals of Statistics*, 38, 1593–1606.